University of Wollongong

Research Online

2006

Morphological changes of a small reef island on a platform reef

Bongkoch Samosorn
University of Wollongong

Follow this and additional works at: https://ro.uow.edu.au/theses

Recommended Citation

MORPHOLOGICAL CHANGES OF A SMALL REEF ISLAND ON A PLATFORM REEF

A thesis submitted in fulfillment of the requirements for the award of

the degree

DOCTOR OF PHILOSOPHY

from

UNIVERSITY OF WOLLONGONG
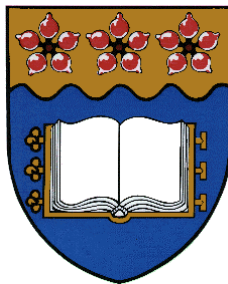
by

Bongkoch Samosorn, M.S. (Civil Engineering)

School of Earth and Environmental Sciences

University of Wollongong

Wollongong, Australia

November 2006

CERTIFICATION

I, Bongkoch Samosorn, declare that this thesis, submitted in fulfilment of the requirements for the award of Doctor of Philosophy, in the School of Earth and Environmental Sciences, University of Wollongong, is wholly my own work unless otherwise referenced or acknowledged. The document has not been submitted for qualifications at any other academic institution.

Bongkoch Samosorn

November 2006

ABSTRACT

This study examines: i) the morphological evolution of a small sand cay on a platform reef over past millennia; ii) changes in its shoreline over past decades; and ii) contemporary characteristics of waves on the reef platform. The study site is Warraber Island located on a platform reef in Torres Strait, Australia. The study is based upon: i) detailed radiocarbon dating; ii) 3-D morphological reconstruction using a DTM; and iii) field measurement of island topography, waves and wind.

Temporal patterns of evolution were assessed based on radiocarbon dating on both bulk samples and on specific components. Bulk radiocarbon ages are indicated to be unreliable for the determination of time of sand deposition. However, ages from shells provide a more appropriate indication of time of deposition of sand in this reef setting. Shell ages imply the continual accretion of the island over the past 3,000 years with a long-term rate of accumulation of approximately 900 m^3/y. Successive stages of accretion, and episodic progradation are indicated by prominent beach ridges.

Variations in island shore position over shorter time scales were examined based on island shape over the past 40 years (1966-2004). Significant change of island shape has occurred only on the southwestern and northeastern ends, rotating in a clockwise direction; the island appears to have undergone net accretion on the northeastern end and erosion on the southwestern end.

Wind climate and medium-term wind patterns were reconstructed. The E-SSE winds, especially ESE and SE winds, have been dominant with winds from the W-NNW sector subordinate. The influence of sunspot periodicity and ENSO on the wind patterns is not discernible but the initiation of solar magnetic cycle was found to coincide with times of the low magnitude of wind effect.

Wave conditions on the reef platform were examined based on the spectra of waves that were measured at a location close to the windward reef rim and five locations around the island. Development of spectral components and saturating conditions were also investigated. Wave characteristics were normally tidally modulated and related to the local wind system. In addition to incident wind wave components generated off the reef, incident short-period wave and infragravity wave components generated on the reef were prominent around the island. Combinations of these three components generate higher and shorter waves on the windward side of the island, and smaller and longer waves on the leeward side of the island. These wave characteristics can initiate movement of sediment around the island and on the island beach.

Probable wave conditions in relation to topographical development over the period of island evolution are discussed based on the contemporary wave conditions on the reef platform. Wind climate and associated patterns of waves and sediment transport are major influences on island shape in response to seasonal influence. Changing wind patterns and wave conditions in relation to nearby reefs, and human activities on the island were examined to identify probable causes of change in island shape over the past 40 years. Over the coming decades, the island is likely to be maintained by the transport of sediment already on the reef flat to the island. Further adjustments of the island morphology are anticipated due to changes in climate and sea level. However, even if there is a gradual rise in sea level, sediment supply to the island is still anticipated because of the greater capacity of waves to entrain and transport sediment, presently abundant on the reef flat.

TABLE OF CONTENTS

CHAPTER 7   CONCLUSIONS

LIST OF FIGURES

only spot heights; and b) using both spot height and breaklines

wave gauge; and b) atmospheric pressure measured using a
baroTROLL located at the airfield on the island

LIST OF TABLES

SYMBOLS AND ABBREVIATIONS

f_N	Nyquist frequency (Hz)
f_p	peak frequency (Hz)
g	gravitational acceleration (m/s^2)
h	water depth (m)
h_b	breaker depth (m)
k	wave number (m^{-1})
u_m	maximum horizontal velocity (cm/s)
D	grain diameter or equivalent sedimentation diameter (cm)
E	wave energy (m^2)
F_c	non-linearity parameter
H	wave height (m)
H_b	breaking wave height (m)
H_i	incident wave height (m)
H_{max}	maximum wave height (m)
H_{mo}	energy-based significant wave height (m)
H_{rf}	reef-flat wave height (m)
K_p	linear wave theory transfer function
N	empirical correction factor
T	wave period (s)
T_p	peak wave period (s)
T_1	mean wave period (s)
U_{10}	wind speed at a standard(10 m) elevation (m/s)

U_A	wind-stress factor
U_w	threshold orbital velocity (cm/s)
W	settling velocity (cm/s)

δ	non-dimensional depth ($\delta = gh/U_{10}^2$)
ξ	surf similarity parameter
ε	bandwidth parameter and non-dimensional energy
ϕ	Phi unit of grain size (D (millimeters) = 0.5^{ϕ})
ρ	fluid density (g/cm^3)
ρ_s	grain density (g/cm^3)
ρ_γ	submerged particle density ($\rho_s - \rho$) (g/cm^3)
μ	fluid dynamic viscosity (g/cm s or poise)
θ	angle between wave crest and bottom contour
θ_{wl}	Shield-type parameter (dimensionless threshold orbital velocity)
ν	non-dimensional peak frequency ($\nu = f_p u10/g$)
x	fetch (m)
χ	non-dimensional fetch ($\chi = gx/u10^2$)

AGD66	Australian Geodetic Datum 1966
AGD84	Australian Geodetic Datum 1984
AHO	Australian Hydrographic Office
AMS	Accelerator Mass Spectrometry radiocarbon dating
ANS	Australian National Spheroid
AMG66	Australian Map Grid 1966
AMG84	Australian Map Grid 1984

DEM	Digital Elevation Model
DTM	Digital Terrain Model
GDA94	Geocentric Datum of Australia 1994
GRS80	Geodetic Reference System 1980 spheroid
LADS	Laser Airborne Depth Sounder
LAT	Lowest Astronomical Tide
TIN	Triangular Irregular Network
WAM	WAve Modeling

ACKNOWLEDGEMENTS

To Professor James Kirby, Dr Fengyan Shi and Wen Long for advice in using REF/DIF and FUNWAVE, and to Don Battersby for assistance on the RV Kirby research vessel.

To the Torres Strait Regional Authority and the Warraber Island Council for permission to work and support on Warraber Island: Ted Billy and Clara Tamu, and the residents of Warraber Island for generous hospitality.

To my lovely wife, Siritron, who has greatly cared, constantly supported, and been next to me no matter what circumstances.

CHAPTER 1

INTRODUCTION

1.1   Thesis Statement

Reef islands on coral reefs comprise some of the lowest-lying lands in the world, often only a few metres above present mean sea level. They form the only land available for several atoll nations in the Pacific and Indian Oceans, such as Kiribati, Marshall Islands, Tokelau, Tuvalu and Maldives, and are culturally and economically valuable to indigenous people living there. In addition, they support tourism, are locations for navigational aids and weather stations, and are sanctuaries for birds and sea animals.

Reef islands are readily mobilised due to being largely composed of unconsolidated sediments and appear susceptible to even small variations in environmental conditions. Morphological changes to reef islands have been reported from many reef settings, attributed to both natural processes, such as seasonally alternating wind patterns and storms, or/and anthropogenic impacts, such as boat channel construction.

It has been widely suggested that globally the level of the sea is rising and will accelerate in the future due to global warming caused by the greenhouse effect, but with uncertainty as to rates of change (IPCC, 2001; Church et al., 2004). This has resulted in great concern about inundation (sea flooding) and erosion, especially of low-lying coasts and reef islands (Roy and Connell, 1991; Leatherman and Beller-Simms, 1997; Nunn, 2000). An increase in inundation is also expected to lead to an increase in the landward reach of wave action resulting in substantial morphological changes to reef

islands. This will impact on both people and economies of the islands. In order to develop proper, effective planning strategies and management, it is essential that there is a clear understanding of the physical response of reef islands to changes in these environmental factors.

In earth sciences, the ability to predict future conditions of a geomorphic system depends primarily on historical information about its former conditions and investigations of its present dynamics (Schumm, 1991). In the case of reef islands, therefore, understanding the past depositional chronology of islands together with present insight into reef-island dynamics in relation to sedimentation and other contemporary driving hydrodynamic forces should be beneficial for predicting probable reef-island conditions in the future. However, studies of the long-term evolution of the reef islands and short-term changes in their shorelines have been scarce. This is especially the case in estimating volumetric changes through time, and developing evolutionary sediment budgets. In addition, the characteristics of primary hydrodynamic factors affecting reef-island development and stability are little known, though these are an important component to understanding reef-island dynamics.

The present study thus aims to examine: i) the morphological evolution of a reef island over past millennia (geological time scale); ii) changes in island shoreline and associated volume over past decades (engineering time scale); and iii) contemporary characteristics of waves, particularly around the island, which is a primary hydrodynamic driving factor influencing the island development and stability. The field site for this study has been a small sand cay "Warraber Island" on a platform reef "Warraber Reef" in Torres Strait, Australia.

This chapter begins with an overview of the distribution and classification of reef islands, placing a sand cay such as Warraber Island, in a broader classification scheme

of reef islands. The formation, morphology and morphological changes of sand cays are then described in Section 1.3. A digital terrain model (DTM) is applied in this thesis to enhance a dimension of morphological reconstruction and analysis of a reef island, from conventional two dimensions to three dimensions, enabling sediment volume calculation. Thus Section 1.4 introduces the DTM and its applications in coastal and reefal studies. In Section 1.5, previous research on Warraber Reef is described. In the final section, Section 1.6, the specific objectives and an outline of the thesis are presented.

1.2   Geographic Distribution and Classification of Reef Islands

Reef islands are low-lying landforms built on a reef surface as a result of the accumulation of the skeletal remains of reef organisms. They are found in the Indian Ocean, Pacific Ocean and Caribbean Sea where coral reefs occur. There are, for example, more than 10,000 reef islands in the Indonesian Seas (Tomascik et al., 1997), more than 300 reef islands in the Great Barrier Reef region (Gourlay, 1988), more than 1,200 reef islands constituting the Republic of the Maldives (Risk and Sluka, 2000), and many in the Caribbean (Steers and Lofthouse, 1940; Thorpe and Stoddart, 1962; Folk, 1967).

The term "reef island" encompasses a range of different types of islands. An early attempt to classify reef islands resulted from an expedition in 1939, whereby Steers classified coral cays along the Jamaican coast into three types: cays of sand and shingle on a windward shore, cays of relatively small sizes with mangrove, and sand cays with a well-developed 'promenade' on the windward side (Steers and Lofthouse, 1940). Stoddart extended this classification to the coast of British Honduras (now Belize)

during an expedition in 1959-60 and separated cays into two main types, sand cays and mangrove cays which were further divided into those with or without sand ridges (Thorpe and Stoddart, 1962). Folk (1967) identified five types based on cays on Alacrán Reef, off the coast of Mexico, and recognised four phases of cay evolution, ranging from a smooth sand phase to a vegetated flat phase.

On the Great Barrier Reef three types of reef islands were recorded by Steers (1937); namely, sand cays, shingle cays and low wooded islands. Fairbridge (1950) developed a more detailed classification of reef islands on the Great Barrier Reef, including unvegetated sand cays, vegetated sand cays, shingle cays, sand cays with separate shingle ramparts (or low wooded islands), and islands with an exposed platform of older, emerged coral-reef materials. While Fairbridge's classification accounts for reef-island types within the northern Great Barrier Reef (Stoddart et al., 1978a), Stoddart and Steers (1977) extended the Fairbridge classification in order to embrace a wider range of reef islands found elsewhere, such as on Indo-Pacific atolls and in Florida. Their classification, based primarily on morphology or sediment character, and secondarily on vegetation, includes: i) sand cays, ii) sand cays with shingle ridges (motu), iii) shingle cays, iv) mangrove cays, v) mangrove cays with windward sand ridge, vi) low wooded island and vii) emerged reef-limestone islands (Stoddart and Steers, 1977). Figure 1.1 shows schematic examples of reef-islands types described by Stoddart and Steers (1977).

As a result of difficulties in applying the Fairbridge classification to all islands of the Great Barrier Reef, Hopley (1982), in addition to previously recognised criteria including location of the reef flat, sediment sizes and presence or lack of vegetation, developed a reef-island classification using further criteria such as the number of islands on the reef top, their degree of complexity and the overall morphology in relation to the

4

Figure 1.1. Schematic examples of reef-island types described by Stoddart and Steers (1977).

presence or absence of centripetal processes. The classification of reef islands on the Great Barrier Reef by Hopley (1982) includes four groups: i) unvegetated solitary islands; ii) vegetated solitary islands; iii) multiple islands; and iv) complex low wooded islands. This classification has also been applied to reef islands in the archipelago of the Indonesian Sea (Tomascik et al., 1997).

The small reef island that is the subject of this research is a vegetated sand cay (Figure 1.1a) in Torres Strait, Australia, and belongs to the vegetated solitary islands type of Hopley (1982). It represents one of the simplest of the reef-island types and was chosen in order to understand morphological development and the dominant processes affecting sand-cay accumulation.

1.3   Sand Cays

Sand cays are generally found on the leeward end of platform reefs (Hopley, 1982; Gourlay, 1990), on the reef flat of large fringing reefs (Stoddart, 1975; Tomascik et al., 1997) and on barrier reefs or atolls where they occur either along the leeward rims near reef passages (Thorpe and Stoddart, 1962; Richmond, 1992), on the outer rims on the leeward side (Folk, 1967) or on patch reefs in the lagoon (Guilcher, 1988; Woodroffe, 1992; Ali, 1997). Their formation, morphologies and morphological changes are reviewed consecutively.

1.3.1.   Formation of Sand Cays

Sand cays are a result of interrelationships between geological, biological and physical processes (Gourlay, 1988). Hopley (1982) suggested that the formation of sand cays depends primarily on three factors: i) sediment availability; ii) convergence of waves on the reefs; and iii) the ability of waves to transport sediment. Conditions of these factors favourable for sand-cay formation are related to morphology of reef platforms on which sand cays are built (Gourlay, 1988).

Reef-Platform Development

It is necessary for a reef platform to develop a near horizontal surface before a sand cay can be built on it. Modern reefs started to grow shortly after the pre-Holocene foundations on which they are established were inundated during the Holocene transgression. Two distinct patterns of sea-level rise have been recognised in reef areas during the Holocene, one relating to reef areas in the Caribbean, which experienced

6

decelerating rates of sea-level rise until present, and another derived for the Indo-Pacific and eastern Australian region, where the sea achieved its present level about 6,000 years ago (Davies and Montaggioni, 1985). Reefs can adopt keep-up, catch-up or give-up strategies in relation to sea-level rise (Neumann and Macintyre, 1985). In the Great Barrier Reef the growth of modern reefs has been dominated by catch-up mode after up to 2,000 years delay of reef colonisation after the pre-Holocene foundations are inundated (Davies and Hopley, 1983).

Generally, reef growth is most prolific on topographic highs and the most rapid rates of growth occur around the reef rim, especially on shallower substrate on the windward side (Scoffin et al., 1978). It has been suggested that the actual time at which individual reefs reach sea level has been dependent on a combination of: i) the depth of foundation beneath the modern reefs; ii) the vertical growth rates of the reef; and iii) the patterns of sea-level change (Hopley, 1982). Once reefs approach sea level, reef growth is increasingly dominated by lateral progradation.

The morphology of Holocene reef platforms is influenced by the depth and morphology of the antecedent surface, the rates of sea-level rise and the rates of carbonate production. Based on the interacting influence of those factors, Hopley (1982) proposed an evolutionary model of Holocene shelf reefs, involving six stages ranging from the juvenile stage of which most parts of reefs are submerged, the mature stage when reefs reach sea level and the reef flat develops, to the senile stage when lagoons are infilled completely and planar reefs develop.

The time at which island deposition commenced is governed primarily by the duration of time needed to form platforms suitable for waves able to transport available sediments to converge at focusing points on reefs. Depth of an antecedent substrate and size of a reef platform are the factors that determine how long it takes for a suitable

7

platform to be built (Gourlay, 1990). The oldest cays, therefore, are most likely to be formed on smaller Holocene reefs that grow over a shallower substrate, requiring less time for reefs to reach sea level and for infilling the lagoonal area to form platform reefs. On the northern Great Barrier Reef, reefs reached the present sea level by about 6,000 years BP (Stoddart et al., 1978b). Gourlay (1990) suggested that it might take further approximately 2,000 years for the subsequent filling of the lagoonal area and the oldest cays on the Great Barrier Reef region appear to have begun to form on reefs about 4,000 years ago.

Sediments and Their Movement on Reefs

The sediments contributing to a sand cay are almost exclusively produced on the surrounding reef. They are mostly carbonate composed primarily of aragonite and calcite, and are derived mainly from skeletal fragments of coral, mollusc or *Halimeda,* which are aragonite, or foraminifera and coralline algae, which are generally calcite (Scoffin, 1987). A minor proportion of non-skeletal carbonate grains is generally derived from ooids, pellets, aggregates and cryptocrystalline particles. Some noncarbonate sediments such as terrigenous sediments and pumice fragments can be present on reefs and islands located close to the mainland or active volcanoes (Tomascik et al., 1997).

Skeletal sediments derived from reef organisms are produced either after death of the organisms, through subsequent physical and biochemical breakdown, or through the destructive processes, particularly bioerosion, that break the skeletons of still-living reef organisms. These different processes of sediment production together with original morphology and internal architecture of sediment-producing organisms are major factors contributing to a wide range of shape and size of carbonate sediments (Scoffin,

8

1987). For example, branching coral physically breaks down to tabular and rod-like fragments of -6ϕ, and gritty fragments of 2ϕ, respectively, (Folk and Robles, 1964) while coral chips of 4 to 6ϕ are produced by sponges boring through massive corals (Scoffin, 1987). By physical breakdown, *Halimeda* disarticulates into whole thin plates of -2 to -3ϕ, and further disintegrates into segments of 0ϕ and subsequently dust of 10ϕ (Folk and Robles, 1964) while foraminiferan tests generally retain their shape but with smaller size due to the loss of complete layers of the structure (Scoffin, 1987). Mollusc shells are fragmented due to mechanical wearing of the organic binder into three particle sizes, namely layers (1-2ϕ), sublayers (5-8ϕ) and unit crystals (11-13ϕ) (Force, 1969). However, reef sediments are generally sand and gravel in size due to high wave energies on reefs (Milliman, 1974) and their sorting is often poor due to the mixture of source organisms (Woodroffe, 2002).

The relative concentration of sediment components on reefs is mainly determined by processes in relation to deposition, and the populations and productivities of the various reef organisms (Milliman, 1974; Kench and McLean, 1996). These factors normally vary regionally, causing sediment components to be distinct between regions (Orme, 1977). For example, as a generalisation, on Caribbean reefs which in general are inundated *Halimeda* is the most important component whereas foraminifera and coralline algae are plentiful on Indo-Pacific reefs which are normally exposed at low tides (Milliman, 1974). As island sediments are mainly derived from the surrounding reef flats, the abundance of sediment-contributing organisms on the reef flat surrounding a sand cay also influences the composition of the beach sediments (Milliman, 1974; McLean and Stoddart, 1978). This aspect of the sediments around Warraber Island has been studied by Hart (2003).

In spite of sediment availability, no sand cays can form if sediments are unable to be transported to where waves converge on reefs. Sediment transport on reefs is primarily determined by sediment properties (shape and density), bedform morphology and the characteristics of the driving hydrodynamic forces (Orme, 1977; Prager et al., 1996). As described above, carbonate sediments within a particular reef generally include a wide range of the combination of sizes, shapes and densities. Therefore, their hydraulic behaviours occur differently in response to the same flow conditions (Maiklem, 1968) and do not observe the modes of sediment transport, generally based on textural analysis developed for terrigenous sediments (Orme, 1977; Halley, 2000). Kench and McLean (1996; 1997) demonstrated that settling velocity is more appropriate than grain-size analysis to apply for studying hydrodynamic behaviour of bioclastic sediments which are usually heterogeneous in nature.

Hydrodynamic currents influencing sediment transport on reefs are generally driven by a complex interrelation between waves, wind and tides (Tartinville and Rancher, 2000; Hearn et al., 2001). In general, the ability of each current component to transport sediments depends on the magnitude of shear stresses applied to the sediments on the bed; therefore, waves dominate the sediment entrainment and bedform formation (Nielsen, 1992). Field studies have indicated that in general wave-induced currents during normal wave conditions are the main component, and are sufficient to entrain and transport the majority of sediments on reefs (Clack and Mountjoy, 1977; Roberts, 1980; Hopley, 1981; 1982; Kench, 1998; Yamano et al., 2000). Sediment transport studied by Hart (2003) on Warraber Reef also indicated the ability of waves to transport sediments under normal climate conditions. Under shoaling waves, the maximum sediment transport by waves occurs just seaward of breaking points (King, 1972). In

reef environments, this usually takes place at about the edge of the reef (Roberts et al., 1992) and subsequently on the reef flat at a cay beach (Hopley, 1982).

Sediments start to move as the threshold of sediment movement is exceeded by wave-induced water particle velocity at the seabed (Komar and Miller, 1973). Kench (1998) applied the concept of *currents of removal,* which winnow away fine-grained material which is readily suspended and leave behind lag deposits of coarser material, to estimate the potential of sediment mobility on the Cocos (Keeling) Islands based on empirically-derived relationships between threshold velocity and the settling velocity of bioclastic sediments. In this thesis, the ability of waves to initiate sediment movement is investigated based directly on wave characteristics measured in the field.

Convergence of Waves on Reefs

Sand cays appear to form at the focusing point where waves converge and sediments are deposited, and it has been suggested that patterns of wave convergence determine shape and orientation of sand cays (Flood, 1979; Hopley, 1982; Flood, 1986; Flood and Heatwole, 1986; Gourlay, 1988). Wave focusing on reef platforms is a result of the combined effects of diffraction, which allows some waves energy to reach the leeward side of the reef, and refraction, which allows waves around the reef rim to move onto the reef and meet at the focusing point.

In general, refraction occurs as waves move at an angle to bathymetric contours and, according to linear wave theory, the degree of refraction depends on wave period, the seaward angle between a wave crest and a contour, the seaward water depth and the shoreward water depth (CERC, 1984). In reef environments, therefore, factors including reef morphology, wave characteristics, tidal range and proximity to nearby

11

reefs are significant to wave refraction and in turn patterns of wave focusing on reef platforms (Stoddart and Steers, 1977; Hopley, 1982; Gourlay, 1988).

Based on a simple refraction model of waves propagating from deepwater to shallow water on a reef with a vertical reef front, Gourlay (1988) suggested that the size, shape and orientation of the reef relative to the dominant wave direction are crucial factors influencing cay formation. For reefs of size much larger than wavelength, focusing points may not be formed due to less energy reaching to the leeside of the reef platform, allowing sediments to be carried over the leeward side of the reef by tidal and wind-induced currents which have no focusing capacity (Gourlay, 1988).

Convergence of waves most likely occurs on circular-shaped and oval-shaped reefs while on ribbon and crescentic reefs a complete focusing point may not be established with the consequence that there are few islands on these reefs (Hopley, 1982). However, cays on circular-shaped reefs are unstable since the focusing point on the reef is readily shifted with changes in wave direction and wave period (Gourlay, 1988). Also, sharp-curved corners of a reef platform can create an abrupt shift in the focusing point with a small change in a wave direction which may explain why reef islands at the corners of atolls are generally wider than elsewhere on the rim (Richmond, 1992).

Shape and size of the focusing point may be changed as a result of changes in the direction and size of the dominant waves and, if a sand cay is already there, this will modify the patterns of sediment transport along the beaches of sand cays (Gourlay, 1990).

Stoddart and Steers (1977) suggested that cays would form further from the seaward edge of reefs in area of greater tidal range together with more exposed to wave action. Small tidal range was suggested as one of primary factors in formation of sand

12

cays in the Caribbean (Steers et al., 1940; Thorpe and Stoddart, 1962). On the Great

Barrier Reef the number of sand cays is relatively less where tidal range is greater than

3 m (Stoddart and Steers, 1977).

Conditions of wave convergence on reefs may also be affected by nearby reefs

interfering with waves fields reaching the reefs (Hopley, 1982; Gourlay, 1988). The

effect of mountains on locations of sand-cay formation on reefs was reported in the

Spermonde Archipelago, south of Celebes, East Indies, where coral cays, that would

normally form elsewhere on the west of the reef flat due to stronger winds associated

with the easterly monsoon, are situated on the east as a consequence of the high

mountains of South Celebes forming a shelter against the force of the east monsoon

(Umbgrove, 1947).

In addition to refraction occurring to incident waves moving onto the reef

platform, the patterns of wave propagation may be further modified on the reef flat due

to local irregularities of reef topography (Gourlay, 1988; Brander et al., 2004; Kench

and Brander, 2006). This affects the patterns of wave focusing and in turn the shape,

size and location of sand cays. The relatively large size of Raine Island, a sand cay on

the northern Great Barrier Reef, is considered to have developed as a result of a shallow

indentation on the leeside of the reef which promotes wave focusing where the island

forms and prevents sediments to be transported into deepwater leeward of the reef

(Gourlay, 1988).

Wave Characteristics on Reefs

Wind-generated waves are a primary hydrodynamic factor influencing the

formation and stability of sand cays (Flood, 1986; Gourlay, 1988) and, consequently,

examination of their characteristics is one of the objectives of this thesis. In contrast to

13

shoaling waves over a gradual sloping shoreface and the relative smoothness of natural beaches, wave characteristics in reef environments are profoundly influenced by abrupt changes in reef morphology and roughness of the reef surface (Hardy and Young, 1996).

Two distinct wave environments in reef regions are recognised (Gourlay, 1990): waves off reefs and waves on reefs. Waves off reefs can be dominated by *seas*, as inside the Great Barrier Reef (Wolanski, 1994), *swell*, such as in Hawaii (Lee and Black, 1978), or a combination of *both,* as occurs in the Caribbean Sea (Roberts et al., 1992) and along the outer Great Barrier Reef (Wolanski, 1994). Gourlay (1990) classified characteristics of waves on reefs, based on five different zones of reef platforms (Figure 1.2), including: i) outer reef slopes where waves are affected by propagation effects; ii) reef edges where wave breaking occurs; iii) reef rims where waves surge after breaking; iv) reef flats where waves reform; and v) beaches of either islands or mainland where reformed waves will break again.
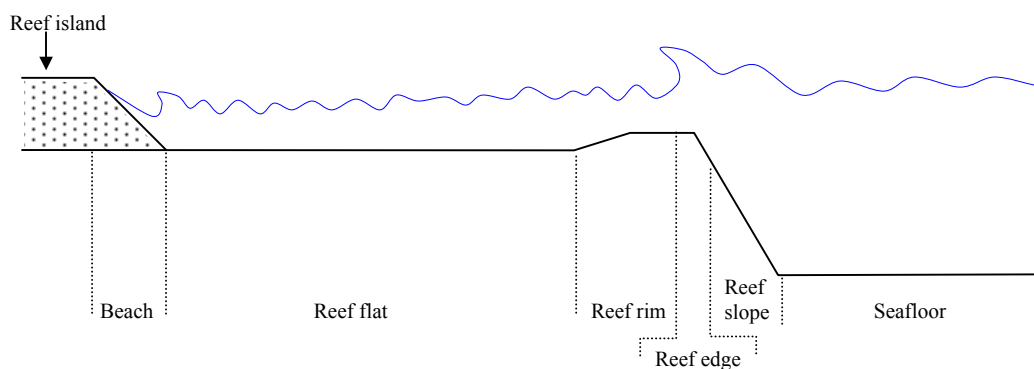
Figure 1.2. Schematic diagram of reef definition in relation to characteristics of waves on reefs.

Waves experience the effects of shoaling and refraction as they approach reefs where water depth becomes variable. However, on the near vertical slope of the reefs, effects of shoaling, refraction and wave scattering are suggested to be small, compared to those occurring on natural beaches (Gourlay, 1990). Wave reflection can be expected

14

to occur on the steep reef front, such as along the outer reef margin of the Great Barrier Reef. However, studies of wave transformation on Yonge Reef (Young, 1989) and John Brewer Reef (Hardy and Young, 1991) found that wave reflection is not significant.

The surf zone generally occurs at, or close to, the reef rim and can be divided into: i) an outer region where waves break; and ii) an inner region where a bore moves landward over the seaward-flowing undertow (Gourlay, 1994). Nelson and Lesleighter (1985) suggested surf zone widths to be proportional to a ratio of incident wave height to water depth on the reef flat *(H/h)*. Gourlay (1994) demonstrated from a laboratory study of regular-wave transformation on the fringing reef along Hayman Island that surf zone widths are between 2 and 3 wavelengths on the reef flat, whereas in field observations values between 2.6 and 5.2 times wavelength were estimated by Hardy and Young (1996).

Normally, waves are random, having a range of wave height and period. Therefore, wave breaking usually occurs over a defined width close to the reef edge (Gerritsen, 1980). Based on monochromatic laboratory results, the widths of the outer region of the surf zone, where breaking takes place, are about one reef-top wave length and that the *H/h* at the breaking point varied from 0.8 to 1.1 (Gourlay, 1994). Hardy and Young (1996) demonstrated from field observation that waves start to break as the ratio of significant wave height at the reef front to reef-flat water depth is greater than 0.5.

As waves break on the reef, energy near the peak frequencies is nonlinearly transferred to higher and lower frequencies. The generation of higher harmonics is generally observed when swell moves over reefs (Lee and Black, 1978; Wiegel, 1990). The transfer of energy to lower frequencies is normally evident in wave spectra from field measurements on reefs (Gerritsen, 1980; Roberts, 1989; Young, 1989; Hardy and

Young, 1996; Lugo-Fernandez et al., 1998b). This transfer of energy to lower frequencies produces the long-period oscillation of the water level or wave set-up fluctuation which promotes current circulation on the reef (Roberts, 1989; Gourlay, 1990; Symonds et al., 1995; Lugo-Fernandez et al., 1998b; Hearn, 1999; Gourlay and Colleter, 2005). Laboratory studies of regular waves moving onto a reef platform with a horizontal reef top and a steep reef front indicated that wave set-up increases with an increase in incident wave height and wave periods, and a decrease in water level on the reef top (Nelson and Lesleighter, 1985; Gourlay, 1996a). Gourlay (1996a) also demonstrated that wave set-up is greater on a confined reef top than on platform reefs with an open lagoon. Wave set-up was found not to occur when incident wave height is smaller than 0.4 times water level on the reef, also corresponding to a condition in which waves move over the reef without breaking (Gourlay, 1994).

Broken waves start to reform as oscillatory waves at the landward end of the surf zone. Reformed wave energy is principally related to breaker types of incident waves. Breaker type can be classified into spilling, plunging, collapsing and surging (Kamphuis, 2000). A plunging breaker dissipates more wave energy than a spilling breaker does and then less energy is left for reformed waves (Gourlay, 1994).

Reformed wave height on the reef flat is a function of water depth over the reef flat and incident wave height (Young, 1989). Hardy and Young (1996) defined the range when depth or incident waves are more dominant on the reef flat. When $H_i/h <$ 0.4, incident waves dominate and when $H_i/h > 0.8$, depth is dominant. In engineering practice, for flat areas within coastal zones over reef platforms, it has been common to apply a ratio of the wave height to water depth (H/h) of 0.78 to design wave heights for coastal works (CERC, 1984). This number was derived from solitary wave theory with an assumption that solitary waves break when the water particle velocity at the wave

crest equals the wave celerity. This number was also found from laboratory studies to be in better agreement with observations for oscillatory waves than solitary waves (CERC, 1984). Nelson (1994), on the other hand, found that the wave height to water depth ratio (H/h) never exceeded a value of 0.55 for shallow-water, oscillatory waves moving over a horizontal bed. The ratio becomes smaller for deeper water, according to his curve of H/h (Nelson, 1994). This value has been also found to be in agreement with field data (Gourlay, 1990; Hardy and Young, 1996; Nelson, 1997).

As reformed waves proceed on the reef, more energy is dissipated by bottom friction, resulting in a reduction in wave height. This may occur slowly over a smooth bottom of a sanded reef flat or significantly over a reef flat occupied by coral thicket (Hopley, 1982). Values of the bottom friction coefficient for a very rough reef surface and very shallow water may be up to one order of magnitude greater than that normally used for a sandy bottom (Hardy and Young, 1991; Lugo-Fernandez et al., 1998b). Gourlay (1990) suggests that for larger reefs, waves at the leeside of the reef or at the island beach on the reef tend to be smaller due to greater energy attenuation from bottom friction.

An understanding of the characteristic wave transformations, particularly across large reef platforms such as of Warraber Reef, and of waves around sand cays is necessary to explain the development and stability of sand cays. However, over recent decades, most of information on wave transformation in reef environments has been derived from field and laboratory studies, particularly on small reef-lagoon systems of fringing reefs, for example, of Hawaii (Lee and Black, 1978; Gerritsen, 1980; Storlazzi et al., 2004), Seychelles (Sheppard et al., 2005), Grand Cayman Island, central Caribbean (Roberts et al., 1975; Roberts, 1980; 1989), St. Croix, US Virgin Islands (Lugo-Fernandez et al., 1998a; Lugo-Fernandez et al., 1998b), Hayman Island,

Australia (Gourlay, 1994), and Japanese mainland and islands (Nakaza et al., 1990; Tsukayama and Nakaza, 2000).

Fewer studies have examined wave transformation on reef platforms (Young, 1989; Gourlay, 1996b; Gourlay, 1996a; Hardy and Young, 1996; Brander et al., 2004; Kench and Brander, 2006; Kench et al., 2006). These studies have been further extended by mathematical models (Gerritsen, 1980; Young, 1989; Hardy and Young, 1991; CERC, 1993; Massel and Gourlay, 2000). However, most of those studies on reef platforms only focused on wave transformation over short distances over the reef rim. Exceptions are the studies by Brander et al. (2004), and Kench and Brander (2006).

Brander et al. (2004) examined wave transformation across the Warraber reef platform, described later in Section 1.5. Kench and Brander (2006) subsequently examined characteristics of wave behaviour on different reef flat environments, based on wave data on reef flats of Warraber Island, the Cocos (Keeling) Islands and a shingle cay on Lady Elliot Island. The present study builds on the observations by Brander et al. (2004) in order to gain a clearer idea of wave characteristics on a reef platform, particularly around a sand cay, which has been scarce.

1.3.2. Morphology of Sand Cays

Sand cays are the simplest of the reef-island types. Even so there is a range of morphologies that can occur. The most consistent morphological feature of sand cays, as well as of most other types of reef islands, is their low elevation with relative flat upper surface and steep beaches.

Their elevation is principally determined by wave run-up (Stoddart, 1964; McLean et al., 1978; Hopley, 1992) and is usually not more than approximately 1 m above high spring tide (Steers, 1929; Stoddart and Steers, 1977). On a number of sand cays on the northern Great Barrier Reef, two terraces have been identified of which the younger lower terrace occurs at about 3.4-4.4 m above MLLS, and fronts an older central higher terrace at about 4.3-5.5 m above MLLS (Stoddart et al., 1978a). Such terraces, with comparable levels and similar vertical separation, have also been recognised on sand cays on low wooded islands on the northern Great Barrier Reef (Stoddart et al., 1978a). McLean et al. (1978) suggested that such terraces occur as a result of different magnitude of wave action influenced by different levels of the sea over the late Holocene. However, Stoddart (1964) has described a similar high-elevation terrace on sand cays in the Caribbean, which have not experienced a high-stand of sea level during the late Holocene, and attributed these to a combined function between sediments generated during storm and natural vegetation trapping those sediments.

Beach ridges are also common part of sand-cay topography (Steers, 1937; Stoddart, 1964; Folk, 1967; Richmond, 1992; Woodroffe, 1992) but mechanisms associated with their forms have not been described. They are normally prominent along windward sides. Their alignment, generally following the shape of the sand cay, reflects the growth history of the sand cay (Richmond, 1992).

There is a wide variety of shapes that sand cays can adopt, ranging from elongate, to oval and equidimensional (Hopley, 1982). Sand spits are also normally found as part of sand-cay shape at one or other end of sand cays. They generally have a triangular shape with their base attached to the cays. They are the most mobile areas and are often observed to shift seasonally in response to the reversal of local wind patterns (Hopley,

1982; Woodroffe, 1992). The orientation of the long axis of sand cays surveyed along the Queensland coast, Australia, was found to be about 45° to the prevalent wind direction (Steers, 1929; Fairbridge and Teichert, 1948), similar to that found for sand cays on Alacrán Reef in the Caribbean (Folk, 1967). A more extensive survey of the northern Great Barrier Reef in 1973 however indicated the more variable orientation than that previously suggested (Stoddart et al., 1978a). Shape and orientation of sand cays are primarily determined by the patterns of focusing waves (Flood and Heatwole, 1986).

The size of sand cays covers a wide range; for example, Indonesian cays range from less than 0.5 ha to over 15 km^2 (Tomascik et al., 1997) and those in the Great Barrier Reef from less than 1 ha to over 1 km^2 (Hopley, 1982). Larger sand cays are more stable than smaller ones (Hopley, 1990). Size of sand cays however appears unrelated to size of reefs. Tomascik et al. (1997) suggested that size and shape of sand cays show some relationships to the elevation of cays above sea level, larger cays having the higher elevation and oval-shaped cays having their central portion elevated slightly above the surrounding area.

Vegetation is a prominent component of sand cays of this type, which ranges from herbs and grasses to a tall broadleaf woodland. Types and distribution of vegetation are related to morphological development of sand cays, spatial variation in environments and disturbance by human or animals either indigenous or introduced by human (Stoddart et al., 1978a). Generally, large or more stable part of sand cays has a dense broadleaf forest, whereas smaller or less stable portions of sand cays are occupied by herbs, grasses and low scrub. The initiation of vegetation on sand cays is probably brought about by drift seeds and birds are particularly important in the dispersal of seeds of plants (Hopley, 1982).

When it has become established, vegetation helps to stabilise sand cays by binding loose sediments with roots, and to increase size and elevation of sand cays through trapping sediments carried either by wind or waves (Steers, 1929). The stability provided by vegetation may also enable beachrock to form, further increasing the stability (Hopley, 1982). Beachrock is normally found in an intertidal zone, and represents seaward-dipping strata of sand along the beach face, formed as a result of cementation of sand. It can form within less than a year to over periods of several years (Hopley, 1982). Exposure of lines of beachrock indicates beach retreat with outcrops representing former beach positions prior to the erosion occurring (Stoddart and Steers, 1977).

1.3.3. Morphological Changes of Sand Cays

Ephemeral sand banks may be formed on platform reefs as a result of sediment supply and its entrainment and transport by wave action. Subsequently, over sufficient periods of steady and suitable conditions, sand cays can become stable enough to allow vegetation to permanently develop on them, further increasing their resilience as vegetation sand cays. However, sand-cay morphology will have varied as a result of changes in sediment supply, changes in wave action or some combination of these, in response to changing environments as it evolves.

Changes in morphology of sand cays and their evolution occur at various time scales. Our knowledge of the Holocene evolution of reefs and reef islands suggests a depositional history over millennia. On the other hand, erosion may be instantaneous, or occur in a short period during an erosional event. It has been found useful to consider coastal landforms at several different scales: i) instantaneous; ii) event; iii)

engineering; and iv) geological (Cowell and Thom, 1994). In this study morphological changes of sand cays over geological and engineering time scales are examined and compared with instantaneous field-based measurements of wave and wind characteristics.

Sand-Cay Evolution over a Geological Time Scale (Millennia)

In considering reef-island evolution over a Holocene timescale of thousands of years only gross morphological changes of reef islands can be determined. As much of the material which comprises reef islands is amenable to radiometric dating, reef-island evolution is usually demonstrated along transects across the islands, based largely on dates of sediment samples at major topographic features along those transects. Over the past decades, however, there have been relatively few attempts to develop a chronology of reef-island deposition (Stoddart, 1969; Guilcher, 1988; Roy and Connell, 1991; McLean and Woodroffe, 1994).

In the case of sand cays, early attempts on the Great Barrier Reef suggested two phases of sand-cay evolution (McLean et al., 1978). A high terrace, which is the major part of sand cays, formed around 3,500 years BP and a low terrace around 2,700 years BP. They also suggested that the occurrence of such high and low terraces can be attributed to wave action during higher and lower sea level, respectively, over the late Holocene.

Woodroffe (1992) examined the evolution of sand cays on atoll rims in the Maldives. They are presently characterised by a relative flat surface of main, central part and a gradual decrease in elevation towards lagoonal and seaward sides with high ridges presented on the seaward sides. He suggested that the sand cays have developed in the last 3,000 years after reefs probably have reached slightly higher level of the sea.

22

However, patterns of the sand-cay evolution were not shown due to insufficient dates (Woodroffe, 1992). On the other hand, Kench et al. (2005) indicated that reef islands in the Maldives formed from a central node, mainly vertically 1,000-1,500 years earlier than those in the Pacific Ocean and appear to have attained present morphology since approximately 4,000 years ago.

Woodroffe et al. (1999) proposed several different models of reef-island evolution over the past 3,000 years. Figure 1.3 shows several different models of the evolution of a typical sandy reef island on an atoll rim comprising an oceanward ridge, a lagoonward ridge of lower elevation and a central depression. The models are shown in terms of isochrons of sediment deposition, schematically represented by the 3,000-, 2,000- and 1,000 year isochron. They describe island development in relation to sediment supplied to the reef islands from either oceanward or lagoonward, or both sides. The islands are viewed as growing out from the central core, or accreting mainly on the oceanward side,

Figure 1.3. Models of reef-island evolution (isochrons in ka) (after Woodroffe et al. (1999)).

23

the lagoonward side, or growing by vertical accretion. Rollover and overwash as well as longshore transport are also recognised as processes that may operate to generate different patterns of island evolution.

The models additionally suggest that island evolution can be in a single episode or through erosional processes, resulting in smaller islands than in the past. Patterns of evolution shown in Figure 1.3 can also be regular, episodic, accelerating or decelerating. Woodroffe (2000) noted that different reef islands might have evolved through more than one of these processes.

The models provide a fundamental framework for considering how reef islands may have evolved. However, few studies have extended this work to examine the chronology of reef-island deposition, or how it might vary in different reef settings. Radiocarbon dating of foraminiferal sands on Makin in Kirabati indicates gradual oceanward progradation of that sand cay (Woodroffe and Morrison, 2001). Kench et al. (2005) presented a revised model of reef-island evolution on an atoll in the Maldives, described above, based on intensive topographic and subsurface studies including stratigraphic and ground-penetrating radar surveys, and bulk radiocarbon dating results.

Difficulties have arisen in determining patterns of reef-island evolution from radiocarbon dating of carbonate sediment samples due to the fact that a radiocarbon age yields an estimate of the time of death of skeletal organisms, whereas deposition may occur some time later after an undefined period of transport, breakdown, erosion and redeposition (Woodroffe, 2000). Depositional history appears to be easier to reconstruct for rubble or shingle cays where episodic extreme events dominate sediment transport. Subject to storms in this setting, the time interval between death and deposition of coarse boulders and rubble is reasonably short due to rapid transport principally driven by extreme events. Examples include the rubble ridges on Lady Eliot

Island (Chivas et al., 1986) and Curacao Spit (Hayne and Chappell, 2001) on the Great Barrier Reef, and rubble ridges on islands on Funafuti atoll, Tuvalu which were impacted by Hurricane Bebe (Maragos et al., 1973; Baines and McLean, 1976).

In contrast, in reef environments where sand cays form, the sand may have gone through a history of re-entrainment and redeposition prior to being deposited on the islands (Woodroffe, 1992). McLean et al. (1978) also pointed out that the lack of modern ages for sand cays on the northern Great Barrier Reef probably results from dating on bulk samples, giving the average age of all components of which many may be derived from reworking of the older sediments. Therefore, reconstruction of sand-cay deposition based on such sediment samples can give rise to periods of sand-cay evolution earlier than anticipated. This point will be identified in the present study, in conjunction with reconstruction of morphological evolution of Warraber Island.

Changes of Sand-Cay Morphology over an Engineering Time Scale (century and decade)

Over an engineering time scale, morphological changes to sand cays are recognised in more detail, mainly involving adjustments to their shape and size in conjunction with the exposure of beachrock and conglomerate, and the formation and migration of sand spits (Flood, 1977; Stoddart et al., 1978a; Hopley, 1982; Flood, 1983; 1986; Flood and Heatwole, 1986; Frank and Jell, 2006). For example, morphological comparisons made on three sand cays on the northern Great Barrier Reef between 1929-1938 and 1973 revealed that Combe and Michaelmas have decreased in size, from 4.93 to 4.57 ha and from 3.13 to 2.90 ha, respectively, with a corresponding increase in area of exposed beachrock, whereas Stapleton has increased in size from 3.96 to 4.67 ha (Stoddart et al., 1978a). Similar results of comparisons over the same period were also

reported for sand cays of the Capricorn and Bunker Groups, including one sand cay without change, three sand cays increasing in size, two sand cays decreasing in size and one sand cay migrating to the northwest (Flood, 1977). Frank and Jell (2006) reported that between 1928 and 2001 a sand cay on Low Isles Reef has migrated eastward and has decreased in size by approximately 20%.

Such changes are principally attributed to changes in wave conditions inducing a shift in focusing points and different conditions of sediment movement (Flood and Heatwole, 1986). Information on waves, the primary hydrodynamic influence on the formation and stability of sand cays, is needed over several decades in order to investigate changes in sand-cay morphology. However, few if any studies are backed by this detailed wave information. In areas where sea (wind-generated waves that are still in area of generation) is dominant, it is common practice to examine morphological changes or physical processes operating on reefs and sand cays based, instead of wave information, on wind data which are normally available at meteorological stations over a longer period of time (Stoddart and Steers, 1977; Hopley, 1981; Wolanski, 1986).

Investigations of morphological changes of sand cays based mainly on wind conditions has been widely described; for example, in the Laccadive-Maldive group (Sewell, 1932), on Ata atoll in the Maldives (Ali, 1997), off the coast of British Honduras, now called Belize (Thorpe and Stoddart, 1962), on Alacrán Reef, Mexico (Folk, 1967), in Jamaican waters (Steers and Lofthouse, 1940), on Indonesian reef islands (Umbgrove, 1947), on a low wooded island in the Great Barrier Reef (Fairbridge and Teichert, 1948), in the northern Great Barrier Reef (Stoddart et al., 1978a) and at the southern end of the Great Barrier Reef (Flood, 1977; Flood, 1983). Flood (1986) suggested that sand cays experience wind fluctuations at three time scales, namely

annual cycles of seasonal fluctuations, the occasional cyclones and a long-term shift of wind patterns.

Fairbridge and Teichert (1948) noted the seasonal change in shape of a sand cay on a low wooded island on the Great Barrier Reef, in association with seasonal movement of curving sand spits at the eastern and western ends of the sand cay. Off the coast of Belize the northeast trade winds which are dominant promote sand-cay stability by building up spits whereas north winds occurring seasonally during winter cause sand cays to erode (Thorpe and Stoddart, 1962). Ali (1997) examined the seasonal changes in morphology of uninhabited sand cays on Ata atoll in the Maldives, which are situated in the monsoon zone. He indicated different patterns of changes in island shape, primarily as a result of the degree of exposure, influence of adjacent reef area, and island and reef orientation.

Bayliss-Smith (1988) demonstrated that in general storms favour shingle-cay (motu) accretion but are destructive to sand cays. McLean and Woodroffe (1994) developed these ideas into a model to explain differences in atoll reef-island morphology in terms of frequency of storm occurrence. However, Flood (1986) suggested that storms could be either constructive or destructive to sand cays, depending on the path and intensity of the cyclones, and the state of the tides. For example, Heron Island, a sand cay on the southern Great Barrier Reef, was accreted after tropical cyclone "Simon" in 1980 whereas the island was eroded in 1976 when the island was hit by tropical cyclone "David" (Flood, 1981). Flood (1981) pointed out that low tides favour accretion and high tides allow larger waves to erode the island. Stoddart (1964) noted severe erosion occurring on sand cays located on the right of a storm track during hurricane "Hattie". The magnitude of change on sand cays due to storms also depends on stabilising factors; for example, the islands with larger areas

27

covered by vegetation tend to undergo less erosion. In the Caribbean, Stoddart (1964) indicated that sand cays with natural vegetation are higher after storms due to trapping of sediments generated during storms by natural vegetation.

Flood (1983, 1986) documented changes in the shape of sand cays within the Capricorn Group on the southern Great Barrier Reef between 1969 and 1982. He noted evident sand-spit reorientation on the leeward ends of the sand cays and suggested that such changes were attributed to a shift of approximately 45° in long-term wind direction, analysed from 1962-1980 wind data recorded at Heron Island. Flood (1988) found correlations between changes in wind direction recorded at Heron Island between 1962 and 1980, and sunspot cycles and times of El Niño-Southern Oscillations (ENSO), but he found that the relationships were not strong. The relationships between long-term wind patterns and environmental factors, and the influence of long-term wind patterns on the island morphology are examined in the present study.

In addition to the effect of changing wave conditions, sand-cay stability can also be impacted by interference from local ecology and human activities. For example, a study of the morphological changes on Green Island, a sand cay on the Great Barrier Reef, between 1936 and 1978 revealed that erosion that has occurred on the island is mainly attributed to a dense cover of sea grass trapping and binding sediments normally interchanged between the island and the adjacent reef flat (Hopley, 1982). On Heron Island, a sand cay on the southern Great Barrier Reef, it was found that a boat channel constructed in 1945 has induced most of the erosion occurring since around 1960 on the western spit (Hopley, 1982). In general, it interferes with the interchange of sediments between the reef flat and the island, allowing sediments to leave the reef top through the channel under an influence of tidal currents. The construction built to protect the shore

from erosion has also subsequently activated shoreline erosion in their vicinity (Flood, 1986).

1.4   Digital Terrain Model (DTM), and Coastal and Reefal Studies

As described above, changes in island morphology are normally determined from 2-D topography in conjunction with dating results for changes over a geological time scale, and island shape and size, derived from field surveys and aerial photographs, for changes over an engineering time scale. In order to extend a dimension of understanding of morphological changes of sand cays, digital terrain models (DTM) can be applied to reconstruct the topography of island surface and consequently associated sediment volume can be estimated.

A DTM is normally modelled by regular grids, called a digital elevation model (DEM) or an irregular network of points, called a triangular irregular network (TIN). A DEM is generated by interpolating input data whereas a TIN is derived by structuring input data (Raper, 1999). DEMs are the most available form because of the ease of computer implementation, compatibility with other geographical data and low cost. They cannot, however, represent discontinuities such as ridges and peaks well (Zeiler, 1999). TINs have several advantages in surface generation, especially for areas having abrupt changes like reefs and reef islands which can be modelled more accurately using more points or some data as edges in TINs to capture abrupt changes in topography (Burrough and McDonnell, 1998). Incorporation of the original data in surface structure as nodes or edges preserves all of the precision of input data (Bratt and Booth, 2002). Therefore, TINs are applied in the thesis to model the topography of the reef and island.

DTMs are increasingly used for the assessment of temporal changes in coastal landform morphologies, representing surfaces in 2.5-dimension or ever 3-dimension (Raper, 1999). A sequence of DTMs is useful to create a time series for animations so as to understand landform behaviour (Dixon et al., 1998; Raper, 2000; Andrews et al., 2002). Also, associated volumetric changes can be estimated from a 3-dimensional model of the surface, and this approach is adopted in the thesis. For example, DTMs have been constructed in order to examine dune morphodynamics of the Outer Banks of North Carolina, USA (Andrews et al., 2002) and in northeast Tasmania, Australia (Mowling and Coleman, 2003), longer term geomorphological change and tidal-related processes in the Humber Estuary, England (Hardisty et al., 1998), and the impact of colliery spoil on the beaches in northeast England (Humphries and Ligdas, 1997).

In reef environments, DTMs have been applied generally to construct reef morphology, for example, of the Great Barrier Reef, called GBRDEM (Lewis, 2001) and submerged, living patch coral reefs in the Gulf of Carpentaria (Harris et al., 2004). DTMs were also applied to examine changes in the location and shape of sandwaves on the seabed in Torres Strait (AUSGEOnews, 2004). However, a DTM has rarely been applied in examining reef-island morphology.

1.5 Previous Research on Warraber Reef

Warraber Island is a vegetated sand cay located on Warraber Reef, a platform reef in Torres Strait (Figure 1.4). It has been visited by a number of groups of researchers to investigate aspects of evolution of its reef platform, its morphological development and reef-top processes that occur there. Results from these investigations that are pertinent to the present study are described in this section.

Figure 1.4. Locations of: a) Torres Strait; b) Warraber Reef in Torres Strait; and c) Warraber Island on the leeward end of Warraber reef platform.

The evolution of Warraber Reef was investigated by Woodroffe et al. (2000), based mainly on the stratigraphy and radiocarbon dating of cores taken across the reef flat. Large heads of the massive microatolls *Goniastrea* and *Porites* occur on the flat area at an elevation considerably above that to which corals are now able to grow. Radiocarbon dates on the microatolls on the elevated reef flat indicated that this part of the reef platform reached sea level approximately 5,300 years BP when the sea was around 0.8-1.0 m higher than present (Woodroffe et al., 2000). This is also supported by dates on coral at a level commensurate with the reef flat within cores through the island, taken in 1990 as part of the Water Resource Study. The reef crest and the reef flat on the northwestern corner of the reef platform were found to be much younger than the elevated reef flat and radiocarbon ages imply this area is younger. The dating

31

results indicated that the surface morphology of the Warraber-Reef platform is entirely Holocene and that the reef grew over an antecedent Pleistocene surface which was encountered at a depth of approximately 6.0 m in a core near the island (Figure 1.5).

Figure 1.5. Schematic cross-section of Warraber Reef with tentative isochrons, in thousands of years (based on Woodroffe et al. (2000)).

The dates on the microatolls on the emergent reef flat implied that this central portion of the platform started to form first by 5,000 years BP as sea was falling to the present level and lateral reef growth was dominant thereafter (Figure 1.5) (Woodroffe et al., 2000). The evidence suggested that the reef has grown with rapid vertical accretion of 5-11 mm/y along the southern rim of the reef while rapid rates of 5-8 mm/y occurred along the northern rim.

The evolution of Warraber Island was initially investigated by Rasmussen and Hopley (1996), suggesting five major stages of island development based on the maturity of soil and vegetation, and concentric beach ridges that could be differentiated from aerial photographs (Figure 1.6). They inferred that island progradation started at the oldest northwestern corner, building towards the southeast in stages 2 and 3, accreting to the east in stage 4 and to eastsoutheast in stage 5 with the most recent development of sand spits at both ends of the island (Rasmussen and Hopley, 1996).

Figure 1.6. Historical changes to Warraber Island (after Rasmussen and Hopley (1994))

A preliminary chronology of island development was subsequently reported by Woodroffe (2000) based on radiocarbon dating of bulk sand samples taken from backhoe pits across the island. The radiocarbon dating results indicated an episode of formation between around 4,000 and 2,000 years ago, followed by steady state thereafter. These two preliminary studies suggest that Warraber Island is a simple sand cay that has undergone a history of accretion that would be suitable for further study in this project.

Rasmussen and Hopley (1996) also observed changes in island shoreline over a period of 1966-1987 based on a comparison of a series of aerial photographs and found that Warraber Island has undergone a period of reorientation in a clockwise direction. They analysed wind data between 1951 and 1992, recorded at Thursday Island, and suggested that the reorientation of the island is caused by a shift of winter wind patterns to a more southerly direction. However, they commented that it is uncertain as to how

long this present trend may last due to limited wind records. The present study therefore extends this work to examine more recent data.

The relationships between the morphologic, hydrodynamic, ecological and sedimentological characteristics of the Warraber reef platform have been studied as the focus of a complementary PhD project by Hart (2003). Based on the six surveyed transects across the Warraber reef platform (Figure 1.7), Hart divided the reef flat into two main reef areas, comprising the raised, sandy reef flat on the east of the island and the deeper area on the west of the island.
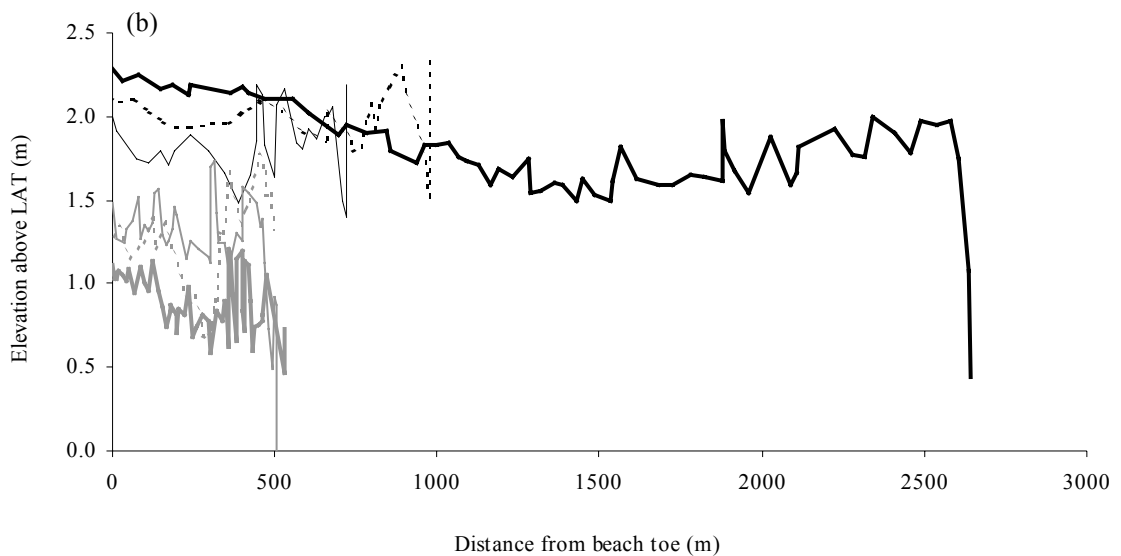
Figure 1.7 Six surveyed transects starting from the beach toe across the Warraber reef flat (after Hart (2003)): a) locations of transects; and b) topography along transects (RT1━━, RT2 -----, RT3 ——, RT4 ----, RT5 —— and RT6━━).

Hart classified nine ecological zones, four on the eastern reef flat and five on the western reef flat, based on variation in four commonest cover types, coralline and brown algae, coral and bare substrate, and in the presence of less common organisms (Figure 1.8). Generally live molluscs dominate zone 1, patches of coralline and brown algae dominate zone 2, coral prolifically grows in deeper areas especially along the reef rim (zones 3, 6, 8 and 9) and foraminifera abundantly live on the raised reef rims (zones 4 and 7). Zone 5 is characterised by reef rock overlain with a layer of muddy sand and is mainly bare of organisms.

Figure 1.8. Ecological zones on the Warraber reef flat: 1) sandy reef flat with molluscs; 2) sandy reef flat with algae; 3) sandy reef flat with coral; 4) E raised algal rim; 5) fine sand reef flat; 6) mixed coral; 7) W raised algal rim; 8) dense branching coral; and 9) dense mixed coral, and sediment composition for samples from the reef flat (larger circles), and island and beach (smaller circles): data represent a synthesis of more than 200 samples by Hart (2003).

Hart indicated that the cover and distribution of live organisms have more influence on sediment compositions on the reef flat than the contribution of carbonate production by each parent organism across the reef flat. Overall, sediments on the reef flat were found to be dominated by mollusc (35%) and coralline algae (26%), with a subordination of coral (13%) (Figure 1.8). Mollusc shells were also found to be the most common constituent of the island beach (average 55%) with coralline algae as the

second most common component (average 16%) (Figure 1.8). Mollusc shells were mostly composed of gastropod (80-87%). Preliminary composition analysis of sediment samples (Figure 1.9) collected from pits along the runway across the island by Hart (2004, per. comm.) also indicates that overall, molluscs and coralline algae have been the major components of the samples, in average accounting for approximately 35 and 34% of total sediment, respectively, over the evolution of the island.
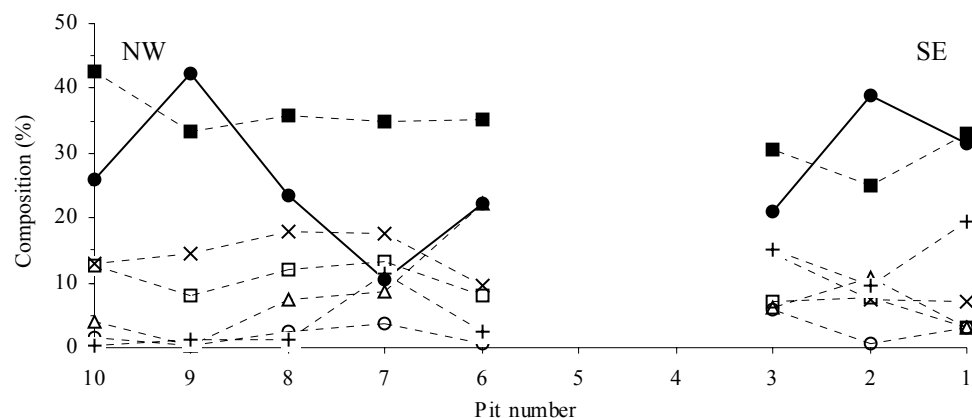
Figure 1.9. Composition (%) of island sediments collected at the base of pits across the island (gastropod —●—, coralline algae ---■---, coral ---x---, *Halimeda* ---□---, other molluscs ---Δ---, foraminifera ---o--- and other components ---+---). There are no data from pit number 4 and 5 due to being cemented material.

Sediment textural analysis indicated that modal settling speeds of the reef-flat and island-beach sediments ranged from −1.5 to −4.5 Psi and −1 to −4.75 Psi, respectively, with the dominant mode in both beach and reef-flat samples of −3.25 Psi (Hart, 2003). Two main groups of settling speeds for the five commonest individual constituents were recognised, the group of mollusc shells, coral and coralline algae fragments, which has faster modal settling speeds ranging between −4 to −4.75 Psi, and the group of foraminifera and *Halimeda*, which has slower modal settling speeds ranging between −3.24 to −3.47 Psi (Hart, 2003). Fine sediment (<4 ϕ) was mostly found on the west of the reef flat and was maximum in the boat channel.

36

Hart undertook current and sediment measurements for 2 periods, during the SE winds (July-August 2001) and the NW winds (February-March 2002). Based on observations of current patterns on the reef flat around the island, Hart found that during the SE winds the mean current directions were found to correspond roughly to the prevailing wind directions whereas during the NW winds the mean current directions were variable due to low speeds or frequently absent in speed of the NW winds. In general mean current speeds were higher (9.5-21.1 cm/s) during the SE winds than those (3.6-16.4 cm/s) during the NW winds and faster currents occurred at windward and shallower areas (Hart, 2003).

Measurement of sediment transport around the island periphery and on the inner (zone 1 in Figure 1.8) and central eastern reef flat (zone 2 in Figure 1.8) showed that the rates of sediment movement were greater (1-67 g/hr) during the SE winds than those (0-15 g/hr) during the NW winds. Overall, the greatest rates of sediment transport were found to occur adjacent to the northeastern and southwestern ends of the island, and on the inner eastern reef flat (zone 1 in Figure 1.8).

Hart concluded that that most of reef flat and island beach sediments (>-5.25 Psi) were potentially transported under normal (non-storm) hydrodynamic conditions, that overall the reef platform is a relatively closed system in terms of sediment transport with the dominant directions of sediment transport across the reef platform towards the island, and that there is the exchange of sediments between the island beach and the adjacent reef flat; the island beach sediment is mainly supplied by the adjacent reef flat (zone 1), of which coarser constituents are selectively retained on the beach, whereas fine materials may be transported back to the reef flat nearby. Hart's study provides important background on and characteristics of sediment transport across the reef

platform, and forms a foundation on which the present study expands, by examining the island and its evolution in more detail.

Spatial and temporal variations in wave characteristics and energy across the Warraber reef platform were investigated by Brander et al. (2004). In their study, waves were measured at six different locations along a transect RT1 (Figure 1.7a), from the base of the island southeast to the reef rim. Wave parameters were estimated and wave energy was calculated for 5 bands of wave components including: i) incident short period waves (0-3 s); ii) incident wind waves (3-8 s); iii) incident swell waves (8-20 s); iv) infragravity waves (20-100 s); and v) far-infragravity waves (>100 s).

They indicated that wave energy across the reef flat is dominated by incident wind wave frequencies which are strongly correlated to water depth. Incident short-period waves were found to be dominant during low water level and their energy tends to increase shorewards. They indicated that the wave environment off Warraber Reef was dominated by swell with periods of 8-10 s and wave height between 1.4 and 1.8 m during the experiment. However, because significant attenuation of swell wave energy occurs between the reef rim and the outer reef flat, swell wave energy is minimal in the energy spectra at all locations at high tide (Brander et al., 2004).

According to significant wave height to water depth ratio, they suggested that during the experiment waves were not saturated and also that the potential for sediment entrainment on the reef platform are only active during periods of higher water or extreme events. This low energy on the reef platform is related to the large reef width, rapid attenuation of energy on the outer reef, and marked topographic variations across the reef (Brander et al., 2004). These relationships are examined further in this study.

1.6   Objectives and Thesis Outline

This study aims to examine: i) the evolution of sand-cay morphology over past millennia (geological time scale); ii) changes in island shore over past decades (engineering time scale); and ii) contemporary characteristics of waves on a reef platform. The study builds upon previous studies of Warraber and is based upon: i) detailed radiocarbon dating; ii) 3-D morphological reconstruction using DTM; and iii) field measurement of island topography, waves and wind.

In order to understand reef-island morphological development in general, it is better to start from a simple situation, both landform and process. Warraber Island has been chosen for this study because it is a simple reef-island system, comprising a small sand cay sitting on a relatively flat reef platform, located outside the storm-belt zone and having a minimal influence from the mainland in terms of sedimentology. In addition, some preliminary studies, described above, have examined reef history, ecology, sediments and wave characteristics, which are all related to the island morphology.

In Chapter 2, the present morphology and morphological evolution of Warraber Island over past millennia (geological time scale) are investigated. Spatial and temporal patterns of morphological evolution are determined, past island morphologies and geometries are reconstructed, and associated volumes are calculated. These evolutionary patterns are temporally examined through bulk samples and component-specific AMS dates to determine the depositional history of Warraber Island. At a broader scale, the morphology of Warraber Reef and Torres Strait is outlined in relation to morphological development of Warraber Island.

In Chapter 3, changes in island shape with associated sediment volume over past decades (engineering time scale) are examined. The changing patterns of island shape are identified, shore topography of the island where significant changes have occurred is reconstructed and associated sediment volumes are calculated. In Chapter 4, wind data are analysed in order to construct the wind climate and medium-term wind patterns for the region, which are applied to assess the wave climate in the region in Chapter 5 and possible causes of changes in island shape identified in Chapter 3. The relationships between medium-term wind characteristics and environmental factors including ENSO and solar activity are also investigated.

In Chapter 5, temporal and spatial variations of wave spectra, spectrally derived wave characteristics and energy, as well as wave-saturating conditions, on the reef platform are examined. Significant spectral components and their origins are identified. Dominant wave environments in the region are deduced from wave information on the reef and wave climate in the region is assessed in relation to local wind climate developed in Chapter 4. The ability of waves to initiate sediment movement is also investigated.

In Chapter 6, probable wave conditions in relation to the morphological evolution of Warraber Island over past millennia are discussed in conjunction with results of wave analysis in Chapter 5. Seasonal change and probable causes of decadal changes in island shoreline over the past 40 years identified in Chapter 3 are also discussed, based mainly on results of wind analysis in Chapter 4, wave conditions on the reef, examined in Chapter 5, and the effect of nearby reefs on wave fields propagating towards the island. The implication of island change over these two time scales for probable future conditions of Warraber Island is also considered. In this chapter, considerations in

selecting and applying wave models to examine patterns of wave focusing on platform

reefs are given. In Chapter 7, the principal findings in this study are summarised.

CHAPTER 2

MORPHOLOGICAL EVOLUTION OF WARRABER ISLAND

OVER PAST MILLENNIA (GEOLOGICAL TIME SCALE)

2.1. Introduction

This chapter focuses on the morphology of Warraber Island and its evolution over past millennia (geological time scale). As described in Chapter 1, physical setting of the region and morphology of the reef on which the island is built are important factors influencing sedimentation and hydrodynamic processes around the island. Therefore, this chapter begins with (Section 2.2) the general setting of Torres Strait in which Warraber Reef is located, using a simple DTM constructed at a coarse resolution constrained by availability of data at suitable scales. The morphology of Warraber Reef is also important and is outlined, based on the results of previous studies, and a DTM of the present topography of the reef is generated from a range of data. The reef-top surface is reconstructed in some detail, as a basement for calculating the island volume to determine the depositional history of Warraber Island.

Section 2.3 focuses on the present morphology of Warraber Island, including construction of a DTM of the present island topography and the general description of island morphology. In Section 2.4, the depositional history of Warraber Island over past millennia is investigated. It involves determination of spatial and temporal patterns of island evolution, reconstruction of morphological evolution of the island and calculation of rates of progradation and associated volumetric changes.

In this study, all morphological analyses and reconstructions were carried out in ArcGIS 8.3 (ESRI, 2002). The projected coordinate system used for this study is the

Map Grid of Australia 1994 (MGA94, zone 54). MGA94 is a UTM map projection of the geographic coordinate system using the Geocentric Datum of Australia 1994 (GDA94), and the Geodetic Reference System 1980 (GRS80) spheroid (ICSM, 2003). All elevations are reduced to Lowest Astronomical Tide (LAT).

2.2. Morphology of Warraber Reef Platform

2.2.1. Morphology of Torres Strait

Torres Strait (Figure 2.1) in which Warraber Reef is situated is a shallow shelf separating the northern tip of the Australian mainland at Cape York from Papua New Guinea. The location of the Strait is between 142^0-144^0E and 9^0-11^0S.
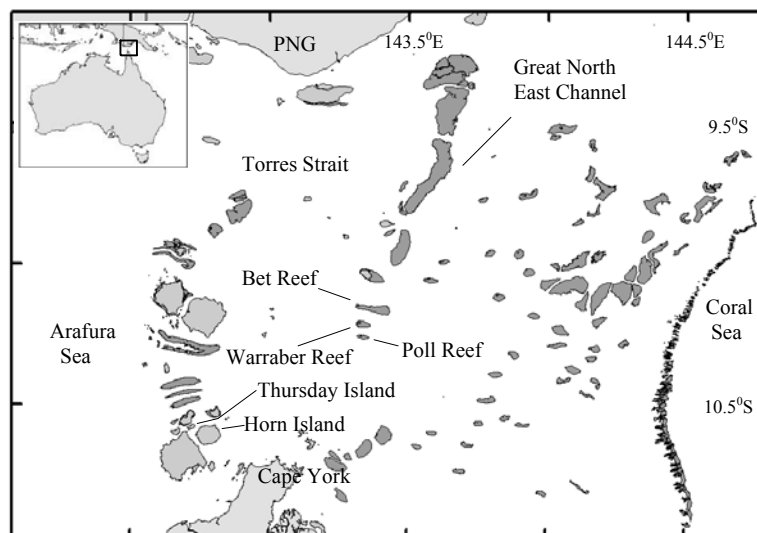
Figure 2.1. Torres Strait.

Torres Strait is bounded on the west by the Arafura Sea, on the east by the Coral Sea and connected to the Gulf of Papua through the Great North East Channel. It was named after a Spanish explorer "Luis Vaez De Torres" who joined the Spanish

expedition through the Strait in 1606 (Parkyn, 1930). The Strait was formed between 8,500 and 6,500 years ago as the land bridge that existed between Australia and New Guinea was flooded by a rising sea level during the postglacial transgression (Barham and Harris, 1983). It is characterised by shallow water, much less than 20 m, with sea-floor sediments revealing a large sediment input from the Fly River delta to the north-east and the degree of reworking by the tides (Harris, 1995).

The islands in the Strait comprise high islands of basic volcanic rocks on the east, low sand cays in the middle, high islands of acidic volcanic and granitic rocks on the west, and low islands with mangrove, mud and peat overlying dead coralline platforms to the northwest (Barham and Harris, 1983). Reefs are well developed in Torres Strait, with large platform reefs and coral shoals occurring throughout the Strait forming a hazard to shipping, and fringing reefs growing around all the high islands. High rates of water flux and the presence of the Coral Sea water mass during the dry season (March-November) favour prolific reef growth in this region (Maxwell, 1968). Reef morphology in many areas exhibits east-to-west orientation, reflecting the influence of strong tidal currents flowing through the Strait between the Arafura Sea on the west and the Coral Sea on the east (Jones, 1995). Strong tidal currents together with shallow water promote vertical homogeneity of temperature and salinity within the Strait (Wolanski, 1994). Strong tidal currents in this region are generated as a result of dissimilar and out-of-phase tidal systems in the Coral Sea and the Arafura Sea (Bode and Mason, 1995). Tidal ranges of approximately 4 m and tidal currents of up to 4 m/s characterise this strait (Amin, 1978).

Torres Strait is dominated by ESE winds between April and November and NW winds between January and February. More details of wind conditions are analysed in Chapter 4. Information on wave climate is largely absent in this region, as is often the

case for reef environments. In the Great Barrier Reef region the wave model, called WAMGBR, has been adapted from WAM, which is designed for open water and gradual variations of bathymetry, for use in complex-reef geometry (Hardy et al., 2001). No information however is available from the model for constructing wave climate in Torres Strait. Young (1999) has generated a global climatology of ocean wind and wave conditions based on a combination of satellite remote sensing and wave model predictions. However, no results are specific to Torres Strait. As demonstrated by Young (1989) the reef complex along the Great Barrier Reef shelf exerts considerable attenuation on energy of waves moving across the shelf from the Coral Sea. Therefore, waves in Torres Strait probably are principally governed by locally generated waves. Wave characteristics in this region, impinging on Warraber Reef and Island, are examined in Chapter 5, based on field measurement of waves on Warraber Reef.

An attempt has been made to create a DTM of Torres-Strait topography. This generalised model may be useful as a preliminary bathymetric model for further research relating to wave climate, mass flux and the estimate of carbonate production. The DTM of Torres-Strait topography is modelled using a TIN and its areas are divided into: i) the seafloor; ii) the reef front; and iii) the reef flat. A similar, but more detailed DTM is constructed for Warraber Reef in the following section. Available data for constructing the Torres Strait DTM include: i) digital mapping (polygons) of features in Torres Strait produced by CSIRO; and ii) Laser Airborne Depth Sounder (LADS) and a nautical chart from the Australian Hydrographic Office (AHO).

Existing digital mapping data for Torres Strait include polygons of five features: mainland; island; reef; water; and foreshore. Only the first three features were used for the construction of the DTM (Figure 2.2a). These were originally in AGD66 but were reprojected to MGA94 for analysis. LADS data consist of a series of data surveyed

between 1994 and 1999, based on the World Geodetic System 1984 (WGS84) and referenced to LAT. Details of LADS datasets are shown in Table 2.1 and coverage areas are shown in Figure 2.2b.

Figure 2.2. Data for constructing the Torres Strait DTM: a) digital mapping of Torres Strait, digitised from the AUSLIG 100k series and satellite imagery by CSIRO; b) coverage areas of LADS datasets surveyed between 1994 and 1999 by AHO; c) coverage areas of a 1998 nautical chart from AHO; and d) a coverage area of a DTM of Torres Strait topography.

Table 2.1 Details of LADS datasets.

Series	No. Datasets	Survey Start	Survey End	Horizontal Datum	Vertical Datum
HI206	8	6-May-1994	1-Dec-1994	WGS84	LAT
HI222	5	22-Jun-1995	28-Nov-1995	WGS84	LAT
HI236	4	16-Oct-1995	4-Apr-1996	WGS84	LAT
HI255	1	12-Feb-1997	29-Apr-1997	WGS84	LAT
HI258	1	20-Nov-1997	4-Dec-1997	WGS84	LAT
HI293	2	29-Jan-1999	24-Apr-1999	WGS84	LAT

The AHO nautical chart (chart No. AUS00839) is in TIFF format georeferenced to WGS84, with water depth referenced to LAT. Its coverage area is shown in Figure 2.2c. Due to very small differences of about 2-3 cm in horizontal distances between WGS84 and GDA94, the transformation to GDA94 was not undertaken for this chart. The bounding polygon for a DTM of Torres Strait topography was defined according to the coverage of the nautical chart and LADS data (Figure 2.2d).

The approach to generate a DTM of Torres Strait is a generalisation, based on limited data, and similar to that used for the Great Barrier Reef by Lewis et al. (2001). The similar approach will be used to model Warraber-Reef topography in the following section. The surface of reefs was defined using polygons of reef perimeters. In view of the scarcity of information about the reef-platform surface, it was assumed in this model that all reef-flat surfaces are flat and 2 m in elevation above LAT, and the base of the reef is horizontally 50 m from the reef edge. The 2-m height above LAT of reef-flat surfaces is an average elevation of Warraber Reef flat, as shown in a later section, and the 50-m horizontal distance was assumed based on data from CSIRO lobster surveys along transects across the reef front. The reef-front areas were therefore simply constructed as a 50-m buffer of the reef-flat polygons.

The seafloor data were derived from soundings from LADS and on-screen digitised points derived from contours on the nautical chart in areas where LADS data are not available. Data from LADS contain a large number of data points that are greater than necessary and cause problems in display and computation. Therefore, LADS data were reduced, using a function "Create Subset" in the Geostatistical Analyst extension (Johnston et al., 2001). All reduced LADS datasets were then merged and the data that are outside the boundary were deleted. In areas in which water depth has not been surveyed, especially along the eastern boundary of the model, interpolated data

were produced using a kriging interpolator. The 3D topography of Torres Strait is shown in Figure 2.3.
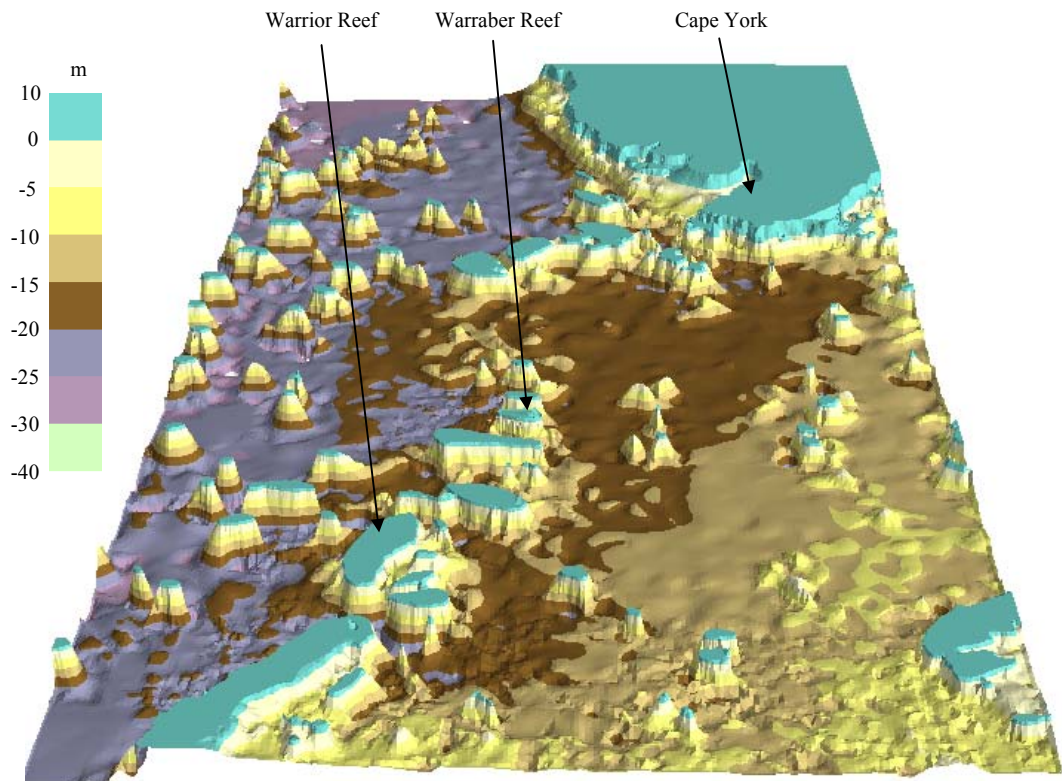
Figure 2.3. 3D model of Torres Strait (viewed from the north with 200x vertical exaggeration). Depth scale is referenced to LAT. Note, this view is looking south towards Cape York peninsular.

Water depth over this part of Torres Strait increases from approximately 10 m below LAT to the northwest (the lower right corner of Figure 2.3) to approximately 30 m below LAT to the southeast (the upper left corner of Figure 2.3). This part of Torres Strait comprises a number of reefs and shoals, particularly to the east (on the left of Figure 2.3). It is therefore likely that only small energy of waves generated in Coral Sea by the SE trade wind can penetrate into this region. In addition, these reefs may limit fetch for waves locally generated in this region. Waves arriving to reefs on which reef islands exist, such as Warraber Reef, may have already gone through diffraction and refraction due to nearby reefs. This results in complex patterns of waves arriving to the

48

reefs, intensifying difficulties in examining morphological changes of reef islands on these reefs.

2.2.2. Topography of Warraber Reef

Warraber Reef is located in the central of Torres Strait and comprises the central of three parallel reefs, called the Three Sisters, the reef to the north called Bet and that to the south called Poll (Figure 2.1). The morphology of Warraber Reef can be described as a planar-reef type, according to the shelf-reef classification of Hopley (1982) (Figure 2.4).

Figure 2.4. Aerial photograph of Warraber Reef and Island, taken in 1966.

Warraber Reef has a pear shape with approximately 5.0 km long in the west-east orientation and approximately 2.5 km wide in the north-south orientation. Its shape which is elongated in the west-east orientation reflects characteristics of strong tidal currents in this region (Woodroffe et al., 2000). Warraber Reef is influenced by a mixed tide with a maximum tidal range of 4.0 m.

The topography of Warraber Reef is important because it influences wave conditions and sediment movement on the reef. It also gives an idea of the pattern of former reef growth and determines the ecology of the reef and reef flat. Ecological and sedimentological characteristics of the reef top have been described by Hart (2003) and are outlined in Section 1.5. However, other less accessible parts of the reef are poorly known and their topography can only be approximated by modelling.

In order to generate the DTM of Warraber Reef, three sections of Warraber Reef are defined (Figure 2.5a): i) the seafloor around the reef; ii) the reef front; and iii) the reef flat.
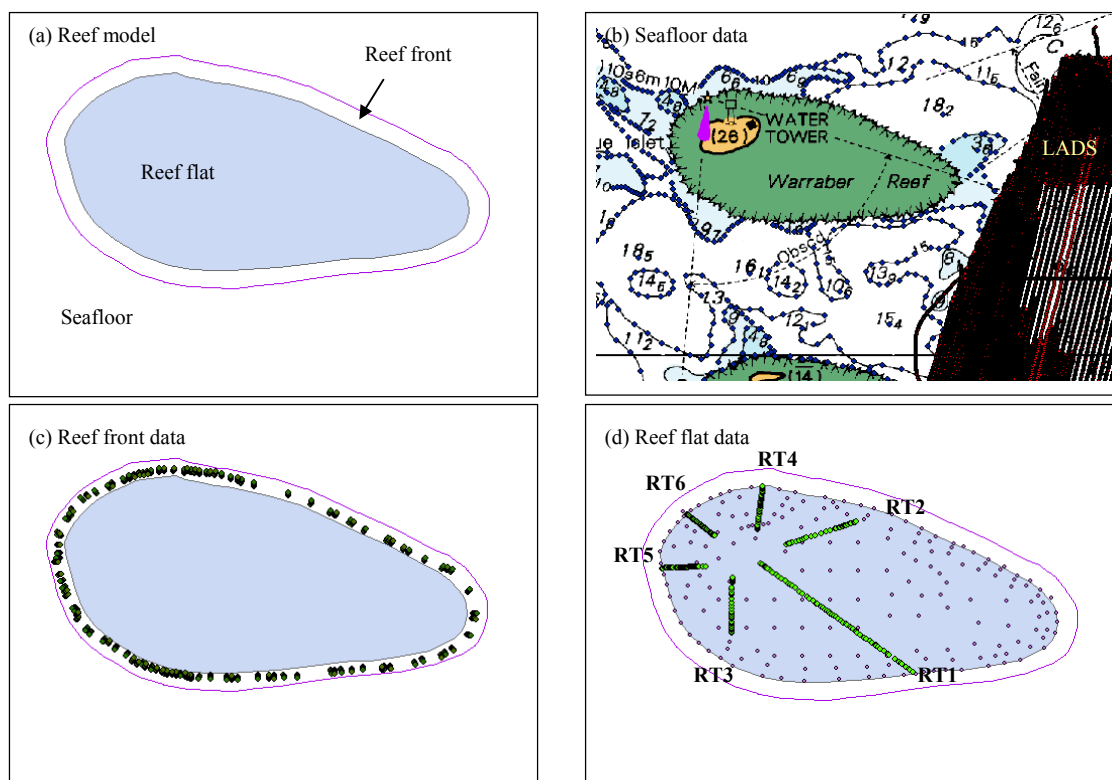
Figure 2.5. Derivation of a topographical model of Warraber Reef: a) definition of three sections; and data for b) the seafloor, c) the reef front and d) the reef flat.

Data used to map the seafloor around the reef were sample points digitised on screen from contours of the nautical chart covering the area around the reef and

soundings from LADS covering the area to the east of the reef, both data provided by the Australian Hydrographic Office (Figure 2.5b). The number of data points in each LADS dataset was reduced to prevent difficulty in display and computation, following the same approach applied for the construction of the Torres Strait DTM in the previous section. The reduced LADS data were then combined with digitised bathymetry, particularly points sampled along isobaths, for seafloor generation.

Bathymetric data for the reef front were derived from observations made by CSIRO divers during lobster surveys (Figure 2.5c). The raw field notes collected during these lobster surveys by CSIRO (Skewes et al., 1997) were interpreted in conjunction with CSIRO staff and provided water depth estimates, but without tidal correction, at survey stations around the reef rim and along transects across the reef front. Sixty transects were used for the construction of the reef-front bathymetry. It was assumed that the base of the reef front is at about the end of the survey transects, which is about 50 m from the reef rim.

The original locations of transect-survey stations along the reef rim, that were obtained from CSIRO lobster surveys, were not at actual positions of the reef rim due to errors in GPS and map digitisation (Skewes et al., 1997). This could be seen, when compared to transects on the reef and GPS records around the periphery of the reef captured by Hart (2003), an outline of Warraber Reef digitised from the AUSLIG 100k series and satellite imagery by CSIRO, and a georeferenced aerial photograph of Warraber Reef flown in 1966 (Figure 2.6). The transect-survey sites along the reef rim from the lobster surveys were displaced towards the southwest approximately 100-200 m from actual positions. Therefore, the reef-rim sites were relocated and a polygon of the reef platform was created based on the new locations of the reef-rim sites.

Figure 2.6. Comparison of data approximating reef-edge locations, indicating a shift of CSIRO lobster survey data (overlaid on aerial photograph taken in 1966). The surveyed transects, described by Hart (2003), are also shown.

Details of elevations of the reef-flat surface (Figure 2.5d) were derived from surveyed transects (RT1, RT2, RT3, RT4, RT5 and RT6) and estimates of spot heights. Initial surveyed transects undertaken during stratigraphic surveys in 1998 were extended during more detailed study of hydrodynamics and ecology in 2001, using a dumpy level along a compass bearing (Hart, 2003). Due to the vastness of the reef flat and limited duration of exposure at low tide for survey, only six transects were surveyed, starting from the beach toe. Topography of the reef flat along the six surveyed transects was shown in Figure 1.7b.

The transect data were insufficient to generate a realistic surface of the reef platform. Spot heights for the non-surveyed areas were therefore estimated based on the field experience of the geomorphologists and ecologists (particularly Deirdre Hart, based on her ecological and sedimentological structures of the reef top) and by visual correlation to the known heights along the transects. The position for each point on transects was calculated from compass bearings and the distances starting from one to three known positions along transects, measured using GPS with geographical

coordinates in AGD66. Data for the reef flat under the island were acquired based on limited information from a drill core undertaken as part of groundwater investigations and considered to be at an elevation of around 2 m above LAT.

In order to be able to capture the variations in the reef topography, the final DTM of reef topography was modelled using a TIN. A TIN allows different resolutions to be used for different areas. Steps to construct the reef topography included preprocessing data, interpolating data in each area to obtain a higher resolution grid, converting grids to point data and constructing a TIN of the whole reef topography from point data (Figure 2.7).
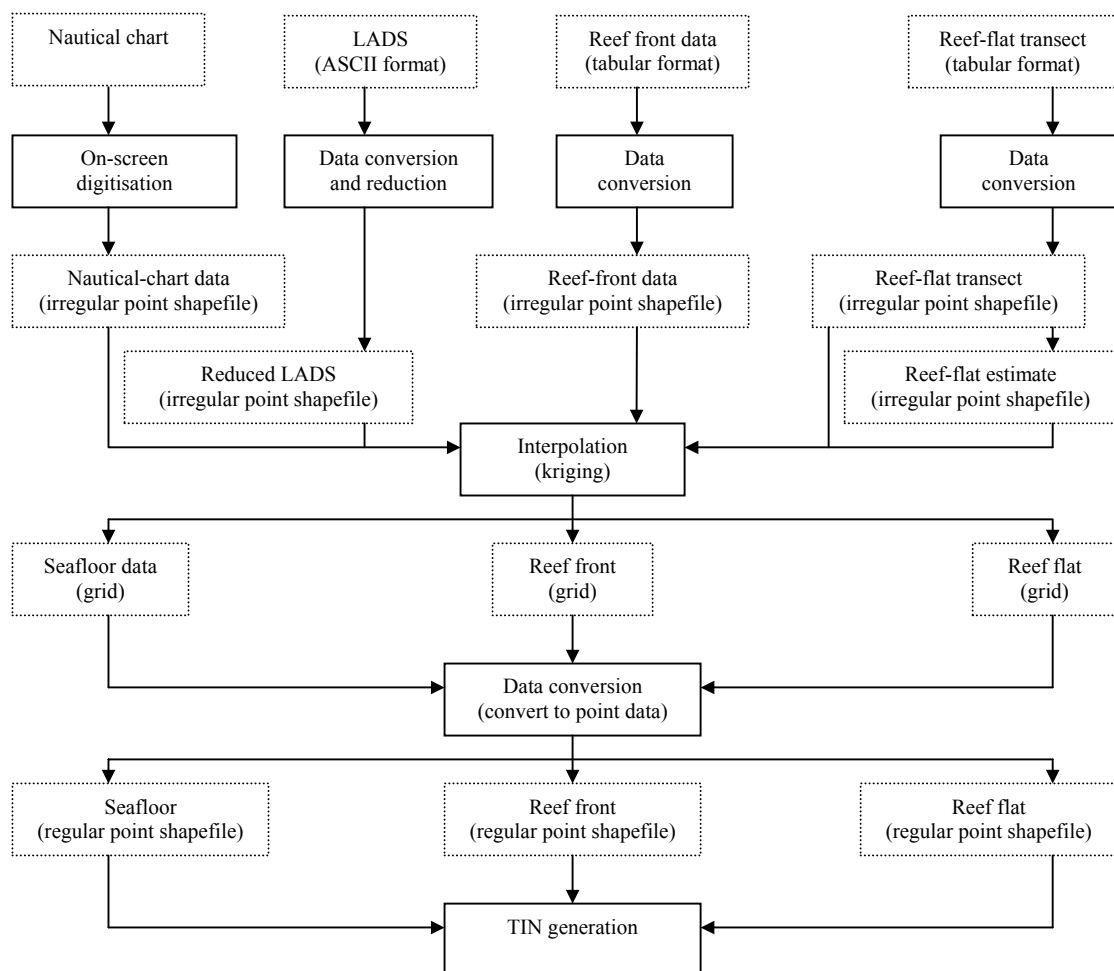
Figure 2.7. Diagram showing steps involved in DTM generation for Warraber Reef.

Preprocessing of data was carried out in ArcMap and involved creating new data in a shapfile format (Vienneau and Bailey, 2001; Booth et al., 2002), converting the original data to shapfiles (Minami et al., 2000), and transforming and projecting their coordinates to MGA94 using ArcToolBox (Tucker et al., 2000).

Interpolated data points instead of the original irregular data points were employed to create a TIN of the reef for several reasons. The irregular data points for the sea floor are mainly derived from contours, the data for seafloor and the reef flat are sparse and all three datasets may not be representative of actual variations of topography. Contour-derived data and sparseness of data can generate flat areas and large areas of planar-facet appearance, respectively, in a TIN. In addition, abrupt changes in elevations generated in a TIN may not exist in actual topography because available data are not located at prominent features. Therefore, the variations of the topography in areas in which no data are available have to be approximated by interpolation.

Interpolation can be performed either through techniques such as spline and kriging on sample data points (Johnston et al., 2001; McCoy and Johnston, 2001), or by the linear or quintic method on a TIN generated from sample data points (ESRI, 2001). Interpolation based on the quintic technique on a TIN can minimise the problem of planar-facet appearance but may not be suitable if the original data points are not at prominent features such as peaks or troughs (ESRI, 2001).

Methods of interpolation on sample point data can be broadly classified into either those of global and local interpolators (Burrough and McDonnell, 1998) or those of deterministic and geostatistical interpolators (Johnston et al., 2001). Global interpolators can be used indirectly in examining and removing the effects of global variations in surface generation (Burrough and McDonnell, 1998) or directly as a

54

generalization of the surface is required if, for example, the data are noisy (McCullagh, 1998). Local interpolators either deterministic such as spline and inverse distance weighted, or geostatistic such as kriging and cokriging are direct interpolation techniques for surface generation.

Investigations have been carried out in order to evaluate which interpolators better perform for surface generation (Kumler, 1994; Carrara et al., 1997; Desmet, 1997; Caruso and Quarta, 1998). However, the conclusion has not been simple; variation of results has occurred, depending on many factors such as types of terrain, sample structure and modelling routine (Dixon et al., 1998). Kriging seems to be the most popular method due to its high performance and its ability to quantify errors due to interpolation, and its suitability when sample points are spatially variable or clumped. Accordingly, in this study interpolation using the kriging method is applied to generate the regular data points for TIN generation.

Interpolations were carried out using the ArcGIS extension, called "Geostatistical Analyst" (Johnston et al., 2001). Basically, interpolations produce the best result if data distribution is normal; therefore, the topographical data having a skewed distribution were transformed to be more normally distributed using a power transformation (Box-Cox) (Johnston et al., 2001). Also, the global trend that can be seen when exploring the data and represented by second-order polynomial was removed.

In the Geostatistical Analyst, the performance of the interpolation is assessed based on results of cross-validation. The cross-validation gives information as to how well the model predicts values for unknown locations, based on four statistical values: i) standardized mean prediction errors; ii) root-mean-square prediction errors; iii) average standard error; and iv) standardized root-mean-square prediction errors. The best results were selected from interpolations having standardized mean prediction errors closer to

zero, smaller root-mean-square prediction errors, average standard error closer to root-mean-square prediction errors, and standardized root-mean-square prediction errors closer to one (Johnston et al., 2001). The grid was converted to point data using "RASTER TO XYZ" (Rathert, 2005), an ArcScript freely downloaded from the ESRI ArcGIS website. The DTM of Warraber Reef is shown in Figure 2.8.
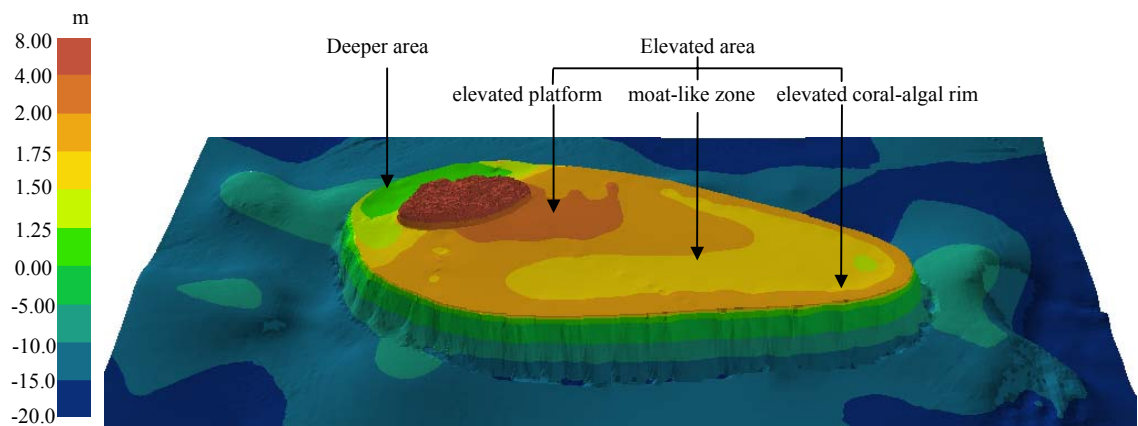
Figure 2.8. 3D topography of Warraber Reef (viewed from the south with 40x vertical exaggeration). Depth scale is referenced to LAT.

The present topography of Warraber Reef comprises two major areas: the reef flat and the reef front. According to the model presented in Figure 2.8, the area of the reef flat is approximately 11 km^2 and the reef front approximately 2 km^2; therefore the total area of Warraber Reef is approximately 13 km^2. Water depth at about the reef base is approximately 15-20 m below LAT.

The reef flat is distinguishable, based on the difference in gross elevation, into two main areas (Hart, 2003) (Figure 2.8): the elevated area on the east of the island, which is the main part of the reef flat; and the deeper area on the west of the island. Elevations of the eastern area tend to decrease gradually from an elevated platform of approximately 2 m above LAT to elevation ranging between 1.25-1.75 m above LAT in a narrow moat-like zone (Figure 2.8). Elevation of a coral-algal rim is approximately 2 m above LAT. Elevations of the deeper reef flat on the west of the island range from 0

to 1.5 m above LAT. Tidal levels in the vicinity of Warraber Reef are shown in Table 2.2, based on tidal prediction at Poll Island (see its location in Figure 2.1), the closest secondary port. According to tidal levels in this area, the elevations of the elevated platform and coral-algae rim are approximately at the elevation of MSL and thus much of the elevated area is exposed for approximately 50% of a tidal cycle whereas the western reef flat experiences more submergence (Hart, 2003).

Table 2.2 Tidal levels at Poll Island (Australian Hydrographic Service 2001)

2.3. Morphology of Warraber Island

The general topography of Warraber Island was described by Rasmussen and Hopley (1996) who inferred that the island had accumulated in a series of stages. More detailed topographic data will enable a clearer definition of the geomorphology of the island, and will enable the calculation of mass sediment budgets. When combined with dating, this will enable a determination of volume of sediment deposited over time.

The present topography of the island was constructed from computer-aided design (CAD) files, produced by Schlencker Mapping using photogrammetry from a series of colour vertical aerial photographs taken in 1998 at a scale of 1:4000. In ArcGIS, a CAD file is generally presented with two types of data: CAD drawings and CAD datasets. CAD drawings have no attribute tables whereas CAD datasets do. Basically, CAD

datasets include features represented by points, polylines and polygons and those of points and polylines were used in island-topography construction. The topography of the island was modelled by a TIN using points and polylines as mass points and break lines, respectively.

Man-made structures, including a large water storage system, a breakwater and road networks (Figure 2.9), that can affect the generation of actual topography and the volume calculation of the island have to be removed from the data before further analyses. In ArcMap, CAD datasets can be directly displayed and queried. However, in order to be editable to remove those features, CAD datasets were transformed to a geodatabase from which corresponding shapefiles were exported.

The projected coordinates of the data were transformed from AMG86 to MGA94. In the area previously occupied by the water storage system, beach ridges existed, running along parallel to the shoreline, as can be seen from historical aerial photographs. Interpolation was undertaken using the kriging method with adjusted anisotropy to conform to the trend of those beach ridges that can be recognised. In summary, data for TIN generation are a point shapefile of spot heights, a point shapefile of interpolated data in an area previously occupied by the water storage system and a polylines shapefile of beach ridges.

The procedure to generate the DTM of the island involves generating a TIN from these data, converting the TIN to a grid using the quintic interpolation, converting the grid to point data and generating a final TIN of the present topography of the island from the point data. A first TIN of the island had an artificial angular view, which is a common characteristic of a TIN. In this TIN construction, similarly, planar-facet appearance was avoided by interpolation. By contrast, interpolation was carried out on

Figure 2.9. Stages in the transformation of the photogrammetrically-derived topographic data for Warraber Island. Water storage system, a breakwater and road networks that were removed from: a) a point shapefile; and b) a polylines shapefile.

a TIN through the quintic technique in ArcToolbox, instead of using the original data

with the kriging method. This is reasonable because the original data consisting of spot

heights and breaklines were photogrammetrically generated on purpose; prominent

features such as beach ridges and beach areas were captured by breaklines and spot

heights were equally distributed. Furthermore, interpolation from a TIN helps to

maintain accuracy so that it is no less than the original data. The point data of the island surface were then generated from the grid for final TIN construction, using the "RASTER TO XYZ" extension (Rathert, 2005). A final TIN of the island topography in 1998 is shown in Figure 2.10
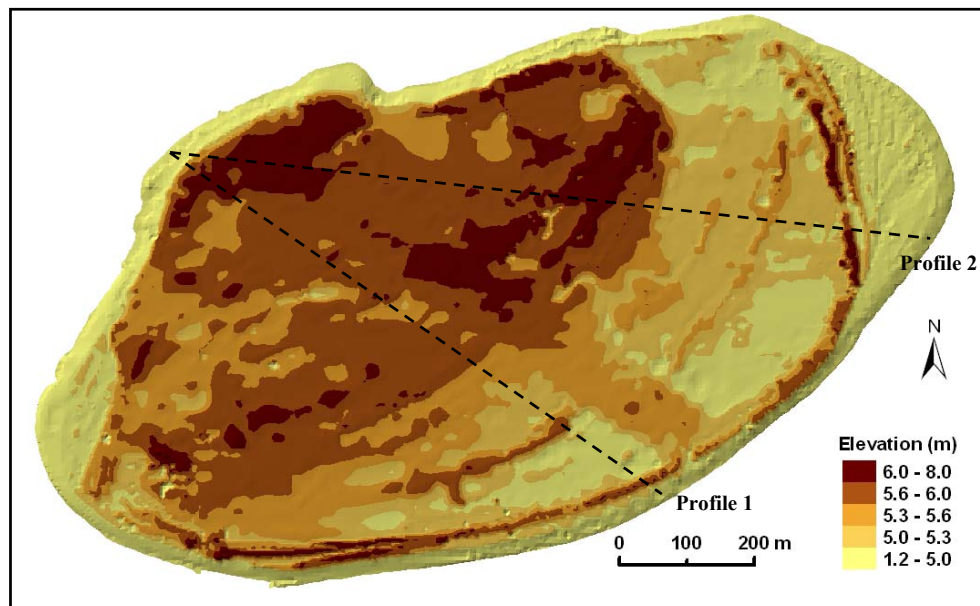
Figure 2.10. Topography of Warraber Island, based on data surveyed in 1998. Two profiles (profile 1 and profile 2) across the island (dashed lines) were extracted from this island model and are shown in Figure 2.11.

Warraber Island is a vegetated sand cay, according to the reef-island classification by Hopley (1982) as outlined in Chapter 1. It sits on the western, leeward end of the Warraber Reef platform (Figure 2.4). The island is oval in shape and is approximately 1,500 m long in the southwest-northeast orientation and approximately 920 m wide in the northwest-southeast orientation. The island is approximately 814,000 m^2 in area and approximately 2,700,000 m^3 in volume, according to the 1998 DTM in Figure 2.10. The highest point, approximately 7 m above LAT, is towards the northwestern corner of the island. Elevations tend to gradually decrease away from that high point with several concentric beach ridges indicating former shorelines, more or less parallel to the

southern shore of the present island. Figure 2.11 shows variations in elevation along the two profiles, indicated in Figure 2.10.
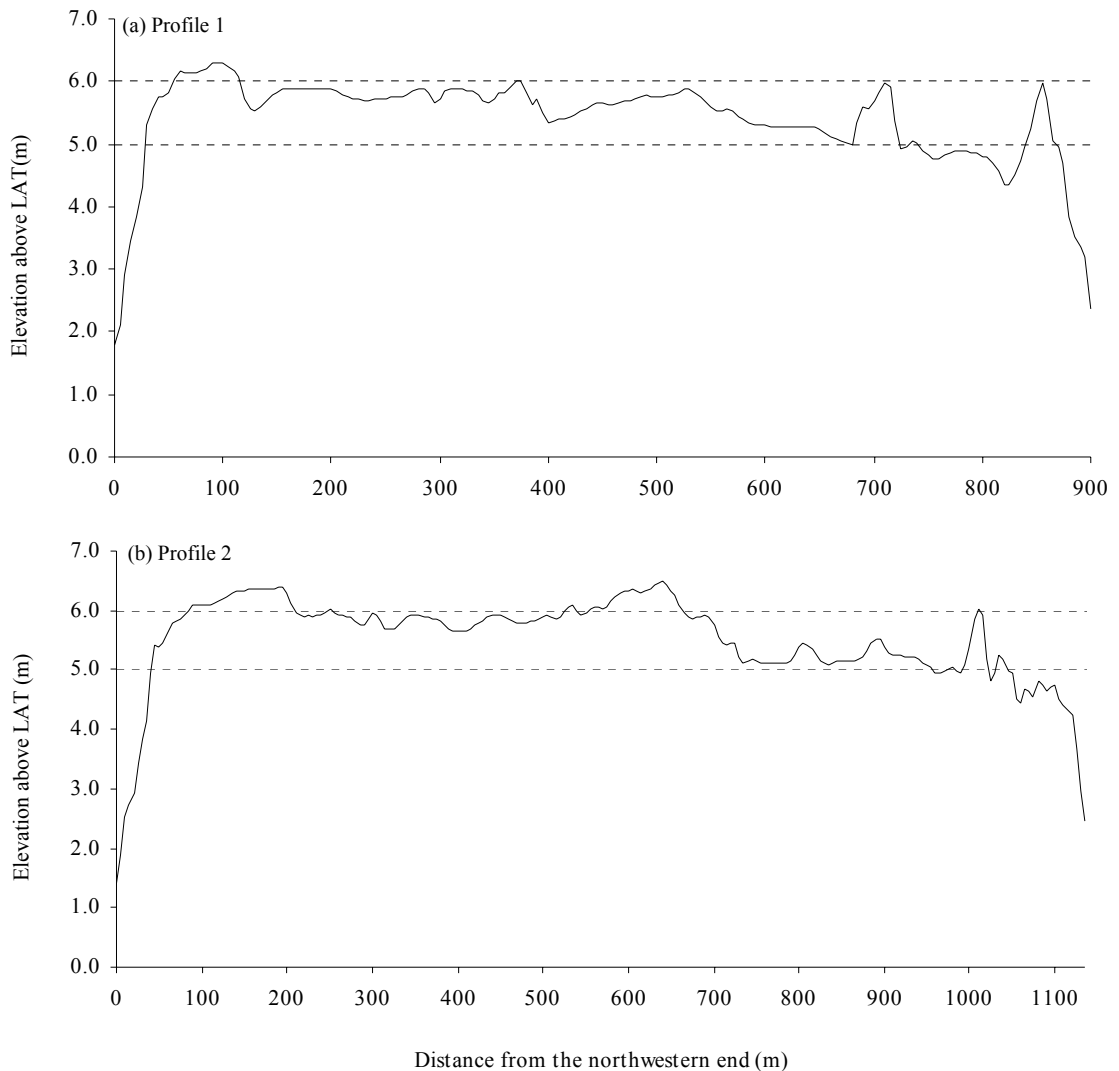
Figure 2.11. Elevations of Warraber Island along (a) profile 1 and (b) profile 2. Their locations are shown in Figure 2.10.

It can be seen in Figures 2.10 and 2.11 that most of the island topography occurs at elevations of between 5 and 6 m above LAT, interspersed with beach ridges some of which are of relatively low amplitude but the more prominent of which rises 1 m above the surrounding topography. Another variation in island topography occurs on the southwestern and northeastern ends of the island. Here elevations are slightly lower than the rest, with an average of 4.8 m and 4.6 m above LAT on the southwestern end

and the northeastern end, respectively. On the northeastern end a series of beach ridges has developed with low sand ridges running along the beach crest. The beach ridges along the southern crest of the island beach are approximately 6 m above LAT and 1 m above the surrounding surface of the island. They are separated into two ridges, one running along the modern shoreline to the west and another terminated at about the southwest corner of the island. The latter probably indicates the trend of the island shoreline shape in the past.

Most of the island is covered by vegetation (Figure 2.12a). To the west of the island the vegetation mostly appears to be natural whereas to the east modified vegetation is evident associated with the village (Rasmussen and Hopley, 1996). Wongi trees, *Manilkara kauki*, are the most widespread forest trees interspersed with planted groves of coconuts, *Cocos nucifera* (Rasmussen and Hopley, 1996).

Figure 2.12. Vegetation and other prominent features on Warraber Island; a) georeferenced aerial photos taken in 1998 showing major constructions and areas of beachrock and b) mangroves growing on low bars in front of beach rock.

Visual observation during fieldwork in 2004 showed exposure of extensive beachrock along the northwestern to northern side of the island and a small outcrop of beachrock along the southern and southeastern beach areas of the island (Figure 2.12a). Young mangroves were also found growing on low sand bars fronting the island around the beachrock at the southern beach area of the island (Figure 2.12b).

Beach morphology of Warraber Island can be classified into three types following the descriptions by Hart (2003) (Figure 2.13).

Figure 2.13. Beach types of Warraber Island: a) Type 1, a short, steep and stepped, concave beach face; b) Type 2, a wide, convex beach face with a gentle break in slope between the beach toe and the reef flat; and c) Type 3, a medium-width, steep and straight beach face. (after Hart (2003)).

Type 1 is characterised by a short, steep and stepped, concave beach face. This type occurs along the northern beach of the island, where there is extensive beachrock backed by a seawall. Type 2 is a wide, convex beach face with a gentle break in slope between the beach toe and reef flat. Beaches around the western and eastern ends are of this type. Type 3 exhibits a medium-width, steep and straight beach face. The southern beach areas fall in to this type 3.

The major constructions on the island are the village settlements on the east of the island, the airstrip, the boat harbour, the seawall along the northern side and the water storage system. Much of the centre of the island was cleared for the airstrip in 1975. The boat channel and harbour were constructed in 1991, and the materials excavated were used for the harbour construction and shoreline protection in front of the community centre (Figure 2.12a). The water storage system was constructed in 1996.

2.4. Depositional History of Warraber Island

Reconstruction of the depositional history of Warraber Island comprises four steps: i) determination of spatial patterns of evolution; ii) determination of temporal patterns of evolution; iii) reconstruction of morphological evolution; and iv) estimate of rates of progradation and associated sediment volume.

2.4.1. Determination of Spatial Patterns of Evolution

The spatial patterns of evolution of Warraber Island have been previously identified on aerial photographs by Rasmussen and Hopley (1996), based mainly on concentric beach ridges. In the present study, the ridges inferred in the earlier study

have been identified in greater detail from the high-resolution DTM of Warraber Island, which was developed in the previous section. Although the island may have gone through continuous accretion throughout periods of evolution, five phases of island evolution were hypothesised by Rasmussen and Hopley (1996) based on configuration of prominent beach ridges. Island shapes corresponding to each phase of evolution are defined by outlines of the beach ridges. Figure 2.14 indicates five phases of the island evolution, including four phases in the past and the last one at present in 1998.
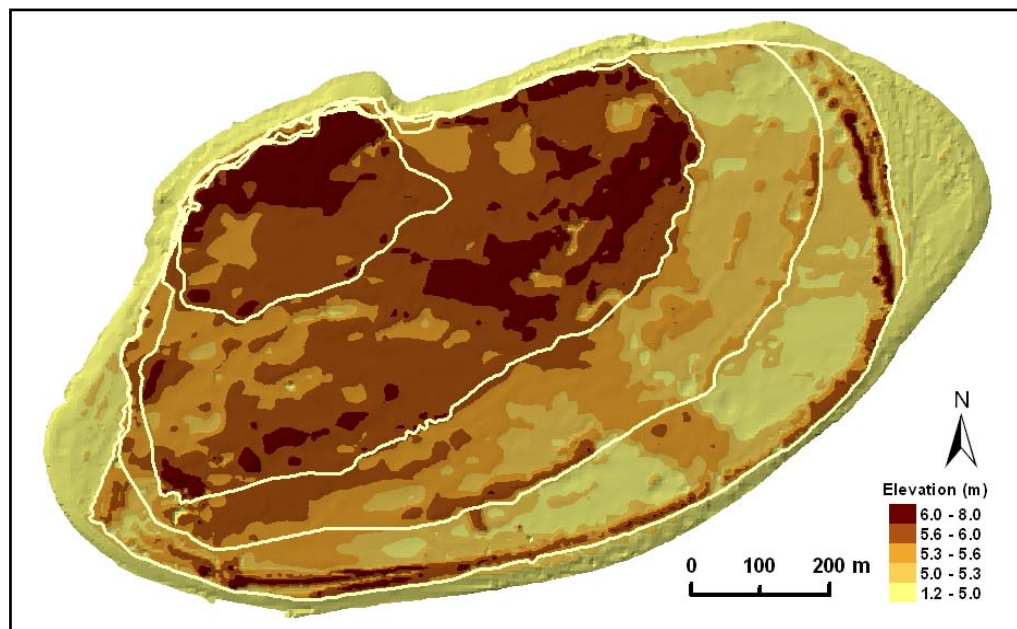
Figure 2.14. Five phases of evolution of Warraber Island, identified based on prominent beach ridges.

2.4.2. Determination of Temporal Patterns of Evolution

Temporal patterns of evolution of Warraber Island have been assessed in three phases, using increasingly refined radiocarbon dating approaches. The first phase involved bulk dates, and the second and third involved AMS dates on specific components.

A series of backhoe pits across the island, adjacent to the runway, was excavated in 1999 and bulk sediment samples were collected at depths between 1 and 2 m below the surface from these pits for analysis. A preliminary investigation on the evolution of Warraber Island, based on radiocarbon dating of bulk sand samples, was initially reported by Woodroffe (2000). The second phase was undertaken in order to examine the reliability of dates on bulk sand samples and a third phase was conducted to verify the results from the second phase.

Individual sand grains of coral, molluscs and foraminifera were chosen from bulk sand samples using a binocular microscope for AMS radiocarbon dating for the second and third phases. Only very small coral fragments (generally about 1 mm or less) could be found and identified based on keys to identification of skeletal components under reflected light (Milliman, 1974). Foraminifera were more easily recognised due to their retained shapes and the least abraded specimens were chosen. Gastropod shells which showed little sign of abrasion, generally retaining their colouration and a sharply pointed spine, were preferentially selected. The 15 samples comprising 6 coral grains, 5 gastropod shells and 4 foraminiferal tests, and 15 samples of 4 coral grains and 11 gastropod shells were sent for AMS dating at ANSTO (Lawson et al., 2000) during the second and third phases, respectively.

The ages of bulk sand samples and AMS ages on individual grain, which are conventional radiocarbon ages (years BP), were calibrated to a calendar BP age (cal BP) using the calibration program, CALIB Rev 5.0.2 (Stuiver and Reimer, 1993). The samples obtained 100% of their carbon from marine sources, so it is necessary to correct for the marine reservoir effect, using the marine98.14C calibration dataset. A ΔR of 50 ± 31, which is obtained from Marine Reservoir Correction Database (Reimer and Reimer, 2000), is applied for reservoir correction for NE region of Australia. The

derivation of this ΔR value is based on 3 museum samples from Torres Strait (Gillespie, 1977; Gillespie and Polach, 1979) and 2 samples from the Gulf of Carpentaria (Rhodes et al., 1980).

The radiocarbon dating results on bulk sand samples are illustrated in Figure 2.15 and Table 2.3. The results of the sequence of radiocarbon dates implied that the island had begun to accumulate towards the northwestern corner of the modern island, where there is presently a conglomerate and fossil beachrock which is exposed on the northern shoreline. With the exception of ages for P10 (3,627-4,013 cal BP) and P8 (3,698-4,088 cal BP), which are not statistically significantly different, episodic progradation towards the southeast is implied with the youngest age, 2,321-2,678 cal BP, occurring in pit P1 in the ridge on the modern shoreline. An age of 3,177-3,473 cal BP from a pit at the site of WS9 (Figure 2.15) appeared consistent with this sequence. The sequence of ages was initially inferred to indicate that there had been negligible addition of sediment to the island over the past 2,000 years once the island had built seaward to its present position.
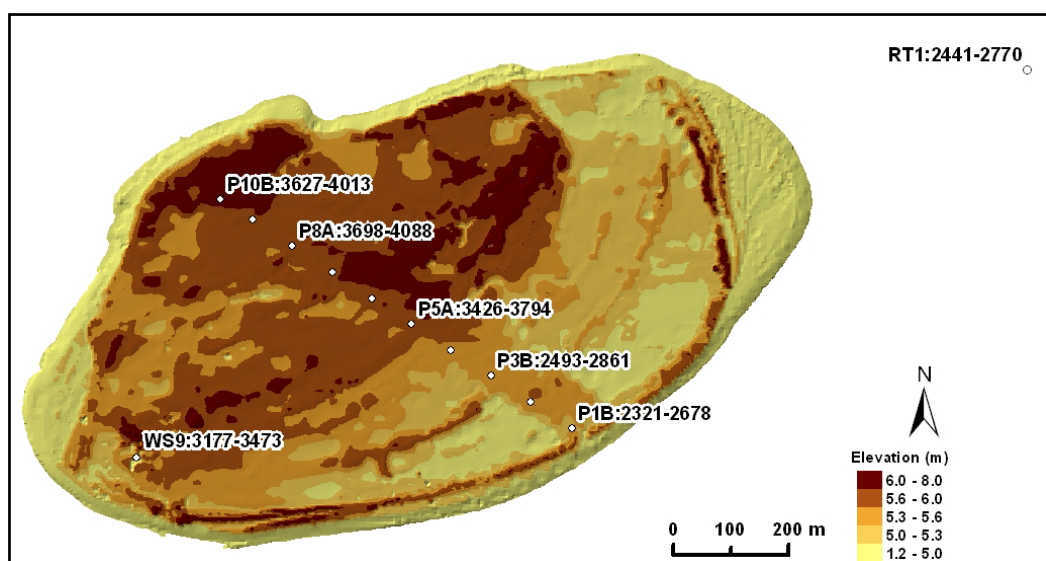
Figure 2.15. Locations of samples with results of radiocarbon dating on bulk sand samples (6 samples from backhoe pits on Warraber Island and 1 sample from the reef flat). Note unit = years cal BP.

Table 2.3. Radiocarbon ages and their associated calibrated ages for bulk sand and individual grains from Warraber Island and reef flat. There is no depth value for WS9, and samples from the beach and the reef flat were collected at the surface.

Sample code	Lab code	Description (m below surface)	$\delta^{13}C$ ($^o/_{oo}$)	Conventional ^{14}C age (Yrs BP±1σ error)	Cal BP 2 σ age ranges
P10B	*Wk8213*	*Bulk sand from the island (2.2 m)*	*0.7*	*3910 ± 60*	*3627 - 4013*
P10B Coral	OZG563	Coral from P10B (2.2 m)	-1.6	4410 ± 50	4335 - 4713
P10B Shell	OZG564	Shell from P10B (2.2 m)	-0.9	2920 ± 40	2463 - 2744
P10B Foram	OZG565	Foraminifera from P10B (2.2 m)	0.0*	5290 ± 140	5291- 5908
P8A	*Wk8212*	*Bulk sand from the island (1.3 m)*	*1.9*	*3970 ± 60*	*3698 - 4088*
P8A Coral	OZG562	Coral from P8A (1.3 m)	0.8	3120 ± 50	2723 - 2995
P7B Shell	OZH751	Shell from P7B (1.8 m)	1.8	2790 ± 50	2322 - 2661
P6B Shell	OZH750	Shell from P6B (2.0 m)	2.8	2230 ± 50	1614 - 1917
P5A	*Wk8211*	*Bulk sand from the island 0.8 m)*	*2.3*	*3730 ± 60*	*3426 - 3794*
P5A Coral	OZG559	Coral from P5A (0.8 m)	-3.1	3920 ± 90	3553 - 4066
P5A Shell	OZG560	Shell from P5A (0.8 m)	1.1	1870 ± 40	1272 - 1491
P5A Foram	OZG561	Foraminifera from P5A (0.8 m)	0.0*	4930 ± 210	4617 - 5651
P4B Shell	OZH749	Shell from P4B (1.3 m)	2.9	1540 ± 40	926 - 1162
P3B	*Wk8210*	*Bulk sand from the island (1.9 m)*	*2.4*	*2990 ± 60*	*2493 - 2861*
P3B Coral	OZG557	Coral from P3B (1.9 m)	-4.0	3650 ± 50	3354 - 3641
P3B Shell	OZG558	Shell from P3B (1.9 m)	0.6	1220 ± 40	632 - 839
P2B Shell	OZH748	Shell from P2B (2.7 m)	2.4	810 ± 50	287 - 493
P1B	*Wk8209*	*Bulk sand from the island (2.2 m)*	*2.7*	*2800 ± 60*	*2321- 2678*
P1B Coral	OZG554	Coral from P1B (2.2 m)	-2.1	1700 ± 40	1082 - 1299
P1B Shell	OZG555	Shell from P1B (2.2 m)	0.3	850 ± 40	314 - 509
P1B Foram	OZG556	Foraminifera from P1B (2.2 m)	0.0*	4780 ± 180	4513 - 5451
RT1	*Wk10830*	*Bulk sand on the reef*		*2930 ± 52*	*2441 - 2770*
RT1 Coral	OZG566	Coral from RT1	0.0*	1760 ± 40	1159 - 1365
RT1 Shell	OZG567	Shell from RT1	0.3	Modern	Modern
RT1 Foram	OZG568	Foraminifera from RT1	0.0*	5770 ± 250	5592 - 6639
WS9	*Wk9421*	*Bulk sand from the island (-)*		*3505 ± 50*	*3177 - 3473*
A2 Shell	OZH752	Shell from the eastern spit (1.43 m)	2.3	990 ± 40	474 - 632
B2 Shell	OZH753	Shell from the eastern spit (1.43 m)	0.9	540 ± 40	0 - 236
C2 Shell	OZH754	Shell from the eastern spit (1.43 m)	3.3	200 ± 40	Modern
BT3 Coral	OZH883	Coral from the beach	1.4	1390 ± 50	736 - 1012
BT3 Shell	OZH884	Shell from the beach	3.9	600 ± 50	42 - 286
BT2 Coral	OZH881	Coral from the beach	1.5	2070 ± 50	1414 - 1732
BT2 Shell	OZH882	Shell from the beach	2.2	490 ± 50	0 - 151
Q1A1 Coral	OZH887	Coral from the reef flat	0.5	2580 ± 40	2064 - 2321
Q1A1 Shell	OZH888	Shell from the reef flat	0.7	Modern	Modern
Q39 Coral	OZH885	Coral from the reef flat	-1.8	4330 ± 60	4180 - 4583
Q39 Shell	OZH886	Shell from the reef flat	2.0	Modern	Modern

Note : * -assumed value as the sample size is to small and no $\delta^{13}C$ measurement was carried out.

The sediments that are supplied to a sand cay are generally produced on the surrounding reef flat (McLean and Stoddart, 1978). This is also the case for Warraber Island where beach sediments are derived from central to inner reef flats (zones 2 and 1, respectively, in Figure 1.8) (Hart, 2003). Therefore, it is expected that radiocarbon ages of sediment on the reef flat are younger than those of sediment on the island as sediment

is transported from sources on the reef flat to be deposited on the island. However, a bulk radiocarbon date on sediment from the reef flat at site RT1, collected by Hart (2003), yielded an unexpectedly old age of 2,441-2,770 cal BP (Figure 2.15).

Radiocarbon ages record time of death of contributing organisms, and can only be used to determine time of sand deposition if there has been rapid transport after death from sources to the site of deposition, and negligible reworking since (Woodroffe and Morrison, 2001). It can be seen in Figure 1.8 that bulk samples collected on the reef flat and the island beach can include various types of sediments. This is also the case of bulk samples collected from pits across the island, as shown by a preliminary analysis by Hart (2004, per. comm.) in Figure 1.9. Ages derived from bulk samples reflect the average of ages of sediment constituents within the samples (Halley, 2000; Harney et al., 2000).

It was postulated that some material from the fossil reef that comprises much of the reef flat around and beneath the island might be incorporated into the sand deposit on the island. In particular, it had been noted that coral fragments can yield ages that are significantly older than other components on other reef islands, such as in the Cocos (Keeling) Islands (Woodroffe et al., 1999). Foraminifera were found to be a major component of a number of sand cays on the Great Barrier Reef (McLean and Stoddart, 1978) and also found to be amenable to transportation by currents during a normal climate (Yamano et al., 2000). Therefore, it was postulated that they might contribute younger ages of sediment components deposited on the island. The reef flat of Warraber Reef is veneered by a thin sediment cover, generally <20 cm thick, and grazed by gastropods, particularly species of *Turridrupa* and *Mitra* (Hart, 2003). Shell sand, often conspicuous as a swash-line ridge, is a prominent feature of the beach at several points around the island and makes up a large proportion of the beach sediment (33-

95%) (Figure 1.8) (Hart, 2003). It was hypothesised that such shells, produced close to the island, might be a more appropriate component to date in order to provide an indication of the time of deposition of sand than other components.

Consequently, a second phase of dating was undertaken using AMS on individual grains of different components to assess the reliability of dates on bulk sand. The results of the second-phase analyses (P10B, P8A, P5A, P3B, P1B and RT1) are shown in Figure 2.16 and Table 2.3, together with the results of the previous bulk dating and the third-phase analyses.

It is immediately apparent that the different components yield substantially different age estimates. It was expected that coral might yield the oldest dates as described above. It was actually the case that individual foraminiferal tests yielded the oldest ages (5,291-5,908 cal BP from the island), with the individual grain from the active sediment on the reef flat (RT1) giving the oldest date of any grain, 5,592-6,639 cal BP. Although the ages on foraminifera have wide age error ranges, the most expedient interpretation is that this part of the reef flat is no longer conducive to foraminiferal production and those foraminifera found on the island or the central reef flat grew in conditions associated with the fossil reef and have undergone entrainment and redeposition over the mid and late-Holocene. Therefore, foraminiferal grains appear inappropriate to interpret the temporal deposition of the island in this reef setting.

Hart's studies indicate that foraminifera presently dominate reef flat sediment samples from around the margin of the reef platform (zone 4 in Figure 1.8), but, as implied from their rapid decrease in successive sediment samples away from the reef crest, are mostly deposited in the slightly deeper 'boat channel' (Hart, 2003).
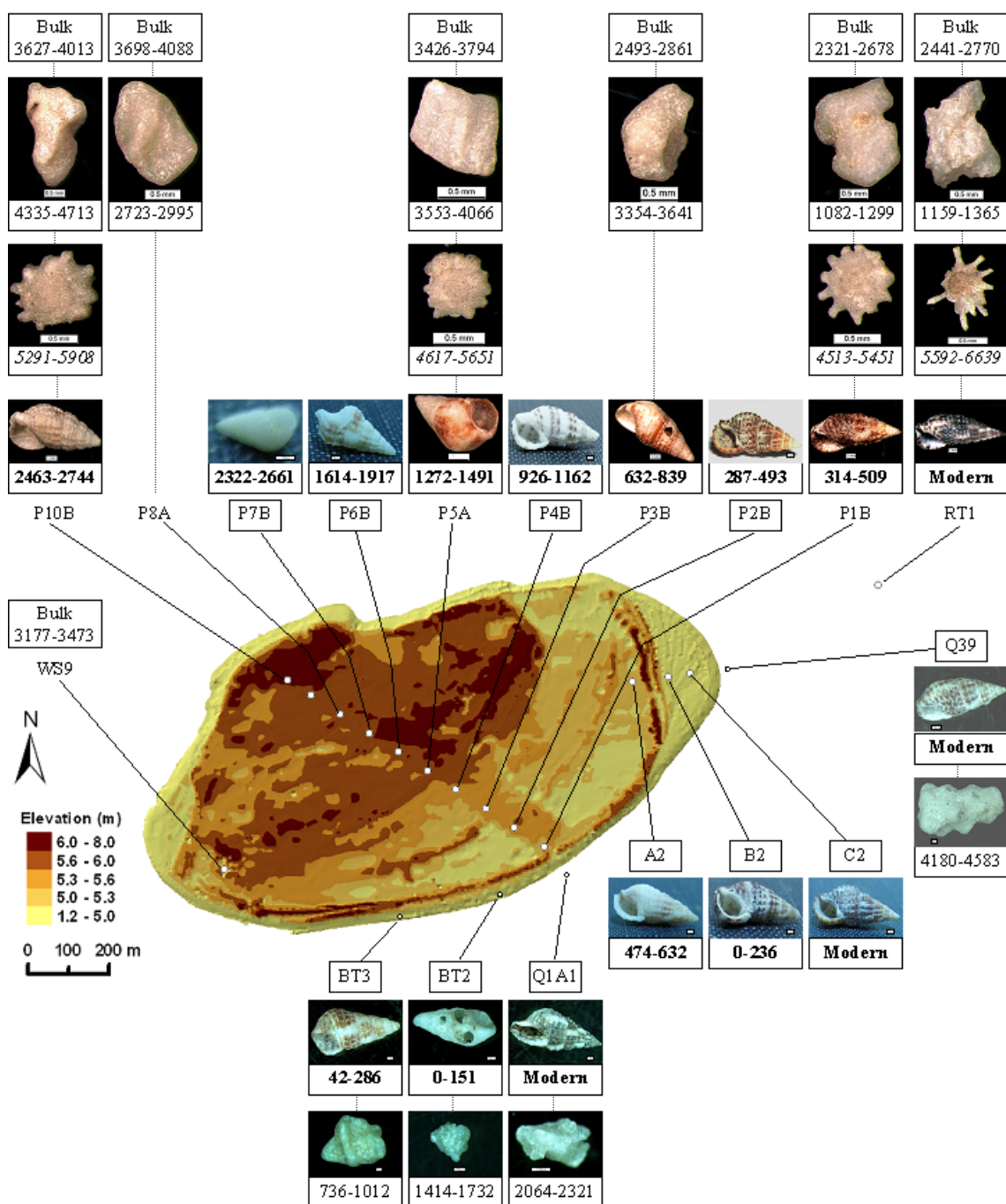
Figure 2.16. Dates of bulk samples (Bulk) from the island and the reef flat and 2 sets of AMS dates on individual grains of coral, foraminifera and shells chosen from bulk samples. All dates are reported with range of 2σ in years cal BP. AMS dates for the second phase are at locations of which names are not in a box (P10B, P8A, P5A, P3B, P1B and RT1) and AMS dates for the third phase are at locations of which names are in a box (P7B, P6B, P4B, P2B, A2, B2, C2, Q39, Q1A1, BT2 and BT3). Dates are in plain text for corals, in italic for foraminifera and in bold for shells. Note scale bar for coral and foraminifera 0.5 mm and for molluscs 1 mm.

71

Ages of coral grains were the least consistent in pattern. Samples of coral grains from P10, P5 and P3 are relatively old (older than the bulk date), whereas those from P8, P1 and RT1 are younger than the bulk date (Figure 2.16). As described above, coral sediments may be derived from the fossil reef flat. In addition, coral grains used for AMS dating are very small fragments, generally about 1 mm or less, meaning that they have gone through several stages of breakdown, requiring a longer period of transport and reworking than simpler, smaller grains derived from other material. Coral sediments currently are primarily derived from deeper areas of the reef flat along the reef rim (zones 3, 6, 8 and 9 in Figure 1.8) (Hart, 2003). Therefore, coral fragments, especially those produced from the live coral along the southeastern reef rim, may take a longer time to be deposited on the island. This implies that individual pieces of coral sand are a poor indicator of time of deposition.

In every case the age on shell is the youngest date for any sample. Components found at the same deposit can be reasonably assumed to be deposited at the same time and, within the same pit, the components having the youngest ages, which imply least time from death to deposition, would be most appropriate to represent time of deposition of islands. Therefore, gastropod shells which give the youngest dates would be the most appropriate component to provide the indication of time of deposition in this reef setting.

Short time interval between death and deposition, which is a required attribute for sediment components used as an indication of deposition, is attributable to fast rates of sediment transport or/and a short distance between sources of sediments and the island. Under the influence of extreme events, the transport rates are high and then sediments that are produced remotely from the island may also be transported to the island in the short time. However, in reef areas that are out of storm zones and where sediment

transport is principally under the influence of normal wave conditions, such as on Warraber Reef (Hart, 2003), the short distance is probably a more significant factor to minimise difference between time of death and that of deposition. This should be the case for shells of gastropods which currently live prolifically on the reef flat adjacent to Warraber Island. Therefore, compared to coral fragments and foraminiferal tests, gastropod shells likely take much less time to be transported from sources to the island.

Compared to other sediment components, gastropod shells also tend to be easier to be transported due to higher buoyancy caused by air trapped inside the chambers of the shells (Maiklem, 1968; Kench and McLean, 1996). In addition, the relative larger size of gastropod shells (Figure 2.16), meaning they protrude above the general level of the sediment, increases their mobility (Kench and McLean, 1996). Prager et al. (1996) also experimentally observed that the coarse fraction of naturally occurring carbonate sands moves before finer-grained components. Gastropod shells are relatively durable, compared to coralline algae, coral and *Halimeda* (Chave, 1964), allowing them to remain within beach deposits for a longer duration and in turn to have been preserved for dating.

It is important to emphasise that these samples were from pits, approximately 1-2 m below the surface, and whereas gastropod shells can be moved opportunistically by hermit crabs, this effect is likely to be minimised in these subsurface samples. In addition, selection of individual grains that looked fresh and little abraded minimised reworking and contamination, which means the date of death derived from radiocarbon dating is closest to that of deposition of the sediment and the ages derived from dating are more reliable. Therefore, it appears that ages derived from gastropod shells are the most appropriate indication of time of deposition within this reef setting. In other situations, however, other components may be more appropriate. For example, on

islands in Kiribati the prolific production of foraminifera on the reef flat immediately adjacent to the island makes them especially appropriate (Woodroffe and Morrison, 2001).

Shell ages indicate that the island began to form around 2,463-2,744 cal BP (P10B) on the northwestern corner of the island and has continually accreted with ages of around 314-509 cal BP (P1B) in the ridge on the modern shoreline and a modern age of the gastropod shell from the sediment collected from the reef flat. This modern age of the gastropod shell from the reef flat is in contrast to all other components within that reef flat sample. Although some time between death and deposition of shells seems highly probable, the sequence of shell ages across the island implies continual addition of sediment to the island. This is in contrast to the interpretation based on the bulk dates, indicating little or no sediment accretion since 2,000 cal BP.

The trend of island evolution implied by AMS dates during the second phase is further verified during the third phase of AMS dates across the island (P7B, P6B, P4B and P2B), and is supported by ages from the northeastern end of the island (A2, B2 and C2), on the southern beach (BT2 and BT3) and on the reef flat close to the island (Q39 and Q1A1) (Figure 2.16). Four AMS dates on shell samples from P7B, P6B, P4B and P2B are consistent with the pattern of sustained accretion of the island, derived from the AMS dates on shells during the second phase (Figure 2.16). The appropriateness of shell grains as an indication of time of deposition is also supported by very young ages of shell grains from the modern beach (BT2: 0-151 and BT3: 42-286 cal BP) and modern ages of shell grains from the reef flat adjacent to the beach toe (Q1A1: Modern and Q39: Modern). On the other hand, dates on coral grains from these locations are anomalously older (BT2: 1,414-1,732, BT3: 736-1,012, Q1A1: 2,064-2,321 and Q39: 4,180-4,583 cal BP) and imply unrealistic and inconsistent patterns of island formation.

74

Ages of shells from the low spit at the northeastern end of the island are consistent with progressive accretion across this area (A2: 474-632, B2: 0-236 and C2: Modern cal BP). This continuous accretion is in agreement with the pattern of active progradation of this area, which can be observed from historical aerial photographs that are presented in the next chapter. The dates on shells at P1B (314-509 cal BP) and A2 (474-632 cal BP) from different locations but at a similar distance behind the same set of beach ridges are not statistically significantly different, supporting the idea that ridges mark former shorelines, and of using beach ridges to define the spatial boundaries of island evolution.

On the inner shelf of the northern Great Barrier Reef dating results from bulk sand samples were reported from sand cays which have similar topography to that of Warraber Island (Stoddart et al., 1978b). The sand cays exhibit two distinct levels, called the high terrace, which is the main part of the islands, and the low terrace, which fronts the high terrace (McLean et al., 1978). Dating on bulk samples from these two distinct levels indicated that the high terrace was generally inferred to have been older than the lower one.

However, they indicated the clustering of dates for the two terraces and no dates younger than 2,000 years BP (Stoddart et al., 1978b). As stated before, dates indicate time of death of sediment-contributing organisms and deposition may have occurred sometimes thereafter. Therefore, the sand cays formed from sediments produced episodically. If applied to describe the evolution of the islands, the youngest age derived from the low terrace can imply that the island accumulation has been inactive since 2,000 years BP which is similar to that of Warraber Island if ages derived from bulk sand samples were applied.

Stoddart et al. (1978b) reported that the low terraces on at least two islands where sediment ages are greater than 2,000 years BP appeared to have formed in large part since 1936. McLean et al. (1978) also strongly suggested that a lack of sediments younger than 2,000 years BP from the low terraces is the result of sources of sediments for the low-terrace formation, which are the reworking of the older cay sands. The reworking of older sediments is also indicated by evidence from one of unvegetated and ephemeral sand cays which are normally thought that they are very young but dating on a bulk sand sample implied that it formed before 2,000 years BP (McLean et al., 1978). On a number of islands on the Great Barrier Reef sediment ages younger than 2,000 years BP are only derived from dating on gravels from unconsolidated storm-deposited banded shingle ridges (Stoddart et al., 1978b). This evidence emphasises that in several cases bulk dates are less reliable than individual grains if right components can be identified to interpret the evolution of island morphology.

In summary, bulk dates in general are likely unreliable for determining chronology of island evolution due to including various types of sediments, some of which may have been reworked and redeposited for considerable time before being incorporated into the island. Gastropod shells appear most appropriate to indicate time of deposition in this reef setting because they are the youngest constituents within the sand samples, live prolifically adjacent to the island, tend to be more amenable to entrainment and transport to the island due to their higher buoyancy and larger size, and relative durability. Ages derived from the gastropod shells imply that the island started to form approximately 2,700 years ago and has continually prograded since. This sequence of ages will be used to reconstruct the morphological evolution of the island in the next section.

2.4.3. Reconstruction of Morphological Evolution

The island appears to have experienced continual accretion over the period of island evolution although the sequence of ridges implies periodic stability interspersed with renewed accretion. However, phases of island evolution are used in this section in order that rates of progradation and volumetric changes can be calculated. The spatial boundary for each phase of island evolution, as described in Section 2.4.1 and associated dates for each phase of island evolution derived from AMS dates on shell in Section 2.4.2 are used to reconstruct morphological evolution of the island. Accordingly, five phases were identified based on morphology and are illustrated in Figure 2.17.
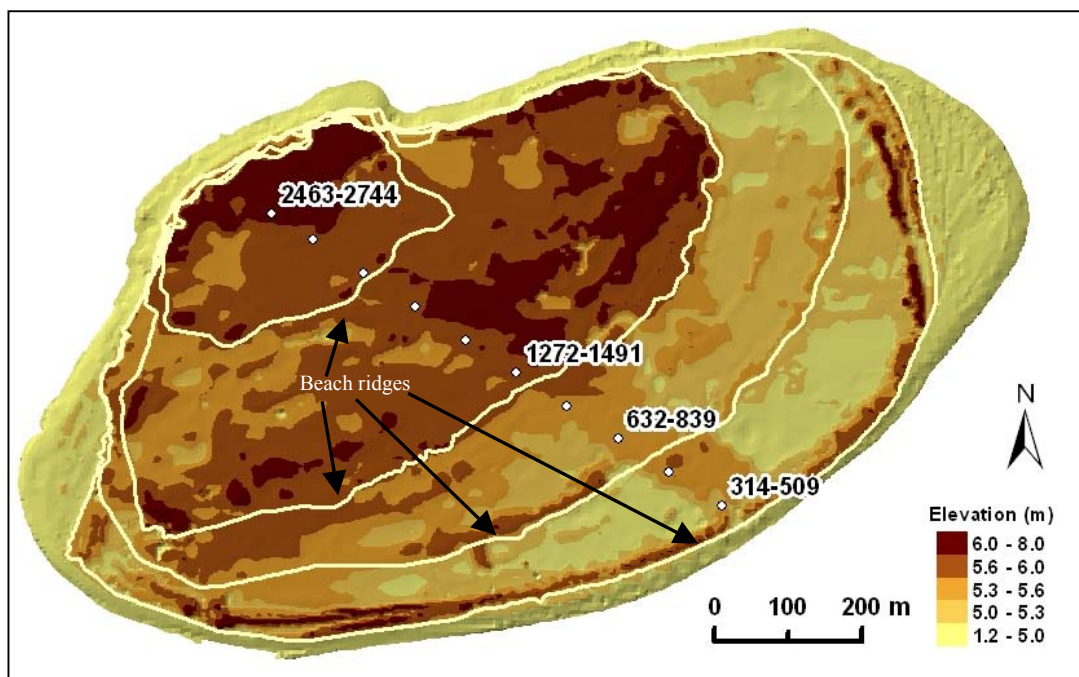
Figure 2.17. Island topography in 1998 with five phases of the island evolution, defined according to location of prominent beach ridges with inferred ages based on interpretation of AMS dates on shells. Note unit = years cal BP.

To reconstruct the island topography in the past, the topographical model (DTM) of the island was separated into: i) the upper surface of the island; and ii) the beach area which runs around the perimeter of the island (Figure 2.18).
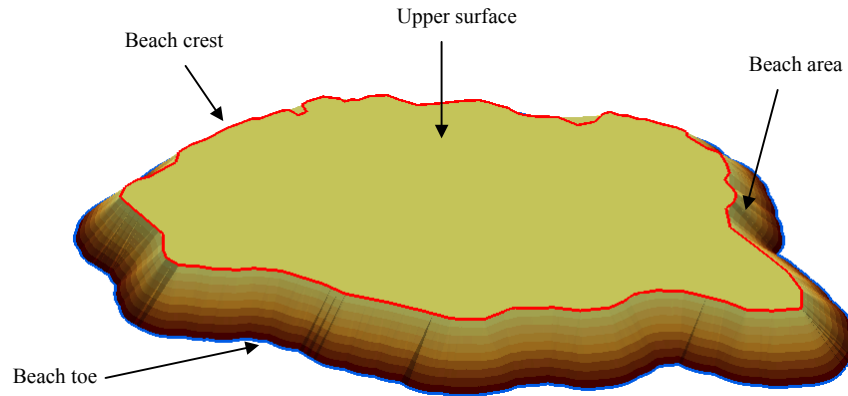
Figure 2.18. Topographical model of the island.

The beach crest was determined where the beach met the upper surface of the island and the beach toe where the beach met the reef flat. It was assumed that over periods of evolution the elevations of the upper surface of the island have remained unchanged and that the island has prograded horizontally in the directions indicated by the radiocarbon dating and the beach ridges. Therefore, the present topographical data corresponding to each phase of island development were employed to create the upper surface of the island at that period.

In spite of the fact that the topography of the past beach area is unknown, former beach area can be approximated by linking the coordinates of the known beach crest to the estimated beach toe. The beach crest at each time interval was determined from the morphology of beach ridges and created as a polygon. The x and y coordinates of the beach toe were calculated using: i) the difference of z between the beach crest and the reef flat at the same position (x and y); and ii) the typical slope of the beach (Figure

78

2.19). The typical slope of the beach is the averaged slope of the present beach profiles (Figure 2.13) and equals to 1/8.
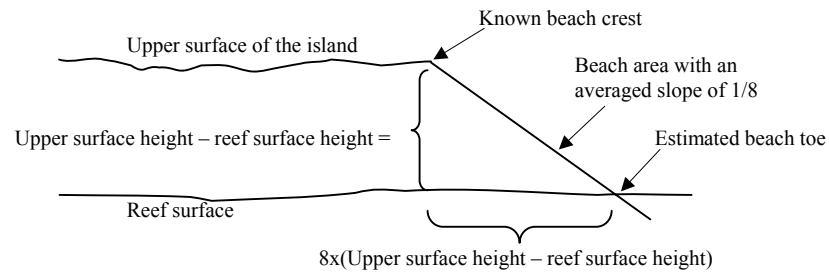
Figure 2.19. Derivation of beach toe positions.

The polygon for each time period, indicated by white lines in Figure 2.17, was created and used as a beach crest. The polygon of the beach crest was converted to a 3D polygon using "convert feature to 3D" in the 3D Analyst extension, with its z values derived from elevations of the island surface. The polygon of the 3D beach crest was also used to select the point data for constructing the final TIN of the island surface at each time interval. The buffer of 2.5 m on both sides of the beach crest was created and used as the mask for calculating the difference of z value between the beach crest and the reef flat at the same position for computing the positions of the corresponding beach toe. Using the average slope of 1/8, the polygon of the beach toe was defined.

To ensure that the island was placed on the reef flat, the z values of the beach toe were assigned from those of the reef flat at the same coordinates, using "convert feature to 3D" in the 3D Analyst extension. A polygon of the beach toe and beach crest, and the point data of the upper surface enabled construction of a TIN of the island surface at each period of evolution (Figure 2.20).

According to Figure 2.20, the island started to form from the northwestern end of the island around 2,700 years ago. Since then, its progradation has expanded
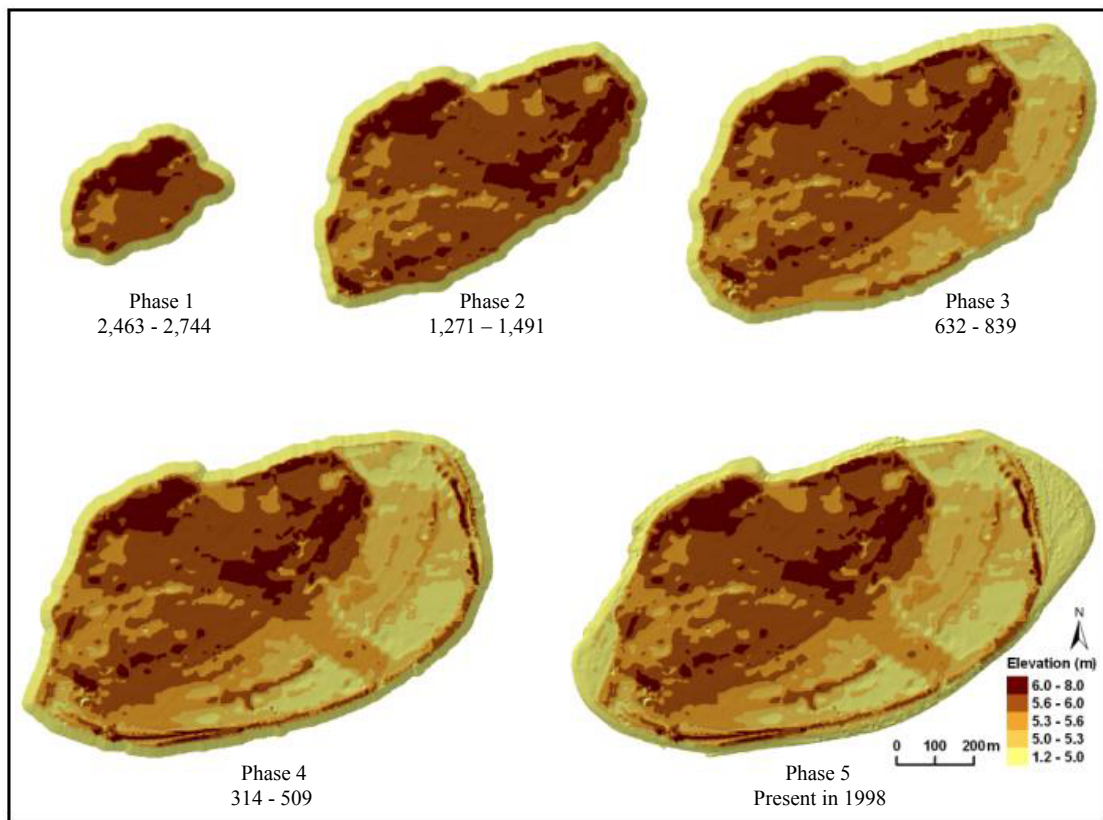
Figure 2.20. Morphological evolution of Warraber Island over the Holocene, identified into five phases. Note unit = years cal BP.

horizontally mainly within an E-S sector with successive beach ridges. During the first one thousand year (phases 1 and 2), an averaged elevation of the island was around 6 m. After that the averaged elevation was reduced to approximately 5 m (phases 3 and 4). During the last 500 years when the continued accretion has mostly occurred on the northeastern and southwestern ends of the island (phase 5), an averaged elevation on both ends has been slightly less than 5 m.

A similar pattern of topographical development was described on sand cays of the inner shelf of the northern Great Barrier Reef (McLean et al., 1978). As describe above, the sand cays of the inner shelf of the northern Great Barrier Reef are mainly characterised by two distinct levels, the older high terrace and the younger low terrace. Differences in elevation between those two levels are around 1.1-3.3 m. McLean et al.

(1978) suggested that the high terrace had formed as a result of wave action not as dunes originated by wind, according to the evidence of weathered drift pumice in surface soil and lens of unweathered pumice at the shallow depth. A thick layer of pumice was also observed at a depth of about 20 cm throughout the higher area of Warraber Island (phases 1 and 2 in Figure 2.20) (Rasmussen and Hopley, 1996), indicating that waves are the primary influence on evolution of Warraber Island.

It has been suggested that variations of sand-cay topography are related to the magnitude of wave run-up which determines the maximum height on a beach, to which sediment can be transported and at which a beach berm normally forms (Stoddart, 1964; Hopley, 1992). McLean et al. (1978) also suggested that differing levels between the high and low terraces on sand cays on the northern Great Barrier Reef are associated with the changing magnitude of wave run-up. The influence of wave action on topographical evolution of Warraber Island will be discussed in Chapter 6, in conjunction with probable wave characteristics during island evolution, assessed from the contemporary wave characteristics analysed in Chapter 5.

2.4.4. Rates of Progradation and Associated Volumetric Changes

Figure 2.21 illustrates patterns of island progradation along the transect across the pits, based on surveyed distance from P10 to other pits and dates on bulk samples and the AMS dates on coral, foraminifera and shell grains. A linear rate of island progradation, based on shell dates, was calculated (a dashed line in Figure 2.21).

According to dates on shell grains, island accumulation commenced around 2,700 years ago and continues until the present along the pit transect with an average linear
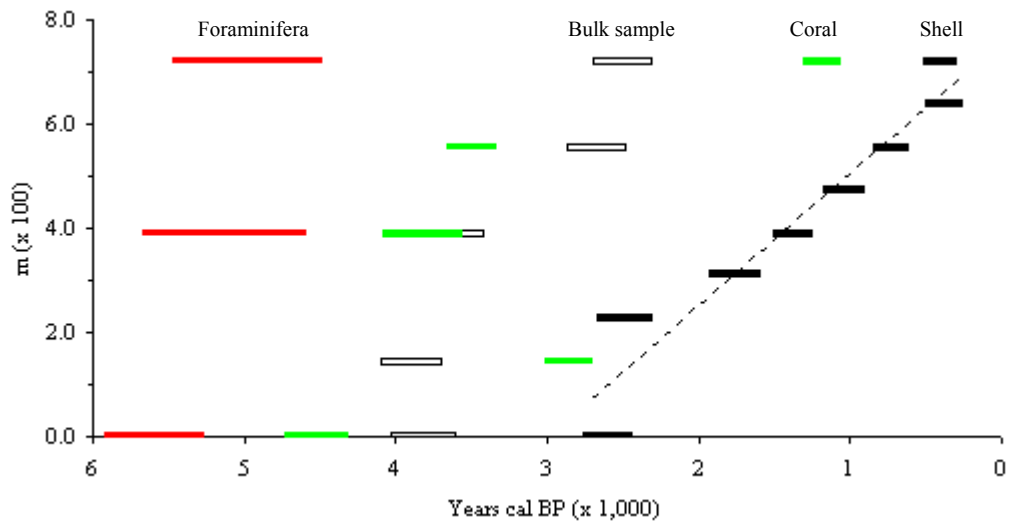
Figure 2.21. Progradation of Warraber Island over the Holocene, based on bulk sand samples and three individual components of coral, foraminifera, and shell. A dashed line represent a linear rate of island progradation which is approximately 0.25 m/yr, based on shell grains.

rate of approximately 0.3 m/yr. This relative rapid rate of progradation implies that deposition and burial is likely relatively soon after death of gastropods.

The volume associated with each phase of island progradation was calculated following a procedure summarised in Figure 2.22. Basically, the volume of the island at each time interval was calculated between the island topography and reef-flat areas overlain by that island topography. The derivation of the surface of the reef was already described in Section 2.2.2 and the island topography at each time interval was already constructed in Section 2.4.3. According to the procedure in Figure 2.22, the next step is to define the reef-flat surface corresponding to phases of the island growth.

The polygons of the beach toe were used to create the associated reef-flat surface. Using the same polygon of the beach toe to create the reef-flat surface assured that the volume of the island was exactly the volume between the island surface and the reef flat. Finally, using the 3D Analyst extension, the volume of the island at each time interval was obtained by subtracting the volume of the reef-flat surface from that of the island surface, both computed over the same plane. The area of the island at each time

82
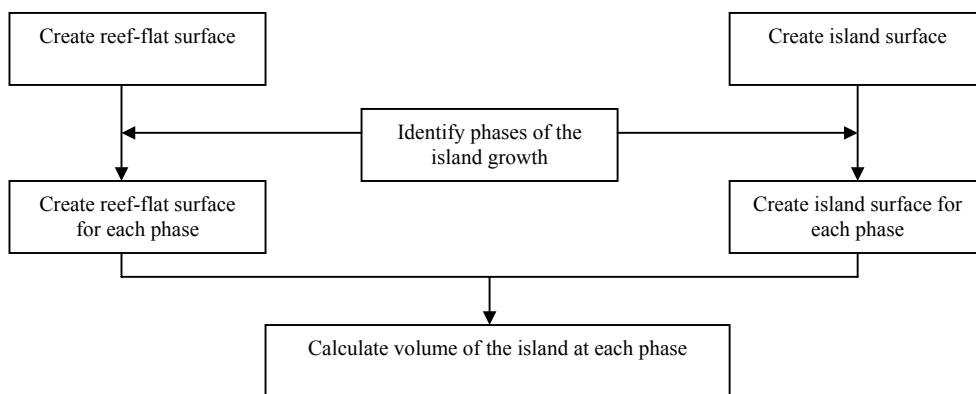
Figure 2.22. Procedure adopted to obtain the volume of the reef island.

interval was also estimated. Table 2.4 shows the estimated volume and area of Warraber Island over a geological time scale and Figure 2.23 illustrates the volumetric change associated with each phase of the island formation, determined based on dates of shell samples. Figure 2.23 also shows the depositional history of the island, based on dates on bulk sand samples and three individual components of coral, foraminifera and shell.

In Figure 2.23, it is obvious that on this island the interpretation based on different individual components of sediment samples gives rise to different patterns of depositional history. Based on the criteria described above, the depositional chronology of the island appears most appropriately derived from the ages of shells. The volume of the island was at least 370,000 m^3 around 2,700 cal BP and appears to have increased continually with a long-term rate of approximately 900 m^3/y, based on the regression line of the shell samples shown in Figure 2.23. The volume of the island in 1998 was over 2,600,000 m^3.

Table 2.4 Volume and area of Warraber Island, based on dates of shell samples

Period (years cal BP, 2σ)	Volume (m^3)	Area (m^2)
2,463 – 2,744	369,841	110,674
1,272 – 1,491	1,384,241	394,144
632 - 839	2,004,428	593,704
314 - 509	2,537,026	772,361
-48 (1998)	2,653,642	813,829
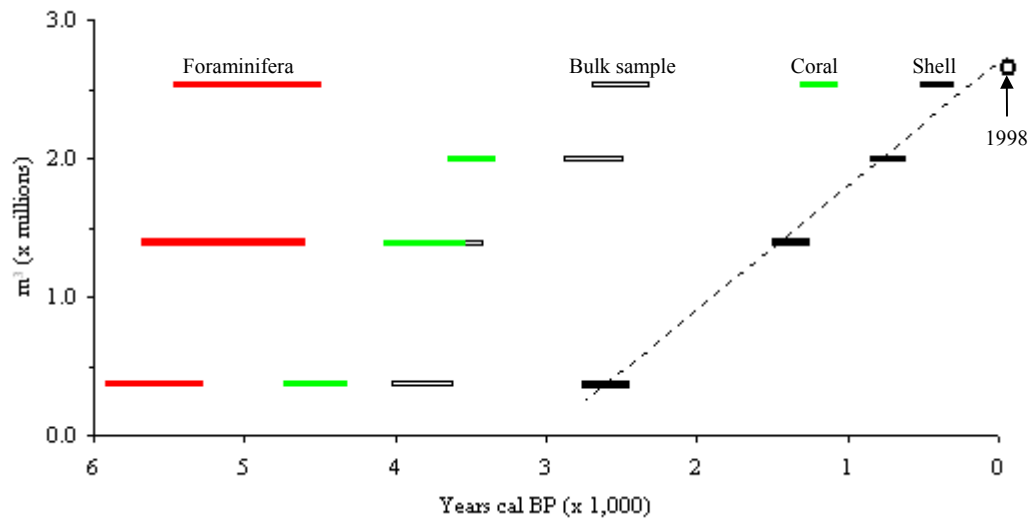
Figure 2.23. Volumetric changes of Warraber Island over the Holocene, based on bulk samples and three individual components of coral, foraminifera and shell samples. A dashed line represents a linear rate of island accumulation which is approximately 900m^3/yr, based on shell grains.

The uncertainty associated with the volume calculation, introduced by the technique applied in Section 2.4.3 for creating the island morphology in the past, was investigated. Two surfaces of the island in 1998 were compared: i) the DTM of the island topography, constructed using present topographical data in 1998 (Section 2.3); and ii) the DTM of the island topography, created following the technique applied for reconstructing the island morphology in the past (Section 2.4.3). Table 2.5 summarises the result of the comparison.

Table 2.5 Uncertainty introduced by the technique applied to construct the past morphology

Base height	Volume (m^3)		Volume difference	
	1998	Calculated 1998	(m^3)	(%)
Reef flat	2,653,642	2,668,990	15,348	0.58

It can be seen from Table 2.5 that the volume calculated from the island DTM generated based on the technique developed in section 2.4.3 is only about 0.6% greater than that calculated from the island DTM constructed from the 1998 topographical data. Therefore, the technique in section 2.4.3 developed for construction of the past island

84

morphology for the reef-island evolution study appears suitable for this reef-island environment.

It should be noted that the depositional rate of approximately 900 m^3/y is calculated based on the volumetric estimates for five phases of island evolution. However, the volumetric estimates do not allow for erosion of the shoreline. At present the extensive outcrops of beachrock are present along the north shore, especially part of the phases 1 and 2 of island evolution, indicating past erosion on this area of the island. Phases of erosion may be also represented by the truncation of individual ridges, especially at their eastern and westernmost points. Rasmussen and Hopley (1996) suggested that Warraber Island was larger over each phase of evolution (Figure 1.6). This uncertainty affects estimation of the depositional rate.

However, the spatial extent for each phase of evolution was determined with reasonable accuracy due to using the high-resolution DTM of the island. In addition, the temporal extent for each phase of island evolution is reliable due to being determined using specific sediment components appropriate for this reef setting. Therefore, the rate of 900 m^3/y reasonably represents the approximate long-term rate of sediment supply to the island. However, over shorter periods in between, fluctuations in depositional rates (higher or lower than 900 m^3/y) can be anticipated. The fluctuation in rates of accretion over past decades will be examined in the next chapter.

2.5. Summary

The morphological evolution of Warraber Island over past millennia (geological time scale) is examined in this chapter, based to a large extent on detailed radiocarbon dating, field observations and morphological reconstruction using DTM. Warraber

Island is a small, vegetated sand cay located towards the western end of Warraber Reef, of which a majority of the reef flat reached the present level by 5,000 years ago. The reconstruction of its depositional history was approached in four steps: i) determination of spatial patterns of evolution; ii) determination of temporal patterns of evolution; iii) reconstruction of morphological evolution; and iv) estimate of progradational rates and associated volumetric changes.

The spatial boundaries of island evolution were primarily determined from the outlines of prominent beach ridges that could be identified on the DTM of the island topography. Accordingly, five phases of island evolution over the Holocene were specified. The temporal patterns of island evolution were assessed in three phases, based mainly on radiocarbon dating on sand samples collected at depths between 1 and 2 m below the surface from 10 pits across the island.

The first phase of dates on bulk sand samples, undertaken by Woodroffe (2000), suggested a relatively discrete episode of evolution followed by steady state. However, older dates on bulk sand samples collected on the reef flat close to the island, which were expected to be very young or modern, suggested the bulk dates might be unreliable as an indication of time of deposition of the island.

AMS dates on individual grains of coral, foraminifera and shell samples during the second phase indicate patterns of island evolution different from that based on bulk dates and also reveal the discrepancy of age determination between different components of sediment samples. The most appropriate sediment for representing time of deposition should be that deposited in shortest time after death. Gastropod shells are the most appropriate indication of time of deposition in this reef environment because they gives youngest age within the same pit, has been prolific on the reef flat around the island, have higher transportability and are durable. Instead of a relatively discrete

episode of evolution followed by steady state, as previously proposed by Woodroffe (2000), the second phase of dating implies that the island appears to have been accreted as a result of continuing supply of sediment. This revised chronology of island evolution is also verified by the AMS dates during the third phase.

Accordingly, during the late Holocene, the island has primarily built horizontally towards the south and east, starting from the oldest part at the northwestern corner of the island which appears to have been in place by 2,700 years ago. The average elevation of the island was around 6 m by 1,500 years ago and was reduced to around 5 m thereafter. The average elevation was slightly less than 5 m over the past 500 years. The estimated volume of the island 2,700 years ago was at least 370,000 m^3 and by 1998 it had reached about 2,700,000 m^3. The volumetric analysis indicates that the island has continually accumulated with a long-term rate of approximately 900 m^3/y over the past 2,700 years.

CHAPTER 3

CHANGES IN WARRABER-ISLAND SHORE OVER PAST DECADES

(ENGINEERING TIME SCALE)

3.1. Introduction

As discussed in Chapter 1, changes in coastal landforms can occurred at different time scales. In Chapter 2, a broad pattern of morphological evolution of Warraber Island over the past 3,000 years was identified. In this chapter, more detail of change in Warraber-Island shore is examined over past decades, based mainly on data from aerial photographs and a field survey. In Section 3.2, shoreline changes are described based on a comparison of island shoreline digitised from aerial photographs and field surveys. In Section 3.3, the topography of island shore is reconstructed using a DTM, and, in Section 3.4, associated volumes are estimated.

3.2. Changes in Island Shoreline

The essential data for this part of the study were obtained from aerial photographs and topographical surveys of beach areas. The aerial photographs are those taken in 1966, 1974, 1981, 1987 and 1998. The elevations of the beach and surrounding reef-flat areas were surveyed during fieldwork in November 2004, using a total station based on ground control points derived from data surveyed by the mapping and consulting company, named Schlencker Mapping Pty Ltd.

Steps to delineate the island shoreline from the aerial photographs involve scanning and georeferencing the aerial photographs, and on-screen digitising the

shoreline of the island from the georeferenced aerial photographs. The georeferenced aerial photographs provide the basis for assessing changes of the shoreline of the island and assessing to what extent the geomorphological trends identified over geological time scales can be detailed at decadal (engineering) time scales.

Contact prints of the aerial photographs were scanned, except that taken in 1966 which was only available in xerographic copy. Details of the aerial photographs and scanning results are given in Table 3.1.

Table 3.1 Details of aerial photographs and scanning results, Warraber Island: 1966 – 1998.

Date	Photo scale	Scan resolution (dpi)	Pixel size (m)	RMSE (m)
18/07/1966	1:48,000	1,200	1.0	-
26/03/1974	1:10,000	1,200	0.2	2.7
02/08/1981	1:13,000	1,200	0.3	0.6
26/11/1987(east)	1:5,000	600	0.2	3.12
26/11/1987(west)	1:5,000	600	0.2	2.74
09/09/1998(183)	1:4,000	600	0.2	0.7
09/09/1998(184)	1:4,000	600	0.2	1.78
09/09/1998(185)	1:4,000	600	0.2	2.66
09/09/1998(186)	1:4,000	600	0.2	1.78
09/09/1998(187)	1:4,000	600	0.2	2.68

The aerial photographs were georeferenced to minimise distortion and subsequent measurement error. The georeferencing step was conducted in ArcMap using the Georeferencing Extension. The main source of ground control points for georeferencing aerial photographs were obtained in consultation with Schlencker Mapping from the planimetric map photogrammetrically derived from 1998 aerial photographs. This planimetric map was originally in AMG86 but was transformed to MGA94. Within the settlement, corners of roads were used as ground control points, and prominent structures along the airstrip were also employed. In the wooded parts of the island remote from the settlement, however, it is hard to find prominent features to use as ground control points. On the older aerial photographs of Warraber Island, trees

or other available features that can be seen on both historical and 1998 aerial photographs are essential and have been used as ground control points.

The 1998 aerial photographs were first georeferenced and subsequently the historical aerial photographs were georeferenced to the planimetric map and the 1998 georeferenced aerial photographs. The two photographs in 1987 and five photographs in 1998 (Table 3.1) were separately georeferenced and then mosaiced into a single image. The root mean square errors (RMSE) produced during georeferencing are generally less than 3.0 m (Table 3.1). It was also found that the locations of beachrock outcrops along the southeast, southwest, west and north of the island, visible in all photographs but not used as ground control points, agree well between the photographs, with estimate error of ±1 m. The final product of georeferenced aerial photographs is shown in Figure 3.1.

On an aerial photograph, shoreline position is commonly mapped using a proxy such as high water line for planar shorelines, or the landwardmost edge of the bluff top or cliff top for high bluffs and cliffed shorelines (Crowell et al., 1991). In this study, in order to calculate the volume of the island, the position of the beach toe was mapped, as an alternative. The beach toe is clearly visible on the aerial photographs and represents the intersection of the island with the reef-flat surface which is generally of known elevation. An effort was made to minimise the error in measurement of the beach toes by locating ground control points around the perimeter of the island, as close to the beach toe as possible.

More effort was required to map the beach toe from the 1966 aerial photograph because only hard copy format was available, and the scale of 1:48,000. Typically, a scale 1:20,000 of aerial photograph is considered as the smallest scale that should be used for mapping a shoreline (Moore, 2000). However, the significance of the 1966

Figure 3.1. Georeferenced aerial photographs, Warraber Island: 1966-1998.

photograph in relation to island change made it appropriate to use what was available. The beach toes were digitised on-screen. Figure 3.2 illustrates the shoreline of the island at each time slice, according to the positions of the beach toe derived from the aerial photographs, together with the beach toe obtained from the field survey in November 2004 obtained using a total station.
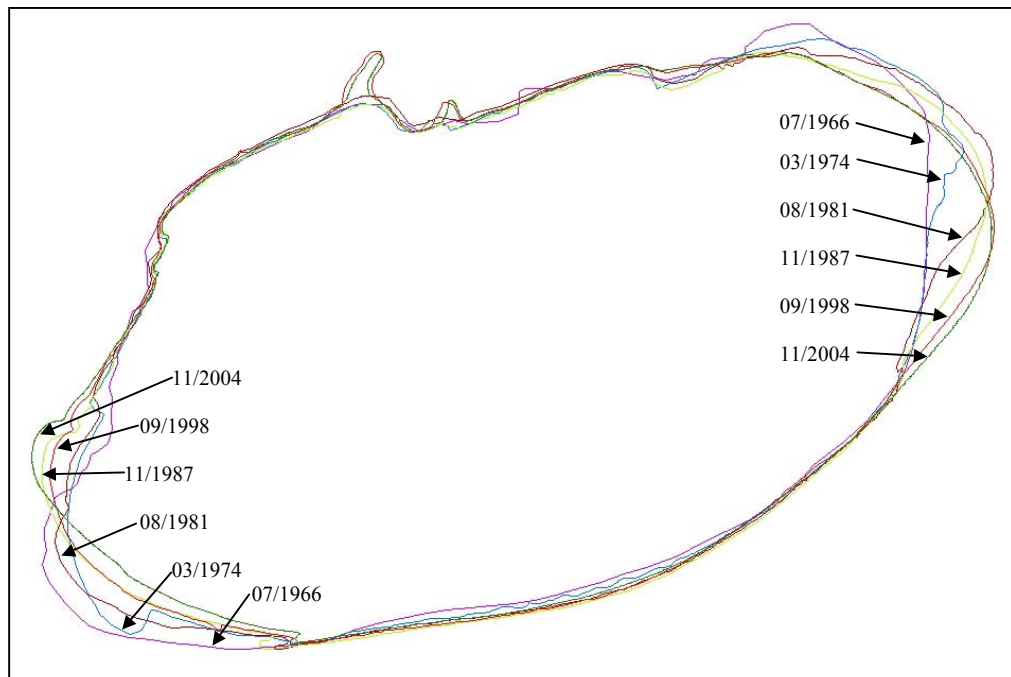
Figure 3.2. Change in shoreline of the island between 1966 and 2004.

It was obvious from a comparison of the digitised island shoreline (Figure 3.2) that, during 1966–2004, significant change has occurred only on the northeastern and southwestern ends of the island in association with sand spits whereas a major part of the island has remained relatively stable, particularly on the northern side of the island which has been fixed by outcrops of beachrock. The comparison suggests that sand spits at both ends of the island have moved in the clockwise direction. As shown In Figure 2.16, the sequence of dates on shells on the northeastern end indicates the continuous addition of sediments on this part of the island (B2:0-236 years cal BP and C2: modern cal BP). This depositional pattern is in agreement with the temporal increase in island size on this part of the island, which was demonstrated in Figure 3.2.

Shoreline changes in association with the movement of sand spits at the ends of sand cays, similar to that observed on Warraber Island (Figure 3.2), have been commonly noted over past decades on sand cays on the Great Barrier Reef (Flood,

1977; Stoddart et al., 1978a; Hopley, 1982; Flood, 1983; 1986; Flood and Heatwole, 1986; Frank and Jell, 2006). Such changes on sand-cay shorelines with the sustained pattern of sand-spit movement over the past decades have been generally suggested to respond to changing patterns of waves on platform reefs due primarily to long-term wind patterns (Flood, 1983; 1986; Flood and Heatwole, 1986). A preliminary investigation of change of Warraber shorelines between 1966 and 1987 by Rasmussen and Hopley (1996) suggested that the rotation of the island in a clockwise direction is attributed to an increase in southerly winds in the region, occurring somewhere between 1975 and 1977. Probable causes of this clockwise movement will be discussed in Chapter 6 in relation to medium-term wind patterns, identified in Chapter 4, wave conditions on the reef, examined in Chapter 5, and the effect of nearby reefs on wave fields moving towards Warraber Reef.

Seasonal patterns of sediment transport around the island were investigated by Hart (2003). However, island shape in response to seasonal influence has not been shown. Probable shape of island in response to seasonal influence will be described in Chapter 6 in relation to wind climate reconstructed in Chapter 4 and associated patterns of sediment transport investigated by Hart (2003).

3.3. Reconstruction of Island-Shore Topography

To calculate the volume associated with the island changes identified in Section 3.2, the DTM of island shore is required. It was clearly shown in Figure 3.2 that only the northeastern and southwestern ends of the island have changed significantly over the past 40 years. The reconstruction of the DTM of the island shore over the past 40 years, therefore, focused only on these two sand spits. A similar approach (Section 2.4.3) and a

topographical model of the island (Figure 2.18) to those previously used for the morphological study over a geological time scale were applied in this chapter to generate the DTM of island shore.

The elevations on the sand spits in 1998 were known. It was assumed that the topography of the upper surface of these parts of the island remained stable and that the island has only been mobilised horizontally. Consequently, the averaged height in these areas derived statistically from 1998 data was used as the elevations of the sand spits in the past. In the same manner as reconstructing the surface of the island over the geological time scale, the historical beach crests were digitised to define the crests of the spits while the island shoreline derived in the previous section was used as the beach toe. The z values of the beach toe were obtained from the reef-flat surface. The z values of the beach crest were assigned using the averaged elevation (4.8 m for the southwest spit and 4.6 m for the northeast spit). Thus, the DTMs of the sand spits were created from 3D polygons of beach crest and beach toe. The DTM of the reef-flat surface corresponding to the spit surface was also created using reef-flat point data as mass point and 3D beach toes as a hard clip. In the same way, the point data of the island and the beach toe were used to construct a DTM of the 1998 spit surface. Eventually, the volume of the sand spits was calculated.

During fieldwork in 2004, the island topography was surveyed using a total station. Beach and surrounding reef-flat areas only were surveyed due to limited duration of exposure at low tide (occurring in early morning and late afternoon). Figure 3.3 shows the spot heights measured using a total station over the survey areas, overlying the 1998 aerial photographs.

Figure 3.3. Spot heights (black dots) on the beach and the surrounding reef flat, measured using a total station.

Northern and northwestern shores were not surveyed because they have a stable configuration, largely dominated by outcrops of beachrock backed by a seawall. Ground control points derived from Schlencker Mapping data were used to start the topographical survey. The total station was generally set up on the reef flat at some distance from the shore and readings taken to the reflector at successive positions on the beach and the adjacent reef flat.

The basic concept of the survey, undertaken with tides exerting a time constraint, was to focus mainly on capturing prominent features. These included beach crests, beach scarps and beach toes, with fewer data points recorded in between for straight beach segments, such as along the southern shoreline, but with more data points for convex beach profiles at the western and eastern ends of the island. This pattern of elevation measurement is appropriate and can give accurate results, particularly, for the DTM construction in a TIN. Under the same assumption that the upper surface of the island topography has remained the same over the period of study, data for the upper

surface of the 2004 topography can be obtained from regularly spaced point data of the 1998 topography, derived from Section 2.3. In summary, data for the 2004 DTM of island topography consist of data from the total station for beach areas and data from the 1998 topography for the upper surface of the island.

The data from the total station were converted to point shapefiles. Figure 3.4 shows the advantage of using additional data of breaklines to capture detail of beach topography.
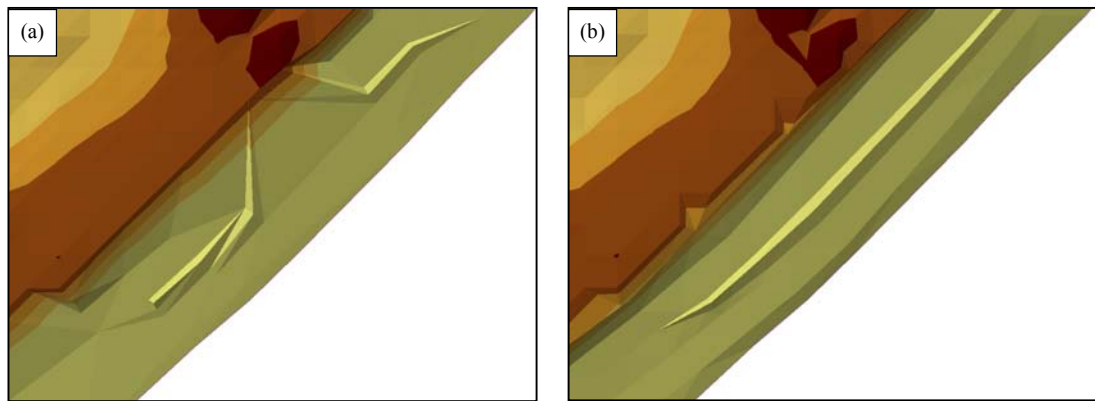
Figure 3.4. DTM generation of the beach areas with a sand ridge: a) using only spot heights; and b) using both spot height and breaklines.

A DTM that is constructed from the original, surveyed spot heights exhibits a spiked surface due to no control breaklines for areas of discontinuity (Figure 3.4a). Breaklines have to be generated from some of the surveyed point data in order to emphasise the prominent features such as beach crests, beach ridges, scarp bases and beach toes, in order for the final DTM to closely represent the actual topography. In Figure 3.4b, for example, a beach with a steep scarp and a sand ridge developed behind beachrock was better represented in a DTM by adding breaklines. In addition, breaklines of the beach areas were created also from surveyed data on the beach in order to control the topography of the beach to follow the pattern of change along the island.

The final DTM of the island topography in 2004 is therefore generated from the spot heights and breaklines for the beach areas and regular point data for the upper surface (Figure 3.5). No linear or quintic interpolation was carried out on the DTM created from the spot height and breaklines because the data were surveyed on purpose and capture the prominent features of the beach areas, existing on the island.
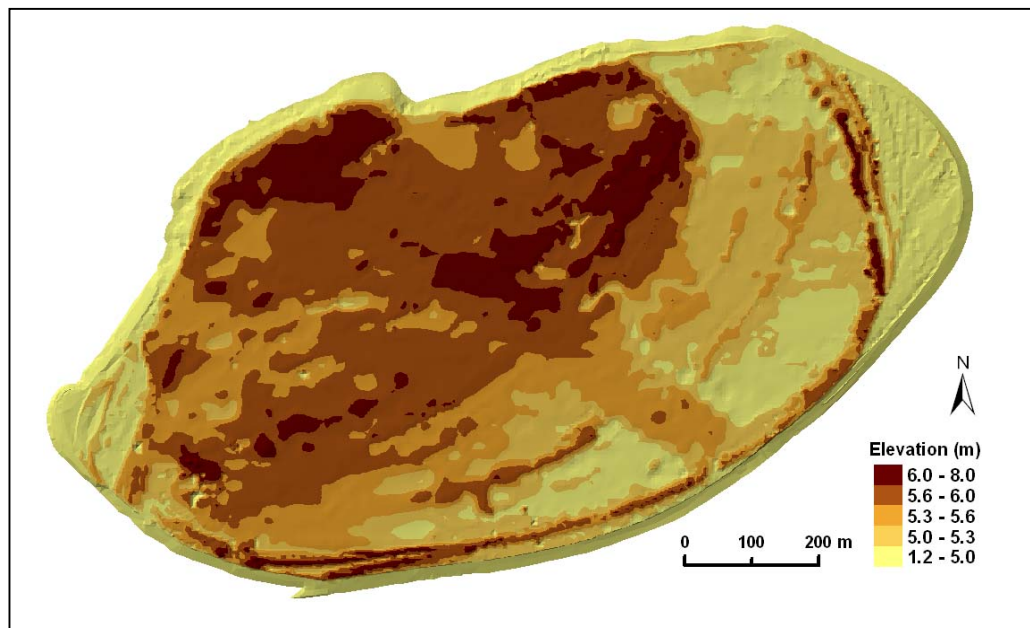
Figure 3.5. Topography of Warraber Island, 11/2004.

3.4. Associated Volumetric Changes

The depositional patterns over the period 1966-2004 are illustrated in Table 3.2 and Figure 3.6a for the northeastern end, and in Table 3.3 and Figure 3.6b for the southwestern end. The total volumetric changes of the island shore over the period 1966-2004 are presented in Table 3.4, based on the sum of the sediment volume of both ends.

Table 3.2 Depositional pattern of Warraber Island between 1966 and 2004 on the NE end.

Period	Volume (m³)	Volumetric change (m³)	Rate of change (m³/y)
1966	44,236	-	-
1974	53,102	8,866	1,108
1981	63,969	10,868	1,553
1987	66,218	2,249	375
1998	67,486	1,268	115
2004	67,098	-388	-65
SUM 1966-2004		22,863 (gain)	
SUM 1974-2004		13,997 (gain)	

Table 3.3 Depositional pattern of Warraber Island between 1966 and 2004 on the SW end.

Period	Volume (m³)	Volumetric change (m³)	Rate of change (m³/y)
1966	79,704	-	
1974	44,585	-35,119	-4,390
1981	49,661	5,076	725
1987	49,993	332	55
1998	38,439	-11,555	-1,050
2004	38,372	-67	-11
SUM 1966-2004		-41,333 (lost)	
SUM 1974-2004		-6,214 (lost)	

Table 3.4 Depositional pattern of the island shore between 1966 and 2004, based on the sum of the sediment volume of both ends.

Period	Volume (m³)	Volumetric change (m³)	Rate of change (m³/y)
1966	123,940	-	
1974	97,687	-26,253	-3,282
1981	113,630	15,943	2,278
1987	116,211	2,581	430
1998	105,925	-10,286	-935
2004	105,470	-455	-76
SUM 1966-2004		-18,470 (lost)	
SUM 1974-2004		7,783 (gain)	
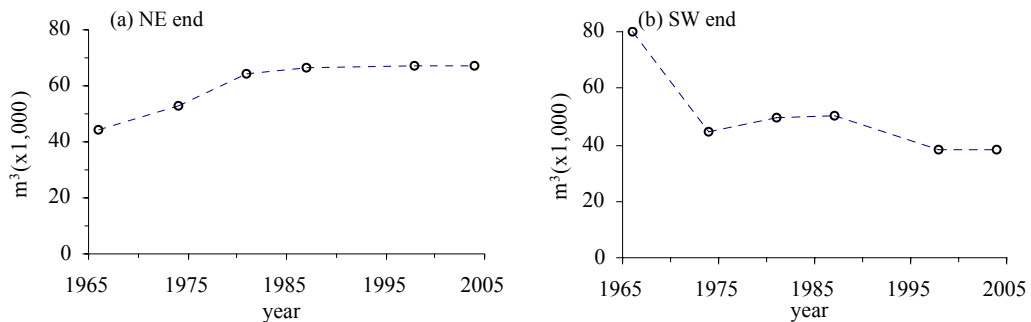
Figure 3.6. Depositional patterns of: a) the northeastern end; and b) the southwestern end of the island over a period of 1966 - 2004.

Figure 3.6a and Table 3.2 show that the volume on the northeastern end has increased continuously from around 44,000 m^3 in 1966 to 67,500 m^3 in 1998 with decreasing rates from approximately 1,000 m^3/y between 1966-1974 to approximately 100 m^3/y between 1987-1998. The volume has been relatively constant between 1998 and 2004. In total, the northeastern end gains approximately 23,000 m^3 over the period 1966 to 2004.

As indicated in Figure 3.6b and Table 3.3, however, change on the southwestern end has occurred differently with periods of accretion and erosion. The volume significantly reduced between 1966 and 1974 from approximately 80,000 to 45,000 m^3 at the erosive rate of about 4,000 m^3/y. The volume between 1974 and 1981 however increased slightly and has been relatively constant between 1981 and 1987. The erosion has recurred between 1987 and 1998 with the erosive rate of approximately 1,000 m^3/y. The volume between 1998 and 2004 has been relatively constant. In total, the loss of the volume of approximately 41,000 m^3 has occurred on the southwestern end of the island between 1966 and 2004. Therefore, between 1966 and 2004 the loss of sediment of approximately 18,000 m^3 has occurred on the island shore, based on the volumetric changes on both ends of the island (Table 3.4).

The high rate of erosion occurring on the southwestern end between 1966 and 1974 could partly reflect error caused by mapping the sand spit from the poorer resolution photography of the 1966 aerial photograph. Excluding the 1966 topography, approximately 6,000 m^3 (or approximately 200 m^3/y) of the sediment has been eroded from the southwestern end (Table 3.3) and approximately 14,000 m^3 (or approximately 500 m^3/y) has been accumulated on the northeastern end (Table 3.2); the island in total has gained approximately 8,000 m^3 (or approximately 300 m^3/y) instead of the loss of

approximately 18,000 m^3 (or approximately 500 m^3/y) found if the 1966 island topography is taken into account (Table 3.4).

Previous studies of sediment transport by Hart (2003) indicated that in general sediments on the reef flat are transported towards the island and are deposited on the island beach with some fine sediments selectively transported back to the reef flat. Although there is some uncertainty of volume estimation due partly to the accuracy of the data, the present study extends Hart's conclusions to identify the island shores where significant accretion and erosion have occurred and to approximate associated volumetric changes of sediments on the island shore over time.

In Chapter 2, a broad pattern of morphological evolution over the past 3,000 years was obtained, the island having continually accreted with a long-term rate of approximately 900 m^3/y. This depositional rate can be considered as an averaged rate over 3,000 years. In this chapter, more detail of a depositional pattern of the island over shorter time scales is detected, involving different rates of accretion over the past 40 years. The broad evolution of island morphology over the past 3,000 years, studied in Chapter 2, and the sustained pattern of dynamic adjustment of the island shoreline over the past 40 years, examined in this chapter, provide the basis to predict probable future conditions of the island in the next century, which will be discussed in Chapter 6.

3.5. Summary

Changes in island shore over the past 40 years (1966-2004) were examined based on reconstruction of the DTM of the island. The essential data were derived from the aerial photographs in 1966, 1974, 1981, 1987 and 1998, and the field survey in 2004.

The aerial photographs were scanned and georeferenced, and the island shoreline was delineated along the beach toe.

A comparison of the island shoreline over a period of 1996-2004 indicates significant change occurring only on the southwestern and northeastern ends of the island, associated with mobile sand spits which appear to have moved in a clockwise direction. However, reversing movement, especially at the southwestern end of the island, occurs in response to seasonal hydrodynamic influence.

Although the sand spits have indicated a similar pattern of rotation in a clockwise direction, the pattern of volumetric changes has occurred differently at both ends. On the northeastern end, the volume has increased continuously with decreasing rates from approximately 1,000 m^3/y between 1966 and 1974 to approximately 100 m^3/y between 1987 and 1998, and been relatively stable thereafter; approximately 23,000m^3 of sediment has been gained between 1966 and 2004. On the other hand, both erosive and accreting periods have occurred on the southwestern end; a high erosive rate of about 4,000 m^3/y between 1966 and 1974, slightly accreting rates between 1974 and 1987, an erosive rate of 1,000 m^3/y between 1987 and 1998, and slightly accreting thereafter. Approximately 41,000 m^3 of sediment has been lost between 1966 and 2004.

However, high uncertainty could occur to the estimated rate of erosion of the southwestern spit between 1966 and 1974 due mainly to error caused by mapping the spit from the poorer resolution photography of the 1966 aerial photograph. The total of approximately 18,000 m^3 of sediment has been eroded from the island between 1966 and 2004 whereas excluding the 1966 topography suggests the accretion of around 8,000 m^3 (approximately 200 m^3/y). This highlights the significance of the accuracy of the data, affecting the interpretation of the depositional history of the island. Nonetheless, whether the 1966 island shore is included or excluded, it can be concluded

that over the past 40 years the island has accreted on the northeastern end and eroded on the southwestern end.

CHAPTER 4

CLIMATE AND MEDIUM-TERM TRENDS OF WIND IN TORRES STRAIT

4.1. Introduction

Waves are the primary factor influencing changes in reef-island morphology. As shown in a following chapter, waves in this region are dominated by local wind-generated waves. Therefore, wind climate is a fundamental element for understanding generation, characteristics and climate of waves in this region and consequently morphological change occurring on reef islands.

Earlier studies of erosion occurring on Warraber Island, undertaken by Liu and Retschlag (1991) and Rasmussen and Hopley (1996), emphasised the island's probable response to wind climate and undertook preliminary analyses of wind data. Hart (2003) in a study of sediment transport on Warraber Reef analysed short-term wind data, between 1995 and 2002, from the meteorological station on Horn Island. The present study reanalyses the wind data between 1951 and 2003 in more detail in order to identify overall, monthly, yearly and medium-term trends of wind climate. The length of the wind data covers the period of shoreline change examined in Chapter 3.

In Section 4.2, information on wind data and wind data analysis are described. The overall wind climate, monthly wind climate and yearly wind climate are developed in Sections 4.3, 4.4 and 4.5, respectively. This information will be taken into account in Chapter 5 to approximate wave climate in this region. In Section 4.5, the medium-term trends of wind climate are also constructed and will be applied in Chapter 6 to explore probable causes of the change in island shape that was identified in Chapter 3. In Section 4.6, the examination is given to the influence of environmental factors on wind

climate in the region. This section focuses on the effect of El Niño-Southern Oscillation (ENSO), sunspot cycles and solar magnetic activity on wind patterns.

4.2. Wind Data Analysis

Wind data for this study were provided by the Queensland Branch of the Bureau of Meteorology (BOM, 2004). They include two datasets, one obtained from the meteorological station on Thursday Island and another on Horn Island (see their locations in Figure 2.1). The data from Thursday Island cover the period between 1951-1992 while the data from Horn Island cover the period between 1995-2003. The station elevations relative to mean sea level are 57.6 m and 4.0 m at Thursday Island and Horn Island, respectively. At both locations, winds were measured at a standard height of 10 m above ground. Wind data had been recorded every 3 hours using an anemograph and, for each 3-hour interval, a record is derived by averaging data for 10 minutes of recording. In order to acquire an accurate pattern of wind, attributed to the main weather systems in the area, the effect of breezes due to the difference in temperatures between land and sea has to be minimised. Generally a sea breeze is stronger than a land breeze and breezes are weak during the transformational period which commonly occurs around 9 pm (Hopley, 1982). Accordingly, only 9 pm data were used in this analysis.

All analysis of wind data was carried out using Excel. The record was found to be incomplete and interrupted with gaps; it was visually examined to identify missing data. The data from Thursday Island (1951-1992) contain 15,341 days with 123 days of missing data (0.8% of the record) while those from Horn Island (1995-2003) contain 3,287 days with 386 days of missing data (12% of the record) (Appendix 1). Due to the

large gap in the data, no combination of the data was performed and the analysis was undertaken based primarily on the data from Thursday Island. The analysis of the data from Horn Island was nevertheless conducted and the results were taken into consideration in examining the yearly wind climate.

Only available data were taken into account for analysis of wind records. Nonetheless, missing data were taken into consideration later in evaluating uncertainty in the wind analysis. The 15,218 days with available data from Thursday Island consist of 1,125 days of calms and 14,093 days of measurable data. The wind data were grouped into 16 compass directions and calm periods. The 16 compass directions include: i) north (N); ii) north-northeast (NNE); iii) northeast (NE); iv) east-northeast (ENE); v) east (E); vi) east-southeast (ESE); vii) southeast (SE); viii) south-southeast (SSE); ix) south (S); x) south-southwest (SSW); xi) southwest (SW); xii) west-southwest (WSW); xiii) west (W); xiv) west-northwest (WNW); xv) northwest (NW); and xvi) north-northwest (NNW).

Wind climate was described in terms of wind effect and wind statistics including the mean wind speeds, the maximum wind speeds and the standard deviation of wind speeds. Wind effect is a cumulative wind speed (Umbgrove, 1947). The data were analysed to establish the overall wind climate by directions, the monthly wind climate by directions, the yearly resultant wind direction and effect, the yearly total wind effect and the medium-term trends of wind effect by directions.

Wind speeds in each direction were summed to derive the total wind effect by directions for constructing the overall wind climate. Wind data were grouped into 16 directions for each month in order to depict the monthly wind climate by directions. The monthly relative frequency of occurrence of wind and calm periods, and the monthly relative magnitude of wind effect were calculated. The statistical values were

calculated for the overall wind climate and the monthly wind climate. Vector analysis was performed on wind data to obtain the u-component (winds moving in the E-W direction) and v-component (winds moving in the N-S direction) for computing the resultant wind direction and effect. The yearly total wind effect and the yearly relative frequency of occurrence of calm periods were also calculated. The medium-term trends of wind effect by directions were generated using 15-year moving average.

4.3. Overall Wind Climate

Figure 4.1 summarises wind climate over a period of 1951-92. Based on wind effect relative to directions, winds in this area can be broadly grouped into four main sectors: i) a N-ENE sector; ii) an E-SSE sector; iii) a S-WSW sector; and iv) a W-NNW sector.

This region is primarily dominated by winds from the E-SSE sector (around 80% of wind effect) and secondarily influenced by winds from the W-NNW sector (around 15% of wind effect) (Figure 4.1a). There are only approximately 2% and 1% of wind effect from the N-ENE and S-WSW sector, respectively (Figure 4.1a). Calm periods occupy approximately 7% of the record.

The distribution of mean wind speeds is relatively symmetrical along a WNW-ESE axis (Figure 4.1b). Higher mean wind speeds are from the W-NNW and E-SSE sectors with the maxima of mean wind speeds of 7.11 m/s and 7.65 m/s from the WNW and the ESE, respectively, and lighter mean wind speeds of less than 4.0 m/s from other two sectors (Figure 4.1b).

Maximum wind speeds are from the W-NNW sector and normally greater than those from the opposite sector (Figure 4.1c). Standard deviation of the wind speeds
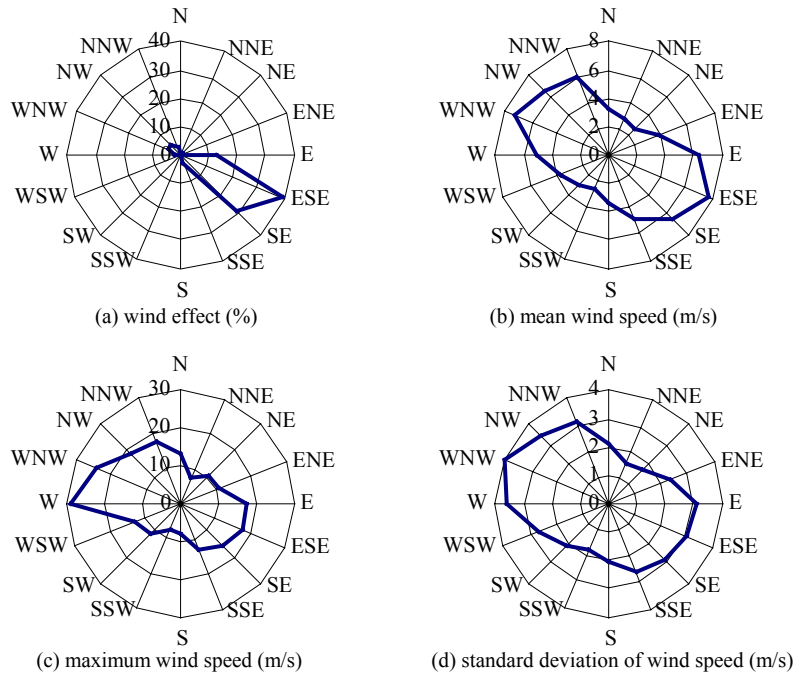
Figure 4.1. Wind climate over the period of 1951-1992: a) relative magnitude of wind effect (%); b) mean wind speed (m/s); c) maximum wind speed (m/s); and d) standard deviation of wind speed (m/s).

indicates that winds from the W-NNW sector are however more variable, especially WNW winds, than those from the E-SSE sector (Figure 4.1d). Therefore, the W-NNW winds exist over a much shorter period than E-SSE winds and are normally characterised by more variable wind speeds with gusts of greater than 20.0 m/s from the W and the WNW while winds from the E-SSE sector are more persistent and exist over a longer duration.

4.4. Monthly Wind Climate

Table 4.1, 4.2, 4.3, 4.4 and 4.5 summarise the monthly wind climate by directions, including the relative frequency of occurrence, the relative magnitude of wind effect, the mean wind speeds, the maximum wind speeds and the standard deviation of wind speeds, respectively. Blank spaces in Table 4.1 and 4.2 indicate that no data fall in those categories while those in Table 4.3, 4.4 and 4.5 mean that either no data fall in

Table 4.1 Monthly relative frequency of occurrence of wind by directions and calm periods (%). A maximum value in each month is given in bold text.

	Jan	Feb	Mar	Apr	May	Jun	Jul	Aug	Sep	Oct	Nov	Dec
N	3.33	3.82	2.69	0.64						0.15	0.72	2.00
NNE	1.47	1.53	1.69	0.56						0.08	0.56	1.61
NE	1.63	1.61	2.30	0.64	0.15	0.16				0.62	1.19	1.84
ENE	2.09	1.70	1.92	1.83	0.39	0.48		0.08	0.32	0.85	3.03	1.92
E	8.91	5.60	8.45	14.91	9.43	3.06	3.06	7.78	13.20	23.15	28.74	**19.37**
ESE	6.51	4.66	15.67	**34.13**	40.03	35.96	36.86	**43.62**	**51.61**	**47.61**	**31.37**	15.37
SE	5.89	4.50	12.98	31.34	**43.51**	**51.97**	**52.94**	42.69	31.24	19.75	16.88	12.45
SSE	1.01	1.36	2.15	2.79	3.63	5.79	5.73	3.65	2.58	3.78	4.38	4.15
S	0.31	0.59	0.84	0.72	0.54	0.80	0.78	0.47	0.16	0.39	0.24	0.38
SSW	0.23	0.42	0.31	0.56	0.08	0.08	0.08		0.08	0.15	0.08	0.23
SW	1.24	1.02	1.31	0.08		0.08		0.08		0.08	0.32	0.54
WSW	1.32	1.53	1.46	0.48	0.08	0.08		0.08		0.15	0.48	1.00
W	8.29	8.40	5.53	1.12	0.08	0.08	0.08			0.23	1.19	5.38
WNW	13.80	16.79	9.29	1.20				0.08		0.31	2.31	6.38
NW	**18.60**	**20.70**	9.14	0.96	0.08					0.08	1.11	7.61
NNW	8.37	9.67	6.22	0.96	0.08					0.08	0.72	4.61
CALM	16.98	16.12	**18.05**	7.10	1.93	1.45	0.39	1.56	0.81	2.55	6.69	15.14
Total	100	100	100	100	100	100	100	100	100	100	100	100

Table 4.2 Monthly relative magnitude of wind effect (%) by directions. A maximum value in each month is given in bold text.

	Jan	Feb	Mar	Apr	May	Jun	Jul	Aug	Sep	Oct	Nov	Dec
N	2.41	3.11	2.07	0.36						0.03	0.29	1.22
NNE	0.84	0.94	1.29	0.35						0.01	0.26	1.04
NE	0.84	0.88	1.42	0.30	0.05	0.21				0.22	0.59	0.94
ENE	1.37	1.23	1.49	1.59	0.37	0.46		0.03	0.17	0.63	2.12	1.42
E	8.01	4.33	9.14	17.01	9.92	3.55	3.52	8.20	14.00	24.82	31.80	**23.84**
ESE	6.76	4.08	**20.18**	**40.12**	**43.90**	39.89	41.18	**50.10**	**56.89**	**54.87**	**42.83**	21.47
SE	4.45	3.37	13.59	32.75	42.55	**50.85**	**49.73**	38.97	26.87	16.09	14.58	12.17
SSE	0.78	1.00	1.44	2.27	2.67	4.56	4.92	2.28	1.96	2.78	3.20	4.03
S	0.08	0.29	0.40	0.32	0.42	0.38	0.53	0.31	0.09	0.18	0.12	0.25
SSW	0.26	0.21	0.19	0.22	0.01	0.02	0.03		0.02	0.04	0.05	0.13
SW	0.75	0.51	1.00	0.02	0.00	0.03		0.08		0.02	0.25	0.35
WSW	0.90	1.38	1.44	0.34	0.02	0.03		0.03		0.12	0.22	0.73
W	11.10	10.02	6.97	0.93	0.02	0.02	0.04			0.06	0.58	5.14
WNW	23.27	26.47	18.20	1.16			0.05			0.10	1.60	9.21
NW	**27.18**	**29.80**	12.82	1.13	0.02					0.01	1.02	11.07
NNW	11.01	12.38	8.37	1.13	0.04					0.03	0.51	6.99
Total	100	100	100	100	100	100	100	100	100	100	100	100

Table 4.3 Monthly mean wind speed (m/s) by directions. Maximum values in each month are given in bold text.

	Jan	Feb	Mar	Apr	May	Jun	Jul	Aug	Sep	Oct	Nov	Dec
N	3.25	3.80	3.21	3.15						1.25	2.11	2.46
NNE	2.57	2.88	3.18	3.46							2.43	2.60
NE	2.31	2.54	2.56	2.65	2.30	**9.55**				2.50	2.60	2.05
ENE	2.93	3.37	3.24	4.83	6.48	6.87			4.25	5.21	3.71	2.96
E	4.04	3.60	4.51	6.36	7.19	8.31	**8.73**	7.91	8.37	7.57	5.85	4.95
ESE	4.66	4.07	5.37	**6.55**	**7.49**	7.95	8.47	**8.61**	**8.70**	**8.14**	**7.22**	5.62
SE	3.39	3.49	4.36	5.82	6.68	7.01	7.12	6.84	6.79	5.75	4.57	3.93
SSE	3.49	3.44	2.79	4.53	5.03	5.63	6.51	4.68	6.00	5.20	3.86	3.91
S	1.15	2.27	1.95	2.51	5.36	3.35	5.09	4.90	4.60	3.28	2.57	2.58
SSW	4.97	2.26	2.58	2.20						2.05		2.20
SW	2.72	2.32	3.18								4.13	2.64
WSW	3.08	4.20	4.12	3.93						5.40	2.40	2.93
W	6.01	5.55	5.25	4.66						1.90	2.57	3.85
WNW	**7.58**	**7.34**	**8.17**	5.39						2.18	3.67	5.81
NW	6.57	6.70	5.85	**6.56**							4.81	5.86
NNW	5.91	5.96	5.61	**6.56**							3.76	**6.10**

Table 4.4 Monthly maximum wind speed (m/s) by directions. Maximum values in each month are given in bold text.

	Jan	Feb	Mar	Apr	May	Jun	Jul	Aug	Sep	Oct	Nov	Dec
N	9.80	12.90	7.70	6.20						1.50	4.10	6.70
NNE	6.70	5.10	6.20	6.20							3.60	7.20
NE	4.10	7.70	5.70	4.10	3.10	10.30				5.10	7.70	5.10
ENE	6.70	10.30	9.30	9.30	9.30	10.80			10.30	9.30	9.30	5.10
E	17.50	8.20	9.80	12.90	13.40	12.90	13.40	**15.40**	**15.40**	15.40	**15.40**	12.90
ESE	10.30	7.70	12.40	**18.00**	**18.00**	**15.40**	**16.50**	**15.40**	14.90	**16.50**	**15.40**	11.80
SE	9.30	7.70	8.80	15.40	12.90	**15.40**	13.40	14.40	**15.40**	13.90	13.90	11.30
SSE	7.20	6.20	10.30	10.30	10.30	13.40	12.90	9.80	12.40	10.30	7.20	9.30
S	2.10	5.10	4.60	5.10	7.20	6.70	7.70	6.20	5.10	6.20	4.10	3.60
SSW	7.20	4.60	5.70	4.10						3.60		4.10
SW	8.20	4.60	11.30								5.70	5.10
WSW	6.70	7.20	12.90	10.30						10.30	4.10	10.30
W	**28.80**	17.00	17.00	10.30						2.60	8.20	15.40
WNW	20.60	**19.60**	**24.20**	11.30						3.10	9.80	15.40
NW	18.50	16.50	15.40	12.90							9.30	**16.50**
NNW	17.50	12.40	15.40	15.40							5.70	16.00

Table 4.5 Monthly standard deviation of wind speed (m/s) by directions. Maximum values in each month are given in bold text.

	Jan	Feb	Mar	Apr	May	Jun	Jul	Aug	Sep	Oct	Nov	Dec
N	2.07	2.40	1.97	1.82						0.35	1.20	1.96
NNE	1.81	1.44	1.24	1.96							0.90	1.57
NE	1.33	1.81	1.33	0.96	1.13	1.06				1.58	1.78	1.23
ENE	1.77	2.22	1.80	2.47	**2.89**	**3.71**			**4.13**	2.87	1.97	1.13
E	2.28	1.88	2.43	2.84	2.78	2.35	2.48	**3.17**	2.68	2.81	2.94	2.62
ESE	2.33	1.91	2.79	2.78	2.64	2.74	**2.72**	2.68	2.61	2.80	**3.11**	2.73
SE	2.05	1.72	2.33	2.38	2.36	2.48	2.58	2.63	2.82	2.90	2.44	2.29
SSE	1.88	1.44	2.16	2.80	2.31	3.03	2.69	2.36	2.18	1.82	1.84	2.15
S	0.68	1.48	1.36	1.39	1.83	1.82	2.27	1.53	0.71	2.28	1.86	0.98
SSW	3.04	1.65	2.13	1.26						2.19		1.66
SW	2.21	1.13	2.73								1.33	1.46
WSW	2.15	2.02	3.42	3.34						**6.93**	1.12	2.63
W	**4.31**	3.24	3.13	2.97						0.82	1.91	3.04
WNW	**4.30**	**3.45**	**4.20**	3.22						0.81	2.34	3.48
NW	3.80	3.29	2.75	2.97							2.49	3.10
NNW	3.18	2.81	3.09	**3.89**							1.63	**3.58**

those categories or a number of data for statistical calculation are less than two. Plots of the relative magnitude of wind effect are also given in Figure 4.2.

Table 4.1 shows that winds from the E-SSE sector and calms generally exist over the whole year while winds from other directions are absent approximately between May and September.   According to the relative frequency of occurrence and calm periods (Table 4.1), and the relative magnitude of wind effect (Table 4.2 and Figure 4.2), the monthly wind climate in this region can be divided into four periods. The first period is between January and February, within which winds are variable with the prevalence of W-NNW winds. In March, which is a period of transition from the W-
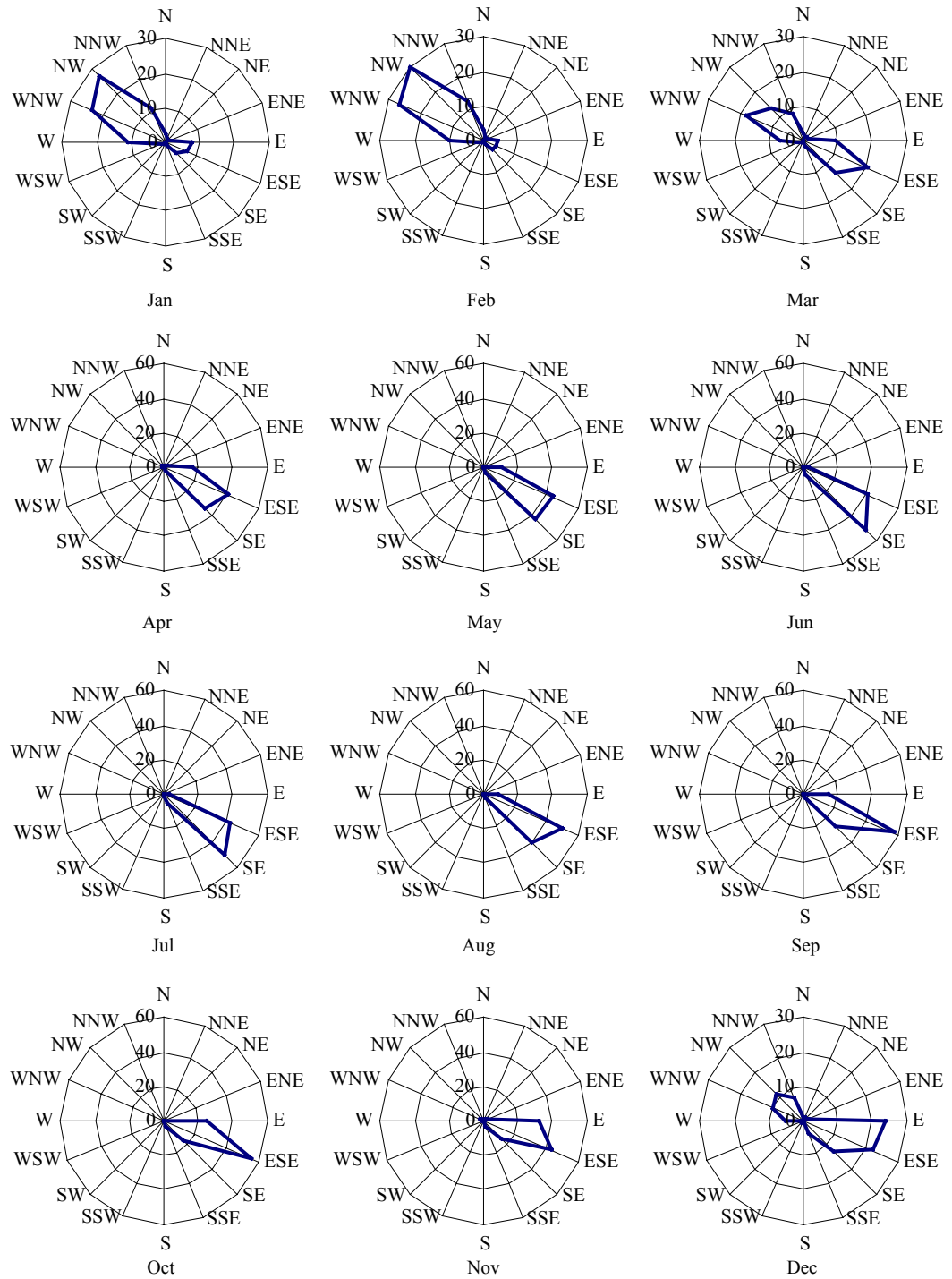
Figure 4.2. Monthly relative magnitude of wind effect (%) by directions.

NNW to E-SSE domination, a calm period is dominant (approximately 18% of times) and winds are variable with a prevailing increase of winds from the E-SSE sector. During these first three months, gusty winds also occur, characterised by very high wind

speeds of more than 20.0 m/s (Table 4.4) but very variable with one standard deviation of wind speed of approximately 4.0 m/s (Table 4.5). From April to November, the dominance of E-SSE winds is very obvious, specifically during May and September wherein winds from the ESE and SE are most significant, contributing more than 80% of the wind effect with one standard deviation of wind speed of less than 3.0 m/s. The maximum wind speeds during this period are generally less than those of the first two periods (Table 4.4). The transition takes place again in December with prevailing E winds and an increase of the wind effect from the W-NNW sector. A calm period is common between December and March, reaching its maximum (18% of time) in March and minimum (0.4% of time) in July (Table 4.1).

The monthly relative magnitude of wind effect is given in Figure 4.3. Around 6% of wind effect occurs in each of the first three months (first and second periods). During the third period, wind effect increases to around 8% in April and peaks at approximately 10% during each month between May and October. It decreases to about 7% at the end of the third period in November and then around 6% in December (the fourth period).
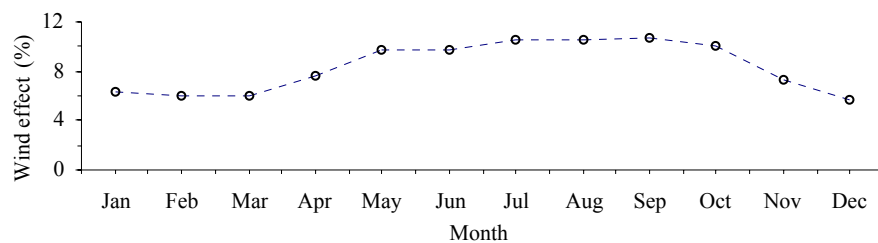
Figure 4.3. Monthly relative magnitude of the wind effect.

4.5. Yearly Wind Climate and Medium-Term Trends of Wind Effect

Vector analysis was carried out on the wind data to compute the yearly resultant wind direction and wind effect. The analysis results of wind data from Horn Island were also included in this section. Figure 4.4a and b show the yearly resultant wind directions and wind effect, respectively, over a period of 1951-2003. Their values are also given in Appendix 2. The results between 1993 and 1995 are not presented because data were unavailable during that period.
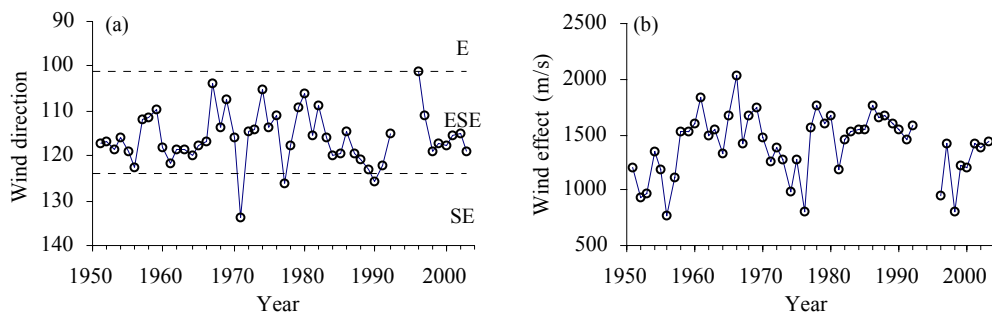
Figure 4.4. Yearly resultant: a) wind direction; and b) wind effect between 1951 and 2003.

It is obvious from Figure 4.4a that the ESE winds have been the prevailing resultant wind component in this region. The resultant wind directions have generally been varied within the ESE sector except in 1971, 1977, and 1990, when they were from the SE and 1996 when they were from the E (Figure 4.4a). Flood (1986) analysed wind data on Heron Island between 1962 and 1980, and indicated a long-term shift in annual resultant wind vectors within a 45$^{\text{o}}$ arc from SSE to ESE in 1964. However, no such a shift has occurred in yearly resultant wind direction (Figure 4.4a)

The resultant wind effect appears to have changed episodically with a period of approximately 20-22 years (Figure 4.4b). During the duration of the record, the

resultant wind effect was first at a low point in 1956, increased with a fluctuation about

its visually estimated trend and then dropped to the low point again in 1976. A second

loop was discernable beyond 1976 with a low point in around 1998, despite incomplete

coverage. The yearly total wind effect (Appendix 2 and Figure 4.5) exhibits the similar

pattern of variation but with less fluctuation than that of the yearly resultant wind effect.

The low points of the total wind effect were at 1952, 1976 and 1998.
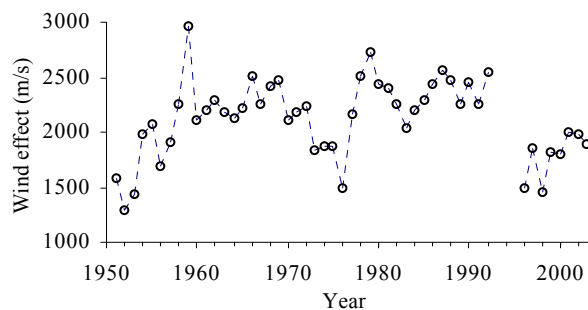
Figure 4.5. Yearly total wind effect.

The yearly percentages of calm periods are illustrated in Figure 4.6a together with

the yearly total wind effect. Calm periods tended to decrease gradually from around

10% in 1951 to about 2% in 1972. In 1973, calm periods increased dramatically and

reached a maximum of 25% in 1976. After 1976, calm periods decreased sharply to

around 3% in 1979 and fluctuated at about 5% until around 2000 and thereafter when

calm periods decreased to less than 5%. As seen in Figure 4.6a, the yearly pattern of the

total wind effect shows an opposite trend of fluctuation to that of the calm periods. A

scatter plot between the wind effect and the calm periods (Figure 4.6b) indicates that

they correlate negatively.

The medium-term trends of wind effect from 16 directions were constructed using

the 15-year moving average (Figure 4.7 and Appendix 3). It is evident that the

influence of the ESE winds has been of most significance on wind climate in this area
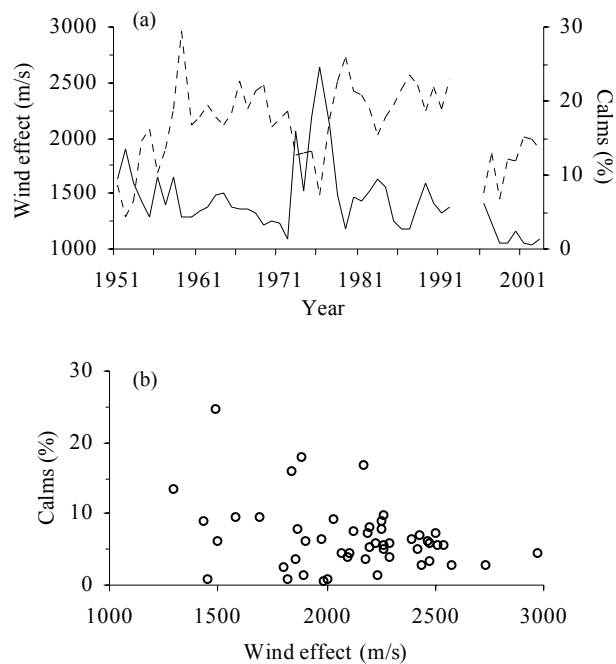
Figure 4.6. a) Yearly total wind effect (---) and yearly relative frequency of occurrence of calm periods (—) and b) a scatter plot between yearly relative magnitude of wind effect and yearly relative frequency of occurrence of calm periods.

all the time (Figure 4.7b). The ESE wind effect appears to have slightly decreased over the middle period of the record. The contribution from the SE winds which are of secondary significance has been relatively stable while the E winds have exhibited a trend opposite to that of the ESE winds (Figure 4.7b).   The wind effect contributed by the S-WSW winds demonstrates a fluctuation but in total is very small, less than 1% of the total wind effect (Figure 4.7c). Abrupt change has occurred to the ENE winds (Figure 4.7a) reaching its maximum at about 2% during the middle period of the record with the WNW winds decreasing during the first half of the record from approximately 6% to less than 4% and relatively stable thereafter (Figure 4.7d). The influence from the W winds (Figure 4.7d) appears to have been relatively stable. Winds that exhibit the increasing trend of wind effect over a period of the record are from the N (Figure 4.7a), SSE (Figure 4.7b), S (Figure 4.7c), SSW (Figure 4.7c) and NNW (Figure 4.7d).

114
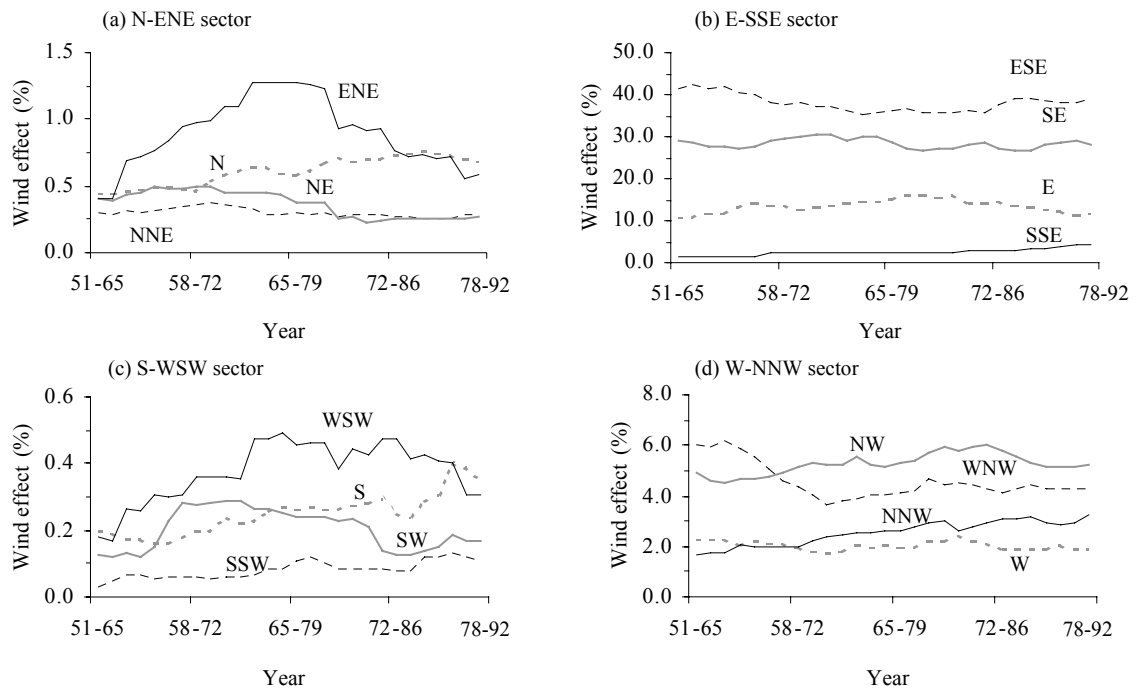
Figure 4.7. Trends of the relative magnitude of wind effect over a period of 1951-1992: a) N-ENE sector; b) E-SSE sector; c) S-WSW sector; and d) W-NNW sector.

4.6. Influence of Environmental Factors on Wind Climate

Solar activity and El Niño-Southern Oscillation (ENSO) have been recognised to play a part in modifying wind fields and consequently to modify wave conditions, resulting in coastal change in several parts of the world. For example, on the central and south coasts of New South Wales, the relationship between times of low sunspot activity and occurrence of erosional events during winter was noted by Stevenson (1980) and the influence of ENSO on beach rotation has been recently recognised (Ranasinghe et al., 2004; Short and Trembanis, 2004). Understanding relationships such as these provides the potential to predict long-term trends of coastal change. An attempt was made in the present study to relate variations of the wind climate to ENSO, sunspot cycles and solar magnetic activity.

ENSO or El Niño Southern Oscillation is the result of a cyclic warming and cooling of the surface ocean of the central and eastern Pacific and its strength can be determined from the normalised difference of surface pressure between Tahiti, French Polynesia and Darwin, Australia (NOAA, 2003). It is a quasi-cyclic phenomenon occurring at irregular intervals of 2-7 years and typically lasts 12-18 months (NOAA, 2003).

Sunspots are cooler areas on the surface of the Sun. Their number, size and duration have varied temporally and spatially, and directly correlate to solar activity which in turn affects the earth's climate. For example, during the Maunder Minimum (1645-1715 AD) when very few sunspots were observed, the climatic period named the "Little Ice Age" developed (Eddy, 1976). The number of sunspots exhibits a cyclic behaviour with periods varying between 7.5-16 years and a mean period of 11.2 years (Burroughs, 2001).

In association with sunspot cycles, strong magnetic fields with the bipolar characteristic of the sunspots was discovered by George Ellery Hale in 1908 (Moussas et al., 2005). The reversal of the polarity of the sunspots occurs regularly at the peak of the sunspot cycle; thus the Sun exhibits an approximate 22-year magnetic cycle (Moussas et al., 2005). The period of the solar magnetic activity is therefore about two cycles of the sunspots.

Visual observation on the graphs in Figure 4.4b and 4.5 indicates the possible relationship between the medium-term wind effect in this region and the solar magnetic activity (a 22-year cycle). Therefore, the resultant and total wind effect shown in Figure 4.4b and 4.5 are plotted against the cycles of sunspot numbers (NASA, 2005) and phases of solar magnetic activity (Landscheidt, 2000) in Figure 4.8. Over the duration

of the wind record, two phases of solar magnetic activity, from 1954 to 1976 and from 1976 to 1996, are indicated in the figure.
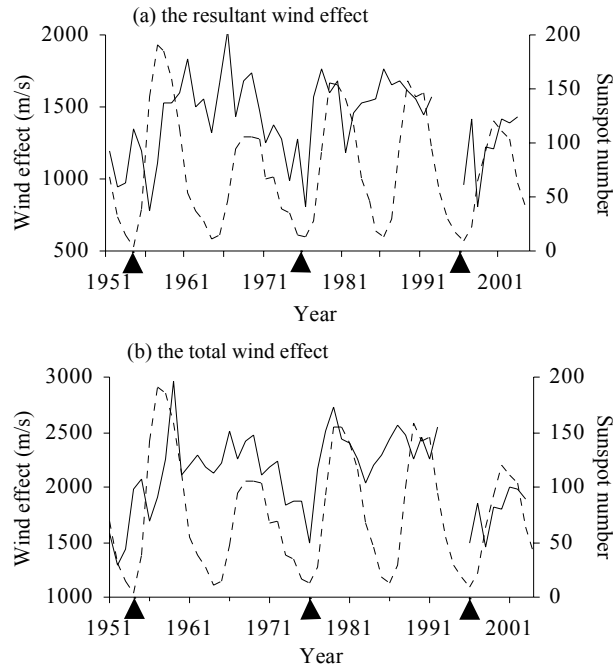
Figure 4.8. Plot of cycles of sunspot numbers (----) with; a) the resultant wind effect (—); and b) the total wind effect (—). The initial phases of solar magnetic activity (1954, 1976 and 1996) (Landscheidt, 2000) are marked by black triangles.

It is seen from Figure 4.8 that patterns of the resultant and total wind effect are reasonably in agreement with a 22-year cycle of solar magnetic activity which comprises approximately two cycles of the sunspot numbers. Both wind effects were lower at about the beginning and ending phases of solar magnetic activity. The discrepancy occurred between a time of lower wind effect and a starting phase of solar magnetic activity in 1954. The resultant and total wind effects were lower in 1956 and 1952, respectively, while a solar magnetic phase began in 1954. This discrepancy may be partly attributed to the greater number of missing data in 1952 (17 data) and 1953 (8 data) all of which occupied a period of high wind effect (Table A1.1 of Appendix 1). A low point of wind effects in 1976 accorded with the start of the following cycle of solar magnetic activity. The lower wind effects between 1993 and 2003 were around 1998

while the initial phase of a solar magnetic cycle was in 1996. Uncertainty of time of lower wind effect during this period is high due to unavailability of wind data between 1993 and 1995, and a great number of missing data between 1996 and 2003 (Table A1.2 of Appendix 1).

Peaks on the total wind effect, particularly occurring about 1958, 1969 and 1980, tended to have coincided with those of the sunspot cycle. However, the influence of the 11-year sunspot cycle on the wind effect is not clear.   Burroughs (2001) suggested that in general the influence of the solar magnetic activity on environments is more obvious than that of the sunspot cycle.

A shorter-term fluctuation about a longer trend of around 22 years of wind effect was examined in relation to ENSO, based on the Southern Oscillation Index (SOI) obtained from the Bureau of Meteorology (BOM, 2005). Analyses involved 12-month moving averages of the monthly SOI and wind data including monthly u-components and v-components, and the monthly resultant wind directions in order to reduce the variability of the data and capture clearer patterns of winds during ENSO occurrence. The approximate 22-year trend that was identified on the u- and v-components of the wind data was estimated and removed using a 4-order polynomial. The scatter plots of the u-components, the v-components and the resultant wind directions against the SOI are illustrated in Figure 4.9 and plots of the time series are given in Figure 4.10.

A positive and a negative number of the SOI indicate a La Niña event (or ocean cooling) and an El Niño event (or ocean warming), respectively (BOM, 2005).   In Figure 4.9, no clear relationships could be found between the SOI, and the three series of the wind data. The v-components (Figure 4.9b) and the resultant wind directions
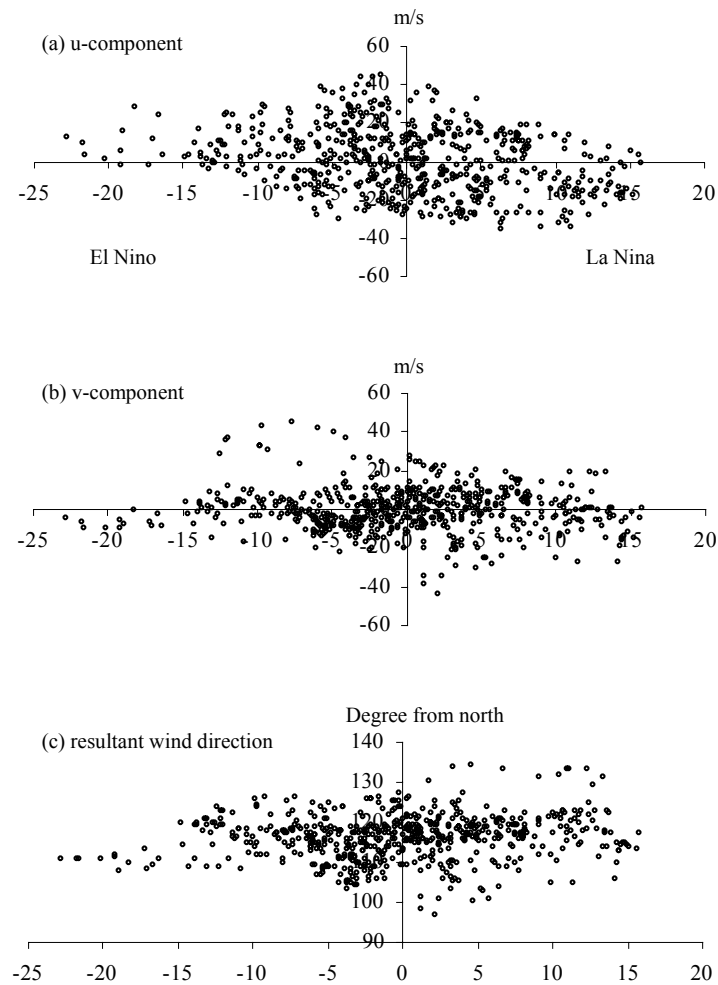
Figure 4.9. Scatter plots of the SOI against: a) the u-component; b) the v-component; and c) the resultant wind direction, after the 12-year moving average and the approximate 22-year trend removal. The values of the u- and v-components less than zero mean they are below the 22-year trend.

(Figure 4.9c) appear more scattered during La Niña events. The only trend that could be detected is on the u-components which appear to have decreased during the La Niña events and increased during the El Niño events (Figure 4.9a). The 1982-83 El Niño is considered as the strongest during the 20th century, as shown in Figure 4.10 by the most negative value of the SOI. In Figure 4.10, however, no prominent signals of the wind could be seen over that period. This is probably due partly to a large number of missing

data between 1981 and 1983 (Table A1.1 of Appendix 1), particularly during May and September when the wind effect is high.
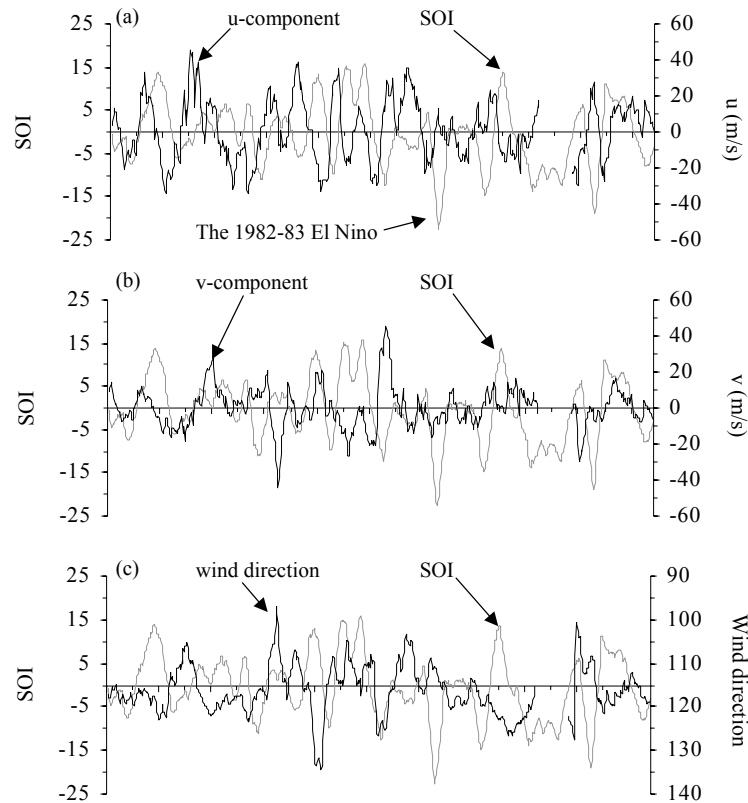
Figure 4.10. Plots of the SOI against: a) the u-components; b) the v-component; and c) the resultant wind direction, after the 12-year moving average and the approximate 22-year trend removal. The values of the u- and v-components less than zero mean they are below the 22-year trend.

Basically, during ENSO the trade winds are weakened; thus wind patterns should be different from a regular pattern. No clear relationships found in this study probably result from the existence of periodicities other than ENSO and the 22-year cycle. In addition, those other components would have more influence on wind, masking the appearance of ENSO signals.

Flood (1988) examined the correlation between long-term patterns of wind direction on Heron Island between 1962 and 1980, and ENSO, sunspots and solar magnetic activity. He found no clear relationships between wind direction, and sunspot

cycles and solar magnetic activity, but noted a more easterly influence of the winds at times of ENSO events. In the present study, the most probable relationship that can be observable is between wind effect and solar magnetic activity.

4.7. Summary

Over the past 40 years, this region has been primarily dominated by winds from the E-SSE sector, in total, contributing approximately 80% of wind effect, and secondarily influenced by winds from the W-NNW sector, in total, contributing approximately 15% of wind effect.

E-SSE winds are prominent between April and November while W-NNW winds are prevalent between January and February. E-SSE winds are characterised by persistent wind speeds with an average of around 8.0 m/s and a standard deviation of less than 3.0 m/s. ESE and SE winds are most significant within the E-SSE sector, especially between May and September when they produce more than 80% of monthly wind effect. Winds from the W-NNW sector are characterised by variable and rare, high wind speeds of greater than 20.0 m/s. March and December are periods of transition from the prevalence of W-NNW winds to E-SSE winds and vice versa, respectively, and generally dominated by variable winds and calm periods.

Yearly resultant wind directions have been most of the time from the ESE with shifts to the SE in 1971, 1977 and 1990, and to the E in 1996. Annually, calm periods are generally less than 10% of time but increased up to their maximum of around 25% in 1976. The resultant and total wind effect appears to have varied with a period of approximately 20-22 years.

The medium-term trend analysis shows that the wind effect from ESE has gradually decreased during the middle period of the record, from SE it has been relatively stable and from E it has varied in opposite directions to that from ESE. Wind effect from N, SSE, S, SSW and NNW tended to have increased over the period of the record.

The analysis of relationships between yearly wind patterns and environmental factors suggested that the influence of a sunspot cycle and ENSO on yearly wind patterns is not clear although some peaks of the sunspot cycle are roughly consistent with those of the total wind effect and the u-components of wind data have decreased during the La Niña. Solar magnetic activity appears to probably relate to the pattern of wind effect, beginning and ending at about the low magnitude of wind effect. However, there seems to be no mechanism that is identifiable that would link wind to solar activity.

CHAPTER 5

CONTEMPORARY WAVE CONDITIONS ON WARRABER REEF

5.1. Introduction

As described in Chapter 1, waves are a major driving force influencing sand-cay formation and stability. They transport sediments to where a focusing point occurs, shape sand cays through patterns of wave convergence and determine sand-cay topography through wave run-up. These processes are primarily influenced by wave characteristics. However, wave characteristics on reef flats, particularly around sand cays, have been little studied. Examination of their characteristics is one of the objectives of this thesis. This chapter therefore examines spatial and temporal variations of wave characteristics, origin of wave spectral components and the influence of waves on the threshold of sediment transport, both on the reef flat and around the island, based mainly on field measurements of wave characteristics in November 2004. This field study extended a preliminary study of wave characteristics and transformation on Warraber Reef undertaken by Hart (2003) and Brander et al. (2004).

The field experiment is outlined in Section 5.2 and wave data analysis is described in Section 5.3. In Section 5.4, patterns of winds, atmospheric pressure and tidal levels occurring during the experiment are reported. The next two sections deal with spatial and temporal variations of wave characteristics and energy for four frequency ranges on the reef flat (Section 5.5) and around the island (Section 5.6), respectively, based on wave spectra. Wave environments off Warraber Reef are identified in Section 5.5, which, together with wind climate derived in Chapter 4, enables an assessment of probable wave climate in this region. Additionally, in these two sections, development

of each spectral frequency range is described and saturating conditions of waves are investigated. Understanding whether or not waves on the reef flat reach their limiting state under various conditions of incident waves off the reef and water depth on the reef flat provides the context for evaluating the impacts of waves on the island stability under change in sea level. In the final section, Section 5.7, the spatial and temporal conditions of the threshold of sediment entrainment are assessed and sediment transport processes on the reef flat are described based primarily on the previous study by Hart (2003).

Results from this chapter, in conjunction with the previous study of sediment transport by Hart (2003), will be applied in Chapter 6 to assess probable wave conditions and sediment transport processes in relation to the evolution of island morphology examined in Chapter 2.

5.2. Field Experiment

A field experiment was undertaken between 24 and 29 November 2004. During that period, a range of instruments was deployed across the reef flat at Warraber Reef to record water pressure, current, atmospheric pressure and wind speed (Table 5.1).

Table 5.1 Instrument deployment during the experiment

Instrument	Sensor type	Number of instruments	Sampling
Kestrel 1000 pocket wind meter	Wind speed	1	-
BaroTROLL	Atmospheric pressure	1	300sec continuous
MiniTROLL pressure sensor	Water pressure	2	2 Hz continuous
NIWA Instrument Systems "Dobie"	Water pressure	1	2 Hz, 17.1 min/30 min
Hardwired KPSI pressure recording system	Water pressure	1	8 Hz continuous
Nortek Acoustic Doppler Velocimeter "Vector"	Water pressure and current	1	8 Hz, 18 min/30 min
InterOcean S4 integrated pressure and current meter	Water pressure and current	2	2 Hz and 5 Hz, 18 min/30 min

Wind data in the field were measured on the windward side of the island twice a day during 25–28 November 2004 using a Kestrel 1000 pocket wind meter. Wind directions were estimated using a magnetic compass measuring the direction of the long ribbon attached to a wooden stick fixed on the beach. Atmospheric pressure was recorded using a baroTROLL installed at the airfield on the island and used for atmospheric-pressure correction for pressure data obtained from a miniTROLL and a Dobie pressure sensor.

Water pressure measurement was undertaken using pressure-type wave recorders including a NIWA Instrument System "Dobie", two InterOcean S4DW wave-current meters, a Nortek Acoustic Doppler Velocimeter (ADV) "Vector", two miniTROLL pressure sensors and a hardwired KPSI pressure recording system with three sealed pressure sensors (Table 5.1). All are standalone units except the KPSI pressure sensors connected to the control unit on a shore for power supply and data acquisition.

The Dobie measured data in bursts of 1,024 s every 30 min at a sampling rate of 2 Hz. Two S4s with a sampling rate of 2 Hz and 5 Hz, respectively, collected data in bursts of 18 min every 30 min. The S4 5 Hz data were linearly decimated to 4 Hz in order that in a 1024-s time series of the data there are 2^n data points, a number of data points required for an algorithm used in wave spectral analysis described in the next section. The decimation was undertaken using a FORTRAN program developed by Stearns and David (1993). Hereafter, the S4 5 Hz data are referred to as S4 4 Hz data. The data from the S4 2 Hz are not included in the analysis due to visually identified errors involving an abrupt shift in a data trend within a burst. The Vector has a sampling rate of 8 Hz and recorded data in bursts of 18 min every 30 min. Only the first 1024-s part within a burst of the Vector data was used for analysis. The miniTROLL and the KPSI measured data continuously with a sampling rate of 2 Hz and

8 Hz, respectively. The miniTROLL and the KPSI data were subsequently separated to be a 1024-s time series every 30 min. The data from the KPSI is only available during daytime. 1024-s time series from the Dobie and the miniTROLL contains 2,048 data points, from the KPSI and the Vector 8,192 data points and from the S4 4 Hz 4,096 data points due to using different sampling rates. A collection of 1024-s time series of water pressure obtained from the sensors every 30 min was used for subsequent wave spectral analysis.

The Dobie was fastened to weights and deployed on the reef surface. The S4 was installed on an aluminium rod fixed on the reef flat, making the sensor approximately 0.20 m high above the reef flat. The Vector was attached vertically to an aluminium pole with the sensor facing down. The miniTROLL was attached to a star picket fixed on the reef surface. The KPSI pressure transducers were laid and fixed on the reef surface and hardwired to the control unit on the beach.

Figure 5.1 depicts the deployment locations around the island and on the reef flat at about the reef edge. The deployment locations around the island include 5 locations, 4 related to the transects (RT4, RT6, RT5 and RT1) defined by previous surveys in 2001 (Hart, 2003) and a new location at the eastern end of the island, hereafter called GZB. The deployment location on the reef flat at the Dobie pressure sensor will be referred to as RF. Different configurations of equipment were deployed on different days around the island due to the limited number of wave and current meters (Figure 5.2). These different configurations of instrument deployments were chosen in order that the distinct wave environments anticipated around the island would be recorded at the same time. In addition, more than one piece of equipment along a transect was deployed in order to investigate spatial variations of wave characteristics from the nearshore towards the island.
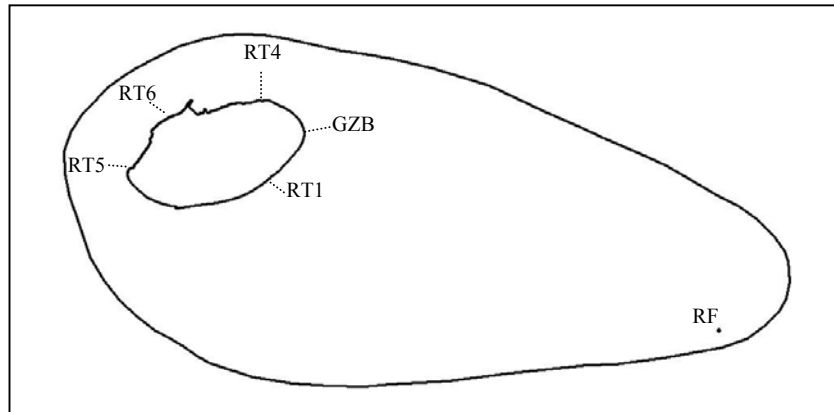
Figure 5.1. Locations of deployments of wave and current recorders on the reef flat (RF) and around the island (RT4, RT6, RT5, RT1 and GZB).
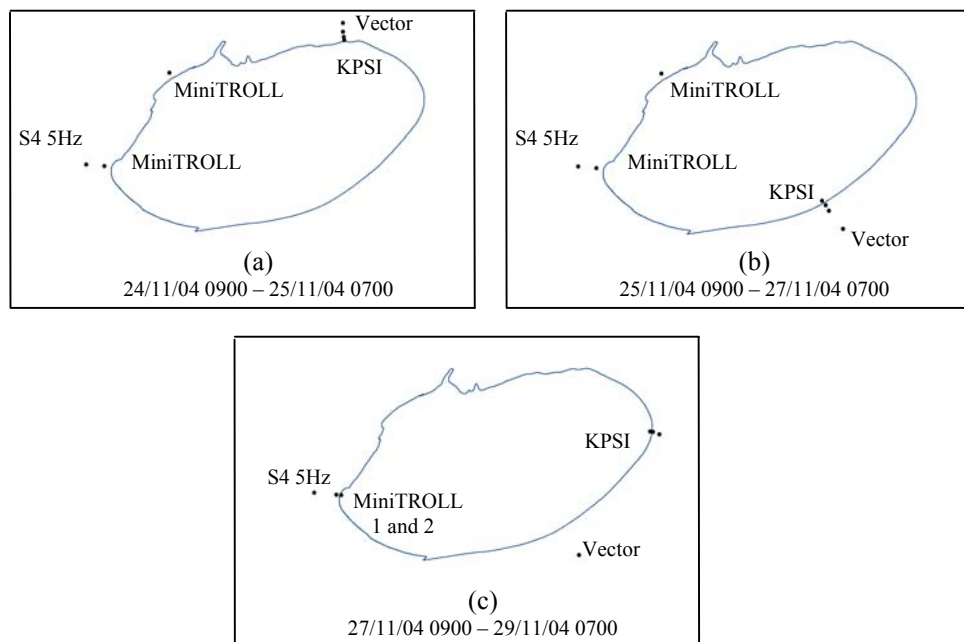
Figure 5.2. Locations and dates of particular instrument deployments around the island.

Ideally, the experiment would have also included measurement of incident waves off the reef in order to understand the relationship between incident waves off the reef and waves on the reef flat, and to be the basis for developing a detailed wave climate in this region. Safety and accessibility issues, however, precluded equipment deployment off the reef. In this study, in order to capture the patterns of waves as close to that of the incident wave as possible, the Dobie pressure sensor was installed close to the eastern

end of the reef flat (RF), about 100 m from the reef edge (Figure 5.1) and the spectral peak of the incident waves off the reef was deduced from the spectra of waves at RF.

5.3. Wave Data Analysis

Spectral analysis based on the fast Fourier transform (FFT) algorithm was used to derive wave parameters from the 1024-s time series of pressure data. FORTRAN programs were developed for analysing the data. The same record length, frequency interval, tapering technique, spectral estimate averaging method and degrees of freedom were used for all time series in order that the results could be compared (Hegge and Masselink, 1996)

The procedures adopted for spectral analysis are primarily those recommended by Bendat and Peirsol (1986). The time series of the data were plotted for visual identification of any trends and outliers. A linear trend was observed, which is attributed to tide level. A polynomial of degree 3 was deployed to detrend the records. The code for trend removal followed Borse (1991). The 4-standard deviation criterion was used to identify outliers. The data that fall outside the 4 standard deviations of the data were removed. Resulting gaps were filled by interpolation using the data at both ends of the gaps. The segment-averaging technique with 50% overlapping was used in order to reduce the variance of the spectral estimates (Bendat and Piersol, 1986). With 50% overlapping, the time series of 1,024 s were divided into 15 segments of 128 s, giving a spectrum having 30 degrees of freedom and a frequency resolution, Δf of 0.0078 Hz. Spectral leakage was suppressed via tapering using a Hanning window. Data tapering reduces bias in the spectral estimates (Krogstad *et al.*, 1999). Fourier coefficients were computed from detrended and tapered data using the FFT technique.

The FFT code is DFFTPACK v 1.0 which is public domain (Swarztrauber and Pumphrey, 1985). A value of $(8/3)^{0.5}$ was applied to each coefficient to compensate for the loss of the variance due to the Hanning tapering. The spectral estimates were obtained from averaging the spectral components over 15 segments.

The energy spectrum obtained at this stage of the wave spectral analysis was the spectrum of water depth measured by a pressure transducer. A pressure-type wave recorder is normally subject to the attenuation of wave action with depth. To convert pressure records to surface waves, in practice, a transfer function, K_p, is applied so as to compensate for the attenuation of wave action with depth and high-frequency cutoff is determined in order to prevent amplifying noise at high frequency regions by the transfer function (NortekUSA, 2002).

A transfer function based on linear wave theory is generally found to be reasonable except in shallow water where effects of nonlinear waves and currents become more dominant (Lee and Wang, 1984). An empirical correction factor, N, is practically applied to the transfer function to account for the difference between theory and observation (Bishop and Donelan, 1987). In the review by Bishop and Donelan (1987), it can be seen that N normally is greater than 1 for longer periods and less than 1 for short periods. Knowles (1983) recommended N derived by Grace (1978) for shallow and closed restricted-fetch estuaries or lagoons which are dominated by waves with periods generally less than 4sec. In this research, N was not evaluated and due to the general trend of N found from previous investigations together with the recommendation for shallow water with sea domination by Knowles (1983), equations of N determined by Grace (1978) were adopted here. Visual inspection of the wave spectra, especially from the sensors at locations around Warraber Island indicated that a maximum value of K_p multiplied by N (NK_p) would not be greater than 10. Therefore,

in this study, NK_p with its maximum value of 10 was applied to convert pressure to surface waves. The FORTRAN program for calculating wave number (k) for NK_p followed Kirby and Dalrymple (1994).

Since the linear transfer function increases rapidly at high frequencies, transforming the pressure signals to surface waves is commonly terminated at a certain frequency beyond which the area is extrapolated using a high-frequency f^n tail (Wolf, 1997), where n varies between −3 and −5, depending on shallow or deep conditions, respectively (Young and Verhagen, 1996b). The high-frequency cutoff can be determined either by using a fixed frequency or using a threshold level being reached by the attenuation factor (Wolf, 1997).

In areas dominated by swell, wave energy beyond 0.5 Hz is normally considered not significant and frequencies at 0.5 Hz or less are used, for instance, by Elgar and Guza (1985a), as the cutoff frequency so that the main portions of the spectrum can be retained and an error attributable to enhancing noise levels at high frequencies can be avoided. In areas where seas are dominant, however, high-frequency components are often found to contribute significant portions to the energy spectrum. Spectra of pressure signals from sensors around Warraber Island show significant levels of energy at high frequencies around 0.5-0.8 Hz (2.0-1.25 s), which were suggested to be wind waves generated locally on the reef flat by Brander et al. (2004). Accordingly, setting the high frequency cutoff is site-specific, depending on the nature of wave conditions in that area and hence has to be determined appropriately in order that the correct portions of the spectra are mostly retained while the influence of noise or aliasing is diminished.

Pressure signals from the Dobie wave gauge start to level off at approximately 0.8 Hz. The cutoff frequency was therefore set at 0.8 Hz and areas between the cutoff frequency and 1.0 Hz were extrapolated using a high-frequency f^5 tail. For the pressure

data from the sensors around the island, the cutoff frequency was set at the frequency when a relative depth (h/L) at that frequency equals to 0.7. Normally, a relative depth of 0.5 is used to determine the cutoff frequency, a value at a boundary between deepwater waves and intermediate waves, according to linear wave theory (Smith et al., 2001). However, in order to have the smooth reduction of spectral energy at the end of a spectrum, this study found the value of the relative depth of 0.7 in combination with the maximum value of NK_p of 10 to be more appropriate for a conversion of the pressure data at the locations around the island. Areas between the cutoff frequency and 1.0 Hz were also extrapolated using a high-frequency f^5 tail.

Several wave parameters were calculated from the wave energy spectra, including the significant wave height H_{mo}, the peak wave period T_p, the mean wave period T_1 and the bandwidth parameter ε. They are defined as (Tucker, 1991)

$$H_{mo} = 4\sqrt{m_0} \ ; \qquad T_1 = \frac{m_0}{m_1} \ ; \qquad \varepsilon = \left(1 - \frac{m_2^2}{m_0 m_4}\right)^{1/2}$$

Where
$$m_p = \sum f^p S(f)\, df$$

The spectral peak T_p was derived from $T_p = 1/f_p$ where f_p defined as (Mansard and Funke, 1991)

$$f_p = \frac{\int f\, S^5(f)\, df}{\int S^5(f)\, df}$$

Compared to other methods for the estimation of f_p, the equation shown above gives less error associated with the determination of f_p (Mansard and Funke, 1991; Young, 1995).

A wave spectrum is divided into 4 different frequency ranges (Figure 5.3), based on the previous wave study on Warraber Reef by Brander et al. (2004). The frequency

ranges include: i) incident short-period wave frequencies of 0.4-1.0 Hz (2.5-1.0 s); ii) incident wind wave frequencies of 0.125-0.4 Hz (8.0-2.5 s); iii) incident swell wave frequencies of 0.05-0.125 Hz (20.0-8.0 s); and iv) infragravity wave frequencies of less than 0.05 Hz (greater than 20 s).
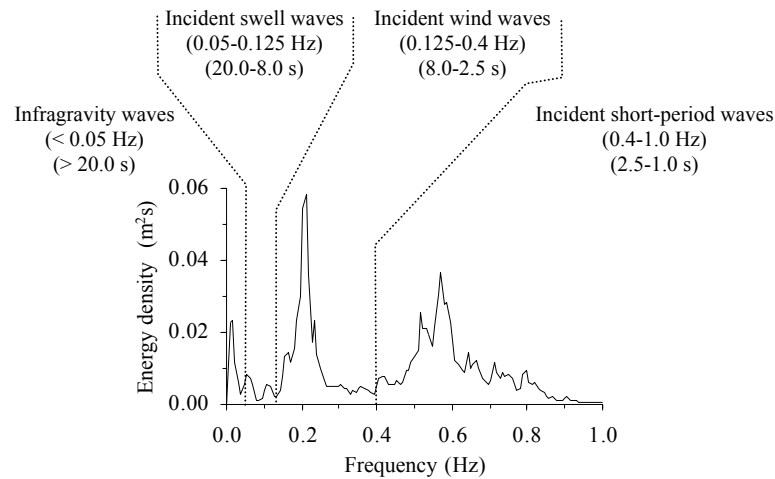
Figure 5.3. Sample wave spectrum with a division of 4 different frequency ranges.

The maximum wave period that can be detectable in this spectral analysis is 128 s according to the length of the data segment. According to spectral shape at the locations around the island, in this study the frequency of 0.4 Hz was found to be more appropriate as the division of frequency ranges between incident wind waves and incident short-period waves than the value of 0.333 Hz that was applied by Brander et al. (2004). The calculation of wave energy was also done from wave spectra for both the whole spectral components and each frequency range defined above.

5.4. Patterns of Winds, Atmospheric Pressure and Tidal Level

Wind speed and directions both from the field and from the meteorological station (Horn Island) are shown in Figure 5.4. Wind data from the meteorological station are

9 am wind recorded at a standard 10 m level. Wind speed from the field shown in

Figure 5.4a is at 10 m, converted based on CERC (1984) from the measurement level of

approximately 1.70 m. Wind speed and directions from both sources exhibit the same

trend. Due to being available for a longer period, hereafter the wind data referred to are

those from the meteorological station. Wind directions over the experiment (24–

29/11/04) were relatively stable from the ESE. Wind speed was 5.11 m/s on the first

day and increased continuously with its peak of 9.81 m/s on 26/11/04 and gradually

decreased thereafter.
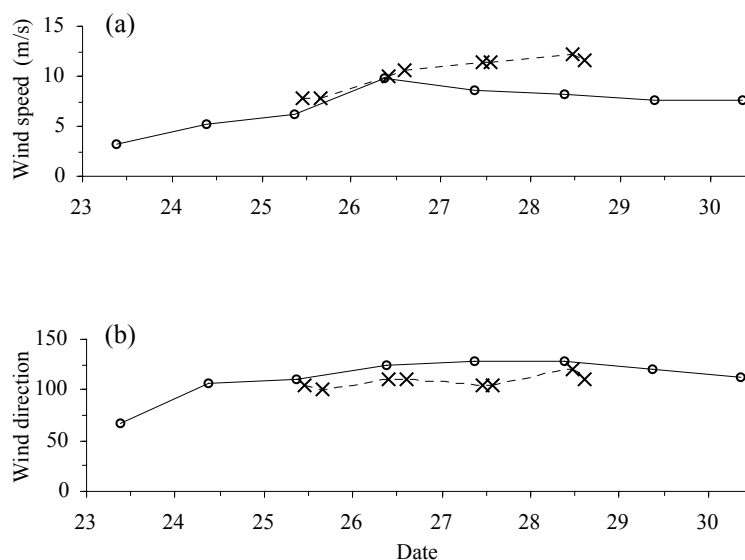
Figure 5.4. a) wind speed and b) wind direction from field observations (--x--) and a meteorological station on Horn Island (─o─).

Figure 5.5a shows the relationship between tides and water depth on the reef flat

derived by averaging data within each time series from the Dobie wave gauge. Water

depth on the reef flat is fundamentally controlled by tides which are a mixed type, a

higher high tide (HHT) around noon, a lower high tide (LHT) around midnight, a lower

low tide (LLT) in the early morning and a higher low tide (HLT) in the afternoon.

133
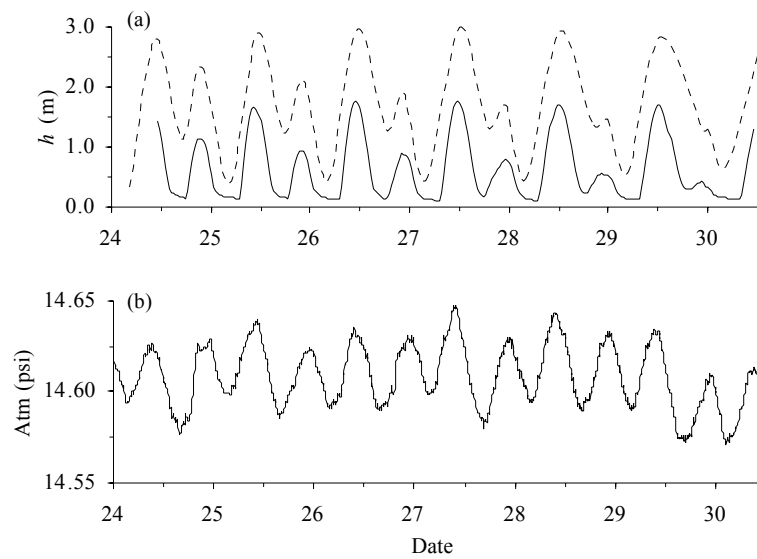
Figure 5.5. Temporal variations of: a) tides (---) and water depth at the Dobie wave gauge (─); and b) atmospheric pressure measured using a baroTROLL located at the airfield on the island. Tides are at Poll Island, which are referenced to the tidal prediction at Twin Island where tides are 28 min later than those at Poll Island.

The reef platform was generally inundated during HHT and LHT whereas during a LLT and most of HLT when tidal levels were below the major part of the reef platform, the reef platform was mostly exposed. At a HHT, water depth increased from 1.66 m on 25/11/04 to 1.78 m on 26/11/04 and slightly reduced to 1.76 m on 27/11/04 and was stable at 1.71 m on 28-29/11/04 (Figure 5.5a).

At a LHT, water depth decreased progressively from around 1.14 m on 24/11/04 to 0.94, 0.87, 0.79, 0.55 and below 0.5 m on 25, 26, 27, 28 and 29/11/04, respectively (Figure 5.5a). During a LLT and most of HLT, water depth on the reef decreased slowly until the next flooding came as a result of water retained on the reef flat gradually draining off the reef platform (Figure 5.5a). Atmospheric pressure obtained from the baroTROLL is shown in Figure 5.5b.

5.5. Wave Characteristics on the Reef Flat at RF

5.5.1. Temporal Variations of Wave Characteristics and Wave Spectra

In general, waves at RF were reformed waves after incident waves broke at about the reef rim, according to visual observations during working on the reef flat. As water depth on the reef flat at RF become shallower than 0.5 m, the pressure signals are more contaminated by an error characterised by flat regions. Therefore, the data having a mean water depth less than 0.5 m were discarded from analysis.

Temporal variations of H_{mo}, T_p, T_1, and ε are shown together with temporal variations of h on the reef flat in Figure 5.6 and the relationship between H_{mo}, T_p, T_1 and ε, and h on the reef flat are illustrated in Figure 5.7. The effect of reef-flat water depth on wave characteristics is obvious (Figures 5.6 and 5.7), particularly, for H_{mo}, as demonstrated in Figures 5.6a and 5.7a. Generally, temporal variations of H_{mo} directly follow a changing pattern of water depth, primarily induced by tides (Figure 5.6a). A daily maximum H_{mo} normally occurred at a HHT, increasing from around 0.22 m on 24/11/04 to around 0.33 m on 25/11/04 and reaching approximately 0.62 m on 26/11/04. The maximum H_{mo} during the field experiment was 0.66 m occurring at a HHT on 27/11/04. After that, daily maximum H_{mo} gradually decreased to 0.62 and 0.54 m on 28 and 29/11/04, respectively. According to values of H_{mo} during the experiment, two events related to wave energy are arbitrarily identified, a low wave-energy event during 24-25/11/04 and a high wave-energy event during 26-29/11/04. Samples of the spectra responding to a low wave-energy event (25/11/04) and a high wave-energy event (27/11/04) are illustrated in Figure 5.8.
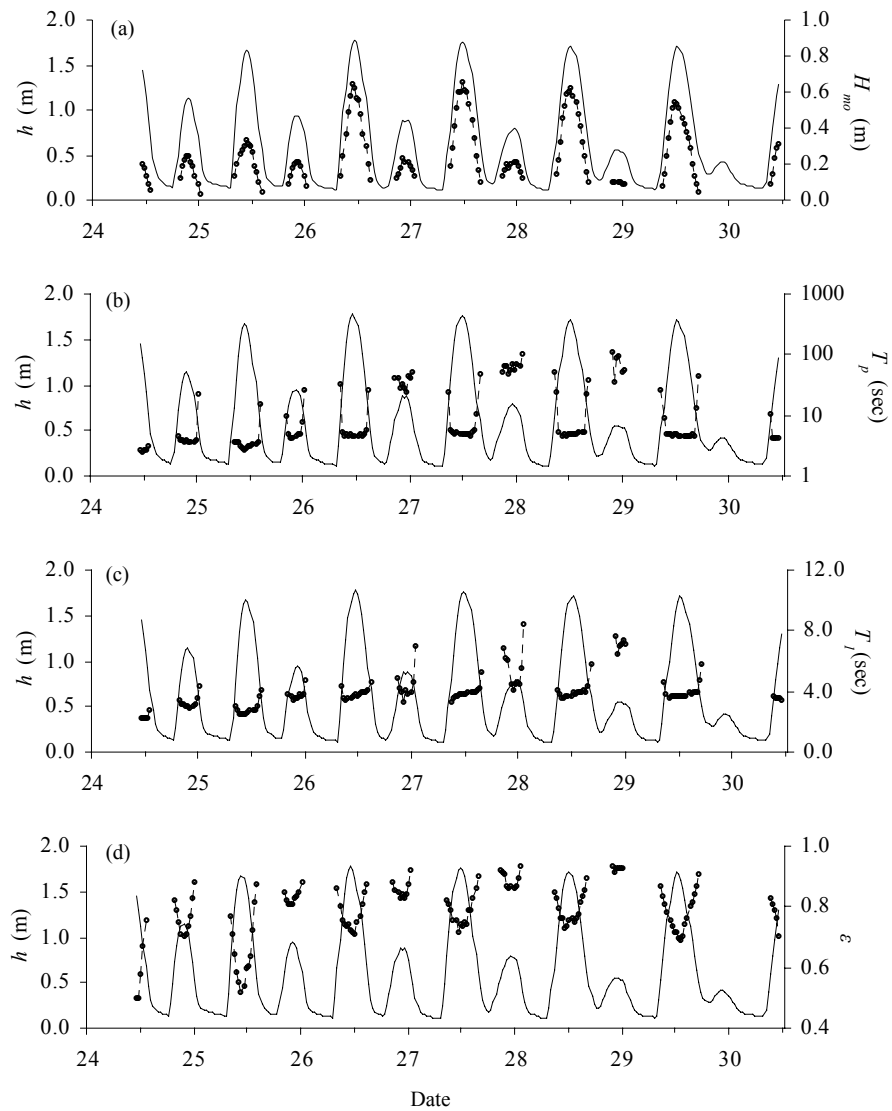
Figure 5.6. Temporal variations of wave characteristics on the reef flat at RF (--o--) between 24–30/11/04: a) H_{mo}; b) T_p; c) T_1; and d) ε, shown together with those of h (—) at RF.

During a tidal cycle, T_p appeared to increase slightly as water depth on the reef flat decreased but became much longer when the water depth was below approximately 0.7 m (Figures 5.6b and 5.7b). Generally, T_p was longer during high wave energy, between 4.5-5.5 s, and shorter during low wave energy, between 2.5-4.0 s (Figures 5.6b and 5.8). At a daily HHT, T_p was around 2.7 s on 24 and 25/11/04, and increased to 4.6 and 4.9 s on 26 and 27/11/04, respectively. The maximum T_p at a daily HHT was approximately 5.1 s occurring on 28/11/04. T_p at a daily HHT slightly decreased to 4.8 s on 29/11/04.
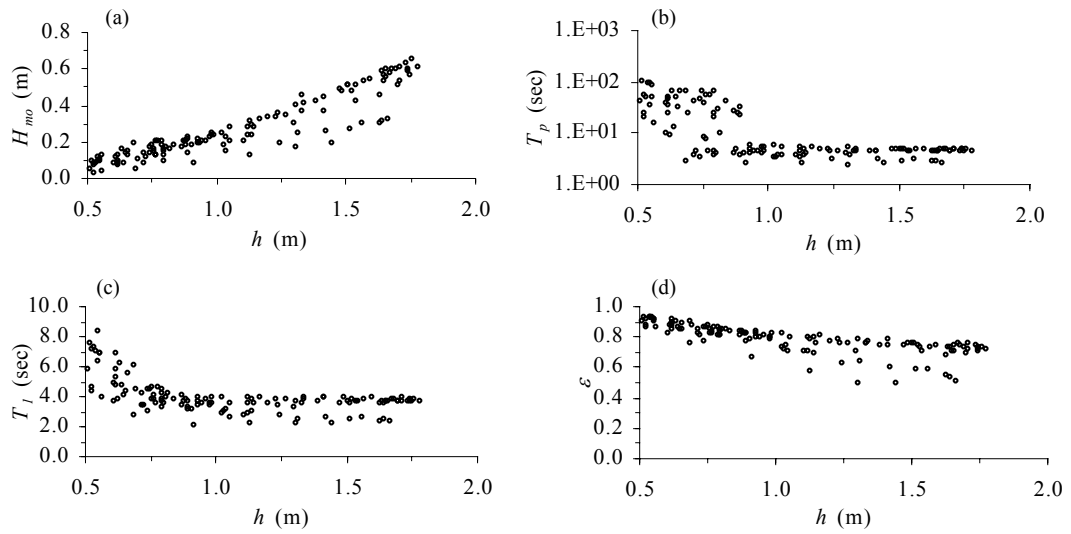
Figure 5.7. Relationship between *h* and wave characteristics: a) H_{mo}; b) T_p; c) T_1; and d) ε, derived from wave data measured at RF over a period of 24-30/11/04.
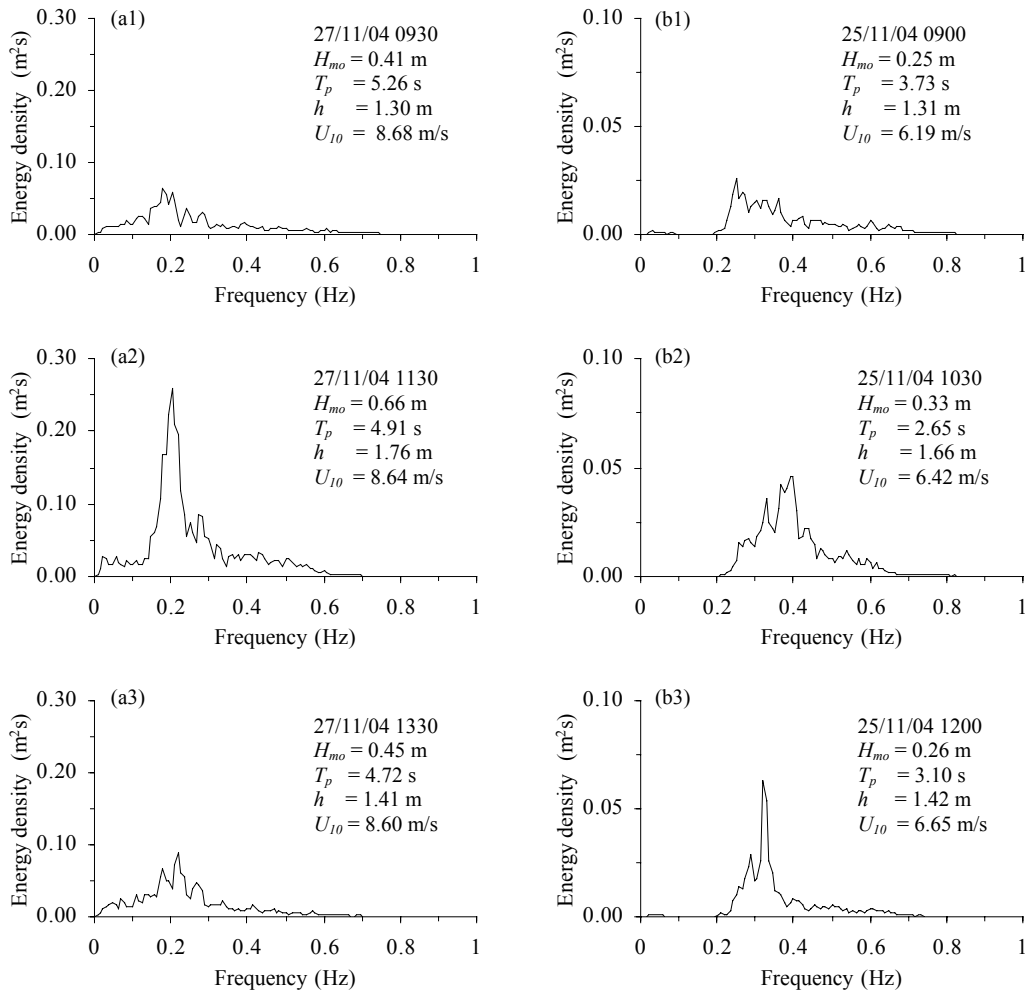
Figure 5.8. Samples of wave spectra during a high wave-energy event on 27/11/04 (a1: flooding tide, a2: high tide and a3: ebbing tide) and a low wave-energy event on 25/11/04 (b1: flooding tide, b2: high tide and b3: ebbing tide).

T_1 also varied similarly but with smaller values, between 3.7-4.0 s during high wave energy and 2.2-2.5 s during low wave energy (Figures 5.6c and 5.7c). T_1 slightly varied during a tidal cycle until water depth was below around 0.7 after which it increased with a decrease in water depth (Figure 5.7c).

Wave spectra are broader-banded when wave energy is spread over a wider range of spectral components and narrower-banded when wave energy only focuses on a narrower range of spectral components. Wave spectra with ε of less than 0.6 are considered to be narrow-banded (Chakrabarti, 1987). According to Figures 5.6d and 5.7d, therefore, most waves were characterised as broad. Only during low wave-energy events at HHT were wave spectra narrow. Generally, at higher water depth, wave spectra exhibited prominent peaks at incident wind-wave components (0.125-0.4 Hz) but became broader with the longer peak periods at lower tide (Figure 5.8).

5.5.2. Wave Energy and Wave Attenuation

Figure 5.9 demonstrates the relationship between water depth on the reef flat at RF and relative wave energy over four ranges of frequencies. Incident wind waves are a major component at this location (Figure 5.9c). They contributed up to about 80% of wave energy during high water level. For water level below approximately 0.7 m, the percentage of incident wind-wave energy decreased (Figure 5.9c) while that of infragravity wave energy increased (Figure 5.9a). The contribution from incident swell wave components (Figure 5.9b) and incident short-period wave components (Figure 5.9d) was normally small, less than 20%. For shallower water, however, swell energy tended to increase (Figure 5.9b). In Figures 5.9c and 5.9d, the scatter during high water
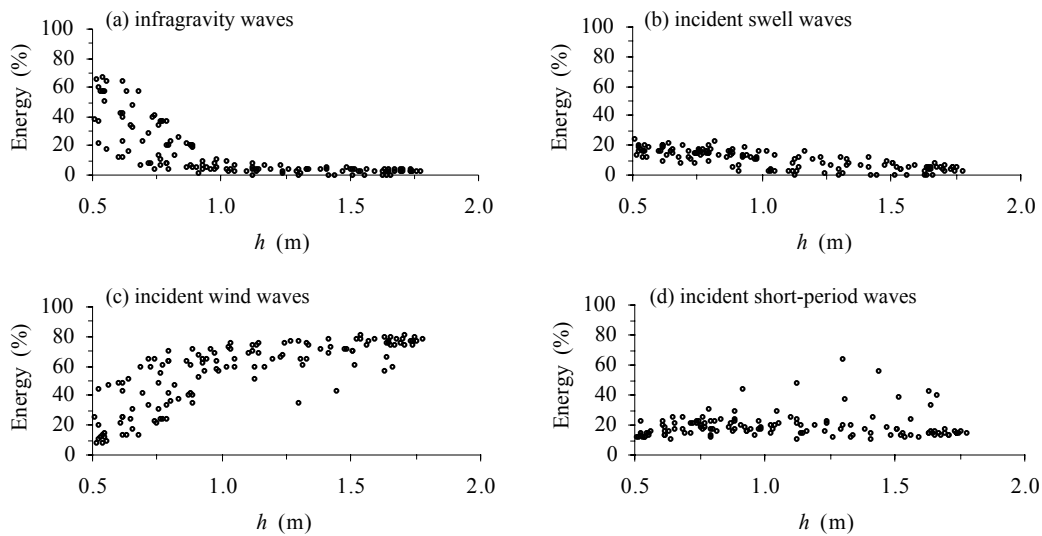
Figure 5.9. Relationships between water depth on the reef flat and relative wave energy over frequencies of: a) infragravity waves (< 0.05 Hz or > 20 s); b) incident swell waves (0.125–0.05 Hz or 8.0-20.0 s); c) incident wind waves (0.4-0.125 Hz or 2.5-8.0 s); and d) incident short-period waves (1.0-0.4 Hz or 1.0-2.5 s) at RF.

depth occurred during low wave-energy events. It indicates more contribution from incident short-period waves and less from incident wind waves. In Figures 5.9a and 5.9c the scatter was found as water depth was below 0.7 m. At water depth below 0.7 m, higher percentages of incident wind waves occurred during low wave-energy events and low percentages during high wave-energy events (Figure 5.9c). In contrast, as water depth was below 0.7 m, infragravity waves contributed more energy during high wave-energy events than during low wave-energy events (Figure 5.9a).

In this study, no incident waves off the reef were directly measured. However, on 29/11/04, incident wave height of approximately 1.5-2.0 m was visually estimated from a dinghy travelling between Warraber Island and Poll Island. In order to estimate wave attenuation between the reef edge and RF during a period of the experiment, the maximum estimated wave height of 2.0 m is presumed to exist on 27/11/04, the day when the maximum H_{mo} of 0.66 m occurred at RF with water depth of 1.76 m. Based on a value of H_{mo} off the reef and that at RF, therefore, approximately 67% of H_{mo} or 90% of wave energy was reduced across the reef rim.

5.5.3. Wave Environments off the Reef and Spectral Wave Components at RF

Studies of wave transformation on a coral reef on the Great Barrier Reef (Hardy and Young, 1996), in Hawaii (Lee and Black, 1978) and at sites in the Caribbean Sea (Roberts et al., 1975; Lugo-Fernandez et al., 1998a) indicated that the frequency of the spectral peak of waves on a reef maintains that of waves off the reef even when wave spectra become broader as a result of energy dissipation and energy transfer. In addition, at Tague Reef, St. Croix, in the US Virgin Islands, Roberts (1989) found that the reef is a more efficient filter for high-frequency waves and only the low-frequency peaks of the forereef spectra persist in the backreef. Therefore, T_p of waves off Warraber Reef could be deduced from T_p derived from wave data at RF, especially during at high tides when water depth has less influence on waves on the reef.

Hardy and Young (1996) studied the relationship between T_p of incident waves and that of waves on the reef flat. They found that when T_p of incident waves is less than 5.0 s, there is close similarity between T_p on both locations. When T_p of incident waves is greater than 5.0 s, however, T_p of waves on the reef flat is slightly shorter probably resulting from more energy removed for longer wave periods due to wave breaking and bottom friction.

Analyses in Sections 5.5.1 and 5.5.2 indicated that waves at RF were generally dominated by incident wind-wave frequencies except during very low water level when infragravity wave frequencies were dominant. Accordingly, wave environments off Warraber Reef during the experiment were possibly characterised predominantly by seas, which are wind waves under the influence of local wind conditions, and have T_p of approximately 4.0 and 6.0 s during low and high wave-energy events, respectively. Sea

domination of waves off Warraber Reef is also suggested by the relationship between wind speeds and variations of wave characteristics at RF, as illustrated in Figure 5.10.
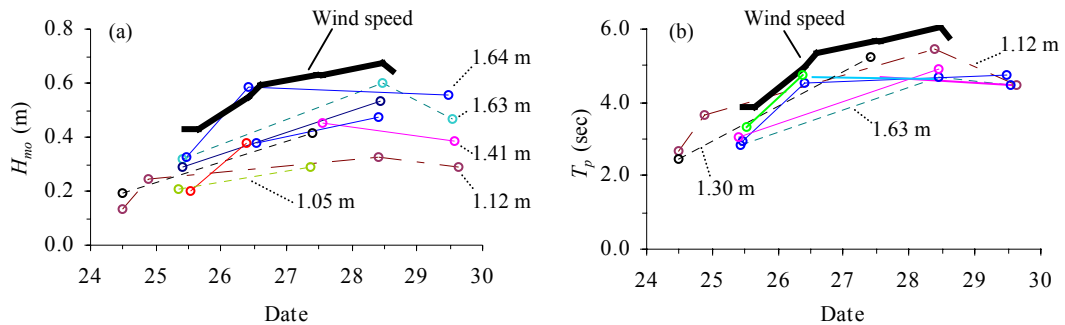
Figure 5.10. Temporal variations of: a) H_{mo}; and b) T_p, for equivalent water depth at RF, compared with variations of wind speeds (━━) obtained from the field over the period of the experiment. Data of H_{mo} and T_p on each line are from the same water depth and only some lines are labelled with water depth due to a limited space. Values of wind speeds are equally reduced so that they can be displayed in the same range of values of H_{mo} and T_p.

Wave characteristics on reef flats are governed by water depth on reef flats and incident wave conditions (Young, 1989). In order to examine only the influence of incident waves, wave parameters at an equal water depth over the period of measurement were selected. Figure 5.10 demonstrates the temporal variation of H_{mo} and T_p over equivalent water depth, compared with variations of wind speeds obtained from the field. Data shown by a circle on the same line are wave conditions (H_{mo} in Figure 5.10a and T_p in Figure 5.10b) occurring at an equal water depth at RF. Different lines are from different water depths. At the same water depth over the period of the experiment, values of H_{mo} and T_p were not constant but tended to increase and peak approximately between 27-28/11/04, similar to a trend of wind-speed variations (Figure 5.10); thus supporting the finding above that wave conditions at RF are primarily influenced by seas which are directly driven by a local wind pattern.

The response time of seas to winds can be approximated using correlation analysis between change in wind speeds and in H_{mo} measured at RF. In order to reduce the

effect of water depth, only H_{mo} at a HHT was chosen for analysis. Figure 5.11 shows results of a correlation analysis with a lag step of 6 h.
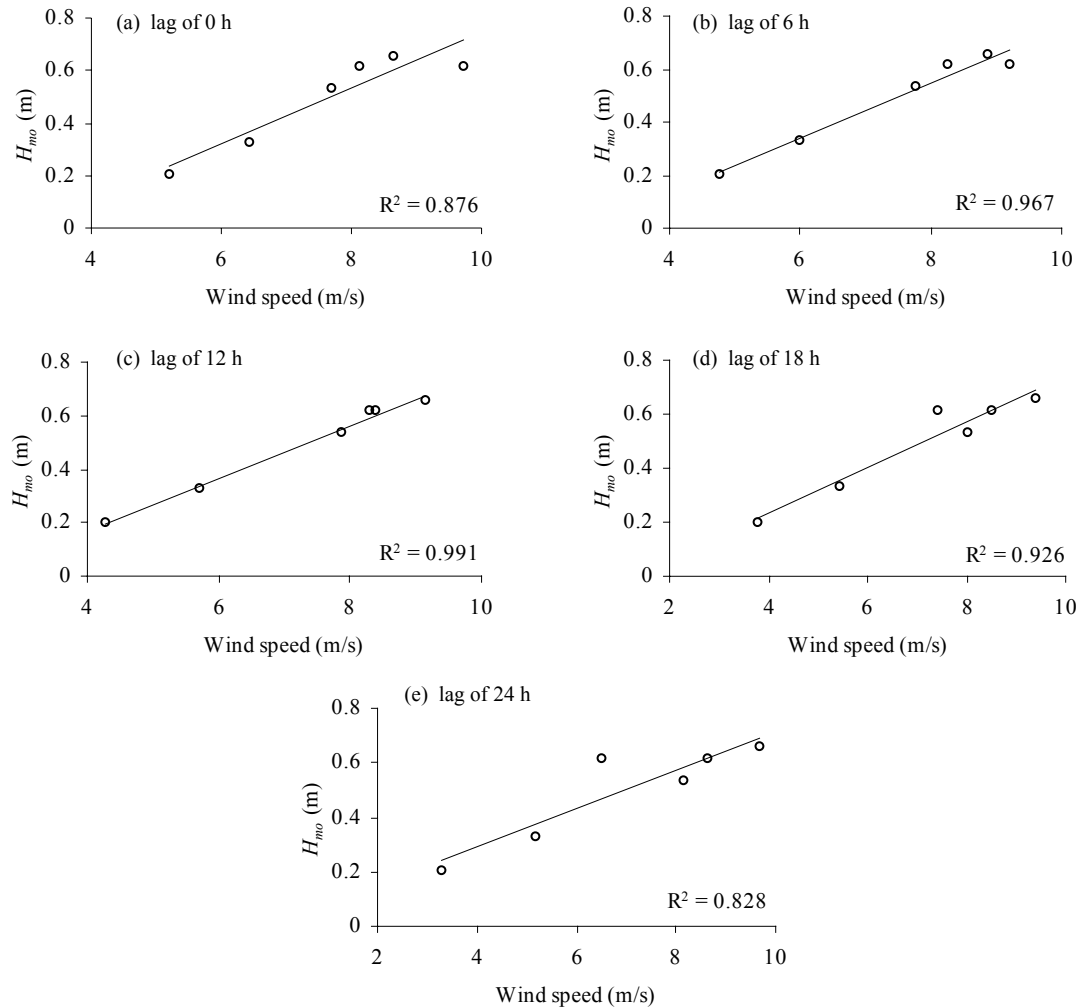
Figure 5.11. Correlation analysis between wind speeds obtained from the meteorological station (Horn Island) and H_{mo} at lags of: a) 0 h; b) 6 h; c) 12 h; d) 18 h; and e) 24 h.

A correlation analysis gave the best correlation coefficient R^2 of 0.991 at a lag of 12 h, suggesting that seas take less than 12 h to respond to wind speeds. Hardy and Young (1996) found the response time of 1 to 2 h during the experiment at John Brewer Reef.

In areas where seas are dominant, swell, which is wind wave not under the influence of local wind conditions, can be more observable only when the energy of seas is small. Therefore, a good time to check if swell is present is when wind is light

and water level is high. Figure 5.12 shows wave spectra at a HHT during low wave energy.
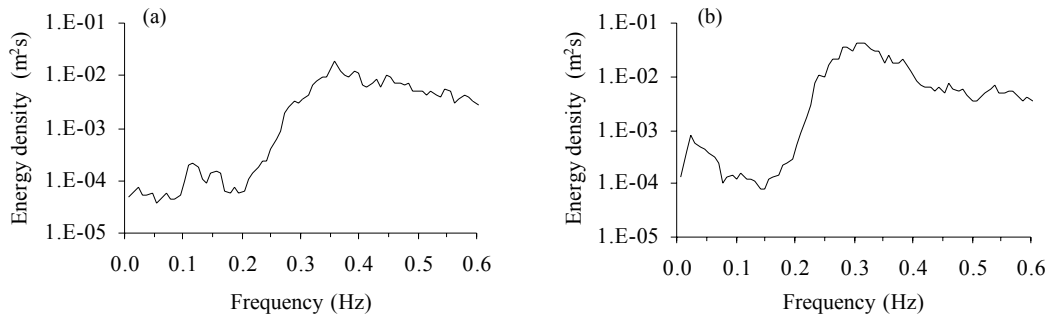
Figure 5.12. Wave spectra at HHT during low wave energy on: a) 24/11/04; and b) 25/11/04, indicating peaks at swell frequencies. Values of wave spectral energy density are plotted using a logarithmic scale so that peaks of swell wave frequencies, which are very small when compared to wind wave components, can be seen.

On 24/11/04 and 25/11/04 during a HHT, peaks of swell at approximately 7.0-8.0 s could be seen and persisted until water depth was below approximately 0.5 m (Figure 5.12a). However, they contributed only less than 0.5% to the spectrum. It can also be noted that as wave energy increased, swell wave components were less clear and infragravity wave components were more obvious (Figure 5.12b). During the high wave-energy event, a swell component was not evident. Therefore, the influence of swell waves on the wave environment at RF is negligible, particularly during high wave-energy events. Most energy found within a swell frequency range, which is shown in Figure 5.9b, is probably not contributed by incident swell waves but rather energy transferred across the spectrum between the incident wind wave and infragravity wave components during the time that incident waves move onto the reef.

As waves propagate over the reef, sub-harmonic (lower frequencies) and super-harmonic (higher frequencies) components of wave spectra are developed as a result of energy transfer from spectral peaks (Gerritsen, 1980). At RF, energy transfer to lower frequency components is observable particularly during low water level, causing the spectra to become broader. Super-harmonic generation is, on the other hand, not

obvious at RF. This is probably due to the fact that seas not swell dominate the wave field off Warraber Reef and that seas are broad-banded.

The super-harmonics of wave spectra are well developed in association with narrow-banded wave characteristics, whereas energy is spread over a wide range of frequencies higher than spectral peaks for broad-banded waves (Elgar and Guza, 1985b). The energy transfer to higher frequency components is generally observed when swell is a major component of incident waves. This has been reported both from field observations of swell moving over the reef (Lee and Black, 1978; Wiegel, 1990) and shallower water (Byrne, 1969; Elgar and Guza, 1985a), and from laboratory experiments of regular waves (Massel, 1983) and irregular waves with spectral peaks of swell components (Kofoed-Hansen and Rasmussen, 1998).

The indefinite generation of super-harmonics in relation to incident shorter-period waves was also pointed out by Hardy and Young (1996) according to the experiment on John Brewer Reef. The super-harmonics however could be indistinguishable from relatively high background energy of high frequency wind waves in wave spectra incorporating both prominent high and low frequency wave components (Guza and Thornton, 1980). The generation of super-harmonics of spectral peaks were also reported in the laboratory experiments when incident waves are very short, for example, having peak frequencies of greater than 0.4 Hz (or less than 2.5 s). In that case, second and third harmonics were developed at very high frequencies of approximately 0.8 and 1.2 Hz, respectively. Those high frequency portions of spectra would not be seen in spectra derived from field measurements probably because of the high-frequency cutoff procedure. In addition, such high frequencies are probably not of engineering concern due to low amplitudes limited by wave steepness.

Basically, wave harmonics are developed as bound waves during incident wave shoaling and subsequently released as free waves when incident waves move across an abrupt change of water depth or break (Kofoed-Hansen and Rasmussen, 1998). Numerical experiments of long-wave transformation on a submerged coastal reef by Karunarathna and Tanimoto (1995) showed that long wave components on the reef top are composed of both free long waves and bound long waves. Therefore, at RF low frequency components of spectra could be a combination of bound long waves and free long waves released as a result of either incident waves breaking or water depth discontinuities at about the reef crest.

5.5.4. Wave Saturation

As seen in previous sections, wave height on the reef flat at RF, which is forced by seas, is significantly limited by water depth on the reef flat. It is necessary to understand whether or not waves on the reef flat reach their limiting state of growth or wave saturation in order that the impacts of incident waves on the island can be anticipated under scenarios of change in sea level.

Saturation of waves on the reef flat at RF was examined based on a curve proposed by Nelson (1994). His curve describes the upper limit value for the ratio H_{max}/h for reformed, oscillatory waves propagating over a horizontal platform in water depth ranging from intermediate water to shallow water and is given by

$$\frac{H}{h} = \frac{F_c}{22 + 1.82 F_c}$$

where F_c is a non-linearity parameter and is defined as (Swart and Loubser, 1979),

$$F_c = \frac{g^{1.25} H^{0.50} T^{2.50}}{h^{1.75}}$$

shallow water waves $\qquad F_c > 500$

transitional water waves $\qquad 500 > F_c > 10$

deep water waves $\qquad 10 > F_c$

Visual inspection of time series of pressure signals was performed in order to select reformed, oscillatory waves from the whole dataset. Data having an average water level greater than 0.9 m were selected and associated H_{mo} was converted to H_{max}. $H_{max} = 1.3 H_{mo}$, based on Glukhovskiy's distribution for wave height in finite water depth (Massel, 1998). For each time series, F_c was computed using H_{max}, h and T_p. Scatter plots of H_{max}/h over ranges of F_c are compared to Nelson's curve in Figure 5.13.
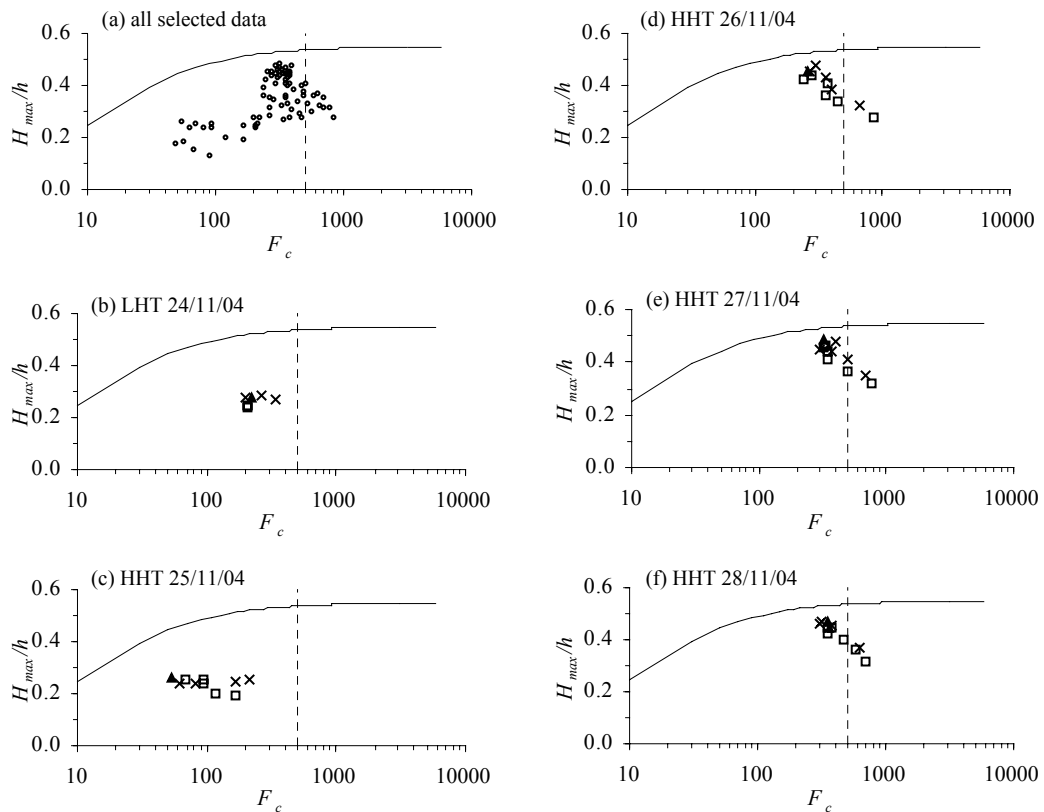
Figure 5.13. Comparison between a curve of maximum H_{max}/h proposed by Nelson (1994) (—) and H_{max}/h from field data: a) all selected data; b) a low wave-energy event at LHT 24/11/04; c) a low wave-energy event at HHT 25/11/04; d) a high wave-energy event at HHT 26/11/04; e) a high wave-energy event at HHT 27/11/04; and f) a high wave-energy event at HHT 28/11/04 (x = flood, ▲ = peak and □ = ebb). On the left side of a dash line is intermediate water and on the right side is shallow water.

Waves on the reef flat at RF approached the limit of H_{max}/h during high wave-energy events (Figure 5.13d, e, and f) whereas they were well below the limit of H_{max}/h

during low wave-energy events (Figure 5.13b and c). Their values of H_{max}/h increased with a decrease of F_c (deeper water wave conditions) and all peaked in an intermediate water wave condition ($10 < F_c < 500$). A shallow water wave condition ($F_c > 500$) was found only during high wave-energy events but well below the limits defined by Nelson's curve. This pattern of H_{max}/h probably results from the different magnitude of energy dissipation due to wave breaking at the reef edge and bottom friction over different levels of water on the reef. The results from a laboratory experiment of wave transformation on a coral reef conducted by Gourlay (1994) indicated that an increase in the ratio of incident wave height to water depth at the reef edge results in more energy dissipation due to wave breaking. Energy dissipation due to bottom friction is a function of horizontal orbital velocity (Massel and Gourlay, 2000) which, based on linear wave theory, decreases with an increase in water level (Komar, 1998). Therefore, the magnitude of energy dissipation due to wave breaking and bottom friction is less at higher water depth on the reef, resulting in an increase of the ratio of H_{max}/h with depth.

It is necessary to emphasise at this point that the a value of H_{max}/h of 0.55 usually referred to as the limit of H_{max}/h is the limit applied for reformed, oscillatory waves over shallow water ($F_c > 500$) across a horizontal bottom. The limiting values become smaller for intermediate water wave conditions ($10 < F_c < 500$), as indicated by Nelson's curve in Figure 5.13. In terms of wave saturation, therefore, values of H_{max}/h less than 0.55 do not mean that waves are not at the limiting level of growth. Similarly, in terms of wave energy, the limiting values of H_{max}/h less than 0.55 are not less significant than the limiting value of 0.55. They occasionally are more important, particularly for engineering design. For example, a value of H_{max}/h of 0.2 at $h = 1.0$ m which implies H_{max} of 0.2 m is much more significant than that of 0.55 at $h=0.1$ m which suggests H_{max} of approximately 0.06 m.

5.6. Wave Characteristics around the Island

5.6.1. Spatial and Temporal Changes of Wave Spectra and Parameters

Wave spectra, and spectrally derived wave parameters and energy contents in different frequency ranges at locations around the island were estimated using pressure data obtained from the Vector (VT), the KPSI, the miniTROLL (MN) and the S4 4Hz. The KPSI includes three pressure sensors deployed together along a transect, the KPSI01 which is furthest from the island, the KPSI02 which is in the middle and the KPSI03 which is closest to the island. There are two miniTROLLs, MN158 and MN162. The field deployment, whereby more than one instrument was deployed along a transect from the nearshore towards the island, was designed to examine spatial variations of wave characteristics across the nearshore towards the island. Time series of pressure signals from those sensors, that are characterised mainly by flat regions, generally occurring during very low water levels, were excluded from analysis.

In the previous section, the swell wave components were found to be very small and only discernible during low wave-energy events. Those peaks of swell waves on spectra at RF during a low wave-energy event on 24/11/04 were also found on spectra at locations around the island, indicating actual presence of swell waves in this region but with very low energy (Figure 5.14). As discussed in the previous section, however, most energy contained within a swell frequency range, in particular during high wave-energy events, is likely attributed to energy transferred between incident wind wave and infragravity wave components. In this section, therefore, energy occurring within a swell wave frequency range is included as part of an infragravity wave range. The higher frequency limit for infragravity waves was also suggested for areas where
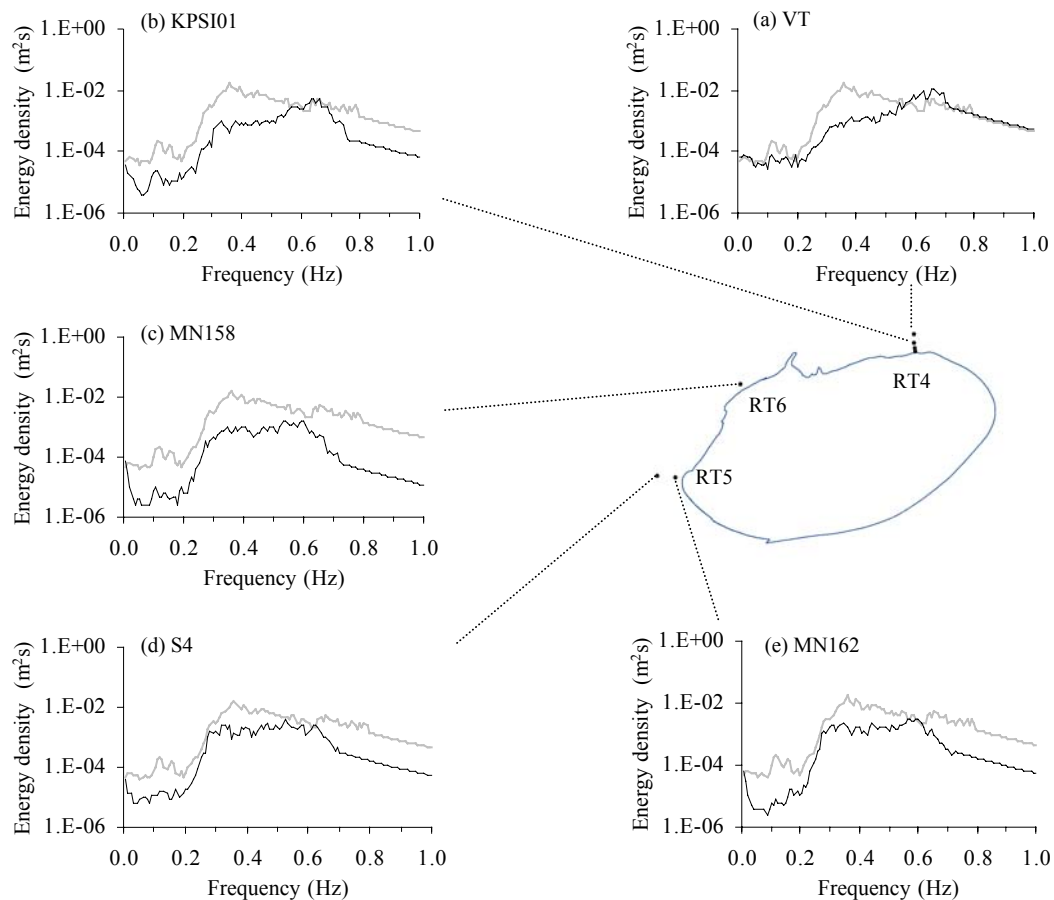
Figure 5.14. Wave spectra at a HHT (1100) on 24/11/04, indicating small peaks at swell wave frequencies, which were seen on wave spectra both at RF (⎯⎯) and at locations around the island (—): a) the Vector at RT4; b) the KPSI at RT4; c) the miniTROLL at RT6; d) the S4 at RT5; and e) the miniTROLL at RT5. The spectra are plotted using a logarithmic scale so that small peaks at swell wave frequencies can be seen.

incident waves are fetch-limited and their frequencies are short (Bauer, 1990). The results from the previous section suggested dominance of sea, not swell, in the wave environment of Warraber Reef during the experiment. The physiography of the reefs that occur throughout the region and persistent ESE winds during the experiment implies probable fetch-limited conditions for sea generation in this region.

Wave spectra, particularly during high wave-energy events, show pronounced peaks in three frequency bands. T_p was not considered in this section since it represents only one frequency band; therefore wave period was described using mean wave period (T_1). Samples of wave spectra, and spatial and temporal variations of wave parameters (H_{mo} and T_1) and energy between 24-28/11/04 are shown in Figures 5.15-5.24.
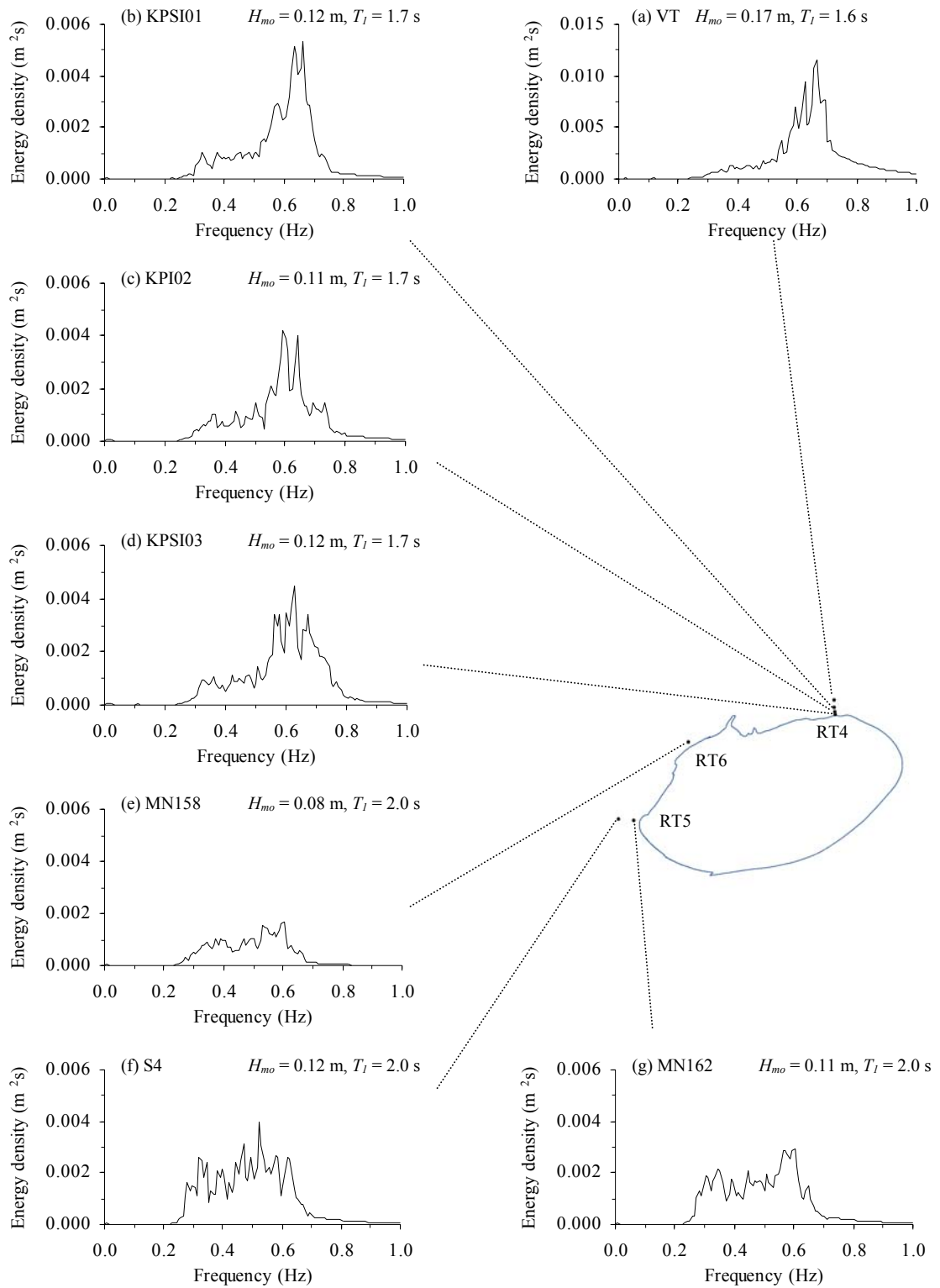
Figure 5.15. Wave spectra at a HHT (1100am) on 24/11/04 from: a) the Vector at RT4; b) the KPSI01 at RT4; c) the KPSI02 at RT4; d) the KPSI03 at RT4; e) the miniTROLL158 at RT6; f) the S4 at RT5; and g) the miniTROLL162 at RT5.
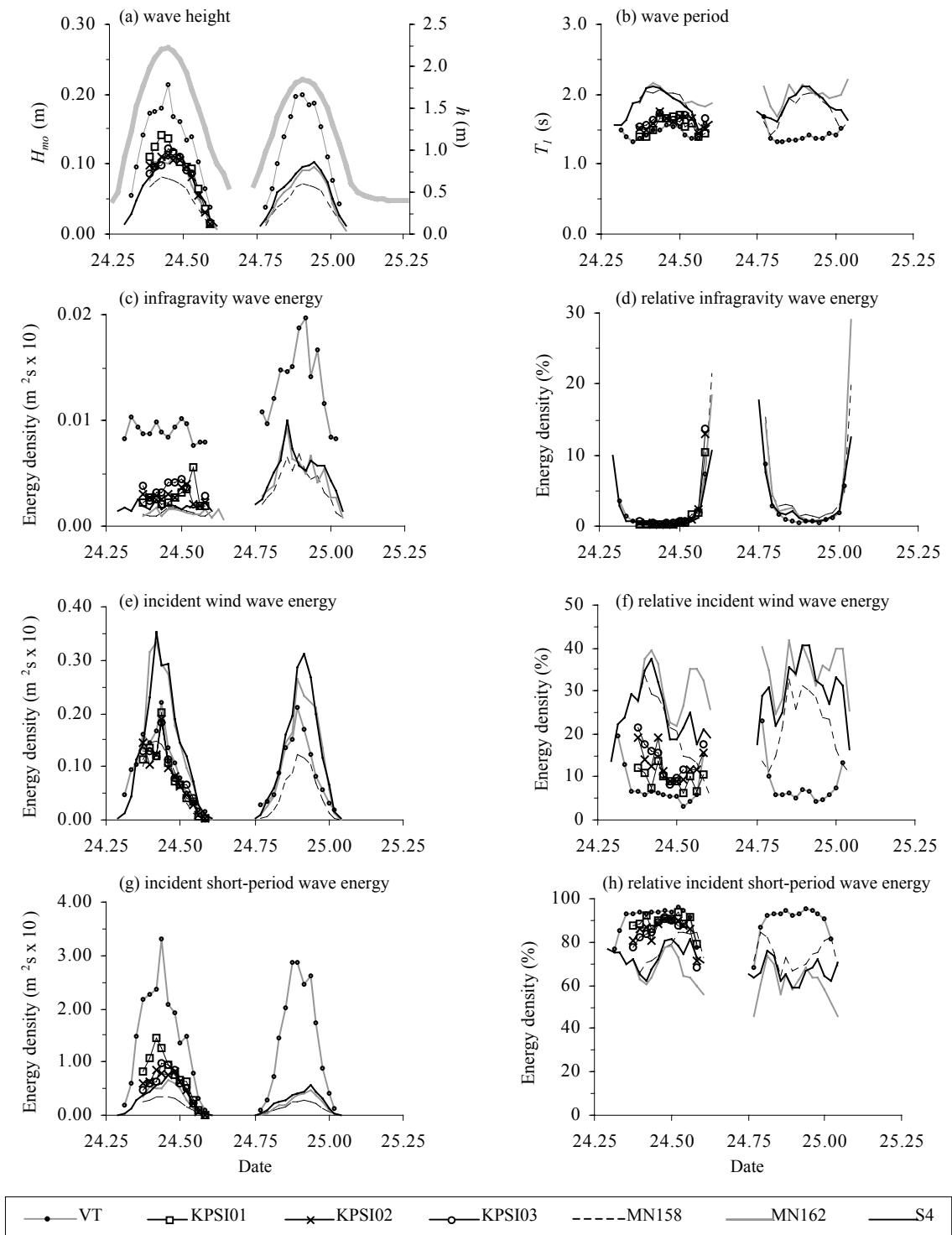
Figure 5.16. Temporal variations of: a) H_{mo}; b) T_1; c) energy of the infragravity wave frequency range; d) relative energy of the infragravity wave frequency range; e) energy of the incident wind wave frequency range; f) relative energy of the incident wind wave frequency range; g) energy of the incident short-period wave frequency range; and h) relative energy of the incident short-period wave frequency range, at different locations around the island (see each instrument location in Figure 5.15) between 24/11/04 0600 (24.25)-25/11/04 0600 (25.25). Water depth on the reef flat (———), derived from S4 data, is also given in (a).
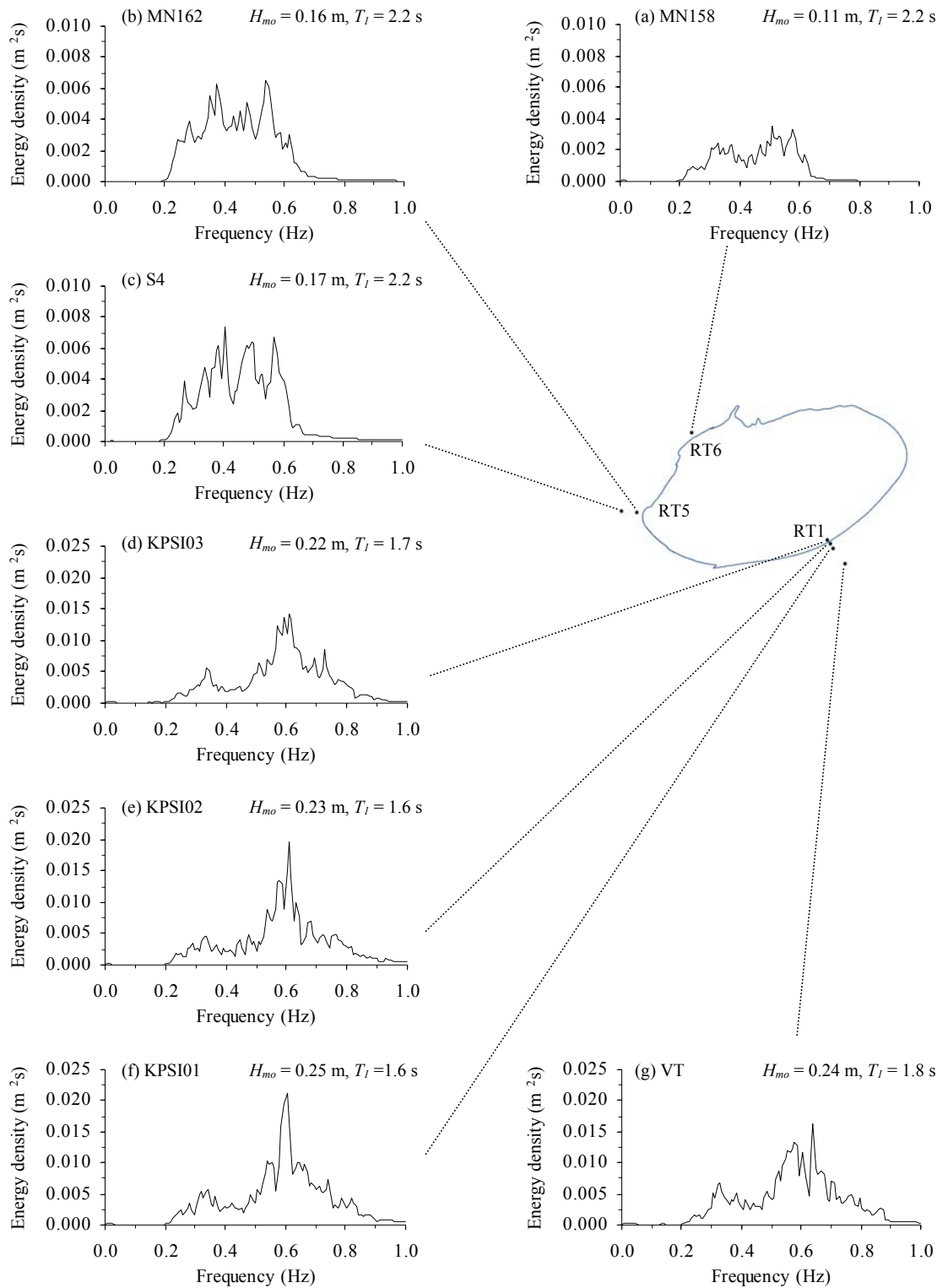
Figure 5.17. Wave spectra at a HHT (1100am) on 25/11/04 from: a) the miniTROLL158 at RT6; b) the miniTROLL162 at RT5; c) the S4 at RT5; d) the KPSI03 at RT1; e) the KPSI02 at RT1; f) the KPSI01 at RT1; and g) the Vector at RT1.
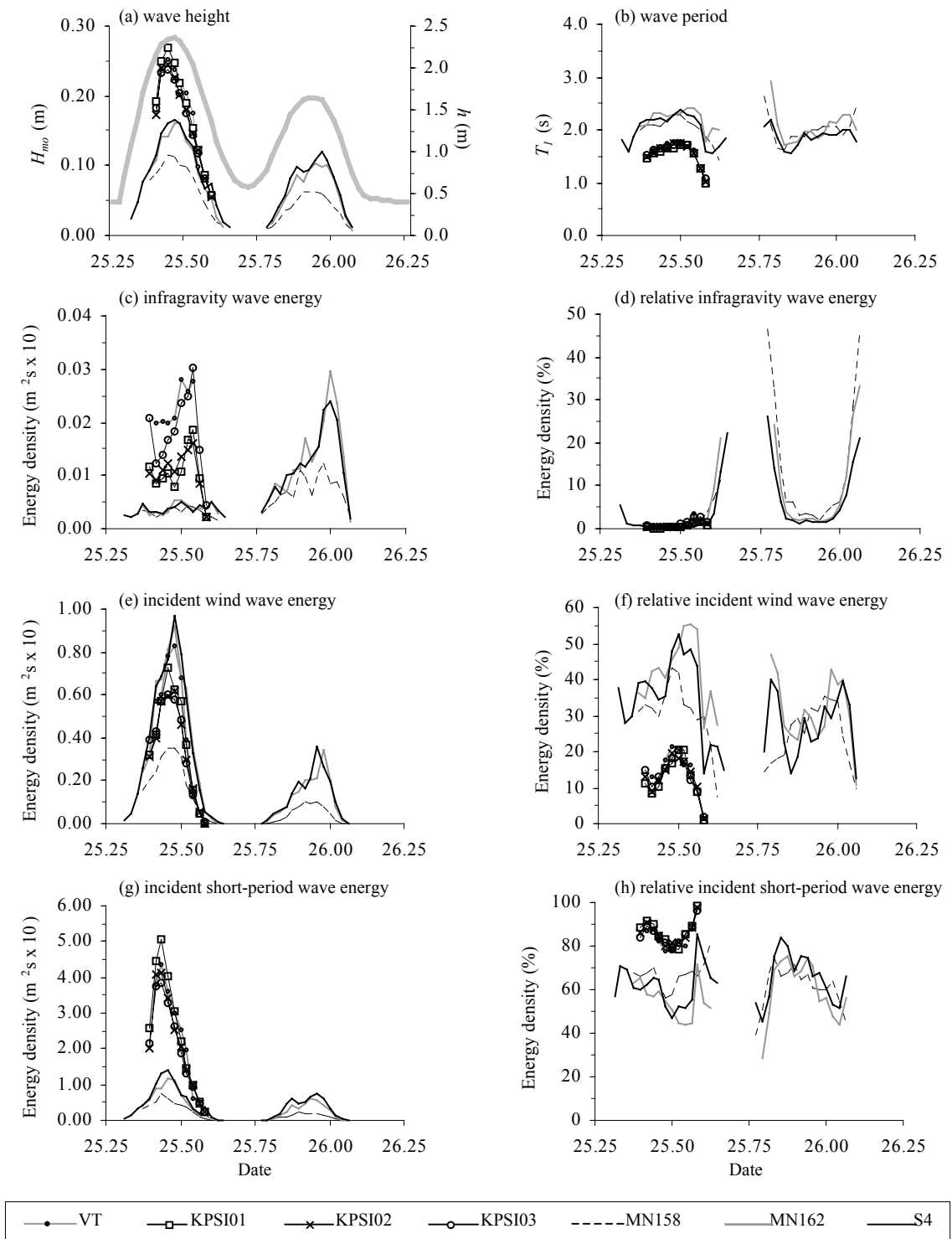
Figure 5.18. Temporal variations of: a) H_{mo}; b) T_I; c) energy of the infragravity wave frequency range; d) relative energy of the infragravity wave frequency range; e) energy of the incident wind wave frequency range; f) relative energy of the incident wind wave frequency range; g) energy of the incident short-period wave frequency range; and h) relative energy of the incident short-period wave frequency range, at different locations around the island (see each instrument location in Figure 5.17) between 25/11/04 0600 (25.25)-26/11/04 0600 (26.25). Water depth on the reef flat (——), derived from S4 data, is also given in (a).
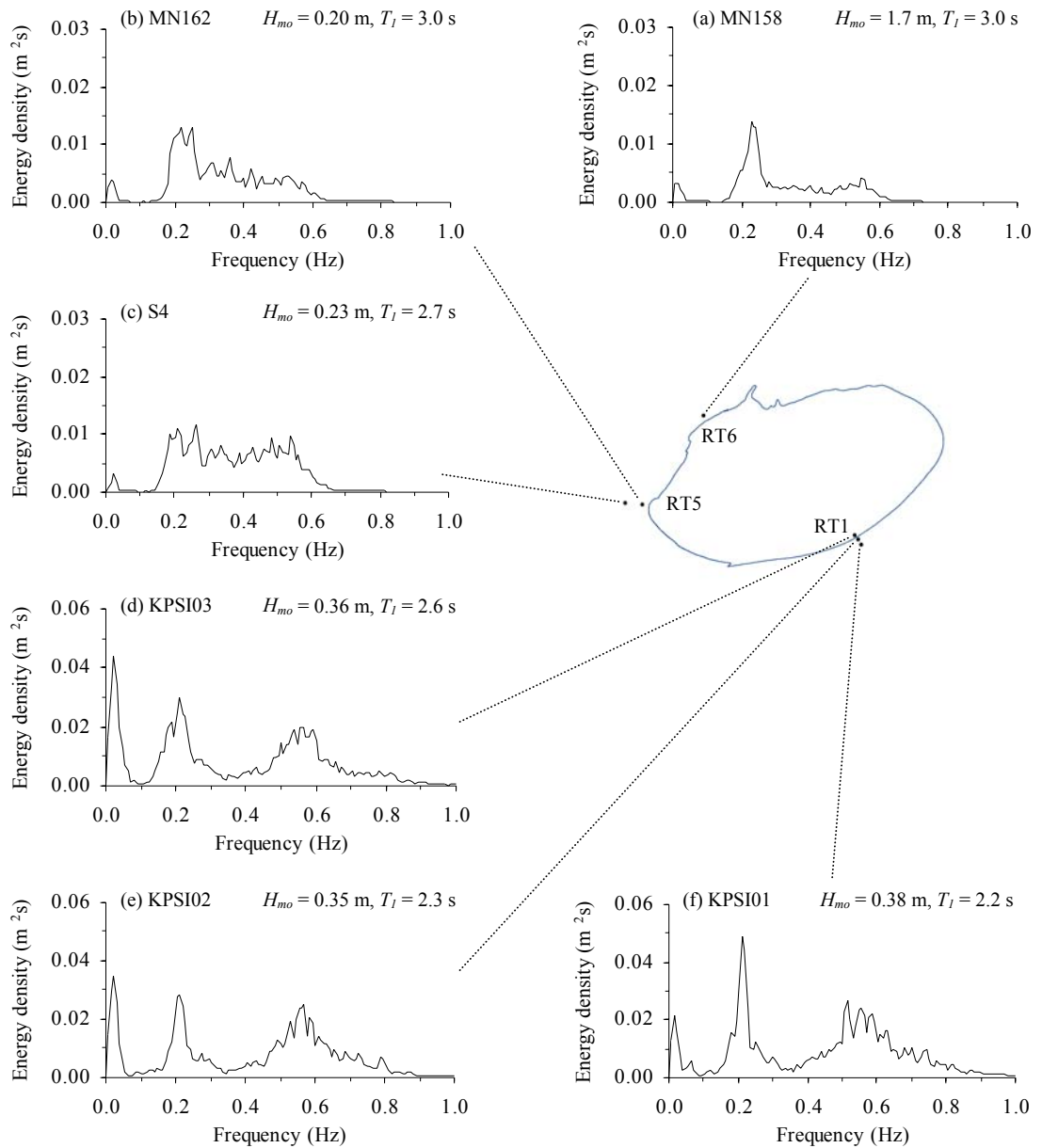
Figure 5.19. Wave spectra at a HHT (1130am) on 26/11/04 from: a) the miniTROLL158 at RT6; b) the miniTROLL162 at RT5; c) the S4 at RT5; d) the KPSI03 at RT1; e) the KPSI02 at RT1; and f) the KPSI01 at RT1. No vector data were available on 26/11/04.

154
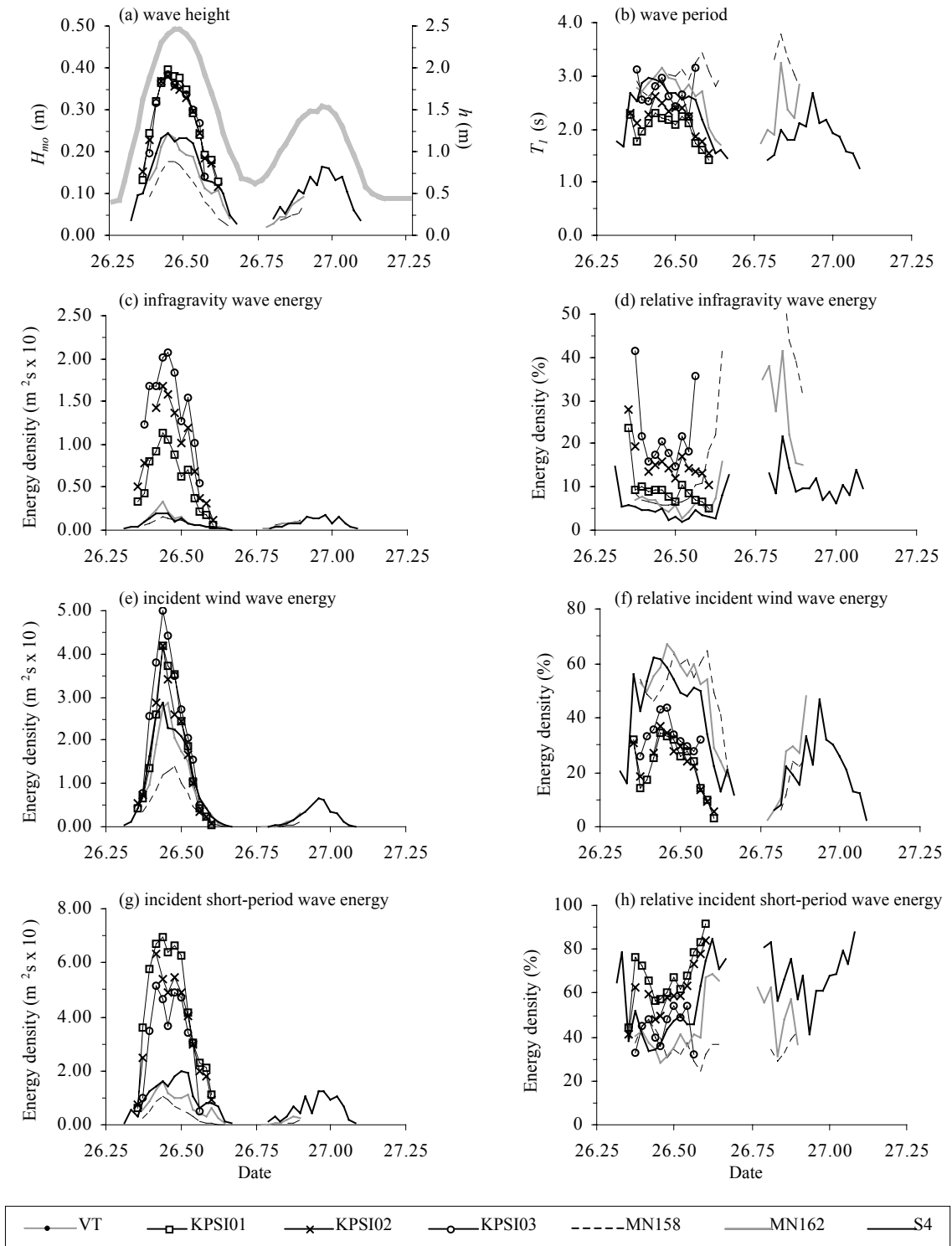
Figure 5.20. Temporal variations of: a) H_{mo}; b) T_1; c) energy of the infragravity wave frequency range; d) relative energy of the infragravity wave frequency range; e) energy of the incident wind wave frequency range; f) relative energy of the incident wind wave frequency range; g) energy of the incident short-period wave frequency range; and h) relative energy of the incident short-period wave frequency range, at different locations around the island (see each instrument location in Figure 5.19) between 26/11/04 0600 (26.25)-27/11/04 0600 (27.25). Water depth on the reef flat (——), derived from S4 data, is also given in (a). No vector data were available on 26/11/04.
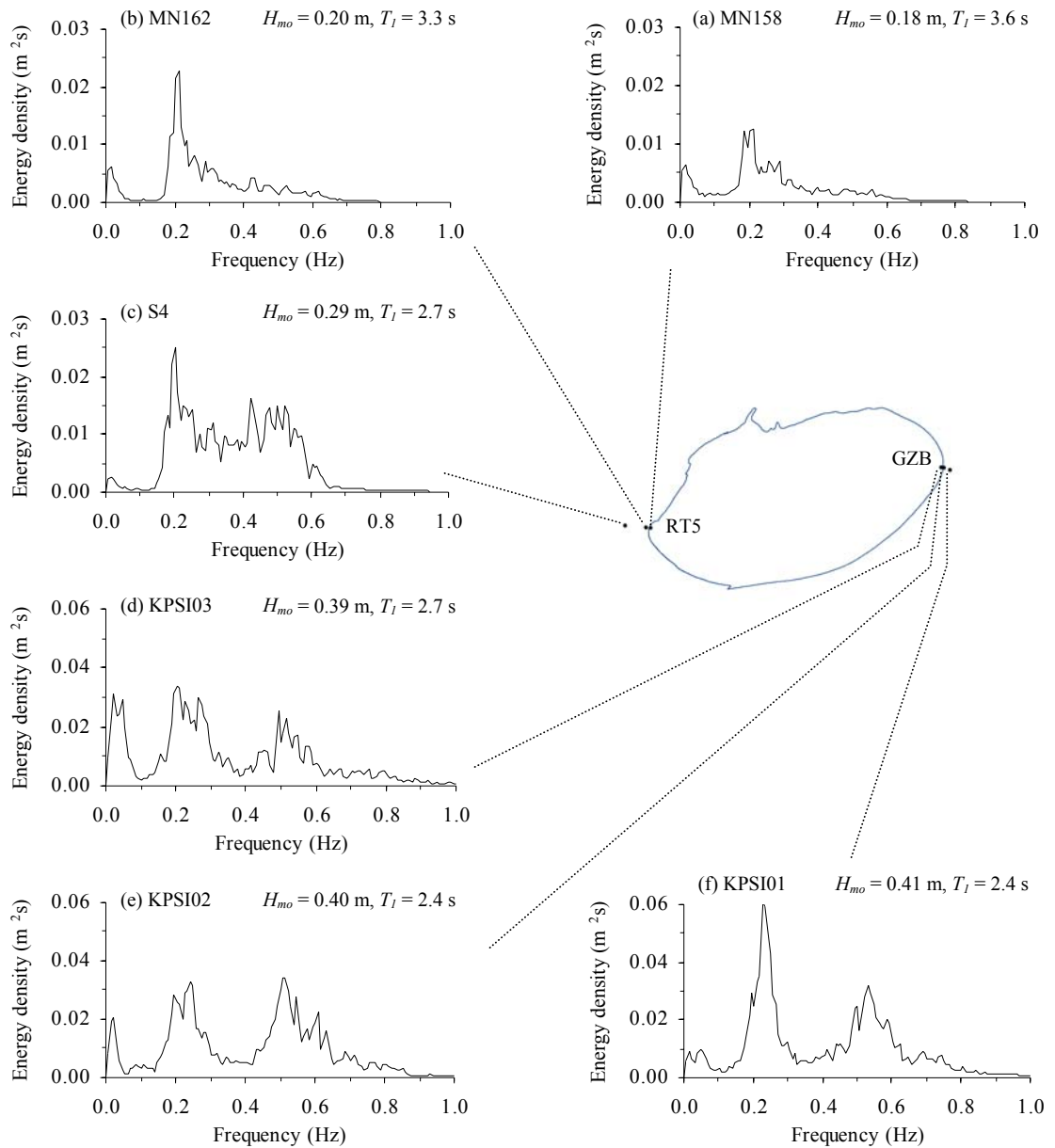
Figure 5.21. Wave spectra at a HHT (1200am) on 27/11/04 from: a) the miniTROLL158 at RT5; b) the miniTROLL162 at RT5; c) the S4 at RT5; d) the KPSI03 at GZB; e) the KPSI02 at GZB; and f) the KPSI01 at GZB. No vector data were available on 27/11/04.
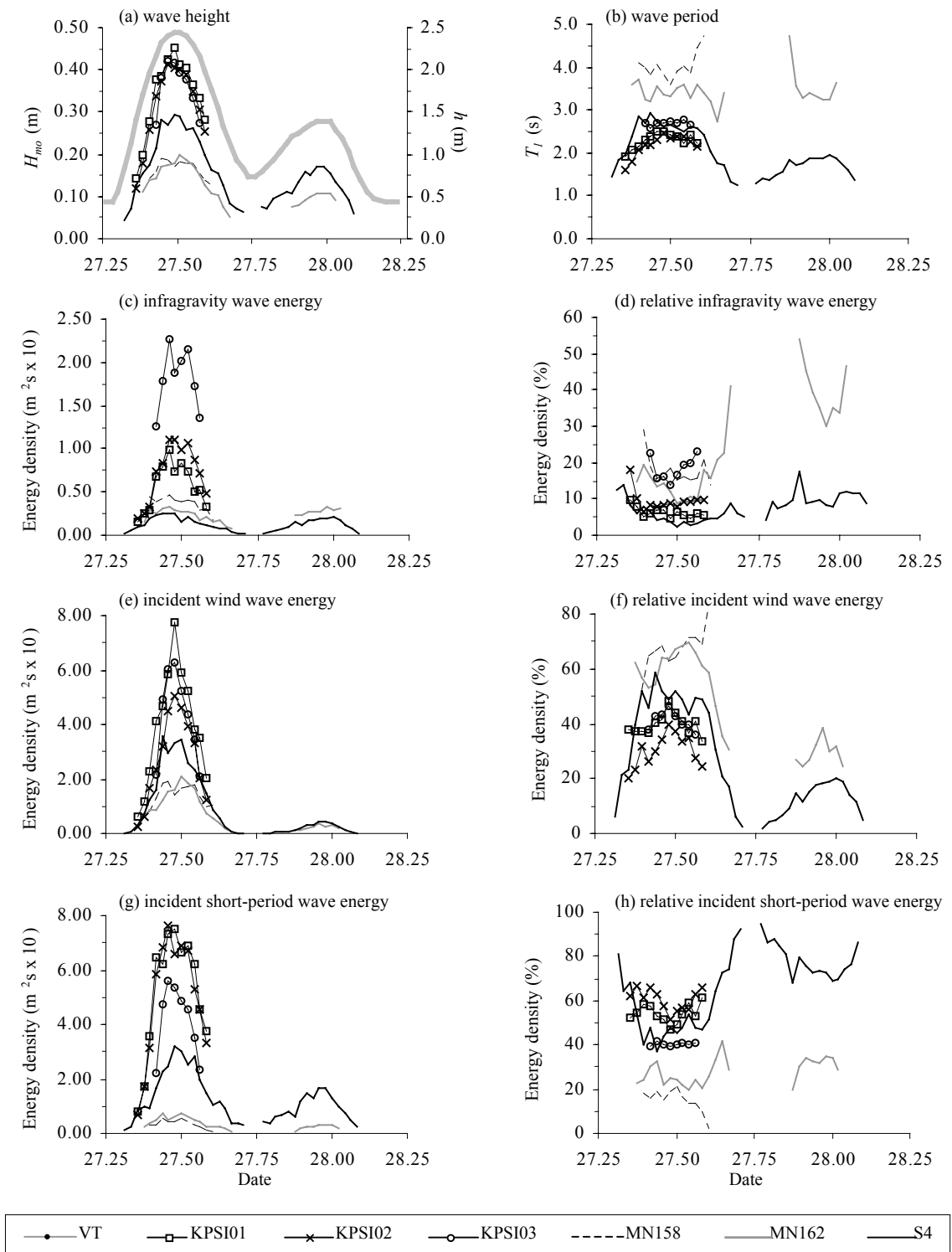
Figure 5.22. Temporal variations of: a) H_{mo}; b) T_I; c) energy of the infragravity wave frequency range; d) relative energy of the infragravity wave frequency range; e) energy of the incident wind wave frequency range; f) relative energy of the incident wind wave frequency range; g) energy of the incident short-period wave frequency range; and h) relative energy of the incident short-period wave frequency range, at different locations around the island (see each instrument location in Figure 5.21) between 27/11/04 0600 (27.25)-28/11/04 0600 (28.25). Water depth on the reef flat (──), derived from S4 data, is also given in (a). No vector data were available on 27/11/04.
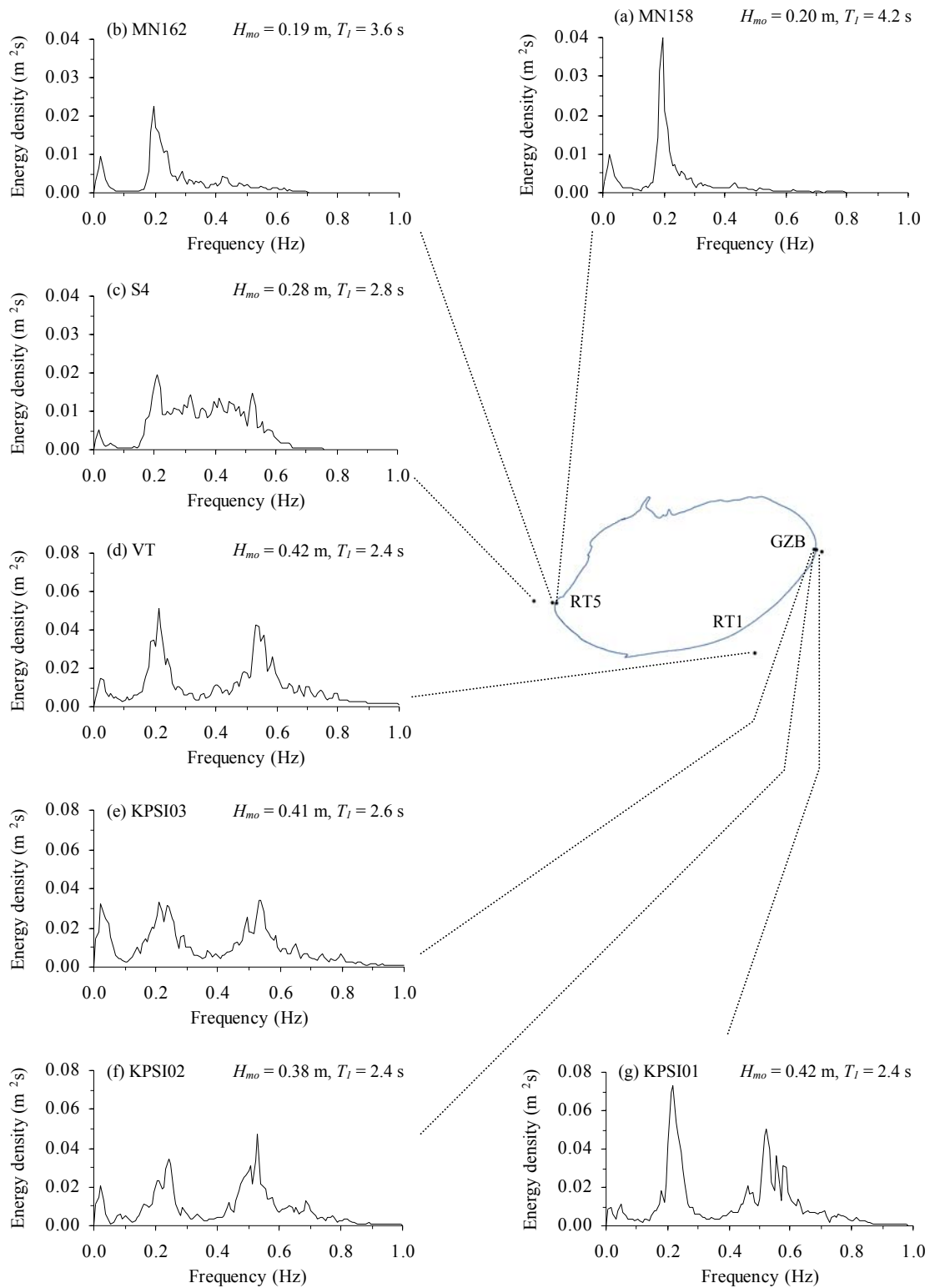
Figure 5.23. Wave spectra at a HHT (1200am) on 28/11/04 from: a) the miniTROLL158 at RT5; b) the miniTROLL162 at RT5; c) the S4 at RT5; d) the Vector at RT1; e) the KPSI03 at GZB; f) the KPSI02 at GZB; and g) the KPSI01 at GZB.
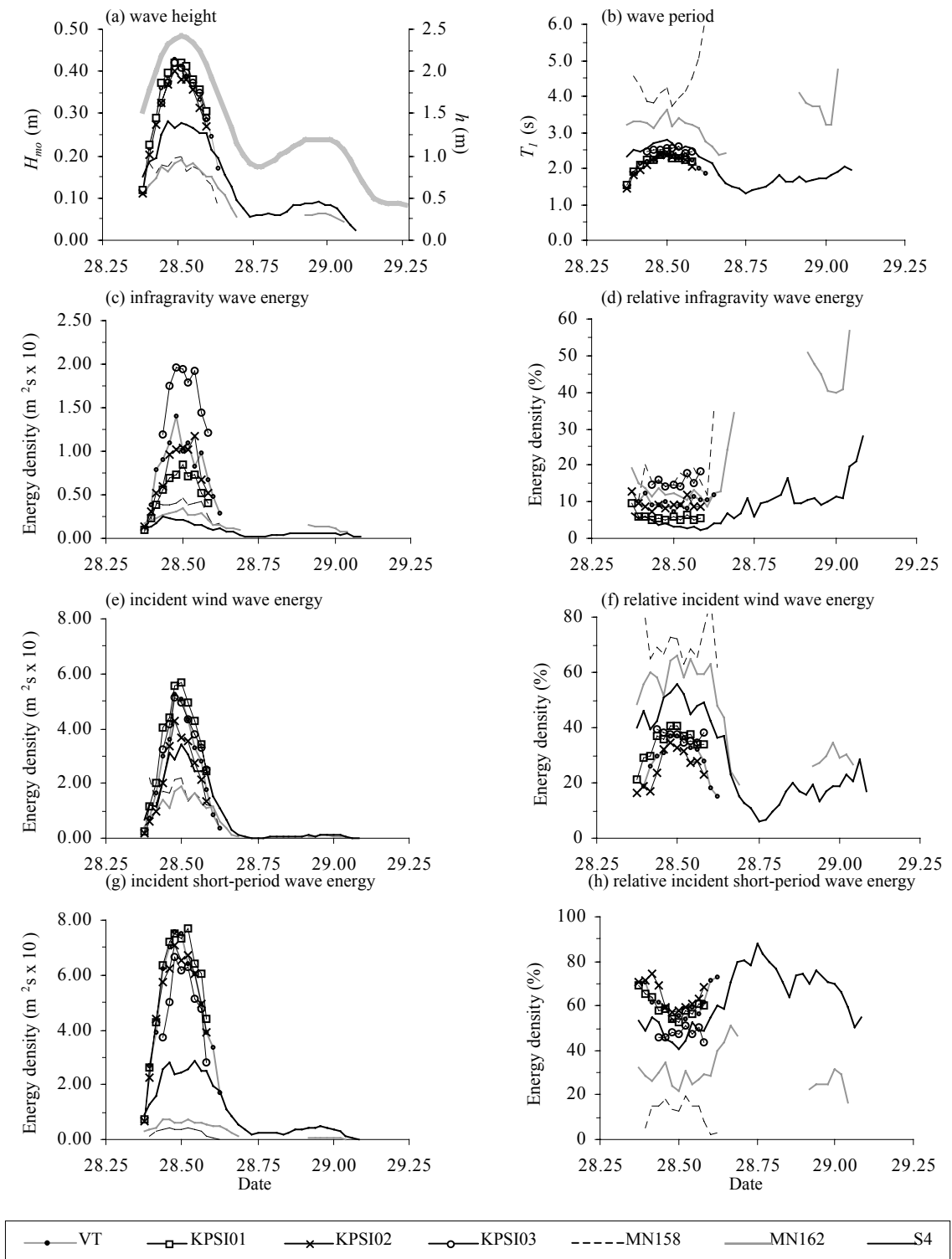
Figure 5.24. Temporal variations of: a) H_{mo}; b) T_I; c) energy of the infragravity wave frequency range; d) relative energy of the infragravity wave frequency range; e) energy of the incident wind wave frequency range; f) relative energy of the incident wind wave frequency range; g) energy of the incident short-period wave frequency range; and h) relative energy of the incident short-period wave frequency range, at different locations around the island (see each instrument location in Figure 5.23) between 28/11/04 0600 (28.25)-29/11/04 0600 (29.25). Water depth on the reef flat (——), derived from S4 data, is also given in (a).

Low and high wave-energy events referred to in this section are those that were defined in the previous section, low wave-energy events during 24-25/11/04 and high wave-energy events during 26-28/11/04.

Wave information during a low wave-energy event on 24/11/04 was obtained from the Vector and the KPSI at RT4, the miniTROLL (MN158) at RT6, and the S4 and the miniTROLL (MN162) at RT5 (Figure 5.15). The maximum values of H_{mo} occurred at the Vector at RT4 which was more exposed to the ESE wind occurring during the experiment while values of H_{mo} from the KPSI at RT4, which were closer to the island, and those from the S4 and the miniTROLL at RT5, which are located in the leeward side, were similar (Figure 5.16a). The lowest values of H_{mo} occurred at the leeward location at RT6, with a maximum value at a HHT of approximately 0.08 m. On 25/11/04, the Vector and the KPSI were moved from RT4 to record data at RT1 which is on the windward side of the island (Figure 5.17). According to wave data at RT6 (MN158) and RT5 (S4 and MN162), values of H_{mo} were slightly greater than those on 24/11/04. Waves at RT1 (VT and KPSI) were higher than those at RT5 and waves at RT6 were found to be smallest (Figure 5.18a). Values of H_{mo} at the peaks of HHT and LHT were similar on 24/11/04 but appeared to be lower at the peak of a LHT on 25/11/04.

Generally, values of T_1 exhibited a slight change over a tidal cycle and tended to increase as water depth on the reef was very low. On 24/11/04, a value of T_1 of approximately 1.5 s at RT4 (VT and KPSI) was slightly smaller than those at RT 5 (S4 and MN162) and RT6 (MN158), which were approximately 2.0 s (Figure 5.16b). On 25/11/04, T_1 of around 2.0-2.5 s at RT5 (S4 and MN162), which slightly increased from around 1.5-2.0 s on 24/1/04, was slightly longer than that at RT1 (VT and KPSI) (approximately 1.5 s) (Figure 5.18b).

In summary, during low wave-energy events waves were shorter and larger at locations exposed to wind (RT4 and RT1) than at locations on the leeward sides (RT5 and RT6). This spatial variation of wave characteristics is attributed to the different magnitude of energy contribution from different wave frequency ranges. On the windward locations (RT4 and RT1), wave energy was dominated by the incident short-period wave range (80-90%) (Figures 5.16h and 5.18h). Spectra at RT4 and RT1 show prominent peaks over the incident short-period wave range (Figures 5.15a, b, c and d, and 5.17d, e, f and g). Spectra at RT5 (S4 and MN162) and RT6 (MN158) contained less percentages of the incident short-period wave energy, approximately 50-80% (Figures 5.16h and 5.18h), and greater percentages of the incident wind wave energy, approximately 20-50% (Figures 5.16f and 5.18f), resulting in less pronounced peaks over the incident short-period wave components (Figures 5.15e, f and g, and 5.17a, b and c).

It is noted that the incident wind wave energy reaching RT5 (S4 and MN162) was much greater that at RT4 (VT and KPSI) and RT6 (MN158) on 24/11/04 (Figure 5.16e), and greater than that at RT1 (VT and KPSI) and RT6 (MN158) on 25/11/04 (Figure 5.18e). The incident wind wave energy at RT6 was comparable to that at the KPSI locations at RT4 on 24/11/04 and much less than that at RT1 on 25/11/04. During these low wave-energy events, the infragravity wave energy was very small, less than 5% of total wave energy (Figures 5.16d and 5.18d). The infragravity wave energy was greater at windward locations (RT4 and RT1) than at the leeward locations (RT5 and RT6) (Figures 5.16c and 5.18c).

During the high wave-energy event on 26/11/04, similarly, waves at RT1, which is on the windward side of the island, were greater than those at RT5 and waves at RT6 were smallest. There was an increase in H_{mo} at all locations, of which the maximum

values occurring at around the peak of a HHT increased from 0.27 m to 0.4 m at RT1 (VT and KPSI), from 0.15 m to 0.25 m at RT5 (S4 and MN162) and 0.10 m to 0.17 m at RT6 (MN158) (Figure 5.20a). T_1 also became longer at all locations, compared to that on 25/11/04, and appeared to increase across the nearshore towards the island (Figure 5.20b). At the peak of a HHT, at RT1 T_1 increased from approximately 2.2 s at the KPSI01 to approximately 2.3 s at the KPSI02 and to approximately 2.6 s at the KPSI03, and at RT5 increased from around 2.7 s at the S4 to around 3.0 s at the MN162 which was similar to that at the MN158 located at RT6 (Figure 5.19).

An increase in values of H_{mo} and T_1 on 26/11/04 was attributed to an increase in wave energy not only over the incident short-period wave components that were dominant during the low wave-energy events but also over the incident wind wave and infragravity wave components. This is clearly seen on spectra, particularly on the windward location (RT1), exhibiting three clearly separated peaks of the infragravity wave, incident wind wave and incident short-period wave components (Figure 5.19).

The infragravity wave energy appeared to increase from the nearshore to the island (at RT1 from KPSI01 to KPSI02 and KPSI03, and at RT5 from S4 to MN162) (Figure 5.20c) and its relative contribution increased with a decrease in water depth. During high water depth on the reef, relative energy contributed by the infragravity wave frequency range increased from less than 5% on 25/11/04 to around 10% at the KPSI01 and to around 20% at the KPSI03 at RT1, and at RT5 and RT6 to around 5% and 8%, respectively (Figure 5.20d). The relative energy contributed by incident wind wave components increased with an increase in water depth (Figure 5.20f) whereas the relative energy over the incident short-period wave components decreased with an increase in water depth (Figure 5.20h). At higher water depth, generally, a wave field at the windward location (KPSI at RT1) was dominated by the incident short-period wave

energy (Figure 5.20h) while at the leeward locations (S4 and MN162 at RT5, and MN158 at RT6) the incident wind wave energy was dominant (Figure 5.20h). As water depth became very low, waves were dominated by incident short-period wave energy with subordination of the infragravity wave energy at all locations, except at RT6 where the infragravity wave energy appeared dominant.

On 27/11/04, the KPSI was relocated to GZB, with the KPSI03 positioned on the mid beach, the KPSI02 at about the beach toe and the KPSI01 in the nearshore, and at RT5 the MN162 was relocated to about the beach toe and the MN158 was moved from RT6 to be installed on the mid beach at RT5. This relocation was intended to examine spectral characteristics of these two different wave environments. According to visual observation, at GZB, which was on the windward side of the island, waves were steeper and larger, and broke more intensely whereas at RT5, which was on the leeward side of the island, waves were calmer and characterised by more regular shape and smaller size.

Wave characteristics between 27-28/11/04 varied similarly. At the windward location at GZB, three sensors (KPSI01, KPSI02 and KPSI03) deployed across the nearshore towards the island indicated that values of H_{mo} were similar spatially and temporally, approximately 0.40 m around the peak of a HHT (Figures 5.22a and 5.24a). On the leeward locations at RT5, on the other hand, values of H_{mo} reduced across the nearshore towards the island, during the peak of a HHT from approximately 0.30 m at the S4 location to approximately 0.20 m at the MN162 and MN158 located at about the beach toe and on the beach, respectively (Figures 5.22a and 5.24a).

At GZB (KPSI), T_1 increased with an increase in water depth, as occurred at the S4 location at RT5 (Figures 5.22b and 5.24b). However, at the MN162 location T_1 was slightly changed and at the MN158 location T_1 appeared to increase with a decrease in water depth (Figures 5.22b and 5.24b). An increase in T_1 towards the island occurred at

both GZB and RT5 but was more evident at RT5, at around the peak of a HHT from approximately 2.7 s at the S4 location to around 3.5 s and 4.0 s at the MN162 and MN158, respectively (Figure 5.22b).   An increase in T_I towards the island at GZB (KPSI) and RT5 (S4, MN162 and MN158) was primarily attributed to a combination of an increase in the infragravity wave energy (Figures 5.22c and 5.24c) and a decrease in the incident short-period wave energy towards the island (Figures 5.22g and 5.24g).

During high water depth, the relative energy over the infragravity wave range increased from approximately 5% at locations on the reef flat to approximately 20% on the beach at both locations (GZB and RT5).   This energy range tended to increase as water became very shallow, particularly at locations closer to the island (Figures 5.22d and 5.24d).   At high water depth, the relative contribution from the incident wind wave energy and the incident short-period wave energy was comparable at GZB but the relative contribution from the incident wind wave energy was greater and increased towards the island at RT5 (Figures 5.22f and 5.24f).   This distinction in relative energy from different frequency ranges was recognised on spectra at two locations, clear peaks evident in incident short-period frequency at GZB but almost absent in incident short-period frequency at the beach at RT5 (Figures 5.21 and 5.23).

In summary, wave environments around the island can be broadly divided into the windward and leeward sides.   In general, waves on windward locations are shorter and larger while waves on leeward locations are longer and smaller.   During low wave-energy events, spatial variations of wave characteristics across the nearshore towards the island are negligible both at the windward and leeward areas.   During high wave-energy events, however, spatial variations of wave characteristics across the nearshore are recognised.   In both sides, longer wave period occurs towards the island and is more evident on the leeward side.   However, wave height on the windward side slightly

164

changes towards the island whereas significant reduction of wave height towards the island occurs on the leeward area. These variations are likely to have significant consequences for sediment movement and island morphology.

5.6.2. Development of Spectral Components around the Island

Incident Wind Wave Components

Figure 5.25 shows a comparison between wave spectra at locations around the island and those at RF. It can be seen in Figure 5.25 that peaks over incident wind wave frequencies at locations around the island correspond with spectral peaks at RF, implying the influence of incident waves off Warraber Reef on wave fields around the island through incident wind wave components.

As waves propagate across the reef platform from the reef rims to the island, their energy is likely to be attenuated as a result of bottom friction. The attenuation of wave energy influenced by incident waves off Warraber Reef can be estimated based on a reduction in incident wind wave energy from RF to the locations on the windward side of the island. Figure 5.26 shows incident wind wave energy at the windward locations at RT1 (Figure 5.26a) and GZB (Figure 5.26b), relative to that at RF.

It is indicated in Figure 5.26a and b that approximately 70-80% of incident wind wave energy was attenuated from RF to the windward side of the island. The attenuation of incident wind wave energy at RT1 and GZB slightly increased over a decrease in water depth, approximately from 80% and 70% to 90%, respectively (Figure 5.26a and b). In Figure 5.26, incident wind wave energy relative to that at RF is also given for the RT5 (Figure 5.26c) which is the leeward location. At RT5 the relative energy increased as water depth decreased (Figure 5.26c). At very low water depth the
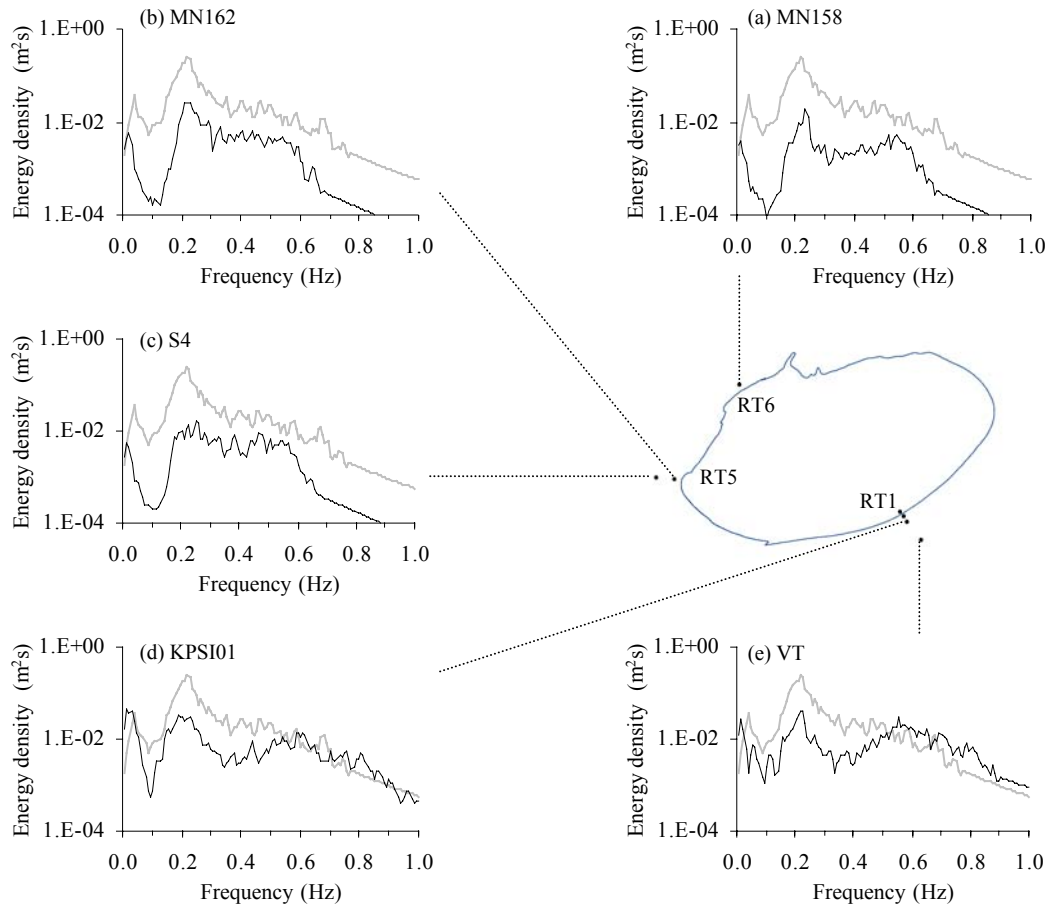
Figure 5.25. Comparison between wave spectra (—) at the peak of a HHT (1100am) on 26/11/04 from: a) the miniTROLL at RT6; b) the miniTROLL at RT5; c) the S4 at RT5; d) the KPSI01 at RT1; and e) the VT at RT1 with a spectrum from the Dobie pressure sensor (—) on the reef flat at RF, indicating peaks over incident wind wave frequency on spectra at locations around the island, that correspond with spectral peaks on spectrum at RF. Values of wave spectral density are plotted using a logarithmic scale due to significant difference in the magnitude between the spectra at RF and those from locations around the island.

relative energy at RT5 rose to more than 100%, meaning that there is more incident wind wave energy reaching this location than reaching RF. This relative energy at RT5 implies the occurrence of wave refraction and diffraction on the western reef rim.

The different patterns of relative energy changes at RT1, GZB and RT5 are likely attributable to the fact that incident wind waves at different locations around the island are generated by incident waves off Warraber Reef refracting and diffracting at different locations along the reef rim and that the elevation of the reef flat at RT5 is lower than the eastern part of the reef flat, where the Dobie pressure sensor was installed. When
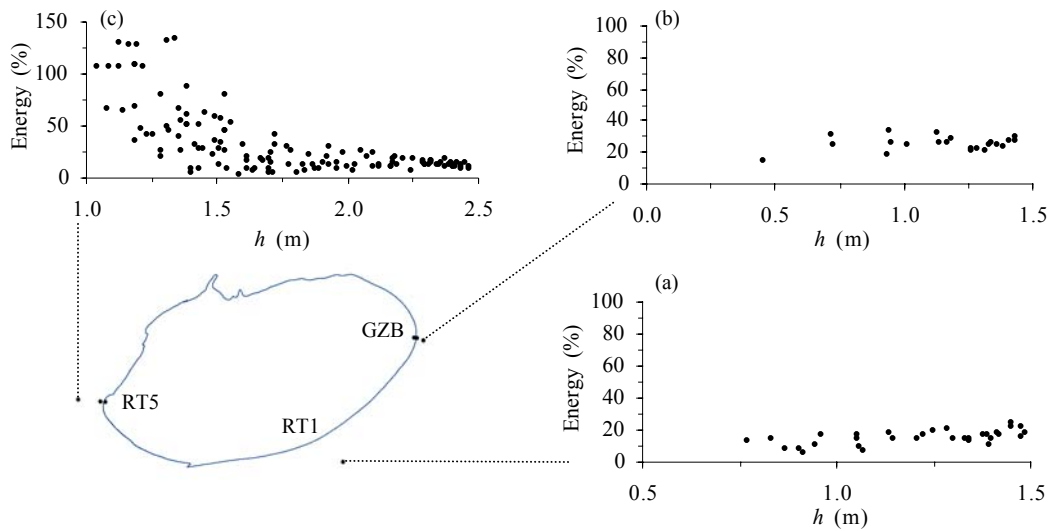
Figure 5.26. Energy of an incident wind wave range (2.5sec < T < 8.0sec) at a) RT1, b) GZB and c) RT5, relative to that of an incident wind wave range at RF.

the eastern part of the reef flat is emerged during the lower tides, waves can still propagate across the western side of the reef flat, which is still submerged. Figure 5.27 shows a comparison between wave spectra at the Dobie pressure sensor and those at the locations around the island during low tides. It is seen that at low tides the spectra at the Dobie pressure sensor have no peaks at the incident wind wave frequencies. On the other hand, the spectra at leeward locations of the island show a spectral peak of incident wind waves. This indicates the occurrence of wave refraction and diffraction of incident waves along the reef rim.

According to Figures 5.16e and 5.27a, incident wind wave energy at RT5 is greater than that at RT4 and according to Figures 5.16e, 5.18e, 5.20e and 5.27c, incident wind wave energy at RT6 is less than that at RT5. This indicates that under the conditions of incident wave off Warraber Reef during the experiment, incident waves moving across the northern side of the reef platform experience more attenuation than waves moving across the western side of the reef platform, resulting in the smaller magnitude of incident wind wave energy at RT4 and RT6.

167
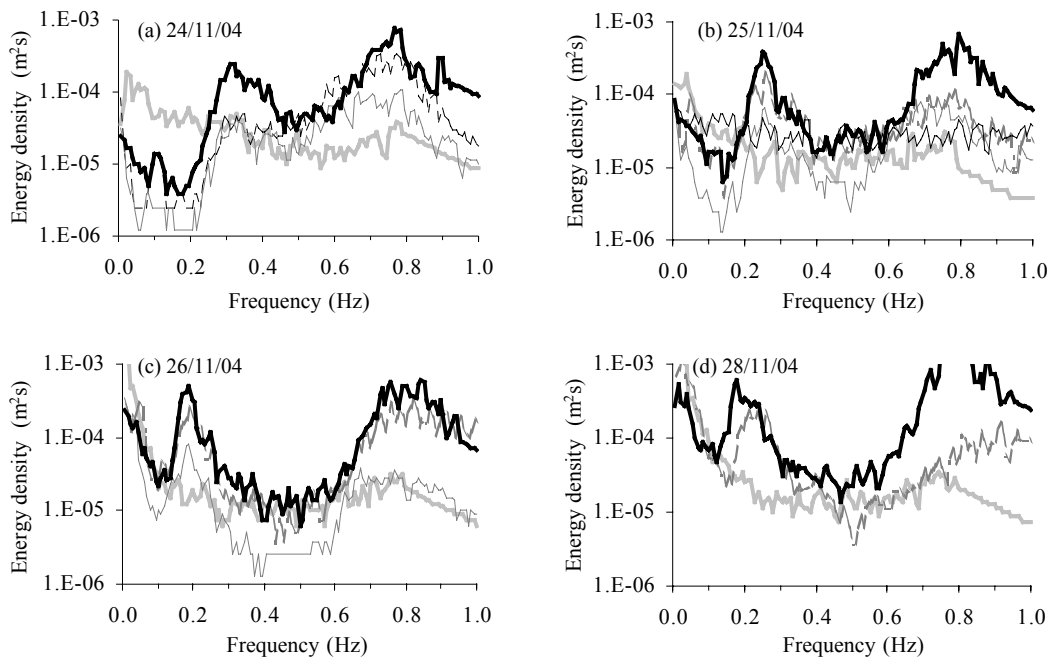
Figure 5.27. Comparison of wave spectra during low tides: a) on 24/11/04 at 1330; b) on 25/11/04 at 1430; c) on 26/11/04 at 1530; and d) on 28/11/04 at 1700. (▬ = Dobie, ▬ = S4 at RT5, ── = Vector at RT4, ─ ‥ = miniTROLL at RT5, ── = miniTROLL at RT6, ----= KPSI at RT4), showing peaks over incident wind wave components at leeward locations (RT4, RT5 and RT6) and no peaks over incident wind wave components at RF (Dobie). This indicates the occurrence of wave refraction and diffraction of incident waves along the northern and western reef rim.

Wave refraction along the northern reef rim is also demonstrated in Figure 5.28 which is a georeferenced aerial photograph taken on 02/08/1981 when ESE and SE winds were prevalent, according to wind data from a meteorological station on Thursday Island.

Figure 5.28. Georeferenced aerial photograph taken on 02/08/1981, showing wave refraction along the northern reef rim. A location of RT4 is shown in the figure.

Infragravity Wave Components

Normally, infragravity waves develop as a result of energy transferred from spectral peaks when waves shoal (Kofoed-Hansen and Rasmussen, 1998). The results of island wave analysis in this section have indicated that the magnitude of the infragravity wave energy at locations around the island appeared to increase with total wave energy and possibly related directly to the incident wind wave energy.

During the low wave-energy events (24-25/11/04) when the incident short-period wave energy was dominant, no infragravity wave components have amplitudes comparable to those of the spectral peaks in the incident short-period waves, unlike those that occurred during the high wave-energy events when peaks over the incident wind wave components were pronounced and amplitudes of infragravity wave components were similar to those of the incident wind wave and incident short-period wave components. In addition, the infragravity wave components at the windward locations contained more energy than those at the leeward locations.

This direct relationship between infragravity waves and incident wind waves is similar to that found on coastal beaches where infragravity waves grow with offshore wave height (Komar, 1998). The infragravity wave components at GZB, RT1 and RT5 also exhibited an increase in their amplitudes across the nearshore towards the island. This pattern of an increase in infragravity energy across the nearshore may be attributable to the presence of edge waves which are a type of infragravity waves (Komar, 1998).

Incident Short-Period Wave Components

Incident short-period wave energy was found to be very significance across the nearshore towards the island at windward locations and in the nearshore at the leeward

side of the island. According to their spectral peaks, they are likely generated locally on the reef platform in response to local wind conditions. Development of incident short-period waves was therefore examined. Data for examining the development of incident short-period waves on the reef platform were selected from the windward locations (RT1 and GZB) of the island in order to correctly estimate wave characteristics under the influence of wind on the reef.

Development of incident short-period wave portions of the spectra at the windward side of the island was found to be dependent on water depth on the reef flat and wind speed (Figure 5.29). At the same mean wind speed, as water depth increases, its energy content increases with a shift of peak frequencies to lower ones (Figure 5.29a). At the same water depth, an increase in wind speed gives rise to an increase in its energy content and a decrease in peak frequencies as well (Figure 5.29b).

Further analysis was carried out to examine the relationships between water depth, and H_{mo} and T_p of the incident short-period waves and compare H_{mo} and T_p of the incident short-period waves to the equations of Young and Verhagen (1996a) in order to see whether the development of the incident short-period waves can be estimated by simplified wave models.
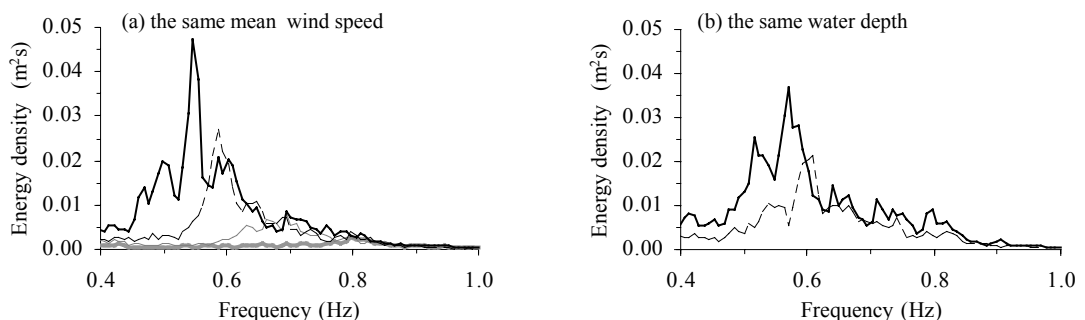
Figure 5.29. Spectral growth of incident short-period wave frequencies: a) the same mean wind speed of 8.8 m/s with different water depths (0.55 m (—), 0.72 m (—), 0.95 m (----) and 1.18 m (━)); and b) the same water depth of 1.28 m with different mean wind speed (6.0 m/s (----) and 8.0 m/s (━)). Data are obtained from KPSI01 at GZB on 27/11/04 for (a), on 25/11/04 1100 for (b) 6.0 m/s and on 26/11/04 1030 for (b) 8.0 m/s.

Previously, equations and curves for forecasting wave conditions in shallow water, which is a function of fetch, wind speed, wind duration and water depth, were given in the Shore Protection Manual volume 1 (CERC, 1984) and later revised by Hurdle and Stive (1989). Young and Verhagen (1996a) proposed equations, which were the modified version of equations presented in the Shore Protection Manual, for wind-wave development in fetch-limited and finite-depth conditions. The equations of Young and Verhagen (1996a) are adopted here for comparing with the field data because of being developed based on the comprehensive study of fetch-limited and finite depth wave growth, and using U_{10}, which is wind speed measured at a standard height of 10 m above ground and generally available from meteorological stations, as wind speed for calculation, instead of using wind-stress factor, U_A, that is used in the Shore Protection Manual, that requires the information on air-sea temperature differences for conversion from U_{10}.

Figure 5.30 indicates the relationships between water depth, and T_p and H_{mo} of incident short-period wave portions of wave spectra. Also, the data are separated into three sets: flood, peak and ebb. During lower-energy events, incident short-period waves during flood have greater H_{mo} than those during ebb. During higher-energy events, however, H_{mo} tends to change similarly both during flood and ebb. Maximum energy of incident short-period waves occurred at high water depth on 27/11/04 and 28/11/04, corresponding to the value of H_{mo} of 0.31 m. T_p appears to increase with depth during flood but be rather stable and slightly higher during ebb. In all cases, T_p was found not to be greater than 2.0 s (0.5 Hz) which is similar to the value estimated by Brander et al (2004). At high water depth, as T_p tends to level off and H_{mo} still increases but slightly, therefore, it is probable that during the experiment incident short-period waves reached their maximum values of T_p while H_{mo} was approaching its limits.
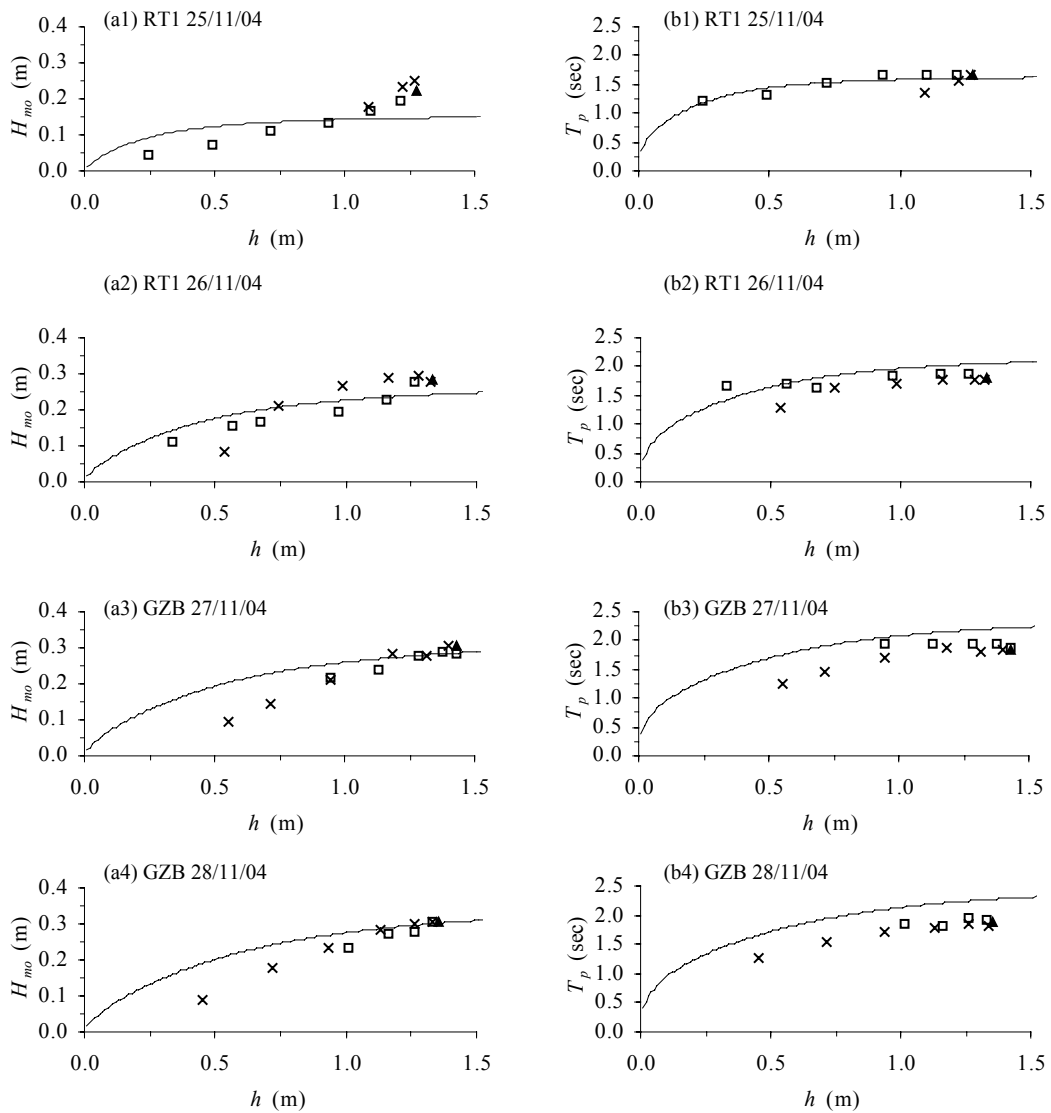
Figure 5.30. Relationships between water depth and H_{mo} (a) and T_p (b) (a1 and b1 at RT1 on 25/11/04, a2 and b2 at RT1 on 26/11/04, a3 and b3 at GZB on 27/11/04, and a4 and b4 at GZB on 28/11/04) (x=flood, ▲=peak and □=ebb). Also curves of H_{mo} and T_p (—) according to Young and Verhagen (1996a) are presented based on fetch = 3500m and (a1 and b1 at RT1 on 25/11/04 U_{10}=7.7m/s, a2 and b2 at RT1 on 26/11/04 U_{10}=10.3m/s, a3 and b3 at GZB on 27/11/04 U_{10}=11.3m/s, and a4 and b4 at GZB on 28/11/04 U_{10}=11.9m/s).

In Figure 5.30, curves of H_{mo} and T_p according to the equations of Young and Verhagen (1996a) are presented. A curve of H_{mo} was calculated from their equation of non-dimensional wave energy, ε, according to $ε=g^2 E/U_{10}^4$ and $H_{mo}=4(E)^{0.5}$ where E is dimensional wave energy. A curve of T_p was calculated from their equation of non-dimensional peak frequency, ν, which equals $f_p U_{10}/g$ where f_p is a peak frequency.

172

Their equations of non-dimensional wave energy, ε, and peak frequency, ν, based on U_{10} and non-dimensional variables of water depth, δ, and fetch, χ, are given as

$$\varepsilon = 3.64x10^{-3}\left(\tanh A_1 \tanh\left[\frac{B_1}{\tanh A_1}\right]\right)^{1.74}$$

$$\nu = 0.133\left(\tanh A_2 \tanh\left[\frac{B_2}{\tanh A_2}\right]\right)^{-0.37}$$

where $A_1=0.493\delta^{0.75}$, $B_1=3.13x10^{-3}\chi^{0.57}$, $A_2=0.331\delta^{1.01}$ and $B_2=5.215x10^{-4}\chi^{0.73}$

In order to calculate non-dimensional wave energy, ε, and peak frequency, ν, given above, U_{10} has been converted from mean wind speed measured in the field on that day, water depth is averaged depth at the site at the time of calculation, assuming the reef elevation along the fetch is flat, and fetch, estimated distance from the Dobie pressure sensor measured in the ESE direction to the island, is treated as constant at 3,500 m. According to the wind data both from the meteorological station (Horn Island) and the field measurement, in this calculation, it is reasonable to presume that the wind duration was not limited, lasting long enough for waves to grow along the fetch. Therefore, the fetch is constant for all cases, values of U_{10} change daily and water depth is depth at the time of calculation.

For H_{mo}, their equation overestimates the values at lower water level and underestimates the values at higher water level, particularly during low-energy events (Figure 5.30a1). For T_p, during low-energy events (Figure 5.30b1), their equation and the data show similarity but, during high-energy events (Figure 5.30b2, b3 and b4), the equation overestimates the values but produces changes similar to a trend of T_p during flooding. In general, their equations are in a better agreement with H_{mo} than T_p.

The trend of H_{mo} and T_p of incident short-period waves during flood is different from that during ebb. The difference is greater during a lower energy event. This can

probably be attributed to tidal currents. During flood the tidal currents roughly follow the direction of incident short-period waves while during ebb the tidal currents approximately flow in the opposite direction to the incident short-period waves.

The discrepancy between the curves of Young and Verhagen (1996a), and the field data probably results from tidal currents, reef-flat topography and bottom friction. The equations were developed based on data from a confined lake with relatively uniform depth and having the small magnitude of bottom friction similar to those in natural beaches. Therefore, no effect of tidal currents was included in equation development. The reef flat across Warraber Reef is actually not flat. The DTM of the reef-flat topography generated in this study using surveyed transects and visual estimates by Hart (2003) shows that the eastern reef flat basically consists of lower areas along the reef rim and higher areas towards its centre. Compared to water depth, the difference in elevations on the reef flat may be less significant during high tides but can exert more influence on fetch determination during lower tides, causing fetch to be shorter. Subsequently, a combination of shorter fetch and shallower water leads to smaller H_{mo} and T_p during low water level. The bottom friction in the reef environment is approximately 1 order of magnitude greater than that existing on natural beaches, due to a combination of a very rough bottom and very shallow water (Hardy and Young, 1991). More energy is, therefore, dissipated, causing waves to have smaller H_{mo} and T_p than those calculated using the equations.

H_{max}/h of the incident short-period waves was also compared with the curve proposed by Nelson (1994) in order to examine saturation of the incident short-period waves. The conversion of H_{mo} to H_{max} was performed using the same equation as used for the data from the Dobie pressure sensor at RF. For each time series, F_c was

computed using H_{max}, h and T_p. Plots of H_{max}/h over ranges of F_c, compared to Nelson's curve are given in Figure 5.31.
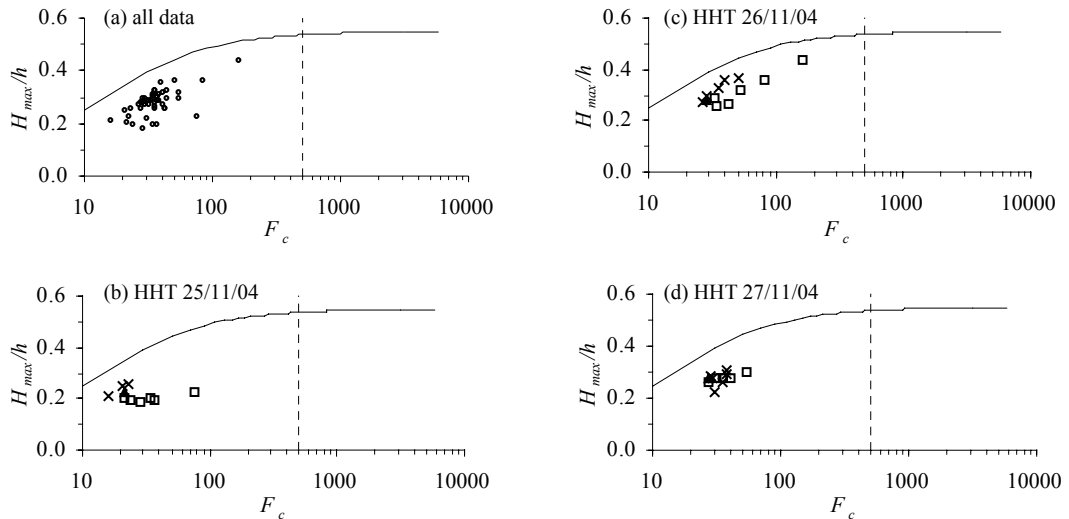
Figure 5.31. Comparison between a curve of maximum H_{max}/h (—) proposed by Nelson (1994) and H_{max}/h of incident short-period waves: (a) all data, (b) HHT 25/11/04, (c) HHT 26/11/04 and (d) HHT 27/11/04 (x = flood, ▲ = peak and □ = ebb). On the left side of a dash line is intermediate water and on the right side is shallow water.

Nelson (1997) investigated height limits of stable waves in two natural distinct environments, the first one, called the top down wave environment, in which stable wave conditions are approached from above as larger incident waves propagating onto a reef are reduced in size, and the second one, called the bottom up wave environment, in which stable wave conditions are approached from below as waves generated on a reef by wind are increased in size. His study was based on field measurements of wave transformation on John Brewer Reef and Lake George for the top down and bottom up wave environments, respectively. He demonstrated that height limits of stable waves both in top down and bottom up wave environments in water of constant depth conformed to the limits defined by the function developed for regular wave experiments. He also concluded that only top down waves can achieve the asymptotic H/h value of 0.55.

The results of wave analysis at RF suggested that in natural occurring top down wave environments, most waves achieve their maximum limits in intermediate conditions, $H_{max}/h < 0.55$. For this bottom up wave environment of incident short-period waves, all field data are intermediate water waves (Figure 5.31a) and H_{max}/h tend to decrease along the curve as deeper wave conditions are approached, especially during high-energy events (Figures 5.31c and d). This pattern of change in H_{max}/h over a tidal cycle is opposite to that of the top down wave environment at RF, in which waves start from the lower values of H_{max}/h in shallower wave conditions and then approach the limits with higher values of H_{max}/h in intermediate water. Values of H_{max}/h of incident short-period waves are all below the curve. Clear alignment of the data along the curve of H_{max}/h together with approaching the limits of H_{mo} probably suggests that during high-energy events incident short-period waves are near the limits of H_{max}/h.

As suggested in the previous section, incident waves off Warraber Reef are dominated by seas. These incident waves were examined in this section to be the main driving force for incident wind wave components on the reef flat. They undergo attenuation as they move across the reef flat towards the island. Therefore, incident wind wave energy becomes smaller from the reef rim towards the island. Growth of infragravity waves around the island is found in the present study to be related to incident wind wave energy on the reef flat. Incident short-period waves that are the main component of wave spectra, especially at windward locations, were proved to be locally generated on the reef platform by the local wind system and their energy probably increases along their fetch across the reef platform. Therefore, it can be summarised that growth of all three wave frequency ranges is related to a local wind system but their magnitude occurs differently around the island depending on locations around the island in relation to main directional influence of wind, the magnitude of

wind speed and reef-top topography, resulting in distinct wave characteristics around the island with potential for differing patterns of sediment movement.

5.6.3. Wave Climate on the Reef Platform

According to spectral analysis of wave data at RF, the wave environment off Warraber Reef during the experiment was predominantly influenced by seas generated by the local wind system and results of wave analysis at locations around the island also suggested the relationships between development of wave spectral components around the island and the local wind pattern. It is normally the case in areas where seas are dominant to determine wave climate from a limited duration of wave information in relation to the relationship between wind data during measurements and the wind climate in the region.

In the present study, winds during the experiment were persistently from ESE with speeds increasing from approximately 5.0 m/s during low wave-energy events to around 7.0-9.0 m/s during high wave-energy events, according to wind data from a meteorological station at Horn Island. Wind analysis in Chapter 4 indicated that Torres Strait has been primarily dominated by winds from the E-SSE sector, accounting for approximately 80% of wind effect in the region. ESE wind is the major component of winds from the E-SSE sector. It exists throughout the year but prominently between April and November, producing approximately 40-50% of monthly wind effect, with its mean wind speeds of around 8.0 m/s and a standard deviation of generally less than 3.0 m/s. Accordingly, wind conditions occurring during high wave-energy events can be considered as modal wind conditions between April and November. This also implies

that general wave conditions occurring on the reef platform and around the island between April and November are similar to those found during the experiment.

According to wind analysis in Chapter 4, December is the transition period between the E-SSE domination to the W-NNW domination with an increase in calm periods. The transition takes place again in March when calms are dominant. The period that may introduce significant wave energy to the island is that between January and February when W-NNW winds are dominant. During this period, windward and leeward sides of the island are reversed (RT4, RT6 and RT5 on the windward side, and RT1 and GZB on the leeward side) and different wave patterns occur due to the difference in wind pattern in relation to reef geometry and reef topography (Hart, 2003). The windward side of the island over this period is characterised by the reef flat with water depth approximately 1.0 m deeper than that on the leeward side and shorter distances from the reef edge to the island at RT6, approximately 500 m, compared to approximately 2,500 m at RT1 on the leeward side (Hart, 2003).

Compared to winds from the E-SSE sector, W-NNW winds have slightly lower mean wind speeds and greater maximum wind speeds of more than 20.0 m/s. WNW and NW winds are the most dominant during these two months but generate monthly wind effects of less than 30% each. To account for 80% of monthly wind effect, wind effect from all directions within the W-NNW sector has to be taken into account whereas only a combination of ESE and SE winds during the E-SSE wind domination generated more than 80% of monthly wind effect. In addition, W-NNW winds have a greater standard deviation of approximately 4.0 m/s. Accordingly, W-NNW winds are more variable both in direction and speed, and waves generated by W-NNW winds are more duration-limited with smaller height and shorter period (Hart, 2003).

No information on swell waves is available in this area. Nonetheless, the location of Warraber Reef in Torres Strait which is bounded on all directions by reefs, islands and mainland suggests that swell waves that may be present in this region at any times of year are likely to be very small. Therefore, it is possible that sea dominates the wave environment off Warraber Reef all year round.

Waves off the reef moving across the reef rim on the windward side, which is deeper, may experience less energy attenuation due to wave breaking. Applying a value of H_{max}/h of $0.55h$ to this area, during highest spring tides, the maximum height that reformed waves could attain after waves break at the reef rim is 1.65 m. The boat channel can allow larger reformed waves due to its deeper water. In addition, the short distance and deeper water depth means less energy is dissipated by bottom friction. This results in a small reduction in wave height across the reef towards the island. Therefore, in some occasions of high wind speeds of more than 20.0 m/s which can occur during the W-NNW wind domination, larger and longer waves can be generated.

Incident wind wave energy at the locations on the windward side, relative to energy of incident waves off the reef, during the W-NNW winds also is possibly greater than that occurring on the windward locations during the influence of ESE winds when waves move over shallower water depth and much longer distances across the reef platform towards the island. Incident short-period waves that are generated on the reef flat and significant during the ESE season, on the other hand, are possibly negligible due to the very short fetch on the western reef flat, compared to the eastern reef flat, and high variation in wind patterns. Wave measurements by Hart (2003) also indicated the absence of incident short-period waves during the domination of W-NNW winds. Therefore, it is likely that waves around the island are primarily dominated by incident wind wave components.

On reefs of a small width with a boat harbour and boat channel, infragravity waves generated when incident waves moves onto the reef may also be significant and, if periods of these infragravity waves are coincident with the natural period of the reef basin, resonant oscillations can be generated (Gourlay, 1990). The resonant conditions can modulate waves on the windward reef flat such that they might reach the island with higher water levels than normal (Nakaza et al., 1990). Therefore, during the W-NNW domination infragravity wave components may contribute significant portions of energy to the wave field on the windward side of Warraber Island. However, the infragravity waves are more absorbed over the larger area of broad reef flats (Gourlay, 1990), which is probably the condition occurring on the reef flat on the lee of the island . On the leeward side of the island, therefore, it is probable that infragravity waves occurring there may be those generated when waves refracting and diffracting along the southern reef rim shoal towards the island on the leeward side.

In summary, incident wind wave is the primary spectral component of waves around the island during the W-NNW wind prevalence. Swell waves and incident short-period waves are negligible. Infragravity waves may be prominent on the windward side of the island in association with resonant conditions whereas infragravity waves found on the leeward side may be those generated by shoaling incident wind waves.

5.7. Threshold of Sediment Transport

Waves moving across the water surface induce an orbital motion of water particles, circular paths in deep water and elliptical paths in intermediate and shallow water (CERC, 1984). At the bottom, water particles move in a to-and-fro horizontal

pattern, with velocity being a function of wave height, wave period and water depth (Komar and Miller, 1973). Sediments start to move as the maximum particle velocity at the bottom (u_m) is greater than the threshold orbital velocity (U_w). The examination of sediment entrainment during the experiment includes two steps, calculation of the maximum horizontal velocity of water particles at the seabed (u_m) and an estimate of the threshold of sediment movement (U_w). U_w and u_m calculated from each time series were then compared to determine if sediment would have been entrained.

The maximum horizontal velocity of water particles at the seabed (u_m) was calculated based on linear wave theory (Komar, 1998).

$$u_m = \frac{H\pi}{T\sinh(kh)}$$

H_{mo} and T_1, derived from wave spectra at RF in Section 5.5.1 and at locations around the island in Section 5.6.1, were used for H and T, respectively. Wave number (k) was calculated using T_1.

The threshold orbital velocity (U_w) in cm/s was calculated based on a method proposed by Le Roux (2001) to predict the threshold of sediment transport under oscillatory waves. The reef flat on Warraber Reef is large. Most of the time, waves move across the reef flat as reformed, oscillatory waves after breaking in the vicinity of the reef rim. The threshold of sediment transport in this consideration, therefore, is that induced by oscillatory waves. The method used by Le Roux represents an advance on previous techniques that were proposed by Manohar (1955), Komar and Miller (1973 and 1975), Hammond and Collins (1979), Soulsby and Whitehouse (1997). Its advantages are that it can be applied for different fluid densities and viscosity, accounts for the dynamic viscosity, needs no value for a wave orbital diameter, uses wave period which is easily determined from the field measurements, and can be applied to both

181

laminar and turbulent flow (Le Roux, 2001). The equation to predict the threshold of sediment transport under oscillatory waves is given by

$$U_w = -0.01 \left[\frac{(\theta_{wl} g D \rho_\gamma)^2}{(\rho \mu / T)} \right] + 1.3416 \left[\frac{(\theta_{wl} g D \rho_\gamma)}{(\rho \mu / T)^{0.5}} \right] - 0.6485$$

where θ_{wl} = Shields-type parameter (dimensionless threshold orbital velocity), g = gravitational constant (cm/s^2), D = grain diameter (cm), ρ = fluid density (g/cm^3), ρ_s = grain density (g/cm^3), ρ_γ = submerged particle density (ρ_s - ρ) (g/cm^3), μ = fluid dynamic viscosity (g/cm s or poise) and T = wave period

T_1 was also used for T in the equation above. Values of ρ of 1.025 g/cm^3, ρ_s of 1.85 g/cm^3 (the mean density of carbonate sediments (Kench and McLean, 1997)), μ of 0.01 g/cm s and g of 981 cm/s^2 were used for U_w calculation. The calculation of θ_{wl} followed Le Roux (2001). Grain sizes (D) used in the equation above can be obtained either using a sieving technique and expressed in terms of sieve diameters or settling technique and interpreted in terms of equivalent sedimentation diameter (the dimensions of a sphere with the same settling rates) (Le Roux, 1998). Kench and McLean (1997) examined differences in grain-size determination for bioclastic sediments between sieve and settling techniques. They indicated that due to the heterogeneous character of bioclastic deposits, sieve-size estimates are different from settled-size determination, that a settling method reflects the hydraulic behaviour of bioclastic sediments and that settled-size estimates are more suitable in examination of sedimentary processes in bioclastic environments. Therefore, grain sizes involved in U_w calculation were derived from transformation of settling velocity (W). A value of ρ of 1.0 g/cm^3 was used in transforming a settling velocity (W) to an equivalent sedimentation diameter (D).

Information on settling velocities of sediments on the Warraber reef flat and on the island beach was obtained by Hart (2003) and was summarised in Section 1.5. In

this study, four values of settling velocities of 4, 8, 16 and 32 cm/s or in Psi unit of -2, -3, -4 and -5, respectively, were chosen for U_w calculation. These four values of settling velocities represent a range of modal settling velocities of bulk fractions of sediment samples on the reef and on the beach of the island. They also cover modal settling velocities of main individual constituents including molluscs, coral, coralline algae, *Halimeda* and foraminifera. Modal settling velocities of these individual constituents are broadly divided into a group of molluscs, coral and coralline algae, of which modal settling velocities range between -4 and -5 Psi, and a group of *Halimeda* and foraminifera, of which settling velocities range between -3 and -4 Psi (Hart, 2003). A procedure proposed by Le Roux (1992) was applied to transform settling velocities to equivalent grain size. The settling velocities of -2, -3, -4 and -5 Psi correspond to equivalent grain sizes of 0.04, 0.08, 0.17 and 0.41 cm, respectively.

The method used here to determine the capacity of waves for sediment entrainment is similar to that, called a *current of removal approach*, applied by Kench (1998) in order to examine and quantify carbonate sedimentary processes in the Cocos (Keeling) Islands, an Indian Ocean atoll. Hydraulic response of carbonate sediment, applied by Kench (1998), was based experimentally on unidirectional flows to establish the threshold of sediment movement, whereas in this study the threshold of sediment movement was determined directly from a wave-induced horizontal orbital velocity at the seabed derived from wave characteristics during the field measurements. Methods for studying sediment transport based on unidirectional flows may be reasonably applied for narrow reef flats where most area is occupied by the surf zone. In the case of Warraber Reef, where the reef flat is very large and most sediment is subjected to oscillatory movement of water particles induced by waves, the relationships developed in relation to oscillatory waves are considered more appropriate.

Figure 5.32 demonstrates temporal and spatial variations of u_m versus those of U_w for four ranges of modal settling velocities of sediments (4, 8, 16 and 32 cm/s). Also, the threshold of sediment entrainment is illustrated in terms of a resultant velocity which is the difference between u_m and U_w in Figure 5.33.

At RF, waves during the low wave-energy events (24–25/11/04) were generally capable of mobilising all sediments with a settling velocity below –4 Psi (16 cm/s) while during the high wave-energy events (26–28/11/04) all four ranges of sediments were mobilised except during a LHT when entrainment condition was similar to the low wave-energy events due to limited wave height by tidal levels (Figures 5.32a and 5.33a).

On 24/11/04 when waves were measured at RT4 using the Vector and the KPSI, at RT6 using the miniTROLL (MN158) and at RT5 using the S4 and the miniTROLL (MN162), wave-induced orbital velocities were deficient in entraining those four ranges of sediment at all locations (Figures 5.32b, c, d, e, f, g and h). On 25/11/04 waves were still incapable of mobilising sediment at RT6 and RT5 (Figures 5.32f, g and h) but movement of sediments with settling velocities less than –4 Psi (16 cm/s) was initiated at RT1 (Figures 5.32b, c, d and e).

On 26/11/04 waves at RT1 were capable of mobilising all four ranges of sediments (Figures 5.32b, c and d) and at RT5 sediments with settling velocities less than –3 Psi (8 cm/s) and –2 Psi (4 cm/s) could be entrained but only around the peak of a HHT and of a LHT, respectively (Figures 5.32g and h). Only sediments with settling velocities less than –2 Psi (4 cm/s) could be entrained at RT6, particularly around the peak of a HHT (Figure 5.32f).
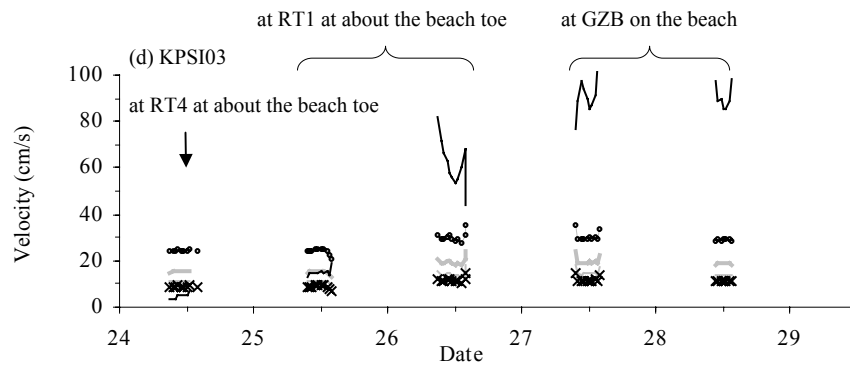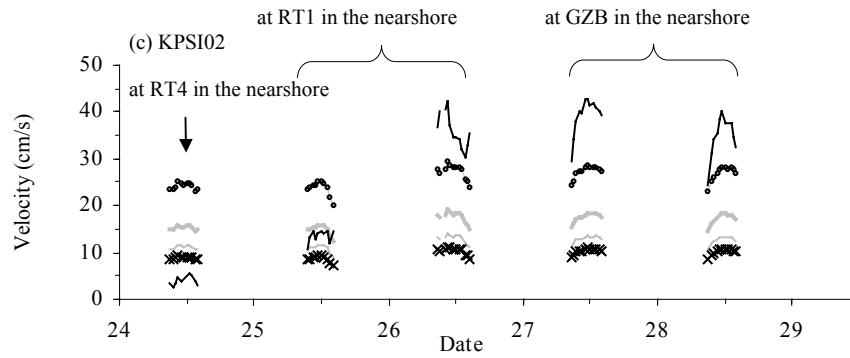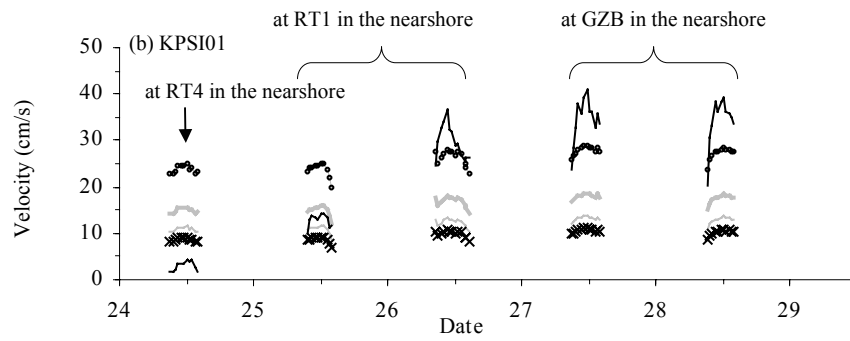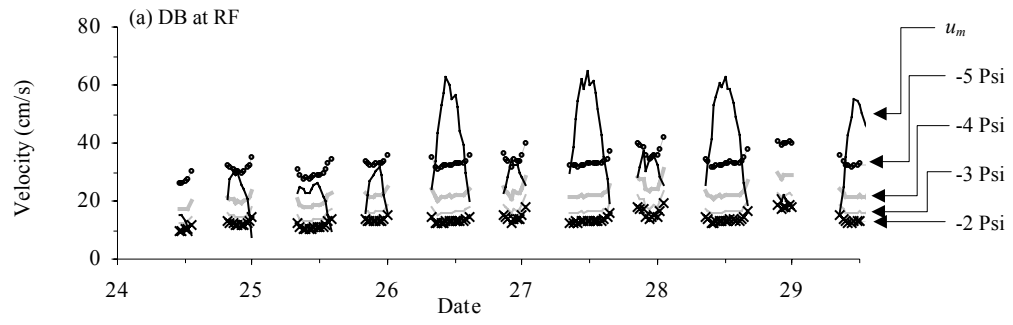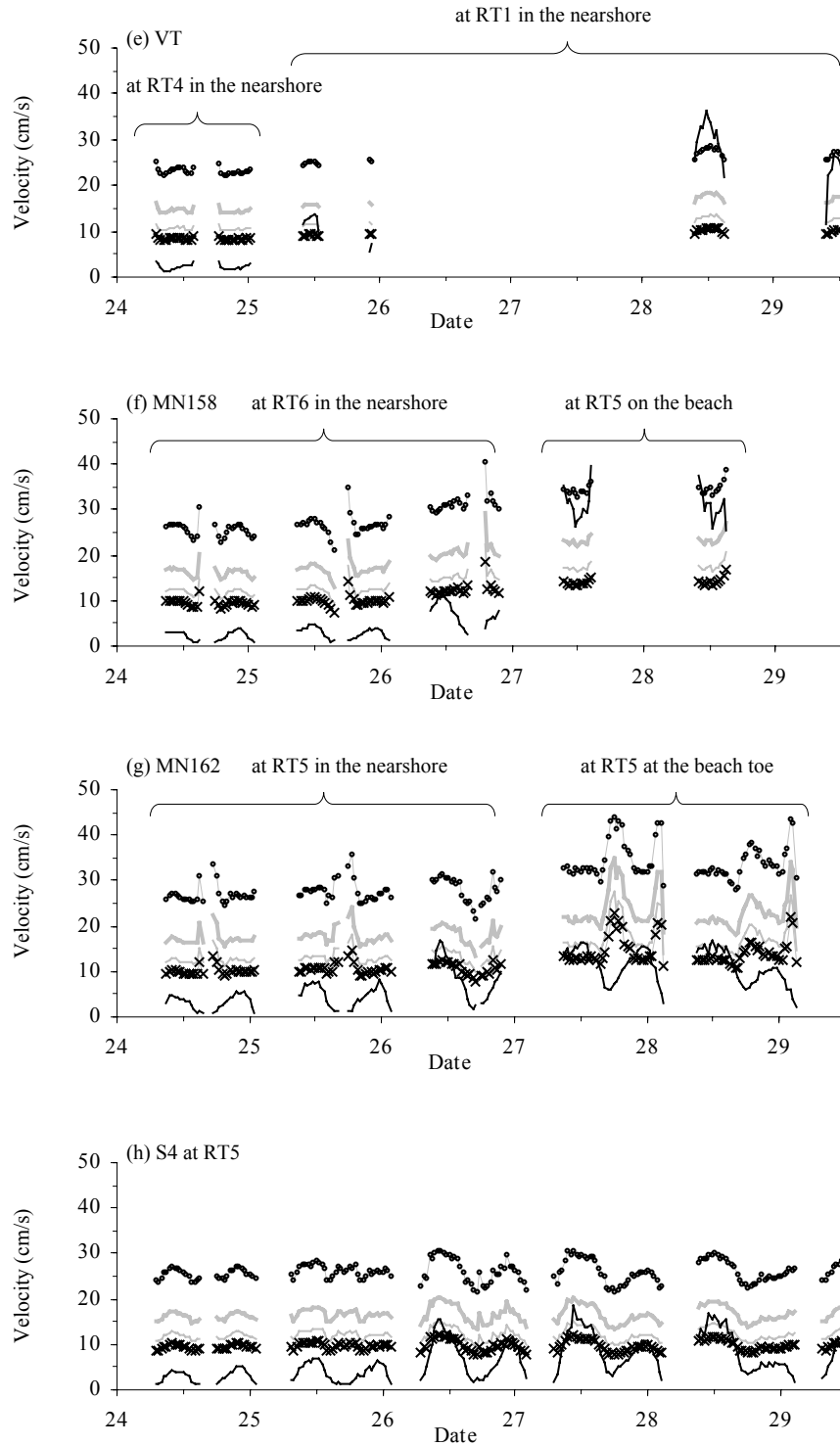
Figure 5.32. Temporal and spatial variations of u_m (——) and U_w of four ranges of modal settling velocities of sediments: –2 Psi ($-_X-$); -3 Psi (——); -4 Psi (▬▬); and −5 Psi (—•—) from: a) DB at RF; b) KPSI01; c) KPSI02; d) KPSI03; e) VT; f) MN158; g) MN162; and h) S4. Their locations are displayed in Figures 5.15, 5.17, 5.19, 5.21 and 5.23. There is no data from the VT between 26–27/11/04.

186

187
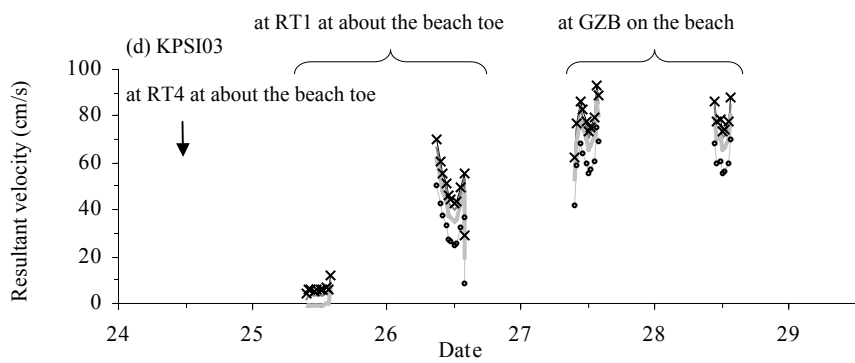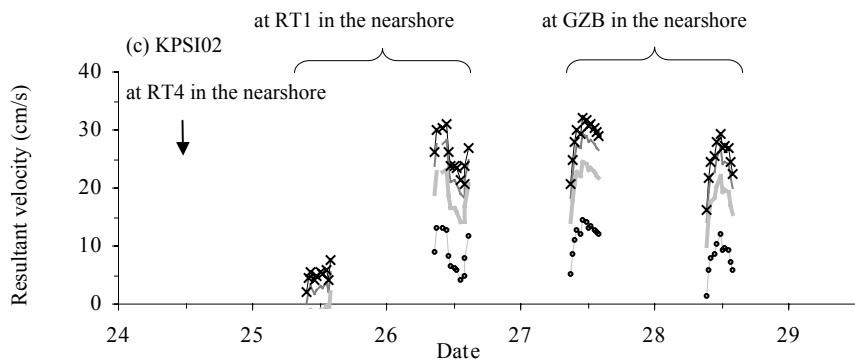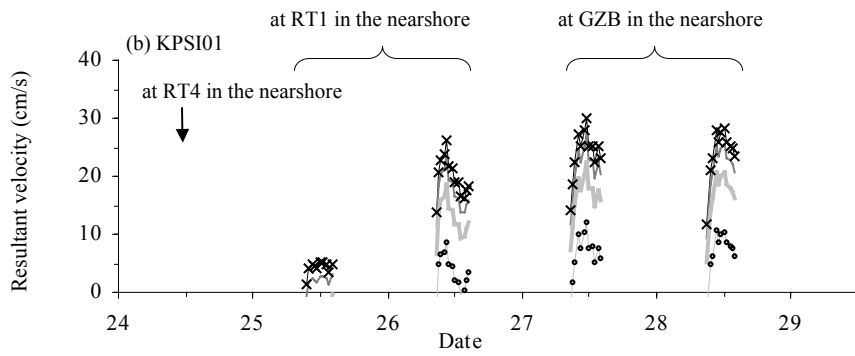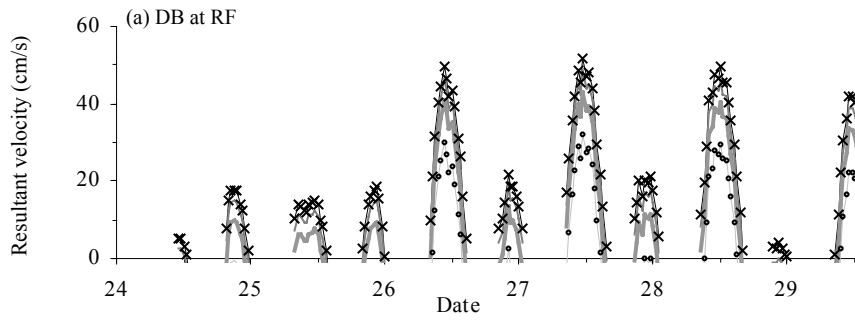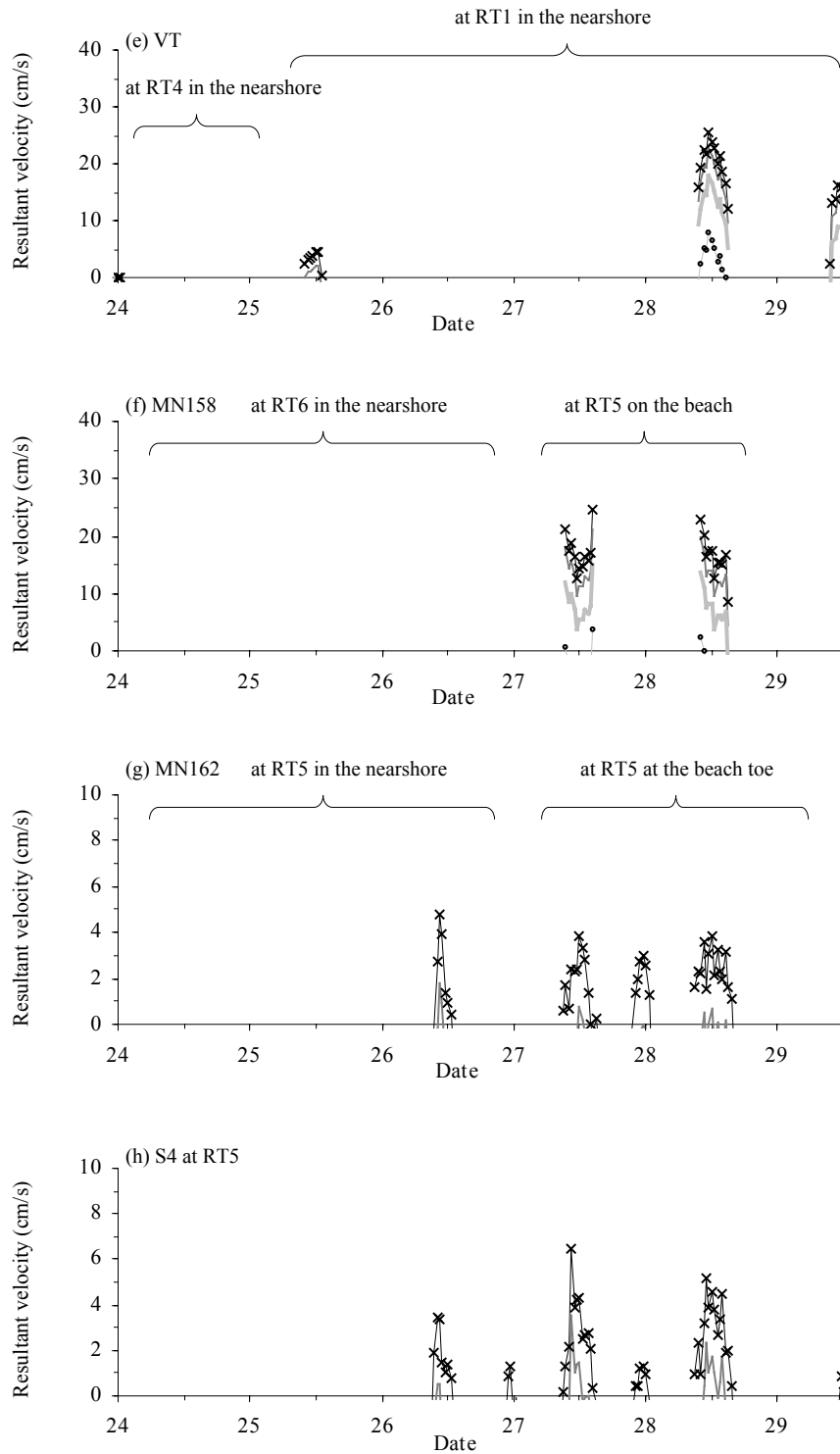
Figure 5.33. Temporal and spatial variations of resultant velocities for four ranges of modal settling velocities of sediments: –2 Psi (x); -3 Psi ( ); -4 Psi ( ); and –5 Psi (•) from: a) DB at RF; b) KPSI01; c) KPSI02; d) KPSI03; e) VT; f) MN158; g) MN162; and h) S4. Their locations are displayed in Figures 5.15, 5.17, 5.19, 5.21 and 5.23. There is no data from the VT between 26–27/11/04.

188

Between 27-28/11/04 waves at GZB (Figures 5.32b, c and d) and RT1 (Figure 5.32e) showed capability for entraining all four ranges of sediments. At RT5 the highest capacity of sediment entrainment occurred on the beach at the MN158 location (Figure 5.32f), able to mobilise sediment with settling velocities less than −5 Psi (32 cm/s) while the entrainment conditions of sediment at the nearshore location (S4) (Figure 5.32h) and the beach toe location (MN162) (Figure 5.32g) were similar to those on 26/11/04.

The relative capability of waves for initiating sediment movement on the reef and around the island is clearly illustrated based on the resultant velocities shown in Figure 5.33. The highest resultant velocities occurred on the beach at GZB (KPSI03) during the high wave-energy events (Figure 5.33d). They appeared to be higher at some stages of flooding and ebbing than at the peak of a HHT. These higher values of resultant velocities probably occurred when this location was dominated by wave shoaling before breaking, resulting in a higher ratio of wave height to water depth at this location. Before and after these periods, this location was probably in the surf zone where wave height decreases after breaking.

The resultant velocities across the nearshore towards the island were similar in magnitude (Figures 5.33b, c and d). Similarly, at RT5, during the high wave-energy events higher resultant velocities occurred on the beach (MN158) (Figure 5.33f) but much lower than those at GZB. The values of resultant velocities at about the beach toe at RT1 (KPSI03) on 26/11/03 (Figure 5.33d) implied that the magnitude of sediment entrainment on the beach at this location was lower but higher than those at GZB and RT5, respectively. However, it is evident that sediment entrainment at all locations was constrained during low water depth.

This finding of spatial variations in the magnitude of potential sediment entrainment around the island is in agreement with results from the previous study of sediment transport by Hart (2003). Hart found that most of reef flat and island beach sediments are potentially transported under normal hydrodynamic conditions and that longshore transport was common around the island.

Hart (2003) also found that the inner reef flat adjacent to the beach on the west of the island, an area where RT4, RT6 and RT5 are located, contained the greater portions of fine sediments than the eastern, elevated reef flat. The present study found that within this inner reef flat on the west of the island sediments with settling velocities of greater than -2 Psi (4 cm/s) were unable to be entrained during the low wave-energy events and that only sediments with settling velocities of –2 Psi (4 cm/s) or less could be mobilised during the high wave-energy events.

Although sediment entrainment is primarily governed by waves (Nielsen, 1992), patterns of sediment transport may be more complex due to combined effects of different driving forces generated by wave, wind and tide (Tartinville and Rancher, 2000; Hearn et al., 2001). As indicated by Hart (2003) from the sediment transport measurements in July when wind was primarily from the ESE, similar to that during the present study, at any one location sediment may be transported both in alongshore directions, and on and off shore directions. In general, the dominant directions of sediment transport across the reef platform are on-shore towards the island, corresponding with the prevailing wind directions (Hart, 2003). However, as shown by sediment trap results from the southeast transect, at locations closer to the reef rim sediment transport was dominated by alongshore movement (Hart, 2003). This may reflect spatially varying magnitude of influence between wave-generated currents

moving towards the island and tide-generated currents moving in an east-west direction on sediment transportation on the reef.

This variation in patterns of sediment transport is also in agreement with the spatially developing patterns of incident wind wave and incident short-period wave components. Incident wind waves are waves off the reef that probably lose significant energy due to wave breaking at about the reef edge. Their energy is dissipated due to bottom friction as they propagate across the reef platform. On the other hand, incident short-period waves were found to be wind waves generated on the reef platform and their energy likely increases along their fetch across the reef platform towards the island. Therefore, total wave energy at about the reef rim is probably low because energy of incident wind waves is small as a result of wave breaking at about the reef edge and incident short-period waves may just start to develop, resulting in domination of tide-generated currents transporting sediments in an alongshore direction. This also implies that sediments (coral and foraminifera) that are produced around the reef rim, especially the southeastern rim, may undergo more complex patterns of transportation towards the island, resulting in more time taken for transportation than shells of gastropods living close to the island.

As suggested in Section 5.6.3, wave conditions observed during the experiment represent the wave characteristics generally occurring on Warraber Reef and around the island. As found from a previous study by Hart (2003), sediments on the reef platform can be transported under normal wave conditions. Therefore, sediment transport processes are commonly active on Warraber reef platform and on the beaches of Warraber Island, particularly during higher water depth, with the higher magnitude on the windward side of the island.

Development and stability of sand cays on platform reefs were generally considered based primarily on the residual energy of waves breaking at about the reef edge (Hopley, 1982; Gourlay, 1988). They suggested that on large reef platforms waves may lose their capacity to transport sediments before reaching focusing points. However, the findings in this study and the finding by Hart (2003) indicate that on the large Warraber reef platform there are significant proportions of wave energy developed on the reef platform, and sediments both on the reef flat and around the island can be entrained, transported and deposited on the island beach.

5.8. Summary

A field experiment was conducted at Warraber Reef in November 2004 in order to extend the earlier studies of Hart (2003) and Brander et al. (2004), and to gain more insight into spatial and temporal variations of wave characteristics, origin of wave spectral components and the influence of waves on the threshold of sediment transport, both on the reef flat and around the island.

Subsurface pressure signals were measured using pressure-type wave recorders at one location on the reef flat close to the reef edge (RF) and 5 locations around the island (RT1, RT4, RT5, RT6 and GZB). Surface wave energy spectra were estimated from subsurface pressure data using the FORTRAN programs developed for wave analysis, based on the fast Fourier transform algorithm. Wave parameters including the significant wave height (H_{mo}), the peak wave period (T_p), the mean wave period (T_1) and the bandwidth parameter (ε) were derived from the wave spectra. Wave energy was also estimated for four spectral frequency ranges: i) incident short-period wave frequencies of 0.4-1.0 Hz (2.5-1.0 s); ii) incident wind wave frequencies of 0.125-0.4

Hz (8.0-2.5 s); iii) incident swell wave frequencies of 0.05-0.125 Hz (20.0-8.0 s); and iv) infragravity wave frequencies of less than 0.05 Hz (greater than 20 s).

Wave characteristics both at RF and at locations around the island vary temporally with depth on the reef flat, which is influenced by tides. At RF, in general incident wind waves are a main wave component except during very low water depth when infragravity waves are dominant. The occurrence of swell waves is observable but with very small energy. The evidence of prominent spectral peaks at incident wind waves and the direct relation found between winds and wave characteristics suggest sea as the primary wave environment off Warraber Reef. Waves at RF approach their limiting state of growth during high wave-energy events.

Whereas incident wind waves are the main component of wave spectra at RF, at locations around the island distinct wave spectra have occurred as a result of different combinations of infragravity wave, incident wind wave and incident short-period wave. These combinations of wave components result in larger and shorter waves on the windward side than those on the leeward side. At a HHT, during the low wave-energy events waves are approximately 0.2 m and 1.7 s on the windward side and approximately 0.1 m and 2.0 s on the leeward side. At a HHT, during the high wave-energy events waves are approximately 0.4 m and 2.5 s on the windward side and approximately 0.3 m and 3.0 s on the leeward side.

Spatial variations of wave characteristics across the nearshore towards the island are evident during the high wave-energy events but negligible during the low wave-energy events. In general, wave period increases towards the island, which is more obvious on the leeward locations. Wave height, on the other hand, changes slightly towards the island on the windward locations but significantly decreases towards the island on the leeward locations.

All three frequency ranges are found to be related to the local wind system. Incident wind waves are forced by seas while incident short-period waves are generated locally on the reef platform and can be approximated using the equations of Young and Verhagen (1996a). Energy of incident wind waves is likely to be reduced towards the island due mainly to bottom friction whereas energy of incident short-period waves likely increases along fetch towards the island. Infragravity wave energy is found to increase as waves shoal towards the island and increase with energy of incident wind waves.

The wave climate on the reef platform is primarily dominated by wave conditions observed during the experiment representing wave conditions occurring during the period between April and November when ESE and SE winds are dominant and is secondarily dominated by wave conditions generated by W-NNW winds during the period between January and February. W-NNW winds are more variable in directions and speeds, and consequently waves generated during this period are more duration-limited with smaller height and shorter period. During this period incident wind waves are probably dominant whereas incident short-period waves may be small due to the very short fetch across the reef flat. Infragravity waves may be observable on the windward side of the island as a result of resonant oscillations and on the leeward side of the island as a result of shoaling incident wind waves.

In general at all locations both RF and around the island sediment entrainment is modulated by tides. At RF, waves can entrain most reef-flat sediments during the high wave-energy events. At locations around the island, the highest capability of waves for initiating sediment movement occurs at GZB (windward side) on the island beach while waves in the nearshore on the windward side can entrain most sediment during the high wave-energy events. At the leeward locations, in general only sediments with slow

settling velocities (less than –2 Psi) can be mobilised, except on the beach at RT5 where

sediments with faster setting velocities can be entrained. The least capacity of waves on

the leeward side for entraining sediment is in accordance with results from the previous

study by Hart (2003) that the inner reef flat adjacent to the beach on the west of the

island contained the greater portions of fine sediments than the eastern, elevated reef

flat.

CHAPTER 6

DISCUSSION

6.1 Introduction

In this chapter, evolution of the island morphology over geological and engineering time scales, examined respectively in Chapters 2 and 3, is discussed with respect to probable patterns of primary hydrodynamic forces operating on the reef over these two time scales.

Section 6.2 discusses probable conditions of waves over a period of island evolution in relation to the morphological evolution of Warraber Island over the past 3,000 years, examined in Chapter 2, based on the contemporary wave conditions examined in Chapter 5.

Section 6.3 discusses probable shape of Warraber Island in response to seasonal hydrodynamic influence and probable causes of a sustained pattern of shoreline changes on Warraber Island over the past 40 years, examined in Chapter 3. Seasonal response of the island shoreline is discussed based on wind climate in the region, analysed in Chapter 4, and associated patterns of sediment transport examined by Hart (2003). In relation to a sustained movement of the island, both the effects of environmental factors and human activities are considered. Environmental influence is discussed based on medium-term trends of wind effect, investigated in Chapter 4, the effects of nearby reefs on wave conditions impinging on the reef and island, and contemporary conditions of unhabitated vegetated sand cays on reefs nearby. Human activities under consideration include the construction of seawalls and the boat channel.

In Section 6.4, the implications for probable future conditions on Warraber Island are discussed and in the final section, Section 6.5, the potential for selecting and applying wave models for wave focusing on platform reefs is described.

6.2 Wave Conditions and Evolution of Warraber Island over the Past 3,000 Years (Geological Time Scale)

It was demonstrated in Chapter 2 that the averaged elevation of Warraber Island had decreased during its evolution from an average of around 6 m over the first 1,000 years to an average of around 5 m and to slightly less than 5 m on northeastern and southwestern ends of the island during the most recent 500 years.

This evolutional pattern of Warraber Island, decreasing in average elevation towards the windward rim, differs from the schematic reef island proposed by Woodroffe et al. (1999), in which elevation is greatest towards the oceanward rim (Figure 1.3). It should be noted that the models of reef-island evolution proposed by Woodroffe et al. (1999) have been developed based principally on studies of reef islands on atolls. In general windward or oceanward reef flats of the islands on atolls are swell-dominated and narrower than those fronting sand cays on reef platforms which are generally located towards the leeward end. Progradation of reef islands across the reef flat towards the atoll rims reduces the oceanward area of the reef flat and in turn allows greater wave action to operate on the islands, resulting in higher oceanward rims of the islands (Kench et al., 2005).

The pattern of topographical variation on Warraber Island, shown by the detailed DTM, is similar to those described for sand cays on the northern Great Barrier Reef by McLean et al. (1978). They suggested a reduction in wave action in association with a

fall in sea level to deposit sediment on sand cays during the late Holocene to explain the terrace-like topography on those sand cays.

Topographical variation on sand cays is directly determined by the magnitude of wave run-up which influences the maximum height on a beach to which sediment can be transported and at which the beach berm normally forms (Stoddart, 1964; McLean et al., 1978; Hopley, 1992). The magnitude of wave run-up is directly proportional to incident wave height (Komar, 1998). In the case of sand cays on reef platforms, incident wave height should be the height of waves on reefs before breaking on the island beach. Therefore, geological-time scale variations of wave height on Warraber Reef would have occurred over the period of evolution, resulting in variations of island topography.

It has been suggested that wave height on reefs is determined by water depth on the reefs and the height of waves off the reefs (Young, 1989). It is not always the case that waves are higher with greater depth; this depends on whether the depth-dominating condition is dominant (Hardy and Young, 1996). Whether or not waves on Warraber Reef could be higher in order to create the greater elevation of the island margin together with probable wave conditions over the period of island evolution can be assessed from a consideration of the contemporary conditions of waves on the reef.

As indicated in Chapter 5, wave fields on Warraber Reef, particularly around the island, are influenced by both wave components generated off and on the reef. It was found in Chapter 5 that the contemporary wave climate off Warraber Reef is dominated by seas. The influence of swell on Warraber Reef was found to be negligible. At present, the nearly continuous ribbon reefs on the shelf edge of the northern Great Barrier Reef appear to limit the penetration of oceanic swell or large waves generated outside the Great Barrier Reef; thus locally generated waves are dominant inside the

Great Barrier Reef (Murray and Ford, 1983; Hopley, 1984; Young, 1989; Wolanski, 1994).

During the Holocene transgression, wave conditions would have been considerably different. Reefs initially established over antecedent foundations and then grew vertically, catching up with sea level (Woodroffe et al., 2000). Before the shelf edge reefs reached sea level, larger waves could have penetrated further landward, resulting in a period of higher wave energy along the mainland coast of the Great Barrier Reef, termed the Holocene "high energy window" (Hopley, 1994). Ribbon reefs on the northern Great Barrier Reef were found to have approached the sea surface at similar periods to the nearshore reefs on the northern Great Barrier Reef (Hopley, 1977). However, in the case of Torres Strait, a period of high wave energy is likely to have been less effective due to the shallow depth at which the antecedent foundations for modern reefs occur (Hopley, 1984). Even if the reef platform initially formed under conditions of higher wave energy, the modern reef morphology on Warraber Reef in particular, but also on many reefs in Torres Strait, appears to have been largely developed before the formation of Warraber Island. Wave environments off Warraber Reef have been dominated by seas over the period of island evolution.

The location of a sand cay on a platform reef generally reflects the primary direction of hydrodynamic forces (Flood and Heatwole, 1986). Warraber Island, sitting on the leeward margin of Warraber Reef, would, therefore, appear to have been formed under a wave climate dominated by easterly winds throughout the period of island evolution.

As indicated in Chapter 5, wave height at locations around the island increases with water depth, even at the leeward location (RT6) during low wave-energy events (24-25/11/04), suggesting that the depth-dominating condition is a common occurrence

for wave environments around the island. Therefore, waves around the island tend to be higher as water depth on the reef is greater. The characteristics of waves around the island are a result of the combined influence of incident short-period waves, which are wind waves originated on the reef platform, incident wind waves, which are forced by wind waves off the reef platform, and infragravity waves, which are directly related to incident wind waves.

Incident short-period waves are more prominent on the windward side of the island and their growth is fetch-limited with their energy dependent primarily on water depth on the reef and wind speed. Their saturating conditions, examined in Chapter 5, suggest that they grow near to their limit during high wave-energy events. Therefore, their energy tends to depend primarily on water depth.

Incident wind wave components at locations around the island are driven by waves off the reef, which is primarily controlled by ESE-SE wind speeds, and are tidally modulated. In general, their energy is attenuated at about the reef rim due to wave breaking, and across the platform due mainly to bottom friction. Wave analysis in Chapter 5 indicated that wave energy at RF, which is primarily dominated by incident wind waves, varies with depth and wind speeds, and at the peak of HHT it approaches its limiting growth. This implies that the energy of incident wind waves on the windward side of the island, which is directly related to that at RF, is more sensitive to water depth on the reef than wave energy off reef (more depth-dominated).

Any increase in energy of waves off the reef above the high wave-energy events presently experienced, therefore, has little effect on the magnitude of incident wind wave components on the windward side of the island. However, an increase in energy of waves off the reef may have more influence on incident wind waves on the leeward side of the island. This is due to the fact that the height of waves off the lee of the reef

is smaller as a result of wave diffraction (CERC, 1984) and that water depth over the reef flat on the leeward side of the island is approximately 1 m deeper (Hart, 2003). The effect of diffraction on the wave field on the lee of the reef was clearly observed from RV Kirby during surveying the reef-front topography in October 2004. The sea was very rough on the windward side of the reef, making operation of the vessel difficult, whereas on the lee of the reef the sea was very calm. The combined effect of smaller height of waves off the reef due to diffraction and the deeper reef flat causes incident wind waves on the reef flat on the leeward side of the island to be less depth-dominated and more sensitive to energy of waves off the reef. Therefore, while an increase in energy of waves off the reef may only slightly affect incident wind waves on the windward side of the island, it can considerably increase energy of incident wind waves on the leeward side of the island.

Variations of incident wind wave energy also have an influence on the magnitude of infragravity waves, as the magnitude of infragravity waves appears to increase with an increase in incident wind wave energy. Wave analysis in Chapter 5 also shows an increase in infragravity wave energy with depth.

According to these contemporary wave conditions, higher waves, which are required in order to generate the greater magnitude of wave run-up to build the higher island surface in the past, can be attributed primarily to higher sea level. Greater wind speeds can introduce more energy on wave fields on the reef platform when accommodation space on the reef platform increases due to an increase in sea level. This assessment of probable wave conditions also supports the idea that the higher sea level is required for higher island topography, similar to that suggested by McLean et al. (1978) for sand cays on the northern Great Barrier Reef.

The history of sea-level change in Torres Strait is important, but is incompletely known over the period during which the island has evolved. Figure 6.1 shows a compilation of data for the northern Great Barrier Reef (Lewis et al. in preparation).

Figure 6.1. Age-height plot of calibrated radiocarbon dates on coral microatolls from the northern Great Barrier Reef, based primarily on data in Chappell (1983) and Larcombe et al. (1995) (based on Lewis et al. in preparation)

The interpretation of sea level for the northern Great Barrier Reef is based on a dataset of more than 45 microatolls, corals constrained in their upward growth by exposure at low tide. Chappell (1983) considered that the simplest interpretation was that sea level had fallen gradually. This interpretation has been re-assessed by Larcombe et al. (1995) and Baker and Haworth (2000) who have inferred several oscillations of sea level during the past 6000 years (Figure 6.1).

Few data are available on changing relative sea levels for Torres Strait during the Holocene. Barham (2000) used the top of modern and fossil *Porites* spp. microatolls from western Torres Strait as a relative datum and argued that sea level fell from a high of around 1.4 m above MLWS 6,000-5,500 years BP to 0.7 m above MLWS around 4,000 years BP. Similarly, Woodroffe et al. (2000) used microatolls on Hammond, Yam and Warraber Islands to infer that sea level was at least 0.8-1.0 m higher than present 5,800 years BP falling gradually until at least 2,300 years BP. However, the microatolls have not been surveyed in with sufficient precision, nor are there enough

dates to reconstruct the detail of relative sea-level history across the region. It is also likely that there has been hydro-isostatic flexure across the shelf in response to sea-level rise and flooding of the land bridge between Australia and New Guinea (Nakada and Lambeck, 1989), with the implication that relative sea-level history differs between individual reefs as found across much of the Great Barrier Reef (Smithers et al., 2006).

Both Barham (2000) and Woodroffe et al. (2000) propose sea levels were between 0.8-1.4 m higher around 5,500-6,000 BP falling to modern levels within the past 3000 years. The large microatolls on the reef flat at Warraber attest to flourishing coral communities on the top of the Warraber reef platform around 5,000 years ago. There have been considerable changes in reef and associated ecosystems since that time with development of intertidal sand and carbonate mudflats and seagrass communities in western Torres Strait (Barham, 2000), and progradation of the reef and infill of shallow reef flat depressions on the less turbid reef systems (Woodroffe et al., 2000). The geomorphological/resource trends associated with human use of resources in western Torres Strait over the past 3,000 years, have been paralleled by the development of sand cays in central Torres Strait.

According to the relationship between the pattern of topographical variation across Warraber Island and an increase in wave height with depth on Warraber Reef, it can be hypothesised that over the period of island evolution the sea level over this reef area has fallen, possibly in a step-like pattern with at least three time intervals, perhaps 1,500 years ago, between around 1,500 and 500 years ago, and 500 years ago until present.

A prominent feature of the surface topography of Warraber Island, discriminated from the DTM, but otherwise only poorly detectable from the earlier aerial photographs, is a series of beach ridges. Ridges mark out former shorelines on the island and provide

the clearest evidence for progradation to the south and east. The top of several of the beach ridges has aeolian sand deposits indicating incipient dune formation. The origin of beach ridges is poorly understood (Curray, 1996; Tanner, 1996). Even where there have been ongoing surveys over decades, as at Moruya in southeastern Australia, the factors that lead to the formation of a specific ridge and its preservation by the development of successive more seaward ridges remain elusive (McLean and Shen, 2006).

The presence of a thick layer of pumice at a depth of about 20 cm throughout the higher area of Warraber Island (phases 1 and 2 in Figure 2.20) indicates that the development of ridges on Warraber Island has been influenced by wave action (Rasmussen and Hopley, 1996). Beach ridges constructed by wave action and later capped by dunes imply that progradation of the shoreline has been episodic. A number of possible factors could explain this periodicity, including variability associated with ENSO, the sunspot cycles, the lunar nodal cycle, and shorter-term variations in sea level, or some combination of these and other effects (Tanner, 1995).

The depositional history derived from radiocarbon dating, as described in Chapter 2, indicates that Warraber Island has accreted continually over the past 2,700 years or more, and the total volume of sand, as well as the rate of accretion marked by the most prominent ridges, indicates a long-term rate of accumulation of approximately 900 m^3/y. It is important to emphasise that this rate of accumulation has been estimated over the whole period of 2,700 years and is based on phases on radiocarbon dates which have error terms of several decades, and which do not mark the exact time of deposition, but a period of shell production prior to the death and ultimate burial of shell material.

6.3   Seasonal and Decadal Changes in Warraber-Island Shape

6.3.1. Seasonal Change in Island Shape

As indicated in Chapter 4, Warraber Reef and Island have been predominantly dominated by ESE-SE winds between April and November with subordination of W-NNW winds between January and February. As demonstrated in Chapter 5, this wind pattern is a primary control on wave characteristics on the reef. The mean current directions were also found to correspond to the prevailing wind directions, which is prominent during the ESE-SE winds but not evident during the W-NNW winds (Hart, 2003).

It was shown in Chapter 5 that sediment movement was active during normal wave conditions. Sediment transport has been shown to be common during normal wave conditions with the domination of on-reef directions towards the island, both on the eastern and western reef areas (Hart, 2003). Overall rates of sediment transport were higher during the prolonged periods of ESE-SE wind domination than during the short season of W-NNW wind domination. Extensive sediment trap data collected by Hart (2003) has shown that considerable volumes of sediment are mobilised on the reef flat during most tidal cycles, and these preliminary studies emphasised the significance of longshore transport which has been analysed over longer time scales in this study.

Change in island shape in response to the seasonal hydrodynamic influence described above can be observed in vertical aerial photographs acquired over the past four decades and analysed in the present study. Among the aerial photographs available, the change in island shape during the domination of W-NNW winds is clearly seen in the 1974 aerial photograph taken on 26th March, at about the transition period

from the W-NNW wind domination to the E-SSE wind domination (Figure 6.2). This photograph is therefore a good representation of the shape of the island after it has been influenced by W-NNW winds.

Figure 6.2. Georeferenced aerial photograph taken on 26th March 1974, showing the well-developed sand spits on the southwestern and northeastern ends of the island after an influence of W-NNW winds. Locations of RT5 and RT4 are shown in the figure.

In Figure 6.2, it can be seen that spits were well developed at both ends, implying strong driving hydrodynamic forces causing sediments to be transported from the northern side of the island along the beach towards the southern side. The shape of sand spits developed at both ends of the island is in accordance with patterns of sediment transport previously studied by Hart (2003). Sediment transport was dominantly on-shore and alongshore to the south along the shoreline at the southwestern end of the island, whereas sediment transport was dominantly alongshore to the south along the shoreline at the northeastern end of the island (Hart, 2003). At sites on RT4 and RT5

(see locations in Figure 6.2) more sediment movement was also recorded during the W-NNW wind domination than during the ESE-SE wind domination (Hart, 2003).

The 1974 conditions of longshore transport and clearly developed sand spits were probably established under uncommon, but seasonal, wind conditions in which the W-NNW wind effect over the first three months of 1974 was greater than an average and the E-SSE wind effect, which normally exists throughout the year, was absent in the first two months (Table 6.1).

Table 6.1 Difference of the wind effect in 1974 from the mean value (unit=m/s).

	Jan	Feb	Mar	Apr	May	Jun	Jul	Aug	Sep	Oct	Nov	Dec
N	4.6	-4.4	-0.2								3.2	
NNE		-0.1										3.0
NE												
ENE									2.8	8.4	14.3	
E			-11.5	-16.5	-16.2			63.7	56.2	70.5	-9.5	-20.6
ESE			-13.6	-7.7	-3.4	10.7	44.3	-56.2	-3.8	-70.8	-61.3	-12.2
SE			-16.0	16.1	-33.0	-17.5	-4.5	-38.9	-20.2	-25.8	-13.7	-7.9
SSE							-9.4					-2.7
S					2.1		0.1					5.3
SSW												0.8
SW												1.6
WSW		1.5										
W	-0.8	-5.0									0.7	
WNW	27.2	13.1	4.2									-5.5
NW	-5.6	5.9	61.5									-14.2
NNW	33.3	0.9	8.3								8.4	2.5

There is no data on island shape during the ESE-SE wind domination in 1974 for establishing seasonal change in island shape. Nonetheless, patterns of sediment transport from a previous study by Hart (2003) and evidence along the beach identified from the aerial photographs taken during the ESE-SE wind domination but in other years may also be useful. During the ESE-SE wind domination, sediment transport previously measured by Hart (2003) indicated on-shore sediment transport and alongshore sediment transport to the north around the southwestern end of the island. This pattern of sediment movement to the north along the southwestern end of the island is also supported by the degree of exposure of the beachrock area that could be clearly seen during the W-NNW wind domination in 1974 (Figure 6.3a) but was less

during the ESE-SE wind domination in 1981 (Figure 6.3b), and was almost under the sand in 1987 (Figure 6.3c) and 1998 (Figure 6.3d) during the ESE-SE wind domination.

Figure 6.3. Increase in sand accumulation on the west of the island: (a) 1974; (b) 1981; (c) 1987; and (d) 1998.

A decrease in beachrock area along this side of the island also implies the long-term residual deposit of sediments transported to the north along this section of the island. In some years, for example in 1987 (Figure 6.3c) and 2004 (Figure 3.2), the well-developed shape of sand spits, similar to that occurring in 1974 (Figure 6.2) but in an opposite direction, also developed during the ESE-SE wind domination. Therefore, it is apparent that the sand spit on the southwestern end of the island seasonally moves in opposite directions in response to seasonal patterns of sediment transport.

At the northeastern end, records of sediment transport during the ESE-SE winds showed domination of alongshore sediment transport but without dominant directions, moving both to the north and south (Hart, 2003). In addition, Figure 3.2 shows that the

northeastern end of the island has not moved northwards during this season, like that occurring on the southwestern end. However, on the adjacent reef flat sediments transported towards the north during this period were evident on the aerial photograph as a sand bar on which a steep, curved front has developed (Figure 6.4).

Figure 6.4. Development of a sand bar on the northeast of the island: (a) 1974; (b) 1981; (c) 1987; and (d) 1998.

The seasonal transformation of the sand bar was also surveyed in the field by Hart (2003). The sand bar with the steeply sloped face was developed with a prograding rate towards the north of about 1 m per week during the domination of SE winds but during the domination of NW winds, that sort of sand bar had disappeared and the sand was spread out over the reef flat (Hart, 2003). The reshaping of sand bar during the influence of NW winds also implies strong longshore transport towards the south along the northeastern end of the island during the influence of W-NNW winds. In Figure 6.4, the accumulation of a sand bar has appeared clearer since 1987 (Figure 6.4c). This

also implies the long-term residual deposit of sediment transported to the north along the northeast of the island.

6.3.2. Probable Causes of Decadal Changes in Warraber-Island Shoreline over the Past 40 Years

At decadal (engineering) scale, interpretation of aerial photographs in Chapter 3 shows that there is an aggregated movement of sediment on the western and eastern extremities of the island into a pattern in which the spits are reshaped and undergo a clockwise movement. Aerial photographs, except that in 1974, were taken in the same season, between April and November, when winds from the E-SSE sector are dominant. Comparing the island shape during the same season over a long period of time allows the trends of shoreline change, caused by residual sediment transport, to be detected. Therefore, it can be inferred that the movement of the island at both ends in a clockwise direction is the result of long-term influencing factors.

In general, change in island shape responds to patterns of wave convergence and ability of waves to transport sediments (Flood and Heatwole, 1986). Aston (1995) suggested that round islands on near circular reefs and elongate islands on more linear reefs behave differently, reflecting wave focusing. As shown in Chapter 5, waves on Warraber Reef are influenced by local wind patterns. In order to have such a sustained pattern of change in island shape, wind characteristics over the period of 1966-2004 would be expected to follow a trend consistent with that of island change. It should be noted that the medium-term trends of wind effect, analysed in Chapter 4, cover only a period from 1951 to 1992 due to a large gap between 1993 and 1995 (Table A1.2 of Appendix 1). Only preliminary attempts, outlined in Section 6.5, have been made in the

present study to determine patterns of wave convergence on Warraber Reef due to very complex environments including topography on the reef and effect of nearby reefs on wave patterns towards the island. Therefore, in the present study probable causes of that movement at the ends of the island will be discussed based on relative magnitude of wave energy generated by wind from different directions and the medium-term trends of wind effect.

Rasmussen and Hopley (1996) initially reported the changing pattern of Warraber shoreline over a period of 1966-1987 and suggested that an increase in influence in the region of winds from southerly directions, particularly from the SSE, is the cause of this change. The medium-term wind analysis in Chapter 4 (Figure 4.7) showed that winds with an increasing trend of wind effect over a period of 1951-1992 are from the N, SSE, S, SSW and NNW but their effect individually has been very small. The SSE winds give less than 5% of the total wind effect. ESE winds have been dominant all the time, contributing around 40% of the total wind effect, with a subordination of SE and E winds, contributing around 30 and 10% of the total wind effect, respectively. Note that wind effect here refers to a cumulative wind speed.

As demonstrated in Chapter 5, waves affecting Warraber Island include both those generated on and off Warraber Reef. Those waves are primarily driven by regional wind patterns. Therefore, an increase or decrease in wind effect from any direction will modify wave conditions both on and off Warraber Reef. In the case of Warraber Reef, however, a change in wave characteristics, caused by changes in wind pattern, is not straightforward, due to reef shape in relation to directions of wind-generated waves and interference from nearby reefs with the wave field approaching the reef.

It was found in Chapter 5 that incident short-period waves are one of the major wave components on the reef. Their energy depends on water depth on the reef flat,

wind speed, wind duration and fetch. It can be seen in Figure 2.4 that fetch, which can be approximated from the distance between the reef edges and the island, varies in response to wind direction. Fetch is longer for winds from the directions between E and SE. According to the relative magnitude of the wind effect and fetch, therefore, E-SE winds can generate larger incident short-period waves than those generated by winds from other directions.

It is demonstrated in Chapter 5 that incident wind waves on Warraber Reef are driven by waves off the reef. Warraber Reef is the central of three parallel reefs, called Three Sisters (Figure 2.1). It is flanked on the north by Bet Reef and on the south by Poll Reef. Therefore, both Bet and Poll reefs interfere with the wave field moving towards Warraber Reef. The reefs act like an off-shore breakwater creating a shadow zone with smaller wave height due to wave diffraction behind the reefs. Generally, in a shadow zone wave height is smaller at locations further from the ends of a breakwater (CERC, 1984).

Figure 6.5 illustrates water areas where Bet Reef and Warraber Reef interfere with waves moving from the W, WNW, NW, NNW and N, while Figure 6.6 illustrates water areas that are interfered by Poll Reef and Warraber Reef when waves move from the S, SSE, SE, ESE, and E. Shadow zones are shown in white areas in both figures. Only waves from the east to south sector and west to north sector were considered because they are the dominant approach directions.

Bet Reef begins to have an effect on the wave field moving towards Warraber Reef when waves propagate from the NNW (Figure 6.5d) and N (Figure 6.5e) and Poll Reef begins to interfere with the wave field moving towards Warraber Reef when waves are from the S (Figure 6.6a) and SSE (Figure 6.6b). The parts of Warraber Reef that
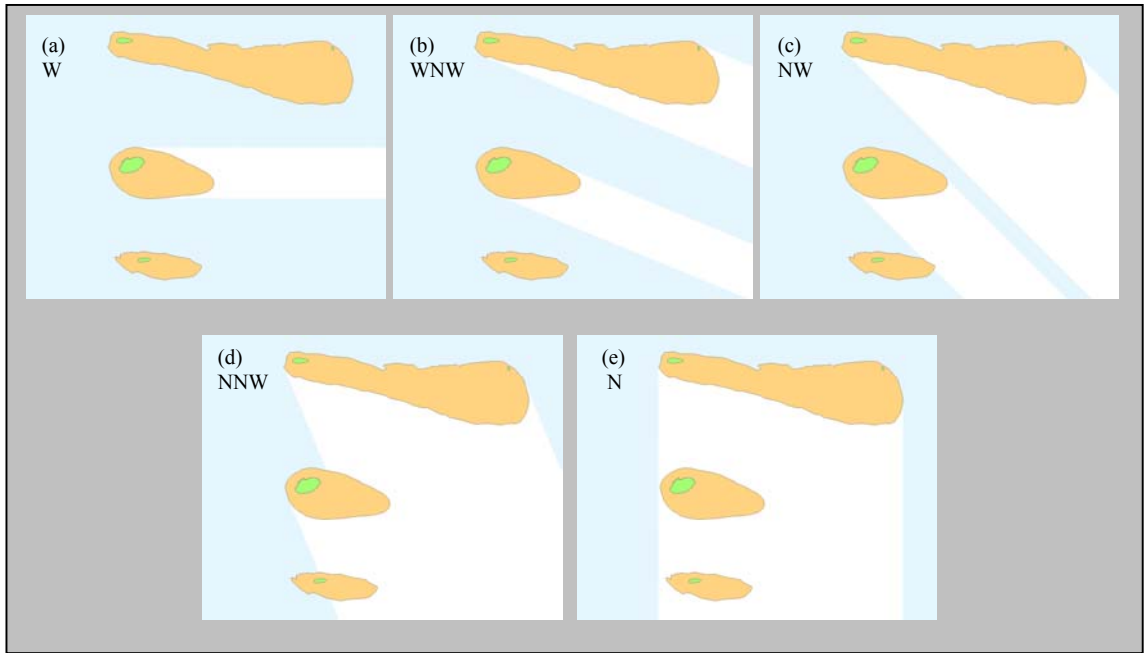
Figure 6.5. The effect of Bet Reef on the wave field moving towards Warraber Reef and the effect of Warraber Reef on the wave field around Warraber Reef. Waves move from: a) W; b) WNW; c) NW; d) NNW; and e) N. White areas indicate shadow zones where wave height is smaller than incident waves due to wave diffraction.
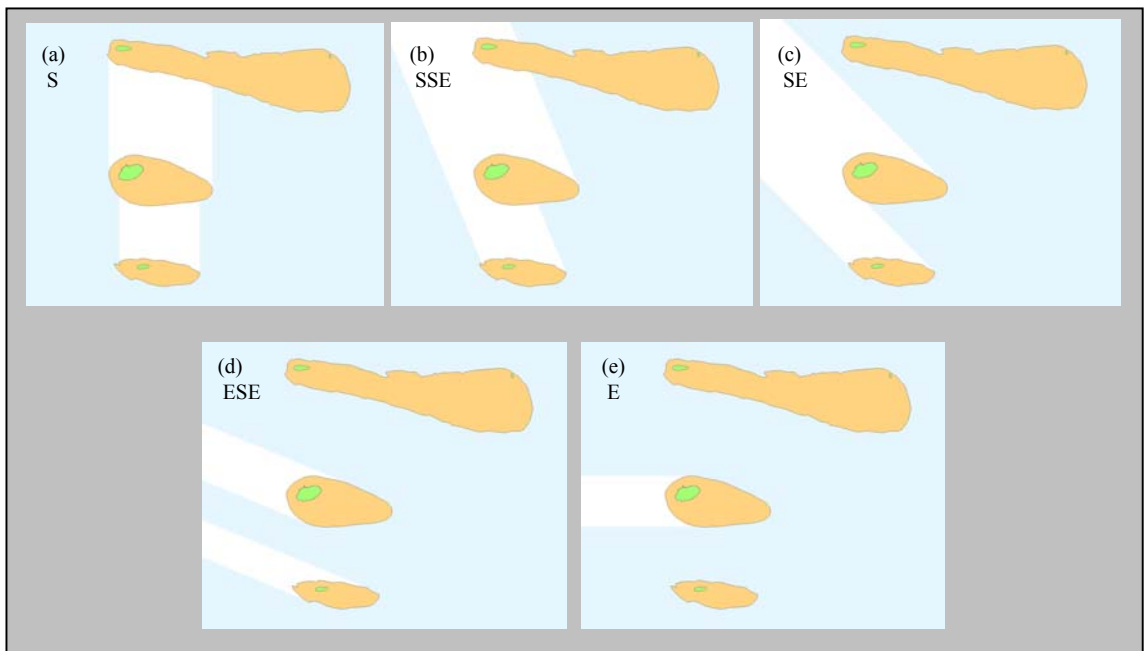
Figure 6.6. The effect of Poll Reef on the wave field moving towards Warraber Reef and the effect of Warraber Reef on the wave field around Warraber Reef. Waves move from: a) S; b) SSE; c) SE; d) ESE; and e) E. White areas indicate shadow zones where wave height is smaller than incident waves due to wave diffraction.

receive full energy from incident waves also vary when an incident wave direction changes (Figure 6.5 and 6.6).

As described above, winds from the N, SSE, S, SSW and NNW seem to be key components in island rotation because they tends to have increased continuously over a period of 1951-92. In Figures 6.5 and 6.6, it appears that Warraber Reef does not receive the full effect of waves generated by winds from the N, SSE, S and NNW due to obstruction by the nearby reefs. It is particularly noteworthy that Warraber Reef is totally within the shadow zone when waves from the N are dominant (Figure 6.5e).

Similarly, the full force of waves from the S can only be felt on the very eastern and western ends of Warraber Reef (Figure 6.6a). Wind-generated waves can be generated in areas between reefs but their height may be small and their period may be short due to the very short fetch. It is likely that waves generated by wind from those directions approach Warraber Reef with reduced height and that they are complex in pattern due to being driven by light and inconsistent winds, and interfered by the nearby reefs. This results in incident wind waves with low energy and complex patterns, having very little influence on the island. Therefore, no clear interaction between waves from those directions and long-term rotation at the ends of the island can be expected.

On the other hand, Warraber Reef is slightly affected by Poll Reef when waves propagate from the SE (Figure 6.6c) and does not experience any effect by the nearby reefs on the wave field approaching from ESE (Figure 6.6d) and E (Figure 6.6e). The ESE wind has been the most significant wind component in the region. Its medium-term pattern indicates a periodic cycle with a minimum between 1963-77 and increasing after that (Figure 4.7b). The SE wind is the second most significant in wind effect but has slightly fluctuated about 30% of the total wind effect (Figure 4.7b). The E wind is

the third most significant in wind effect and has exhibited an opposite cycle to that of the ESE wind (Figure 4.7b).

The medium-term trends of E and ESE winds appear to have been consistent with the patterns of island change. In addition, they can generate both larger incident short-period waves, described above, and incident wind waves on the reef. A combined effect of wind from these two directions may be enough to shift the main wave direction and to have had an effect on Warraber Island during past 40 years. According to trends of wind effect and relative wave energy, therefore, the movement in a clockwise direction at the ends of Warraber Island during the past 40 years has been more likely influenced by a combined effect of E and ESE winds than southerly winds as suggested by Rasmussen and Hopley (1996).

In addition to the influence of environments, such change in island shape can also be influenced by human activities. The most obvious ones on Warraber Island are the boat harbour and channel on the northwestern reef, and seawall along the north shore. In general, these structures could have an effect on island morphology in terms of interference and interruption of waves and sediment transport along the shore of the island (Hopley, 1982; 1990). However, on Warraber Reef they probably have exerted minimal effect on the clockwise movement occurring at the ends of the island during the past 40 years because they were constructed in 1991 and patterns of change are clearly detectable before that date. In addition, this part of the reef is normally subject to much less wave action and sediment transportation due to being on the leeward side of the island during the long period of the ESE-SE wind domination.

During the W-NNW wind domination when this area is on the windward side wave activities and sediment transportation on the western reef flat are generally low (Hart, 2003). This is reflected in sediment texture in this area which contains more fine

sediment than other parts of the reef. Hart (2003) indicated that the boat channel is a minor sink for the finest fractions of sediment on the reef platform and is not a source of reef-flat or island-beach sediment. The major sources of island sediment are on the eastern reef flat (zones 1 and 2 in Figure 1.8) (Hart, 2003). Therefore, it is inferred that the sustained pattern of movement at the ends of the island over the past 40 years has been primarily influenced by environmental conditions.

This inference is also supported by evidence on uninhabited vegetated sand cays on Bet and Poll Reefs. Natural patterns of erosion were observed on Bet and Poll Islands during fieldwork in 2004. Extensive areas of beachrock were found on the northern side of these two islands, similar to those on the northern of Warraber Island. Along the northern side of Poll Island, beachrock outcrops at a clear angle with the present shoreline. Beaches on the southern side of these two islands are smooth and straight with beachrock along some parts of the beaches, similar to that on southern Warraber Island. Extensive beachrock is also found towards the southwestern ends of Bet and Poll Islands, perpendicular to the present shoreline. The location of these outcrops of beachrock is similar to that found on Warraber Island. The occurrence of beachrock at the southwestern ends of Bet and Poll Islands suggests that a clockwise movement of the western ends has also occurred on these two islands. Therefore, the extensive beachrock on the southwest and erosion on the north of Bet and Poll Island are evidence to suggest that environmental factors are the main causes of shoreline changes to the reef islands in this region.

At present, the southwestern shore of Warraber Island is undergoing substantial erosion in association with the movement of the island in a clockwise direction (Figure 6.7). In Figure 6.7, the erosion is clearly indicated by scarps and undercut and

threatened Wongai trees along the shore. This is of considerable concern to people on

the island as the erosion occurs close to the water storage facility.

Figure 6.7. Photograph taken during 2004 fieldwork, showing erosion occurring: a) along the southwestern shore of Warraber Island; and b) at mature Wongi tree along the southwestern shore with waste material at its base to prevent further erosion.

6.4   Implications for Probable Future Conditions on Warraber Island

There has been controversy as to the extent to which reef islands will be threatened by anticipated sea-level rise and global climate change in the next 50-100 years. A study concerning reef-island stability under a rise in sea level by Roy and Connell (1991) suggested that more frequent storms and higher sea level are expected to generate severe erosion on reef islands, causing a reduction in island size and in turn reducing fresh groundwater reserves.

In contrast, Hopley (1992) suggested that over the next 100 years under the influence of anticipated sea-level rise, many reef islands are likely to increase in size as a result of an increase in carbonate production, with more sediments presently abundant on the reef flats able to be transported towards islands. Kench et al. (2005) studying evolution of atoll islands in the Maldives have indicated that sand cays have more resilient morphology than generally recognised, which may add to their ability to resist in the face of anticipated rise in sea level.

As described in Chapter 1, in general development and stability of sand cays is influenced by sediment availability and wave capacity for transporting sediments available on the reef flat to a focusing point (Hopley, 1982; Flood and Heatwole, 1986). At present, the reef flat around Warraber Reef, particularly on the east of the island, is extensively overlain by sediment which is up to 20 cm thick in some areas (Hart, 2003). According to dating analysis shown in Chapter 2, these sediments include those components that are newly produced on the reef flat and those components that have been reworked and redeposited on the reef flat over a period of time. In general, predicted rates of sediment production on reefs are estimated based on predicted rates of carbonate production on the reefs (Kench and Cowell, 2000). That estimation is

generally suitable for reefs on which sediment composition is dominated by coral. In the case of Warraber Reef, sediment composition is dominated by shells and is more related to the cover and distribution of living organisms than rates of carbonate production (Hart and Kench, 2006). Although rates of sediment production on Warraber Reef under a rise in sea level are unknown, over the next century at least there will be supply of sediment, presently lying on the reef flat, to Warraber Island.

Some studies suggested that an increase in wave energy due to deeper water over the reef can generate greater erosion, for example on reef islands on atolls (Yamano, 2000) and beaches behind fringing reefs (Sheppard et al., 2005). However, on large reef platforms such as Warraber Reef the ability of waves to transport sediments to sand cays is of far more concern than the effect of waves on erosion (Hopley, 1982; Gourlay, 1988; Hopley, 1992). According to wave analysis in Chapter 5, while incident wind wave components are attenuated across the reef flat, wave capacity for entraining sediments is augmented by development of incident short-period wave components across the reef flat and an increase in infragravity wave energy in the nearshore towards the island. These waves are depth-dominated; their energy increases with an increase in water depth and more sediment movement can be initiated during higher water depth on the reef flat.

Hart, in her study of sediment transport, also indicated that sediment transport under normal wave conditions on Warraber Reef is active, mainly towards the island, and that the island beach sediments are supplied by the adjacent reef flat, particularly on the east of the island (Hart, 2003). Therefore, under a rise in sea level in the next century the duration and capacity of waves to entrain and transport sediments towards the island will tend to increase, a condition similar to that suggested by Hopley (1992) for sand cays on the Great Barrier Reef.

An increase in wave height on the reef flat due to sea-level rise will increase the magnitude of wave run-up as well. This means that sediments can be transported to a higher level on the island and island elevation is likely to increase as a result of higher sea level. Therefore, an increase in sea level in the future appears likely to increase island size and elevation.

However, it should be noted that locations of a focusing point could be shifted as a result of sea-level change on any reef platforms. The locations of a focusing point on reef platforms is basically related to the magnitude of wave refraction which depends on reef morphology, wave period, and water depth both on and off reefs. The variation in the magnitude of wave refraction due to water depth (Table 6.2) and wave period (Table 6.3) can also be depicted using Snell's law applied to linear waves.

Table 6.2 Variations of wave refraction due to variations of water depth. The magnitude of wave refraction is indicated by the angle between the crest of waves on the reef and the bottom contour ($\theta_{\text{on-reef}}$). $\theta_{\text{on-reef}}$ is smaller for more refracted waves. The magnitude of wave refraction increases with a decrease of water depth.

T=10 s		$\theta_{\text{off-reef}} = 20^{\circ}$
Depth (m)		$\theta_{\text{on-reef}}$
Off-reef	On-reef	
10.5	0.5	4.6
11.0	1.0	6.4
11.5	1.5	7.6
12.0	2.0	8.6

Table 6.3 Variations of wave refraction due to variations of wave period. The magnitude of wave refraction is indicated by the angle between the crest of waves on the reef and the bottom contour ($\theta_{\text{on-reef}}$). $\theta_{\text{on-reef}}$ is smaller for more refracted waves. The magnitude of wave refraction increases with an increase in wave period.

h on reef = 2 m	h off reef = 12 m	$\theta_{\text{off-reef}} = 20^{\circ}$
T (s)		$\theta_{\text{on-reef}}$
3		16.0
6		10.0
12		8.4
20		8.2

In Table 6.2, it assumes that 10-s waves move onto a reef with a vertical front and wave refraction was calculated for water depths on the reef of 0.5, 1.0, 1.5 and 2.0 m, where water depth off the reef is 10 m deeper than water depth on the reef. In Table

6.3, water depth is held constant at 2 m on the reef and wave refraction was calculated for waves with a period of 3, 5, 8, and 12 s. In both cases, the angle between the crest of waves off the reef and the bottom contour ($\theta_{\text{off-reef}}$) is held constant at 20°.

It can be seen from Table 6.2 that an increase in water depth decreases the magnitude of wave refraction and consequently causes the relocation of the focusing point of waves on the reef. The results in Table 6.3 also suggest that incident wind wave components that are driven by waves off the reef moving across the reef front are the wave components that influence the focusing point on the reef platform due to their longer wave period and moving across more variable water depth. Incident short-period wave components may enhance sediment movement on the reef flat, as their energy increases along fetch. However, they contribute little to the development of the focusing point on the reef because they are generated on the reef flat and their propagation is principally dependent on wind direction. This is evident from wave spectra on the windward side of the island, especially close to the island, in which incident wind wave components are prominent but incident short-period wave components are absent. Infragravity wave components do not contribute to the development of the focusing point due to their significance only in the vicinity of the island.

Therefore, it is possible that the focusing point on Warraber reef platform will shift towards the leeward reef rim, if sea level is higher. This shift in the focusing point will induce sediment to be transported along the island beaches towards the leeward end of the island. Although available sediment may have been provided to the island, resulting in an increase in island size, change in island shape can be expected to occur due to adjustment of the island to changes in the focusing point. Even if sea level remains relatively unchanged in the near future, the island is still likely to be affected by

change in the dominant direction of waves on the reef, attributed to change in wind directions. As suggested in Section 6.3, change in the shape of Warraber Island over the past 40 years reflects that natural effect.

Understanding of this dynamic pattern of sand cays in response to environmental conditions is very important for better management of sand cays. Permanent concrete structures are not appropriate to control the adjustment of the island beach, especially on the windward side during the ESE winds on Warraber Island because they will permanently interrupt natural processes of continual exchange of sediment between the reef flat and the island, and sediment transport along the island, resulting in permanent loss of adaptive capacity of the island to environmental conditions. If it is necessary to adopt measures to remedy the erosion problems that presently occur on the beach area, for example along the southwestern end of the island, then soft measures, such as groins of sand bags, are preferable to seawalls because of lower cost and an ability to remove them if no longer required.

6.5   Wave Models and Wave Focusing Studies on Reef Platforms

As described above, sand-cay morphology has continually adjusted to new equilibria, particularly in response to relocation of the focusing point on the reef platform. Refraction diagrams using linear wave theory were constructed by Gourlay (1990) to examine the shift in a focusing point due to changes in dominant wave direction.

Another approach that can simulate a shift in a focusing point more efficiently and accurately is by using wave models. Wave models have been applied in order to examine patterns of wave refraction in some reef areas (Rakha and Abul-Azm, 2000),

but application of wave models to simulate wave focusing on a reef platform has proved difficult.

In this section, it is intended to consider the selection and application of wave models for wave focusing on reef platforms, which might provide the basis for further research in this field. The wave models that were selected for this study are REF/DIF and FUNWAVE, both developed and freely distributed by University of Delaware, USA. An attempt has also been made in this study to undertake preliminary modelling, but more detailed modelling is beyond the scope of this study.

The REF/DIF version that was used in this study is REF/DIF1 version 2.5. It is the weakly nonlinear combined refraction and diffraction model which describes the transformation of wave height and direction as a result of processes including shoaling, refraction, energy dissipation and diffraction (Kirby and Dalrymple, 1994). The model has been developed based on a parabolic approximation of the elliptic mild-slope equation and can correctly predict wave characteristics over irregular bathymetry and around islands that were previously unable to be predicted using ray tracing techniques. It also includes the capability to model wave conditions where currents and bottom friction are present. In the model, wave transformation after breaking is simulated using a model developed by Dally et al. (1985), which was recommended to calculate wave attenuation over reefs (CERC, 1993). Reflected waves are not simulated in this model due to its being developed in parabolic form.

There are some constraints in using this wave model to simulate wave focusing on reef platforms. The first is that the model was developed based on the mild-slope equation; it gives good results for slope up to 1:3 but can qualitatively correctly predict the wave field for steeper slopes. The second is the limited areas of wave equation used in the model. The model uses Stokes wave theory which is valid in deep water. The

model has been extended to predict waves in shallow water by using the Stoke-to-Hedge nonlinear model which describes waves as a solitary wave in shallow water and as Stokes waves in deeper water. The important constraint is the angle of wave direction. The model is restricted to a narrow window of wave direction around the principle direction due to being developed in parabolic form. The angle of propagation around the principle propagation direction is depicted in Figure 6.8.
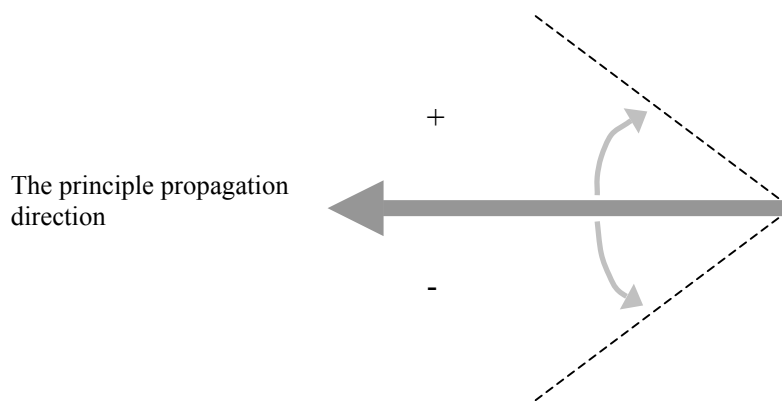
Figure 6.8. Schematic diagram of the angle of propagation around the principle propagation direction.

The model has been developed to simulate the angle of propagation up to ±90 deg (Kirby, 1986). However, an increase in the angle of propagation also increases errors for small angles and the angle of propagation of ±70 deg is the upper limit, a value within which errors for small angles are still small (Kirby, 1986). In order to obtain a focusing point on a reef platform, wave models must allow wave propagation in all directions (360^0). This is a limitation of this wave model to simulate the focusing point on platform reefs.

Preliminary results of this model are given in Figure 6.9 for a maximum angle of propagation of ±40 deg (Figure 6.9a), ±70 deg (Figure 6.9b) and ±90 deg (Figure 6.9c). Bathymetric data in the model is a DTM of a simple circular reef platform with horizontal surface constructed using ArcGIS. FORTRAN programs were developed to
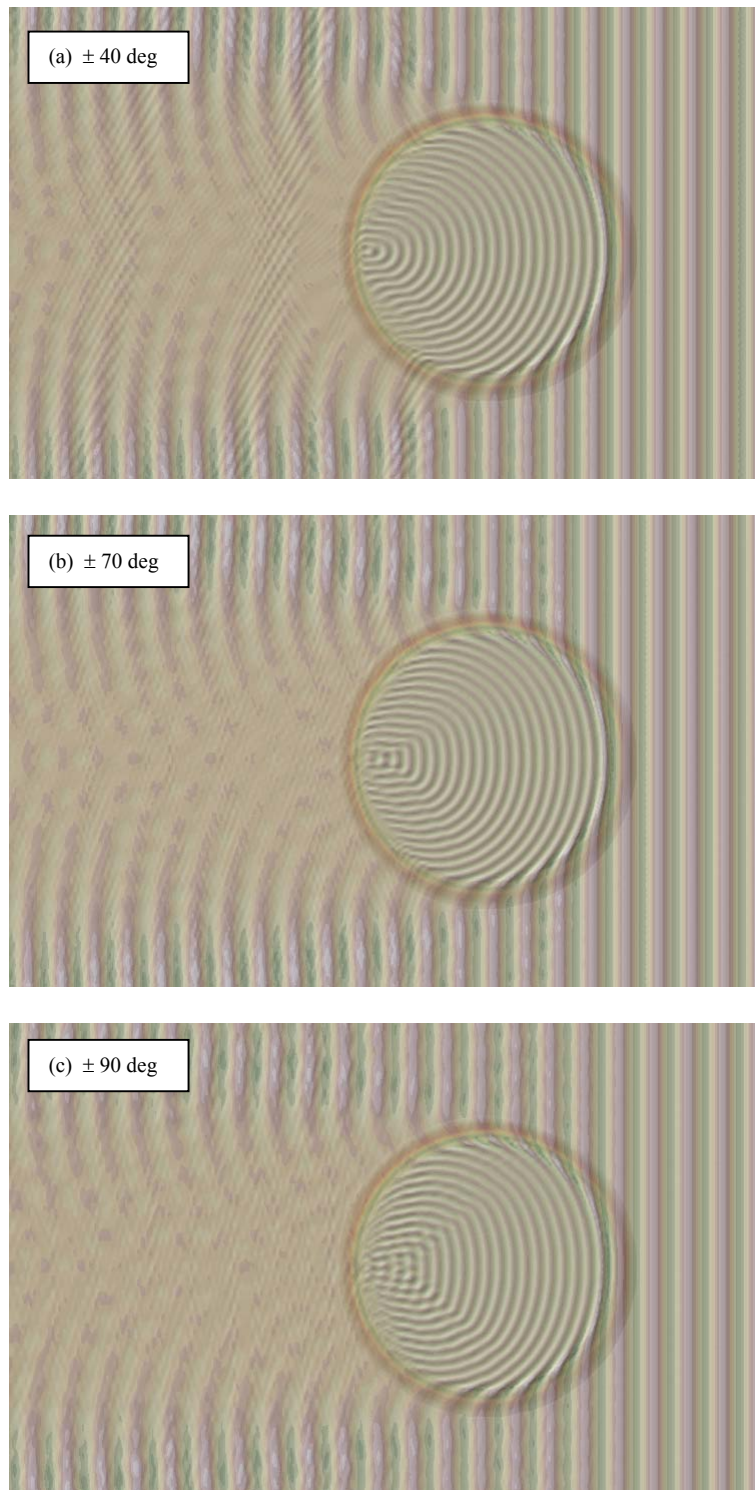
Figure 6.9. Wave focusing patterns on a circular reef using REF/DIF and a maximum angle of propagation of (a) ±40 deg, (b) ±70 deg and (c) ±90 deg. Waves move from right to left.

transform the output from ArcGIS (shapefile) to be in a format for the model and transform outputs from the model to be in a shapfile format in order that the results can be displayed in ArcGIS. Wave height and period is 1 m and 6 s, respectively. Water depth on the reef is 1 m.

Figure 6.9 shows that the model appears to fail to simulate wave refraction around the leeward end of the reef due to the limit of the angle of propagation. As the maximum angle increases, the shape of the focusing point is distorted, being too square (Figure 6.9b and c).

Another wave model examined in this study is FUNWAVE 2 version 1.0.1. FUNWAVE is a fully nonlinear wave model and has been developed based on a Boussinesq equation to study wave propagation in two horizontal dimensions (Wei et al., 1995). Basically, the model simulates temporal and spatial water surface elevations, and spatial velocity components. It was originally based on the shallow water equations and has been extended to include the lowest order of frequency dispersion up to the boundary between deepwater and intermediate water (kh=1 or h/L=0.5). In this model, surf zone hydrodynamics are simulated by introducing an eddy viscosity term into the equations and wave run-up on the beach is modelled using permeable-seabed techniques. Sub- and super- harmonic waves that are generated during wave transformation can be simulated in the model. This model has no restriction on the angle of propagation; waves can propagate in all directions (360^0) (Kirby et al., 1998). Therefore, models of this type have the potential to simulate a focusing point on platform reefs.

However, there are further constraints in applying this model. There are a lot of parameters to be set up before running. Therefore, it is not easy to operate but easily collapses before finishing a run, due to inappropriateness of parameter settings. It is not

user-friendly. The model is designed to be operated in LINUX and its outputs are all in a binary format. Importantly, it requires great computational time and generates large output files, especially for a large area of study. It was found in the present study that this time-consuming computation and large output files limit the model to be applied for the actual scale of the Warraber reef platform.

Computational time depends primarily on time step size which is determined by grid size (Kirby et al., 1998). Time step size must be less than half of grid size. Values of grid size are estimated based on the shortest wavelength that would be likely to be detected on the shallowest area. It is required in the model that wavelength must be equal to or greater than two times of water depth and that grid size must be smaller than half wavelength. For example, for simulating waves with period of 6 s moving in water depth of 0.5 m, grid size must be smaller than 6 m in order that 6-s waves can be detected in 0.5-m water depth. However, a decrease in grid size increases accuracy of results; grid size of up to ten times smaller than wavelength is common in practice (Kirby et al., 1998).

Therefore, a smaller scale of Warraber Reef was used for this purpose. A simple DTM of Warraber Reef was created using ArcGIS. The model size of the reef was reduced to 400 m long and 200 m wide. It was found in this study that the model collapsed before generating outputs for very steep reef-fronts. The DTM with 10-m height, horizontal reef top and a reef-front slope of 1/5 was used in this modelling. The resolution of the reef model is 1 m and the whole running area is 900 m x 600 m. In order to increase the magnitude of wave refraction on the reef platform, longer waves and shallow water on the reef were applied. Wave period is 6 s and water depth on the reef is approximately 0.5 m. A small wave height of 0.1 m was used in this modelling to prevent the running instability.

Similarly, FORTRAN programs were written to convert a shapefile of the reef model to be an input for FUNWAVE and to convert binary outputs of spatial water surface elevation from FUNWAVE to be able to be displayed in ArcGIS. In this study, supercomputer facilities at the Australian Centre for Advanced Computing and Communications (ac3) were used to run this model. A preliminary result is shown in Figure 6.10.
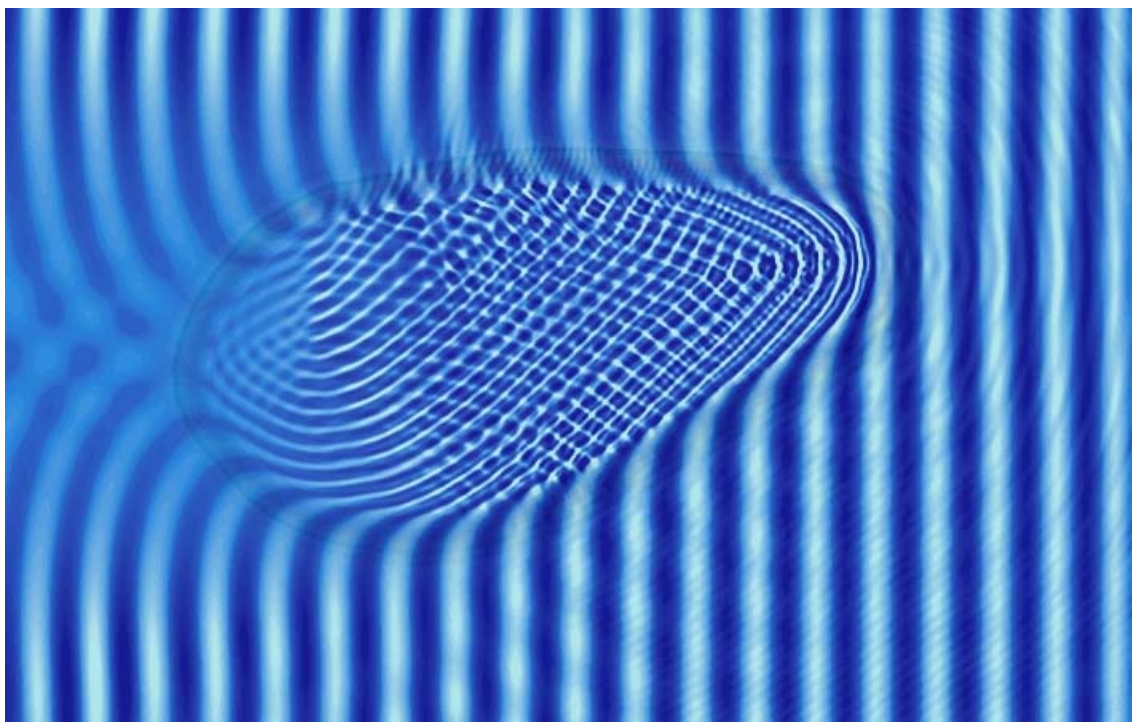
Figure 6.10. Simulation of wave transformation on a reef model using FUNWAVE. Waves move from right to left

As described above, this wave model can simulate waves moving in all directions. Wave refraction around the reef rim, especially at the leeward end, is clear. Water surface elevations shown in Figure 6.10 look complex due to the presence of super-harmonic components of incident waves. This model shows potential in simulating waves focusing but it is only practical at present for a small reef platform. In the near

future, the problems of time-consuming and large output files may be minimised due to rapid advance in computer technology.

However, hydrodynamic processes, and sediment entrainment and transport over reefs are complex and incompletely known. In addition, it has been shown in Chapter 2 that there is presently insufficient survey data to accurately construct at DTM of the reef flat surface. Thus there are presently many constraints to apply such models to investigate waves and related processes on reefs.

CHAPTER 7

CONCLUSIONS

7.1 Introduction

The present study has been undertaken in order to examine: i) the morphological evolution of a small sand cay over past millennia (geological time scale); ii) changes in its shore over past decades (engineering time scale); and iii) contemporary characteristics of waves, particularly around the island. The principal conclusions are summarised in this chapter together with areas where further research can extend these results.

7.2 Morphological Evolution of Warraber Island over Geological and Engineering Time Scales

Warraber Island is a small, vegetated sand cay that has formed at the leeward end of the Warraber reef platform. The platform is built on an older Pleistocene substrate, that is at least 6 m below the surface of the reef; the majority of the reef flat probably reached its present level by 5,000 years ago when the sea level was slightly higher. The island is approximately 1,500 m long by 920 m wide; it has a surface area of approximately 814,000 m^2 and comprises a volume of sand of approximately 2,700,000 m^3.

The broad pattern of geological evolution of island morphology was examined based on a digital terrain model (DTM) and the outlines of prominent beach ridges, that can be detected from it, indicating episodes of island development. Temporal trends of

island evolution were assessed based on radiocarbon dating, both on bulk samples and on individual sand grains of coral, molluscs and foraminifera selected from the bulk samples.

This study showed that caution must be exercised in determining temporal patterns of sand-cay evolution using radiocarbon dating of carbonate sediment samples. In this reef setting bulk dates are unreliable to determine depositional chronology of the island due to the mixed composition of sediments with a wide range of ages on the reef flat. Among the selected individual sediment components, gastropod shells are the most appropriate component to indicate temporal development of island morphology, consistently yielding the youngest ages within the same deposit. Shells are especially suitable in view of the closeness of sediment-contributing organism habitats to the island, transportability and durability. Dates on shell significantly revise the chronological evolution of Warraber Island from an interpretation of rapid accretion for 1,000 years followed by negligible addition of sediment since 2,000 years ago, based on bulk ages, to continual accumulation over the past 3,000 years.

Combining topographic data from the island DTM, associated sediment volume and radiocarbon ages of gastropod shells, the island is inferred to have begun to form at the northwestern corner by approximately 2,700 years ago. Subsequently, it has gradually accreted and gained the volume of approximately 2,700,000 m^3 in 1998. The island has grown with a long-term rate of sediment accumulation of approximately 900 m^3/y. During the first 1,000 years, the island topography had an average elevation of around 6 m and decreased to around 5 m thereafter and lowered to slightly less than 5 m by 500 years ago in association with the development of the southwestern and northeastern ends.

The examination of island morphology over decadal (engineering) time scale focused on changes to the island shoreline over the past 40 years (1966-2004), based mainly on a series of aerial photographs and topographical surveys of beach areas. A comparison of island shoreline indicated that significant change of the island has occurred only on the southwestern and northeastern ends associated with sand spits that appear to have rotated in a clockwise direction.

Volumetric analysis indicated that over the period 1966-2004 the island has accreted on the northeastern end and eroded on the southwestern end. Excluding 1996 data due to accuracy constraints, approximately 14,000 m^3 (or approximately 500 m^3/y) has been accumulated on the northeastern end and approximately 6,000 m^3 (or approximately 200 m^3/y) of the sediment has been eroded from the southwestern end of the island. Reconstruction of shoreline position reveals variation of island shape and volume over a time scale shorter than that recovered from radiocarbon dating, and reveals a pattern of rotation and reworking that implies that environmental factors, such as wind and wave direction might be an important control.

7.3   Contemporary Conditions and Their Implications for Morphological Changes

7.3.1   Wind Characteristics in Torres Strait

Over the past 40 years, this region has been primarily dominated by winds from the E-SSE sector (80% of wind effect) and secondarily influenced by winds from the W-NNW sector (15% of wind effect). The E-SSE winds, especially ESE and SE winds, are persistent and very prominent between April and November whereas winds from the

W-NNW sector are variable with rare, high speeds between January and February. The transition periods occur in December and March when calm periods are dominant.

Vector analysis showed that the yearly resultant wind directions have been most of the time from the ESE and the resultant wind effect appears to have varied in a periodic pattern. The time of the low magnitude of yearly total wind effect was found to be in agreement with that of the initiation of the approximate 22-year cycle of solar magnetic activity, but the significance of this correlation, and the relationships between the wind characteristics and ENSO are not clear.

7.3.2   Wave Conditions on Warraber Reef

Analysis of wave spectra close to the windward reef rim suggested that wave environments off Warraber Reef are dominated by sea not swell. However, wave analysis around the island showed that development and stability of the island are influenced by both wave components generated off the reef (incident wind wave components) and those generated on the reef (incident short-period wave and infragravity wave components).

The magnitude of these three components spatially varies around the island. During the low wave-energy events, incident short-period wave components are dominant, especially on the windward side of the island. During high wave-energy events, all three components are evident, especially at the windward side, whereas incident short-period wave components are small to absent on spectra at the leeward side. As a result of these combinations, waves on the windward side are generally larger and shorter than those on the leeward side. Also, during high wave-energy events, spatial variations of wave characteristics across the nearshore towards the island

are obvious; wave period increases towards the island, especially more evident on the leeward side, whereas wave height changes slightly towards the island on the windward side but decreases towards the island on the leeward side.

The relationship between wind characteristics during a field experiment and characteristics of wind climate in the region suggested that wave conditions during the experiment represent the wave climate during the period between April and November when ESE and SE winds are dominant. Wind climate in the region and the field studies by Hart (2003) also suggested that a significantly different wave climate occurs during the period between January and February when W-NNW winds are prominent and waves are more duration-limited with smaller height and shorter period.

This study provides several insights into wave action and its effect on reef platforms, particularly in relation to sand-cay development and stability. It has been demonstrated that energy of waves forced across the reef crest (incident wind waves) decreases towards the island. However, waves on the reef do not lose their capacity for initiating sediment movement due to the generation of incident short-period wave and infragravity wave components on the reef flat, with their energy increasing towards the island. This interplay between waves from off the reef and those generated on the reef requires further investigation, as the balance is presumably highly reef specific.

Analysis of sediment entrainment showed that wave conditions both on the reef flat close to the reef edge and around the island are capable of initiating sediment movement but with different magnitude. On the reef flat close to the reef edge, waves are capable of entraining most of the sediments (settling velocities less than –5 Psi) during high wave-energy events. Around the island, during high wave-energy events waves in the nearshore on the windward side can entrain most of sediments and the highest capability of wave entrainment occurs on the island beach. On the leeward side

234

of the island only slow settling velocities (less than −2 Psi) can be mobilised in the nearshore whereas faster setting velocities can be entrained on the beach. The threshold of sediment movement generally depends on water depth over the reef, induced by tides.

7.3.3   Implications for Morphological Evolution

The wave climate around the island depends primarily on water depth.   It is inferred that during past millennia wave height on the reef was greater in order to generate higher wave run-up required for creating the higher elevation that is indicated by the topography of the oldest part of the island. This depth-constrained condition and topographical variation of the island also suggests that over the period of island evolution sea level probably has fallen in a step-like pattern with at least three time intervals, identifiable: i) time of island formation-around 1,500 years ago; ii) around 1,500-around 500 years ago; and iii) 500 years ago until present.

Erosion and deposition occur at various points around the island. Whereas decadal change in island shape indicates a sustained rotation in a clockwise direction, reversing trends, particularly at the southwestern end of the island, occur in response to seasonal hydrodynamic conditions. Decadal changes in island shoreline over the past 40 years were found to be primarily influenced by environmental factors. Trends of wind patterns and effect of nearby reefs on wave fields moving towards the island suggested that a combination of wind effect from ESE and E is probably the main cause of change over the past 40 years.

Geological evolution of island morphology, decadal changes in the island shoreline and contemporary conditions of sedimentation, wind and waves on the reef

suggested that future change in island shape is inevitable. The fact that sea level was higher in the past implies that the island will persist if there is only a slight rise in sea level in future. A shift in the focusing point on the reef is a likely response to anticipated sea-level rise over the next century. The pattern of gradual accumulation over past millennia suggests that in future, Warraber Island may increase in size due to availability of sediment, and its supply, enhanced by the higher capacity of waves for entraining and transporting sediment towards the island.

This natural pattern of accretion presumes that human activities do not adversely effect either the production of sediment on the reef (for example decreasing calcification under eutrophic conditions) or the pathway of sediment transport along the island shoreline (for example through construction of seawalls).

Preliminary modelling of wave focusing on platform reefs has been undertaken. It indicates that wave focusing does occur on broad reef platforms and the field observations confirm this tendency for waves to focus sediment on the lee of the platform and form a sand cay. However, at present it is only practical for a small reef platform due to computing ability.

REFERENCES

Ali, M., 1997. Seasonal morpho-sediment changes on islands of Maldives and implications with sea level rise, Proceedings of the 3rd SPREP Meeting on Climate Change and Sea Level Rise in the Pacific, Noumea, pp. 1-13.

Amin, M., 1978. Statistical-Analysis of Storm Surges in Torres Strait. Australian Journal of Marine and Freshwater Research, 29: 479-496.

Andrews, B.D., Gares, P.A. and Colby, J.D., 2002. Techniques for GIS modeling of coastal dunes. Geomorphology, 48: 289-308.

Aston, J., 1995. The relative mobilities of coral cays on the Great Barrier Reef can be modeled. Unpublished MS Thesis, James Cook University, Australia, 267 pp.

AUSGEOnews, 2004. Shifting sands the clue to vanishing seagrasses, Issue no. 75, pp. 32-34.

Baines, G.B.K. and McLean, R.F., 1976. Resurveys of 1972 hurricane rampart on Funafuti atoll. Search, 7: 36-37.

Baker, R.G.V. and Haworth, R.J., 2000. Smooth or oscillating late Holocene sea-level curve? Evidence from the palaeo-zoology of fixed biological indicators in east Australia and beyond. Marine Geology, 163: 367-386.

Barham, A.J., 2000. Late Holocene maritime societies in the Torres Strait Islands, northern Australia-cultural arrival or cultural emergence? In: S. O'Connor and P. Veth (Editors), East of Wallace's line: studies of past and present maritime cultures of the Indo-Pacific region. A.A.Balkema, Rotterdam.

Barham, A.J. and Harris, D.R., 1983. Prehistory and palaeoecology of Torres Strait. In: P.M. Masters and N.C. Fleming (Editors), Quaternary coastlines and marine archaeology: towards the prehistory of land bridges and continental shelves. Academic Press, London, pp. 529-557.

Bauer, B.O., 1990. Assessing the relative energetics of infragravity motions in lakes and seas. Journal of Coastal Research, 6: 853-865.

Bayliss-Smith, T.P., 1988. The role of Hurricanes in the development of reef islands, Ontong Java Atoll, Solomon-Islands. Geographical Journal, 154: 377-391.

Bendat, J.S. and Piersol, A.G., 1986. Random data: analysis and measurement procedures. John Wiley & Sons, Inc., Canada, 566 pp.

Bishop, C.T. and Donelan, M.A., 1987. Measuring waves with pressure transducers. Coastal Engineering, 11: 309-328.

Bode, L. and Mason, L., 1995. Tidal modelling in Torres Strait and the Gulf of Papua. In: J.H. Choat, N.K. Saxena and O. Bellwood (Editors), Recent advances in

marine science and technology'94. PACON International and James Cook University of North Queensland, Townsville, pp. 55-65.

BOM, 2004. Wind data at Thursday Island and Horn Island. Queensland Branch, Bureau of Meteorology.

BOM, 2005. S.O.I. Archives - 1876 to present. http://www.bom.gov.au.

Booth, B., Shaner, J., Crosier, S., Sanchez, P. and MacDonald, A., 2002. Editing in ArcMAP. Environmental Systems Research Institute, Redlands, USA, 462 pp.

Borse, G.J., 1991. FORTRAN 77 and numerical methods for engineers. PWS-KENT Pub. Co., Boston, 722 pp.

Brander, R.W., Kench, P.S. and Hart, D., 2004. Spatial and temporal variation in wave characteristics across a reef platform, Warraber Island, Torres Strait, Australia. Marine Geology, 207: 169-184.

Bratt, S. and Booth, B., 2002. Using ArcGIS 3D Analyst. Environmental Systems Research Institute, Redlands, USA, 268 pp.

Burrough, P.A. and McDonnell, R.A., 1998. Principles of Geographical Information Systems. Spatial Information Systems. Oxford University Press Inc., New York, 333 pp.

Burroughs, W.J., 2001. Climate change: a multidisciplinary approach. Cambridge University Press, Cambridge, 298 pp.

Byrne, R.J., 1969. Field occurrences of induced multiple gravity waves. Journal of Geophysical Research, 74: 2590-2596.

Carrara, A., Bitelli, G. and Carla, R., 1997. Comparison of techniques for generating digital terrain models from contour lines. International Journal of Geographical Information Science, 11: 451-473.

Caruso, C. and Quarta, F., 1998. Interpolation methods comparison. Computers & Mathematics with Applications, 35: 109-126.

CERC, 1984. Shore Protection Manual v.1, U.S. Army Coastal Engineering Research Center, Vicksburg.

CERC, 1993. Wave attenuation over reefs. CETN I-56, U S Army Engineer Waterways Experiment Station, Vicksburg.

Chakrabarti, S.K., 1987. Hydrodynamics of offshore structures. Springer-Verlag Berlin, Heidelberg, 440 pp.

Chappell, J., 1983. Evidence for smoothly falling sea-level relative to north Queensland, Australia, during the past 6,000 Yr. Nature, 302: 406-408.

Chave, K., 1964. Skeletal durability and preservation. In: J. Imbrie and N. Newell (Editors), Approaches to palaeoecology. John Wiley and Sons Inc., Sydney.

Chivas, A., Chappell, J., Polach, H., Pillans, B. and Flood, P., 1986. Radiocarbon evidence for the timing and rate of island development, beach-rock formation and phosphatization at Lady Elliot Island, Queensland, Australia. Marine Geology, 69: 273-287.

Church, J.A., White, N.J., Coleman, R., Lambeck, K. and Mitrovica, J.X., 2004. Estimates of the regional distribution of sea level rise over the 1950-2000 period. Journal of Climate, 17: 2609-2625.

Clack, W.J. and Mountjoy, E.W., 1977. Reef sediment transport and deposition off the east coast of Carriacou, West Indies, Proceedings of the 3rd International Coral Reef Symposium, pp. 97-103.

Cowell, P.J. and Thom, B.G., 1994. Morphodynamics of coastal evolution. In: R.W.G. Carter and C.D. Woodroffe (Editors), Coastal Evolution: Late Quaternary shoreline morphodynamics. Cambridge University Press, Cambridge, pp. 33-86.

Crowell, M., Leatherman, S.P. and Buckley, M.K., 1991. Historical shoreline change - error analysis and mapping accuracy. Journal of Coastal Research, 7: 839-852.

Curray, J.R., 1996. Origin of beach ridges: Comment. Marine Geology, 136: 121-125.

Dally, W.R., Dean, R.G. and Dalrymple, R.A., 1985. Wave height variation across beaches of arbitrary profile. Journal of Geophysical Research-Oceans, 90: 1917-1927.

Davies, P.J. and Hopley, D., 1983. Growth facies and growth rates of Holocene reefs in the Great Barrier Reef. BMR Journal of Australian Geology & Geophysics, 8: 237-251.

Davies, P.J. and Montaggioni, L., 1985. Reef growth and sea-level changes: the environmental signature, Proceedings of the 5th International Coral Reef Congress. Antenne Museum-EPHE, Tahiti, pp. 477-515.

Desmet, P.J.J., 1997. Effects of interpolation errors on the analysis of DEMs. Earth Surface Processes and Landforms, 22: 563-580.

Dixon, L.F.J., Barker, R., Bray, M., Farres, P., Hooke, J., Inkpen, R., Merel, A., Payne, D. and Shelford, A., 1998. Analytical photogrammetry for geomorphological research. In: S.N. Lane, K.S. Richards and J.H. Chandler (Editors), Landform, monitoring, modelling and analysis. John Wiley & Sons Ltd., West Sussex, pp. 63-94.

Eddy, J.A., 1976. Maunder Minimum. Science, 192: 1189-1202.

Elgar, S. and Guza, R.T., 1985a. Observations of bispectra of shoaling surface gravity waves. Journal of Fluid Mechanics, 161: 425-448.

Elgar, S. and Guza, R.T., 1985b. Shoaling gravity waves: comparisons between field observations, linear theory and a nonlinear model. Journal of Fluid Mechanics, 158: 47-70.

ESRI, 2001. TIN interpolation. Arc/Info online documentation in ArcDoc, ArcInfo Workstation.

ESRI, 2002. What is ArcGIS? Environmental Systems Research Institute, Redlands, USA, 76 pp.

Fairbridge, R.W., 1950. Recent and Pleistocene coral reefs of Australia. Journal of Geology, 58: 330-401.

Fairbridge, R.W. and Teichert, C., 1948. The Low Isles of the Great Barrier Reef: a new analysis. Geographical Journal, 111: 67-88.

Flood, P., 1977. Coral cays of the Capricorn and Bunker Groups, Great Barrier Reef Province, Australia. Atoll Research Bulletin, 195: 1-7.

Flood, P.G., 1979. Geomorphology of Tryon Island and Reef. Queensland Naturalist, 22: 113-126.

Flood, P.G., 1981. Coral cays and cyclone. Beach Conservation, 42:6.

Flood, P.G., 1983. Climatically induced changes to the shape of coral cays, southern Great Barrier Reef, Australia, Proceedings of the Inaugural Great Barrier Reef Conference. JCU Press, Townsville, pp. 379-384.

Flood, P.G., 1986. Sensitivity of coral cays to climatic variations, southern Great Barrier Reef, Australia. Coral Reefs, 5: 13-18.

Flood, P.G., 1988. Shoreline changes on coral cays, Capricornia section, Great Barrier Reef marine park, Australia, Proceedings of the 6th International Coral Reef Symposium, Australia, pp. 219-224.

Flood, P.G. and Heatwole, H., 1986. Coral cay instability and species-turnover of plants at Swain Reefs, Southern Great-Barrier-Reef, Australia. Journal of Coastal Research, 2: 479-496.

Folk, R.L., 1967. Sand cays of Alacran Reef ,Yucatan, Mexico: Morphology. Journal of Geology, 75: 412-437.

Folk, R.L. and Robles, R., 1964. Carbonate sands of Isla Perez, Alacran Reef Complex, Yucatan. Journal of Geology, 72: 255-292.

Force, L.M., 1969. Calcium carbonate size distribution on the west Florida shelf and experimental studies on the microarchitectural control of skeletal breakdown. Journal of Sedimentary Petrology, 39: 902-934.

Frank, T.D. and Jell, J.S., 2006. Recent development on a nearshore, terrigenous-influenced reef: Low Isles Reef, Australia. Journal of Coastal Research, 22: 474-486.

Gerritsen, F., 1980. Wave attenuation and wave set-up on a coastal reef, Proceedings of the 17th International Coastal Engineering Conference, Sydney, Australia. ASCE, New York, pp. 444-461.

Gillespie, R., 1977. Sydney University natural radiocarbon measurements IV. Radiocarbon, 19: 101-110.

Gillespie, R. and Polach, H., 1979. The suitability of marine shells for radiocarbon dating of Australian prehistory. In: R. Berger and H. Suess (Editors), Proceedings of the 9th International Conference on Radiocarbon Dating. University of California Press, Los Angeles, pp. 404-421.

Gourlay, M.R., 1988. Coral cays: products of wave action and geological processes in a biogenic environment, Proceedings 6th International Coral Reef Symposium, Townsville, Australia, pp. 491-496.

Gourlay, M.R., 1990. Waves, set-up and currents on reefs cay formation and stability, Engineering in Coral Reef Regions Conference, Magnetic Island, Townsville, pp. 249-264.

Gourlay, M.R., 1994. Wave transformation on a coral reef. Coastal Engineering, 23: 17-42.

Gourlay, M.R., 1996a. Wave set-up on coral reefs. 1. Set-up and wave-generated flow on an idealised two dimensional horizontal reef. Coastal Engineering, 27: 161-193.

Gourlay, M.R., 1996b. Wave set-up on coral reefs. 2. Set-up on reefs with various profiles. Coastal Engineering, 28: 17-55.

Gourlay, M.R. and Colleter, G., 2005. Wave-generated flow on coral reefs-an analysis for two-dimensional horizontal reef-tops with steep faces. Coastal Engineering, 52: 353-387.

Grace, R.A., 1978. Surface wave heights from pressure records. Coastal Engineering, 2: 55-67.

Guilcher, A., 1988. Coral reef geomorphology. Coastal morphology and research. John Wiley & Sons Ltd., New York, 228 pp.

Guza, R.T. and Thornton, E.B., 1980. Local and shoaled comparisons of sea surface elevations, pressures and velocities. Journal of Geophysical Research, 85(C3): 1524-1530.

Halley, R.B., 2000. Eleven things a geologist thinks an engineers should know about carbonate beaches. In: L.L. Robbins, O.T. Magoon and L. Ewing (Editors), Carbonate beaches 2000: First International Symposium on Carbonate Sand Beaches, Key Largo, Florida. ASCE, Virginia, pp. 1-14.

Hammond, T.M. and Collins, M.B., 1979. On the threshold of transport of sand-sized sediment under the combined influence of unidirectional and oscillatory flow. Sedimentology, 26: 795-812.

Hardisty, J., Middleton, R., Whyatt, D. and Rouse, H., 1998. Geomorphological and hydrodynamic results from digital terrain models of the Humber Estuary. In: S.N.

Lane, K.S. Richards and J.H. Chandler (Editors), Landform monitoring, modelling, and analysis. John Wiley & Sons Ltd, West Sussex.

Hardy, T.A., Mason, L.B. and McConochie, J.D., 2001. A wave model for the Great Barrier Reef. Ocean Engineering, 28: 45-70.

Hardy, T.A. and Young, I.R., 1991. Modelling spectral wave transformation on a coral reef flat, 10th Australasian Conference on Coastal and Ocean Engineering, Auckland, New Zealand, Water Quality Centre, Hamilton, New Zealand. Publ. No. 21., pp. 345-350.

Hardy, T.A. and Young, I.R., 1996. Field study of wave attenuation on an offshore coral reef. Journal of Geophysical Research-Oceans, 101: 14311-14326.

Harney, J.N., Grossman, E.E., Richmond, B.M. and Fletcher, C.H., 2000. Age and composition of carbonate shoreface sediments, Kailua Bay, Oahu, Hawaii. Coral Reefs, 19: 141-154.

Harris, P.T., 1995. Muddy waters: the physical sedimentology of Torres Strait. In: J.H. Choat, N.K. Saxena and O. Bellwood (Editors), Recent advances in marine science and technology '94. PACON International and James Cook University of North Queensland, Townsville, Queensland, pp. 149-160.

Harris, P.T., Heap, A.D., Wassenberg, T. and Passlow, V., 2004. Submerged coral reefs in the Gulf of Carpentaria, Australia. Marine Geology, 207: 185-191.

Hart, D. and Kench, P.S., 2006. Carbonate production of an emergent reef platform, Warraber Island, Torres Strait, Australia. Coral Reefs, in press.

Hart, D.E., 2003. Eco-sedimentological environments of an inter-tidal reef platform, Warraber Island, Torres Strait. Unpublished PhD Thesis, University of New South Wales, Australia, 210 pp.

Hart, D.E., 2004. Sediment composition of bulk samples on Warraber Island. Personal communication.

Hayne, M. and Chappell, J., 2001. Cyclone frequency during the last 5000 years at Curacoa Island, north Queensland, Australia. Palaeogeography Palaeoclimatology Palaeoecology, 168: 207-219.

Hearn, C.J., 1999. Wave-breaking hydrodynamics within coral reef systems and the effect of changing relative sea level. Journal of Geophysical Research, 104: 30007-30019.

Hearn, C.J., Atkinson, M.J. and Falter, J.L., 2001. A physical derivation of nutrient-uptake rates in coral reef: effects of roughness and waves. Coral Reefs, 20: 347-356.

Hegge, B. and Masselink, G., 1996. Spectral analysis of geomorphic time series; auto-spectrum. Earth Surface Processes and Landforms, 21: 1021-1040.

Hopley, D., 1977. The age of the outer ribbon reef surface, Great Barrier Reef, Australia: implications for hydro-isostatic models, Proceedings of Third International Coral Reef Symposium, Miami, Florida, pp. 23-28.

Hopley, D., 1981. Sediment movement around a coral cay, Great Barrier Reef, Australia. Pacific Geology, 15: 17-36.

Hopley, D., 1982. The geomorphology of the Great Barrier Reef. A Wiley-Interscience publication, 453 pp.

Hopley, D., 1984. The Holocene "high energy window" on the Central Great Barrier Reef. In: B.G. Thom (Editor), Coastal geomorphology in Australia. Academic Press, North Ryde, N.S.W., Australia, pp. 135-150.

Hopley, D., 1990. The geological an geomorphology of the Great Barrier Reef in relation to engineering problems, Proceedings of the Engineering in Coral Reefs Conference, Magnetic Island, pp. 61-74.

Hopley, D., 1992. Coral reef islands in a period of global sea level rise, Recent advances in marine science and technology, 92, pp. 453-462.

Hopley, D., 1994. Continental shelf reef systems. In: R.W.G. Carter and C.D. Woodroffe (Editors), Coastal Evolution: Late Quaternary shoreline morphodynamics. Cambridge University Press, Cambridge, pp. 303-340.

Humphries, L.P. and Ligdas, C.N., 1997. A GIS application for the study of beach morphodynamics, Proceedings of CoastGIS'97. University of Aberdeen, Aberdeen.

Hurdle, D.P. and Stive, R.J.H., 1989. Revision of SPM 1984 wave hindcast model to avoid inconsistencies in engineering applications. Coastal Engineering, 12: 339-351.

ICSM, 2003. Geocentric Datum of Australia technical manual version 2.2, Intergovernmental Committee on Surveying and Mapping.

IPCC, 2001. Climate change 2001: the scientific basis. Cambridge University Press, Cambridge, 639-694 pp.

Johnston, K., Ver Hoef, J.M., Krivoruchko, K. and Lucas, N., 2001. Using ArcGIS Geostatistical Analyst. Environmental Systems Research Institute, Redlands, USA, 306 pp.

Jones, M.R., 1995. The Torres Reefs, North Queensland, Australia-strong tidal flows a modern control on their growth. Coral Reefs, 14: 63-69.

Kamphuis, J.W., 2000. Introduction to coastal engineering and management. Advanced series on ocean engineering, 16. World Scientific Publishing Co. Pte. Ltd, Singapore, 437 pp.

Karunarathna, H. and Tanimoto, K., 1995. Numerical experiments on low-frequency fluctuations on a submerged coastal reef. Coastal Engineering, 26: 271-289.

Kench, P.S., 1998. A currents of removal approach for interpreting carbonate sedimentary processes. Marine Geology, 145: 197-223.

Kench, P.S. and Brander, R.W., 2006. Wave processes on coral reef flats: implications for reef geomorphology using Australian case studies. Journal of Coastal Research, 22: 209-223.

Kench, P.S., Brander, R.W., Parnell, K.E. and McLean, R.F., 2006. Wave energy gradients across a Maldivian atoll: Implications for island geomorphology. Geomorphology, in press.

Kench, P.S. and Cowell, P.J., 2000. Variation in sediment production and implications for atoll island stability under rising sea level, Proceedings of the 9th International Coral Reef Symposium, Bali, Indonesia, pp. 1181-1186.

Kench, P.S. and McLean, R.F., 1996. Hydraulic characteristics of bioclastic deposits: New possibilities for environmental interpretation using settling velocity fractions. Sedimentology, 43: 561-570.

Kench, P.S. and McLean, R.F., 1997. A comparison of settling and sieve techniques for the analysis of bioclastic sediments. Sedimentary Geology, 109: 111-119.

Kench, P.S., McLean, R.F. and Nichol, S.L., 2005. New model of reef-island evolution: Maldives, Indian Ocean. Geology, 33: 145-148.

King, C.A.M., 1972. Beaches and coasts. Arnold, London, 570 pp.

Kirby, J.T., 1986. Rational approximations in the parabolic equation method for water waves. Coastal Engineering, 10: 355-378.

Kirby, J.T. and Dalrymple, R.A., 1994. Combined refraction/diffraction model REF/DIF 1 Version 2.5: documentation and user's manual. CACR Report No. 94-22, Center for Applied Coastal Research, Department of Civil Engineering, University of Delaware, Newark, DE 19716.

Kirby, J.T., Wei, G., Chen, Q., Kennedy, A.B. and Dalrymple, R.A., 1998. FUNWAVE 1.0: fully nonlinear Boussinesq wave model documentation and user's manual. CACR Report No. 98-06, Center for Applied Coastal Research, Department of Civil Engineering, University of Delaware, Newark, DE 19716.

Knowles, C.E., 1983. On the estimation of surface gravity waves from subsurface pressure records for estuarine basins. Estuarine Coastal and Shelf Science, 17: 395-404.

Kofoed-Hansen, H. and Rasmussen, J.H., 1998. Modelling of nonlinear shoaling based on stochastic evolution equations. Coastal Engineering, 33: 203-232.

Komar, P.D., 1998. Beach processes and sedimentation. Prentice-Hall, Inc., New Jersey, 544 pp.

Komar, P.D. and Miller, M.C., 1973. The threshold of sediment movement under oscillatory water waves. Journal of Sedimentary Petrology, 43: 1101-1110.

Krogstad, H.E., Wolf, J., Thompson, S.P. and Wyatt, L.R., 1999. Methods for intercomparison of wave measurements. Coastal Engineering, 37: 235-257.

Kumler, M.P., 1994. An intensive comparison of triangulated irregular networks (TINs) and digital elevation models (DEMs). Cartographica, 31(2): Monograph 45.

Landscheidt, T., 2000. Solar forcing of El Niño and La Niña. ESA Special Publication, 463: 135-140.

Larcombe, P., Carter, R.M., Dye, J., Gagan, M.K. and Johnson, D.P., 1995. New evidence for episodic post-glacial sea-level rise, central Great Barrier Reef, Australia. Marine Geology, 127: 1-44.

Lawson, E.M. et al., 2000. AMS at ANTARES - The first 10 years. Nuclear Instruments and Methods in Physics Research Section B: Beam Interactions with Materials and Atoms, 172: 95-99.

Le Roux, J.P., 1992. Settling velocity of sphere: a new approach. Sedimentary Geology, 81: 11-16.

Le Roux, J.P., 1998. Entrainment threshold of natural grains in liquids determined empirically from dimensionless settling velocities and other measures of grain size. Sedimentary Geology, 119: 17-23.

Le Roux, J.P., 2001. A simple method to predict the threshold of particle transport under oscillatory waves. Sedimentary Geology, 143: 59-70.

Leatherman, S.P. and Beller-Simms, N., 1997. Sea-level rise and small island states: an overview. Journal of Coastal Research, SI24: 1-16.

Lee, D.Y. and Wang, H., 1984. Measurement of surface waves from subsurface gauge, Proceedings of 19th Coastal Engineering Conference, Houston, Texas. ASCE, New York, pp. 271-286.

Lee, T.T. and Black, K.P., 1978. The energy spectra of surf waves on a coral reef, Proceedings of 16th International Coastal Engineering Conference, Hamburg, Germany. ASCE, New York, pp. 588-608.

Lewis, A., 2001. Great Barrier Reef Depth and Elevation Model: GBRDEM. Technical Report No. 33, CRC Reef Research Centre, Townsville.

Lewis, S.E., Wust, R.A.J., Webster, J.M. and Shields, G.A., A revised sea-level curve for he Great Barrier Reef and eastern Australia over the last 7,000 years. in preparation.

Liu, G. and Retschlag, B., 1991. Evaluation of shoreline erosion and flooding at Warraber Island Torres Strait region. Report CE 91/15, Australian Construction Services.

Lugo-Fernandez, A., Roberts, H.H. and Suhayda, J.N., 1998a. Wave transformations across a Caribbean fringing-barrier Coral Reef. Continental Shelf Research, 18: 1099-1124.

Lugo-Fernandez, A., Roberts, H.H., Wiseman, W.J. and Carter, B.L., 1998b. Water level and current of tidal and infragravity periods at Tague Reef, St. Croix (USVI). Coral Reefs, 17: 343-349.

Maiklem, W.R., 1968. Some hydraulic properties of bioclastic carbonate grains. Sedimentology, 10: 101-109.

Manohar, M., 1955. Mechanics of bottom sediment movement due to wave action, Beach Erosion Board.

Mansard, E.P.D. and Funke, E.R., 1991. On fitting of JONSWAP spectra to measured sea states, Proceedings of the 22nd Coastal Engineering Conference. ASCE, New York, pp. 464-477.

Maragos, J.E., Baines, G.B.K. and Beveridge, P.J., 1973. Tropical cyclone Bebe creates a new land formation on Funafuti Atoll. Science, 181: 1161-1164.

Massel, S.R., 1983. Harmonic generation by waves propagating over a submerged step. Coastal Engineering, 7: 357-380.

Massel, S.R., 1998. The limiting wave height in wind-induced wave trains. Ocean Engineering, 25: 735-752.

Massel, S.R. and Gourlay, M.R., 2000. On the modelling of wave breaking and set-up on coral reefs. Coastal Engineering, 39: 1-27.

Maxwell, W.G.H., 1968. Atlas of the Great Barrier Reef. Elsevier, Amsterdam.

McCoy, J. and Johnston, K., 2001. Using ArcGIS Spatial Analyst. Environmental Systems Research Institute, Redlands, USA, 236 pp.

McCullagh, M.J., 1998. Quality, use and visualisation in terrain modelling. In: S.N. Lane, K.S. Richards and J.H. Chandler (Editors), Landform monitoring, modelling and analysis. John Wiley & Sons Ltd, West Sussex, pp. 95-118.

McLean, R.F. and Shen, J.-S., 2006. From foreshore to foredune: foredune development over the last 30 years at Moruya Beach, New South Wales, Australia. Journal of Coastal Research, 22: 28-36.

McLean, R.F. and Stoddart, D.R., 1978. Reef island sediments of the northern Great Barrier Reef. Philosophical Transactions of the Royal Society of London Series A-Mathematical Physical and Engineering Sciences, 291: 101-117.

McLean, R.F., Stoddart, D.R., Hopley, D. and Polach, H., 1978. Sea level change in the Holocene on the northern Great Barrier Reef. Philosophical Transactions of the Royal Society of London Series A-Mathematical Physical and Engineering Sciences, 291: 167-186.

McLean, R.F. and Woodroffe, C.D., 1994. Coral atolls. In: R.W.G. Carter and C.D. Woodroffe (Editors), Coastal Evolution: Late Quaternary shoreline morphodynamics. Cambridge University Press, Cambridge, pp. 267-302.

Milliman, J.D., 1974. Marine carbonates. Recent sedimentary carbonates, 1. Springer-Verlag, New York, 375 pp.

Minami, M. et al., 2000. Using ArcMap. Environmental Systems Research Institute, Redlands, USA, 528 pp.

Moore, L.J., 2000. Shoreline mapping techniques. Journal of Coastal Research, 16: 111-124.

Moussas, X., Polygiannakis, J.M., Preka-Papadema, P. and Exarhos, G., 2005. Solar cycles: a tutorial. Advances in Space Research, 35: 725-738.

Mowling, F. and Coleman, R., 2003. Temporal-spatial analysis of dune morphology. In: C. Woodroffe and R.A. Furness (Editors), Coastal GIS 2003: an integrated approach to Australian coastal issues. Wollongong Papers on Maritime Policy, No 14. Centre for Maritime Policy, University of Wollongong, pp. 243-255.

Murray, R.T. and Ford, L.R., 1983. Problems in the analysis of data for the assessment of longshore sediment transport: an example from North Queensland, 6th Australasian Conference on Coastal and Ocean Engineering, Brisbane, Australia. Institution of Engineers, Australia, Nat.Conf.Publ.No. 83/6, pp. 21-26.

Nakada, M. and Lambeck, K., 1989. Late Pleistocene and Holocene sea-level change in the Australian region and mantle rheology. Geographical Journal, 96: 497-517.

Nakaza, E., Tsukayama, S. and Hino, M., 1990. Bore-like surf beat on reef coasts, Proceedings of 22nd International Conference Coastal Engineering, Delf, Netherland, pp. 743-756.

NASA, 2005. The sunspot cycle. http://science.nasa.gov/ssL/pad/solar/sunspots.htm.

Nelson, R.C., 1994. Depth limited design wave heights in very flat regions. Coastal Engineering, 23: 43-59.

Nelson, R.C., 1997. Height limits in top down and bottom up wave environments. Coastal Engineering, 32: 247-254.

Nelson, R.C. and Lesleighter, E.J., 1985. Breaker height attenuation over platform coral reefs, 17th Australasian Conference on Coastal and Ocean Engineering, Christchurch, New Zealand, Conference Organising Committee. Vol.2, pp. 9-16.

Neumann, A.C. and Macintyre, I., 1985. Reef response to sea level rise: keep-up, catch-up or give-up, Proceedings of the 5th International Coral Reef Congress, pp. 105-110.

Nielsen, P., 1992. Coastal bottom boundary layers and sediment transport. Advanced series on ocean engineering, 4. World Scientific Publishing Co. Pte. Ltd., Singapore, 324 pp.

NOAA, 2003. El Nino. In: A.M. Babkina (Editor), El Nino: overview and bibliography. Nova Science Publishers, Inc, New York, pp. 1-4.

NortekUSA, 2002. Wave measurements using the PUV method. Doc.No. N4000-720, http://www.nortekusa.com/technotes/TN019.pdf.

Nunn, P.D., 2000. Sea-level changes and their effects on tropical Pacific island environments: The next hundred years, Proceedings of the Pacific Islands Conference on Climate Change, Climate Variability and Sea Level Rise. National Tidal Facility Australia, Rarotonga, Cook Island, pp. 59-62.

Orme, G.R., 1977. Aspects of sedimentation in the coral reef environment. In: O.A. Jones and R. Endean (Editors), Biology and geology of coral reefs, pp. 129-182.

Parkyn, E.A., 1930. The voyage of Luis Vaez de Torres: review. Geographical Journal, 76: 252-256.

Prager, E.J., Southard, J.B. and Vivoni-Gallart, E.R., 1996. Experiments on the entrainment threshold of well-sorted and poorly sorted carbonate sands. Sedimentology, 43: 33-40.

Rakha, K.A. and Abul-Azm, A.G., 2000. Nearshore wave modelling for a beach with coral reefs along the Red Sea, Proceedings 9th International Coral Reef Symposium, Bali, Indonesia, pp. 311-313.

Ranasinghe, R., McLoughlin, R., Short, A.D. and Symonds, G., 2004. The Southern Oscillation Index, wave climate and beach rotation. Marine Geology, 204: 273-287.

Raper, J., 1999. 2.5- and 3-D GIS for coastal geomorphology. In: D.J. Wright and D.J. Bartlett (Editors), Marine and coastal geographical information systems. Taylor & Francis, London, pp. 129-136.

Raper, J., 2000. Multidimensional geographic information science. Taylor & Francis, New York, 300 pp.

Rasmussen, C.E. and Hopley, D., 1996. Warraber Island beach erosion review. Consultancy Report, Edmiston&Taylor, Consulting Engineers & Project Managers, Brisbane.

Rathert, D., 2005. ArcGIS extension "RASTER TO XYZ". Resource Data Inc. http://www.resdat.com.

Reimer, P. and Reimer, R., 2000. Marine reservoir correction database, http://www.calib.org/marine.

Rhodes, E.G., Polach, H., Thom, B.G. and Wilson, S.R., 1980. Age structure of Holocene coastal sediments: Gulf of Carpentaria, Australia. Radiocarbon, 22: 718-727.

Richmond, B., 1992. Development of atoll islets in the Central Pacific, Proceedings of the 7th International Coral Reef Congress, Guam, pp. 1185-1194.

Risk, M.J. and Sluka, R., 2000. The Maldives: a nation of atolls. In: T.R. McClanahan, C.R.C. Sheppard and D.O. Obura (Editors), Coral reefs of Indian Ocean: their ecology and conservation. Oxford University Press, Inc., New York, pp. 325-352.

Roberts, H.H., 1980. Physical processes and sediment flux through reef-lagoon systems, Proceedings of the 17th International Coastal Engineering Conference, Sydney, Australia. ASCE, New York, pp. 209-214.

Roberts, H.H., 1989. Physical processes as agents of sediment transport in carbonate systems: Examples from St. Croix, U.S.V.I. In: D.K. Hubbard (Editor), 12th Caribbean Geological Conference, Teague Bay, St. Croix: West Indies Library, pp. 95-103.

Roberts, H.H., Murray, S.P. and Suhayda, J.N., 1975. Physical processes in a fringing reef system. Journal of Marine Research, 33: 233-260.

Roberts, H.H., Wilson, P.A. and Lugo-Fernandez, A., 1992. Biologic and geologic responses to physical processes: examples from modern reef systems of the Caribbean-Atlantic region. Continental Shelf Research, 12: 809-834.

Roy, P. and Connell, J., 1991. Climatic change and the future of atoll states. Journal of Coastal Research, 7: 1057-1075.

Schumm, S.A., 1991. To interpret the Earth: ten ways to be wrong. Cambridge University Press, Cambridge, 133 pp.

Scoffin, T.P., 1987. An introduction to carbonate sediments and rocks. Blackie & Son Ltd, London, 274 pp.

Scoffin, T.P., Stoddart, D.R., McLean, R.F. and Flood, P.G., 1978. The Recent development of the reefs in the northern province of the Great Barrier Reef. Philosophical Transactions of the Royal Society of London Series B-Biological Sciences, 284(999): 129-140.

Sewell, R.B.S., 1932. The coral coasts of India. Geographical Journal, 79: 449-465.

Sheppard, C.R.C., Dixon, D.J., Gourlay, M.R., Sheppard, A. and Payet, R., 2005. Coral mortolity increases wave energy reaching shores protected by reef flats: examples from the Seychelles. Estuarine Coastal and Shelf Science, 64: 223-234.

Short, A.D. and Trembanis, A.C., 2004. Decadal scale patterns in beach oscillation and rotation, Narrabean Beach, Australia - Time series, PCA and wavelet analysis. Journal of Coastal Research, 20: 523-532.

Skewes, T.D., Dennis, D.M., Pitcher, C.R. and Long, B.G., 1997. Age structure of Panulirus ornatus in two habitats in Torres Strait, Australia. Marine and Freshwater Research, 48: 745-750.

Smith, M.J., Stevens, C.L., Gorman, R.M., McGregor, J.A. and Neilson, C.G., 2001. Wind-wave development across a large shallow intertidal estuary: a case study of Manukau Harbour, New Zealand. New Zealand Journal of Marine and Freshwater Research, 35: 985-1000.

Smithers, S.G., Hopley, D. and Parnell, K.E., 2006. Fringing and nearshore coral reefs of the Great Barrier Reef: episodic Holocene development and future prospects. Journal of Coastal Research, 22: 175-187.

Soulsby, R.L. and Whitehouse, R.J.S., 1997. Threshold of sediment motion in coastal environment, 13th Australasian Coastal and Engineering Conference and 6th Australasian Port and Harbour Conference. HR Wallingford, Oxon, Christchurch, New Zealand, pp. 149-154.

Stearns, S.D. and David, R.A., 1993. Signal processing algorithms using Fortran and C. P T R Prentice-Hall, Inc., New Jersey, 331 pp.

Steers, J.A., 1929. The Queensland coast and the Great Barrier Reef. Geographical Journal, 74: 232-257.

Steers, J.A., 1937. The coral islands and associated features of the Great Barrier Reef. Geographical Journal, 89: 1-28.

Steers, J.A., Chapman, V.J., Colman, J. and Lofthouse, J.A., 1940. Sand cays and mangroves in Jamaica: Cambridge University Jamaican Expedition, 1939 Meeting of the Society, 15 April 1940. Geographical Journal, 96(5): 305-328.

Steers, J.A. and Lofthouse, J.A., 1940. The coral cays of Jamaica. Geographical Journal, 95: 30-42.

Stevenson, B., 1980. Solar cycles and erosional events on the New South Wales central and south coasts. Search, 11: 117-118.

Stoddart, D.R., 1964. Storm conditions and vegetation in equilibrium of reef islands, Proceedings of the 9th Coastal Engineering Conference, Lisbon, Portugal. ASCE, New York, pp. 893-906.

Stoddart, D.R., 1969. Sea-level change and the origin of sand cays: radiometric evidence. Journal of Marine Biological Association India, 11: 44-58.

Stoddart, D.R., 1971. Coral reefs and islands and catastrophic storms. In: J.E. Steers (Editor), Applied coastal geomorphology. Macmillan, London, pp. 155-197.

Stoddart, D.R., 1975. Sand cays of Tongatapu. Atoll Research Bulletin, 181: 16.

Stoddart, D.R., Mclean, R.F. and Hopley, D., 1978a. Geomorphology of reef islands, northern Great Barrier Reef. Philosophical Transactions of the Royal Society of London Series B-Biological Sciences, 284: 39-61.

Stoddart, D.R., Mclean, R.F., Scoffin, T.P. and Thom, B.G., 1978b. Evolution of reefs and islands, northern Great Barrier Reef: synthesis and interpretation. Philosophical Transactions of the Royal Society of London Series B-Biological Sciences, 284: 149-160.

Stoddart, D.R. and Steers, J.A., 1977. The nature and origin of coral reef islands. In: O.A. Jones and R. Endean (Editors), Biology and geology of coral reefs. Academic Press, New York, pp. 60-106.

Storlazzi, C.D., Ogston, A.S., Bothner, M.H., Field, M.E. and Presto, M.K., 2004. Wave- and tidally-driven flow and sediment flux across a fringing coral reefs: Southern Molokai, Hawaii. Continental Shelf Research, 24: 1397-1419.

Stuiver, M. and Reimer, P.J., 1993. Extended ^{14}C database and revised CALIB 3.0 ^{14}C age calibration program. Radiocarbon, 35: 215-230.

Swart, D.H. and Loubser, C.C., 1979. Vocoidal wave theory, Vol. 2: verification. Research Report 360, NRIO, CSIR.

Swarztrauber, P.N. and Pumphrey, H.C., 1985. DFFTPACK V1.0. ftp://ftp.netlib.org:/fftpack/dp.tgz.

Symonds, G., Black, K.P. and Young, I.R., 1995. Wave-driven flow over shallow reefs. Journal of Geophysical Research, 100: 2639-2648.

Tanner, W.F., 1995. Origin of beach ridges and swales. Marine Geology, 129: 149-161.

Tanner, W.F., 1996. Origin of beach ridges: Reply. Marine Geology, 136: 127-130.

Tartinville, B. and Rancher, J., 2000. Wave-induced flow over Mururoa Atoll Reef. Journal of Coastal Research, 16: 776-781.

Thom, B.G., 1974. Coastal erosion in eastern Australia. Search, 5: 198-209.

Thorpe, J.E. and Stoddart, D.R., 1962. Cambridge Expedition to British Honduras. Geographical Journal, 128: 158-171.

Tomascik, T., Mah, A.J., Nontji, A. and Moosa, M.K., 1997. The Ecology of the Indonesian Seas. Periplus Editions (HK) Ltd., Singapore, 1388 pp.

Tsukayama, S. and Nakaza, E., 2000. Wave transformations on coral reefs. In: B.L. Egde (Editor), Proceedings of 27th International Coastal Engineering Conference, Sydney, Australia. ASCE, New York, pp. 1372-1382.

Tucker, C., DeMerchant, I., Bicking, B., Boyd, C., Pardy, J., Conly, M., Prince, G., Kabot, G. and Pengelley, A., 2000. Using ArcToolbox. Environmental Systems Research Institute, Redlands, USA, 105 pp.

Tucker, M.J., 1991. Waves in ocean engineering: measurement, analysis, interpretation. Ellis Horwood, Chichester.

Umbgrove, J.H.F., 1947. Coral reefs of the East Indies. Bulletin of the Geographic Society of America, 58: 729-778.

Vienneau, A. and Bailey, J., 2001. Using ArcCatalog. Environmental Systems Research Institute, Redlands, USA, 294 pp.

Wei, G., Kirby, J.T., Grilli, S.T. and Subramanya, R., 1995. A fully nonlinear Boussinesq model for surface waves. I. Highly nonlinear, unsteady waves. Journal of Fluid Mechanics, 294: 71-92.

Wiegel, R.L., 1990. Transformation of swell over a reef. Shore and Beach, 58: 31.

Wolanski, E., 1986. Observations of wind-driven surface gravity waves offshore from the Great Barrier Reef. Coral Reefs, 4: 213-219.

Wolanski, E., 1994. Physical oceanographic processes of the Great Barrier Reef. CRC Marine Science. CRC Press, Inc., Boca Raton, 194 pp.

Wolf, J., 1997. The analysis of bottom pressure and current data for waves, 7th International Conference on Electronic Engineering in Oceanography, pp. 165-169.

Woodroffe, C.D., 1992. Morphology and evolution of reef islands in the Maldives, Proceedings of the 7th International Coral Reef Symposium, Guam, pp. 1217-1226.

Woodroffe, C.D., 2000. Reef-island sedimentation on Indo-Pacific atolls and platform reefs, Proceedings of the 9th International Coral Reef Symposium, Bali, Indonesia, pp. 1187-1192.

Woodroffe, C.D., 2002. Coasts: form, process and evolution. Cambridge University Press, Cambridge, 623 pp.

Woodroffe, C.D., Kennedy, D.M., Hopley, D., Rasmussen, C.E. and Smithers, S.G., 2000. Holocene reef growth in Torres Strait. Marine Geology, 170: 331-346.

Woodroffe, C.D., McLean, R.F., Smithers, S.G. and Lawson, E.M., 1999. Atoll reef-island formation and response to sea-level change: West Island, Cocos (Keeling) Islands. Marine Geology, 160: 85-104.

Woodroffe, C.D. and Morrison, R.J., 2001. Reef-island accretion and soil development on Makin, Kiribati, central Pacific. Catena, 44: 245-261.

Yamano, H., 2000. Sensitivity of reef flats and reef islands to sea-level change, Proceedings 9th International Coral Reef Symposium, Bali, Indonesia, pp. 1193-1198.

Yamano, H., Miyajima, T. and Koike, I., 2000. Importance of foraminifera for the formation and maintenance of a coral sand cay: Green Island, Australia. Coral Reefs, 19: 51-58.

Young, I.R., 1989. Wave transformation over coral reefs. Journal of Geophysical Research-Oceans, 94: 9779-9789.

Young, I.R., 1995. The Determination of confidence-limits associated with estimates of the spectral peak frequency. Ocean Engineering, 22: 669-686.

Young, I.R., 1999. Seasonal variability of the global ocean wind and wave climate. International Journal of Climatology, 19: 931-950.

Young, I.R. and Verhagen, L.A., 1996a. The growth of fetch limited waves in water of finite depth .1. Total energy and peak frequency. Coastal Engineering, 29: 47-78.

Young, I.R. and Verhagen, L.A., 1996b. The growth of fetch limited waves in water of finite depth .2. Spectral evolution. Coastal Engineering, 29: 79-99.

Zeiler, M., 1999. Modeling our world. Environmental Systems Research Institute, Redlands, USA, 199 pp.

NUMBER OF DAYS WITH MSSING WIND DATA, 1951-2003

Table A1.1 Number of days with missing wind data, 1951-1992, Thursday Island.

Year	Jan	Feb	Mar	Apr	May	Jun	Jul	Aug	Sep	Oct	Nov	Dec	Total
1951	6	3											9
1952				2	4	5	4	2					17
1953									4	4			8
1954													
1955										2			2
1956				2							2		4
1957		1											1
1958													
1959					1		4						5
1960													
1961													
1962													
1963													
1964													
1965									3				3
1966	1												1
1967											1		1
1968				1									1
1969													
1970													
1971	4	4											8
1972													
1973					1								1
1974													
1975													
1976													
1977													
1978				1									1
1979													
1980													
1981							6	10	8		2		26
1982						4	1	2	3				10
1983					2	8	10	2					22
1984	1						2						3
1985													
1986													
1987													
1988													
1989													
1990													
1991													
1992													
Total	12	8		6	8	17	27	16	18	6	4	1	123

Table A1.2 Number of days with missing wind data, 1993-2003, Horn Island.

Year	Jan	Feb	Mar	Apr	May	Jun	Jul	Aug	Sep	Oct	Nov	Dec	Total
1993													
1994						Unavailable data							
1995				9	10		4		2	2	7		34
1996			4	1			21	4	13	2	2	8	55
1997	4	5	9	3	1	2		4	1		1	1	31
1998	1		2		11	6	4	4	5	14	19		66
1999	7	6			1				1		1	11	33
2000			1	2			1	1			2		7
2001			2								1		3
2002		1	1	1		6		1		5	3	6	24
2003		1				2	2	3	5	7	2	2	24

APPENDIX 2

YEARLY RESULTS OF WIND DATA ANALYSIS

Table A2 Yearly results of wind data analysis.

Year	Resultant wind direction (degree)	Resultant wind effect (m/s)	Total wind effect (m/s)	Calms (%)
1951	ESE (117)	1,194.18	1,578.2	9.55
1952	ESE (117)	940.65	1,297.1	13.47
1953	ESE (118)	970.71	1,433.4	8.96
1954	ESE (116)	1,346.51	1,976.7	6.58
1955	ESE (119)	1,189.72	2,073.6	4.41
1956	ESE (123)	771.55	1,688.2	9.67
1957	ESE (112)	1,117.93	1,904.5	6.04
1958	ESE (111)	1,523.22	2,260.8	9.86
1959	ESE (110)	1,521.77	2,968.3	4.44
1960	ESE (118)	1,598.99	2,108.4	4.37
1961	ESE (122)	1,839.66	2,198.1	5.21
1962	ESE (119)	1,496.12	2,293.7	5.75
1963	ESE (119)	1,552.07	2,188.3	7.40
1964	ESE (120)	1,319.96	2,124.4	7.65
1965	ESE (118)	1,670.25	2,224.4	5.80
1966	ESE (117)	2,029.41	2,508.0	5.49
1967	ESE (104)	1,427.01	2,261.9	5.49
1968	ESE (114)	1,678.55	2,423.6	4.93
1969	ESE (108)	1,735.84	2,479.2	3.29
1970	ESE (116)	1,466.14	2,101.3	3.84
1971	SE (134)	1,251.20	2,177.2	3.64
1972	ESE (115)	1,381.36	2,236.7	1.37
1973	ESE (114)	1,279.35	1,840.5	15.93
1974	ESE (105)	989.01	1,864.5	7.95
1975	ESE (114)	1,272.55	1,880.7	17.81
1976	ESE (111)	806.53	1,485.0	24.59
1977	SE (126)	1,562.64	2,166.2	16.71
1978	ESE (118)	1,766.86	2,505.4	7.42
1979	ESE (109)	1,596.36	2,728.5	2.74
1980	ESE (106)	1,674.95	2,431.0	7.10
1981	ESE (116)	1,187.16	2,391.5	6.49
1982	ESE (109)	1,462.22	2,253.1	7.89
1983	ESE (116)	1,522.46	2,030.6	9.33
1984	ESE (120)	1,547.03	2,196.8	8.26
1985	ESE (120)	1,552.10	2,288.7	3.84
1986	ESE (114)	1,758.00	2,438.2	2.74
1987	ESE (119)	1,659.33	2,572.5	2.74
1988	ESE (121)	1,678.97	2,476.3	6.01
1989	ESE (123)	1,605.46	2,250.9	9.04
1990	SE (126)	1,549.02	2,463.6	6.30
1991	ESE (122)	1,446.83	2,259.0	4.93
1992	ESE (115)	1,572.44	2,538.8	5.74
1993				
1994		Unavailable data		
1995				
1996	E (101)	952.13	1,499.8	6.11
1997	ESE (111)	1,415.55	1,859.6	3.59
1998	ESE (119)	808.68	1,450.8	0.74
1999	ESE (117)	1,222.74	1,816.5	0.90
2000	ESE (118)	1,211.47	1,799.2	2.51
2001	ESE (116)	1,420.30	2,007.7	0.83
2002	ESE (115)	1,388.18	1,987.2	0.59
2003	ESE (119)	1,436.01	1,892.4	1.47

APPENDIX 3

15-YEAR MOVING AVERAGE OF WIND EFFECT BY DIRECTIONS

Table A3.1 15-year moving average of wind effect between N and SSE.

Year	N	NNE	NE	ENE	E	ESE	SE	SSE
51-65	9.01	5.93	8.07	8.13	224.08	832.95	589.25	31.70
52-66	9.31	5.93	8.14	8.57	227.83	878.15	596.65	33.98
53-67	9.90	6.85	9.48	14.89	258.65	894.79	589.70	34.85
54-68	10.55	6.54	9.96	15.82	263.31	925.57	608.04	36.35
55-69	11.10	6.95	10.99	17.30	304.07	909.60	612.48	35.83
56-70	11.17	7.50	10.89	18.87	316.21	896.89	622.71	34.84
57-71	10.93	8.03	11.05	21.54	318.55	873.15	659.42	49.41
58-72	10.78	8.16	11.33	22.58	320.41	868.90	678.47	51.92
59-73	12.35	8.37	11.27	22.68	294.43	865.15	686.23	49.59
60-74	12.77	8.05	9.91	24.09	292.54	820.96	676.15	49.87
61-75	13.59	7.71	9.91	24.02	298.95	807.51	664.41	50.37
62-76	13.87	7.19	9.57	27.18	308.83	779.09	623.09	48.46
63-77	13.80	6.03	9.67	27.18	310.27	754.72	639.44	53.71
64-78	12.91	6.27	9.23	27.42	315.17	764.83	641.05	54.86
65-79	12.84	6.44	8.23	28.07	335.16	791.18	626.57	51.97
66-80	13.49	6.24	8.37	27.80	356.68	804.26	597.68	51.96
67-81	14.96	6.58	8.13	27.18	352.37	782.85	590.10	52.56
68-82	15.78	6.00	5.77	20.41	346.40	788.30	600.37	51.70
69-83	14.82	6.04	5.70	20.85	355.16	773.43	588.15	52.77
70-84	15.09	6.07	4.80	19.79	312.47	776.05	608.31	57.95
71-85	15.19	6.03	5.05	20.09	305.71	770.74	622.60	64.82
72-86	16.01	5.95	5.60	16.60	322.77	824.99	588.14	57.50
73-87	16.60	5.82	5.73	15.94	304.37	859.82	587.67	62.13
74-88	17.33	5.69	5.62	16.62	300.60	876.52	599.05	71.07
75-89	17.06	5.65	5.89	15.93	291.51	878.75	634.16	78.73
76-90	17.10	6.03	5.96	16.65	282.15	883.30	655.99	87.72
77-91	16.59	6.79	5.92	13.04	274.39	900.89	687.11	98.41
78-92	16.59	6.82	6.29	13.97	282.29	927.63	665.91	96.81

Table A3.2 15-year moving average of wind effect between S and NNW.

Year	S	SSW	SW	WSW	W	WNW	NW	NNW
51-65	4.06	0.61	2.49	3.59	46.65	121.61	98.98	34.11
52-66	3.99	1.02	2.49	3.55	48.30	123.63	95.49	36.15
53-67	3.69	1.43	2.87	5.71	49.39	131.90	96.77	36.63
54-68	3.89	1.43	2.63	5.71	45.55	130.19	102.97	45.00
55-69	3.66	1.19	3.35	6.92	49.04	125.04	105.81	43.69
56-70	3.70	1.33	5.19	6.71	47.39	113.75	107.07	44.65
57-71	4.15	1.37	6.39	7.02	48.94	103.96	112.58	44.97
58-72	4.52	1.37	6.39	8.29	45.78	100.07	118.43	46.21
59-73	4.56	1.27	6.36	8.16	41.76	92.07	121.38	49.95
60-74	5.31	1.27	6.30	7.95	38.84	80.11	115.54	52.35
61-75	4.87	1.31	6.29	7.79	39.05	83.05	114.09	53.91
62-76	4.94	1.45	5.71	10.12	43.75	83.73	118.55	53.77
63-77	5.49	1.83	5.57	10.09	42.27	86.21	110.99	53.53
64-78	5.80	1.83	5.47	10.57	43.54	86.19	110.68	56.13
65-79	5.80	2.37	5.31	10.03	43.74	90.63	116.89	56.98
66-80	5.97	2.68	5.24	10.17	43.40	92.56	118.13	61.35
67-81	5.80	2.27	5.24	10.20	48.12	101.97	125.63	64.25
68-82	5.87	1.85	5.03	8.49	48.78	96.93	130.23	65.73
69-83	5.93	1.85	5.03	9.69	53.03	97.27	124.80	56.91
70-84	6.07	1.85	4.49	9.17	47.64	95.66	127.42	59.79
71-85	6.38	1.81	2.95	10.27	45.59	93.35	130.38	64.13
72-86	5.52	1.71	2.74	10.33	42.01	89.39	125.83	67.41
73-87	5.35	1.71	2.74	9.19	42.21	94.03	122.61	68.96
74-88	6.41	2.70	3.15	9.53	43.22	98.97	119.53	71.25
75-89	6.89	2.70	3.35	9.33	43.77	96.41	116.93	65.97
76-90	9.33	3.04	4.29	9.25	47.06	99.71	119.11	65.21
77-91	9.26	2.90	4.01	7.19	44.01	100.87	122.07	70.03
78-92	8.44	2.52	4.08	7.33	44.96	102.56	124.86	77.26